UNIVERSITY OF SOUTHAMPTON

FACULTY OF NATURAL AND ENVIRONMENTAL SCIENCES

OCEAN AND EARTH SCIENCES

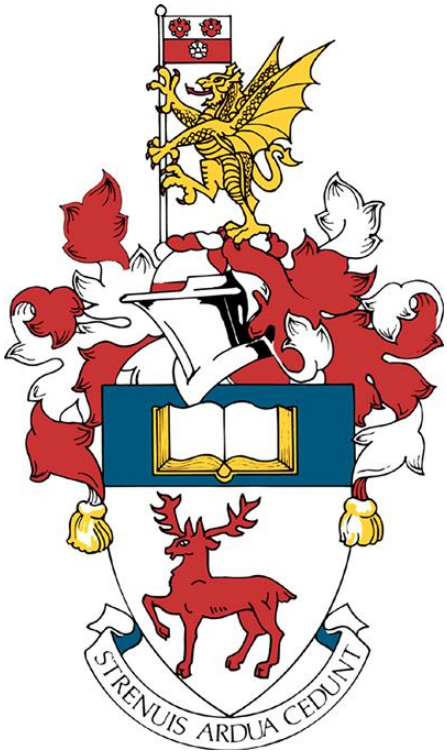

THE 1 MA EVOLUTION OF CONSTRUCTIVE AND DESTRUCTIVE PROCESSES AT THE ISLAND ARC VOLCANO OF MONTSERRAT

By Maya Coussens

Thesis for the degree of Doctor of Philosophy

March 2016

UNIVERSITY OF SOUTHAMPTON

ABSTRACT

Faculty of Natural and Environmental Science
Ocean and Earth Sciences
Doctor of Philosophy

THE 1 MA EVOLUTION OF CONSTRUCTIVE AND DESTRUCTIVE PROCESSES AT THE ISLAND ARC VOLCANO OF MONTSERRAT

By Maya Coussens

Montserrat is a small island arc volcano in the Caribbean island arc. The island comprises three main volcanic centres: Silver Hills, active between 2.5-1 Ma; Centre Hills, active between ~1 to 0.5 Ma; and the Soufrière Hills-South Soufrière Hills volcanic complex, active from ~0.3 Ma. Here an extensive (> 1 Ma) and detailed stratigraphic record is compiled for Montserrat using both the subaerial and submarine (in the form of three International Ocean Drilling Program cores) records. This combined record gives valuable insight into the evolution of volcanic and mass-wasting processes at Montserrat, and may be useful for future hazard mitigation.

The stratigraphic record shows that eruptive styles, volcanic intensity and mass-wasting processes have varied through time. Dome-style eruptions have dominated the past 1 Ma of volcanic activity at Montserrat. At the older edifice of Centre Hills, regular large-magnitude explosive eruptions (represented by >1m thick pumiceous sequences onshore) also occurred, but such explosive eruptions are rare at the younger Soufrière Hills-South Soufrière Hills volcanic complex.

Periods of heightened volcanic activity occurred between 1.1-0.9 Ma, 0.3 Ma, and 0.2-0.1 Ma. Another period of increased volcanism may have also occurred at ~0.5±0.2 Ma. These coincide with periods of increased, mass-wasting, identified at 1.1-0.9 Ma, 0.6-0.5 Ma, 0.3 Ma, and 0.2-0.1 Ma and suggest that increased volcanic activity may facilitate mass-wasting processes. This may be due to increased deposition of material on the island flanks, or increased seismic activity that can trigger collapses.

The ages of the largest landslide deposits (volumes >0.3 km^3) observed offshore of Montserrat also coincide with periods of faster sea-level rises. Analysing the global database, large landslides coincide with rapid sea-level rise at other island arc volcanoes, but not at ocean islands. The reason for this difference in behavior is unclear, but maybe associated with differences in island composition and size, or tectonic regimes.

Contents

List of Figures

Chapter 1

Chapter 2

Chapter 3:

Chapter 4:

Chapter 5:

List of Tables

Appendix

Declaration of Authorship

I, Maya Coussens, declare that this thesis entitled *The 1 Ma evolution of constructive and destructive processes at the island arc volcano of Montserrat* and the work presented within this thesis are the results of my own work.

I confirm that:

- The work was done wholly/ mainly whist in candidature for a research degree at the University of Southampton
- Where any part of this thesis has previously been submitted for a degree or any other qualification at this university or any other has been clearly stated
- Where I have consulted the published work of others is always clearly attributed
- I have clearly identified all quotations from the work of others, and have given the source. With the exception of quotations this thesis is entirely my own work.
- I have acknowledged all main sources of help
- Where the thesis is based on work done by myself jointly with others, I have made clear exactly what was done by others and what I have contributed myself
- Parts of this work has been published/ submitted to journals as:

Wall-Palmer, D., Coussens, M., Talling, P. J., Jutzeler, M., Cassidy, M., Marchant, I., *et al.,* (2014), Late Pleistocene stratigraphy of IODP Site U1396 and compiled chronology offshore of south and south west Montserrat, Lesser Antilles, *Geochemistry, Geophysics, Geosystems,* 15(7), 3000-3020

Coussens, M. F., Wall-Palmer, D., Talling, P. J., Watt, S. F. L., Hatter, S. J., Cassidy, M., *et al.,* (2016), Synthesis: stratigraphy and age control for IODP Sites U1394, U1395, and U1396 offshore Montserrat in the Lesser Antilles, *Proceedings of the IODP*, 340, 19

Coussens. M., Wall-Palmer. D., Talling. P. J., Watt. S. F. L., Cassidy. M., Jutzeler. M., Clare. M. A., Hunt. J. E., Manga. M., Gernon. T. M., Palmer. M. R., Hatter. S. J., Boudon. G., *et al.,* (Submitted), The relationship between eruptive activity, flank collapse and sea-level at volcanic islands: a long-term (>1 Ma) record offshore Montserrat, Lesser Antilles, *Geochemistry, Geophysics, Geosystems*

Coussens. M., Cassidy. M., Watt. S. F. L., Jutzeler. M., Talling. P. J., Barfod. D., Gernon. T. M., Taylor. R., Hatter. S. J., Palmer. M. R., and the MVO, (Submitted), A 1 Myr evolution of explosive volcanic activity: chronostratigraphy of the Centre Hills Volcano, Montserrat, *The Journal of Volcanology and Geothermal Research*

Signed

Date: 30/03/2016

ACKNOWLEDGEMENTS

I would like to thank my four supervisors Peter Talling, Sebastian Watt, Thomas Gernon, and Martin Palmer for their guidance, support, and supervision over the duration of my PhD. Pete, thank you for your vision, and encouragement over the past few years. You have been an endless source of creativity and you have taught me so much. Seb, the past few years have involved big and exciting changes for you and your family with the move to Birmingham and the arrival of both Ruben and Martha, but yet you have been ever-present and committed to my supervision. Thank you so much for all of your enthusiasm, for building my confidence, and also the time that you have invested in my research. Tom, thank you for always having an open office door for whenever I have been stuck. Thank you for your career advice and for encouraging me to be persistent. I shall miss the trips to Tenerife and your comparisons of lava to low-fat natural yogurt. Martin, thank you for all of our interesting tephra-related chats, and thank you for all of your advise on paper writing. You have all been fantastic supervisors, and I cannot thank you enough for all of the time you have spent reading numerous manuscripts and giving constructive feedback. Thank you for giving me this great opportunity.

I would also like to give special thanks to Michael Cassidy, Martin Jutzeler, Deborah Wall-Palmer and Rex Taylor. Mike, you have been so supportive and encouraging during my PhD, thank you so much for all of your help and advice, and thank you for helping me with my fieldwork on Montserrat. I have immensely enjoyed all of our volcanological conversations, including about the migration of pigs with Caribbean accents across Montserrat. Martin, I miss our random afternoon chats and watching your coffee cup collection grow. Thank you for all of your help and guidance over the past few years, particularly with using the Malvern and your constructive feedback on various manuscripts. I have learned a lot about physical volcanology and pumice rafts through our chats. Debbie, you have taught me everything I know about forams. Thank you for your endless patience whilst teaching me how to identify different foraminifera species. You have instilled a new appreciation for marine microfossils.

Rex, thank you for being my panel chair and for all of your help and advise in processing and interpreting geochemical and petrological data. Thank you for always having an open door for whenever I have had a question.

I would like to thank Mike Clare, and James Hunt for their statistical and sedimentological expertise. I enjoyed our conversations and experimenting with new techniques that you both introduced me to. I would also like to thank the MVO, in particular Adam Stinton and Rod Stewart for their support during fieldwork on Montserrat. Also, thank you to Eliza Calder and Paul Cole for interesting discussions on the subaerial stratigraphy of Montserrat, and to Michael Manga for suggesting improvements on manuscripts.

Suzanne MacLachlan, thank you for all of your help in BOSCORF, I am so sorry I managed to use so many plastic pots. Agnes Michalik, Bob and John, Ian Croudace also provided laboratory assistance in NOCS. Also thank you to Dan Barford and Jim Imlach for your help in the laboratories at SUERC and to Ben Buse and Stuart Kearnes at Bristol University.

I would also like to thank lots of the lovely friends I have made in Southampton. Thanks to Stuart Hatter, Holly Elliot, and Katie McFall for all of our volcano-related chats and also for our discussion on various lab techniques. Thank you also to Millie Watts and Meike Gfrarer for the regular use of your sofa/airbed to save me the long commute from Bexhill during lab-intensive periods, and also for even feeding me too!

Thanks to all of my friends in Bexhill and Hastings who have been so supportive and encouraging, particularly the ladies at Bexhill Rowing Club, and those of you at Emmanuel Church Hastings. Jess, Jany, Haz, Bethan, C, Mini Pepper, Abi, Charlie, Laura, and Alex you girls continually inspire me to keep going. Also, special thanks to my family, Mum, Dad, Mussie, Aunty Jas and to my in-laws Paul, Carole, Jean and Thomas. Paul, thanks for offering me a job in the yard when my funding ran out, and

Aunty Jas thank you for letting me stay whilst Jamie was in New Zealand for 3 months and cooking me lots of tasty curry.

Above all, thanks to God, and to my husband, Jamie Coussens. Jamie, thank you so much for all you do, for looking after me whilst I was writing up, and helping me through difficult parts of the PhD. It would have been immeasurably more difficult without you. And thanks to God, who has graciously given me so much, and who has sustained me throughout the duration of this PhD.

Chapter 1:

1. Introduction

1. Project Rationale

The aim of this PhD is to study the long–term (>1 Ma) evolution of volcanic and sedimentological processes at an island arc volcano. Eruption and mass-wasting events present a range of hazards at volcanoes. The nature of these hazards - including their magnitude, frequency and behaviour - can vary through the life cycle of a volcanic system. Single events can involve a variety of connected processes. For example, dome-forming eruptions may lead to instability and mass-wasting, with subsequent landslides that can generate tsunamis (Kokelaar, 2002; Edmonds and Herd, 2005; Trofimovs *et al*., 2008; Wadge *et al*., 2014). Furthermore, specific events, such as major edifice collapses, may change the subsequent nature of volcanism and mark important junctures in the development of a volcano (Longpré *et al*., 2009; Brown *et al*., 2014; Cassidy *et al*., 2015). To understand these relationships, and ultimately resolve the connections between long-term patterns in volcano behaviour and the short-term hazards presented by a volcano, it is necessary to document how volcanism and sedimentary processes evolve over long time scales. In this thesis, I take this approach for the island of Montserrat, combining >1 Ma of Montserrat's onshore and offshore stratigraphies (in the form of IODP drill cores) to develop one of the longest and most complete histories of an island arc volcano. Using this record this study aims to identify 1) how eruptive styles varied at Montserrat over the past 1 Ma, 2) when mass wasting events occurred, 3) what factors triggered mass wasting events, 4) how the frequency of volcanism and mass wasting varied through time 5) and how large landslides (volumes >0.3 km^3) were emplaced.

2. Introduction

Montserrat is arguably one of the world's best-studied island arc volcanoes (Figure 1). Soufrière Hills edifice, the only currently active centre on Montserrat, began erupting in 1995. Since then the island has been under near-continuous observation by the Montserrat Volcano Observatory (MVO). Alongside the continuous gas emission and seismological observations extensive work has been conducted on both the on and offshore deposits. Numerous eruptive and mass-wasting events have been identified, including seven large landslide deposits with estimated volumes between 0.3–20 km^3 (Figure 1)(Roobol and Smith 1998; Smith, 2007; Harford *et al*., 2002; Le Friant *et al*., 2004, 2008, 2010; 2015; Trofimovs *et al*., 2006, 2013; Cassidy *et al*., 2013, 2014; Watt *et al*., 2012a, 2012b; Crutchley *et al*., 2013; Karstens *et al*., 2013). Given the extensive work already conducted on the island of Montserrat, it is logical to extend the work on the island by studying Montserrat's earlier eruptive history.

Within this study, detailed onshore stratigraphic work (Chapter 2) is combined with the study of holes drilled from three International Ocean Drilling Program (IODP) sites (Chapters 3 and 4). The onshore deposits are a sequence of primary and reworked eruptive products. Detailed logging and chemical analysis of the subaerial deposits were used to compile a robust onshore stratigraphy.

Offshore, multiple holes were drilled at IODP Sites U1394, U1395 and U1396 during Expedition 340 in March 2012 (Figure 1). These Holes contain a suite of tephra–fall layers and deposits associated with mass-wasting and eruption events. At Site U1394 Holes extend to ~0.3 Ma, at Site U1395 Holes extend to >1 Ma and at Site U1396 Holes extend to >4 Ma, based on oxygen isotope and paleomagnetic dating. At Site U1394 a large landslide deposit, (Deposit 2) with an estimated volume of 8.4 km^3 is sampled and is one of the few large landslide deposits to be drilled.

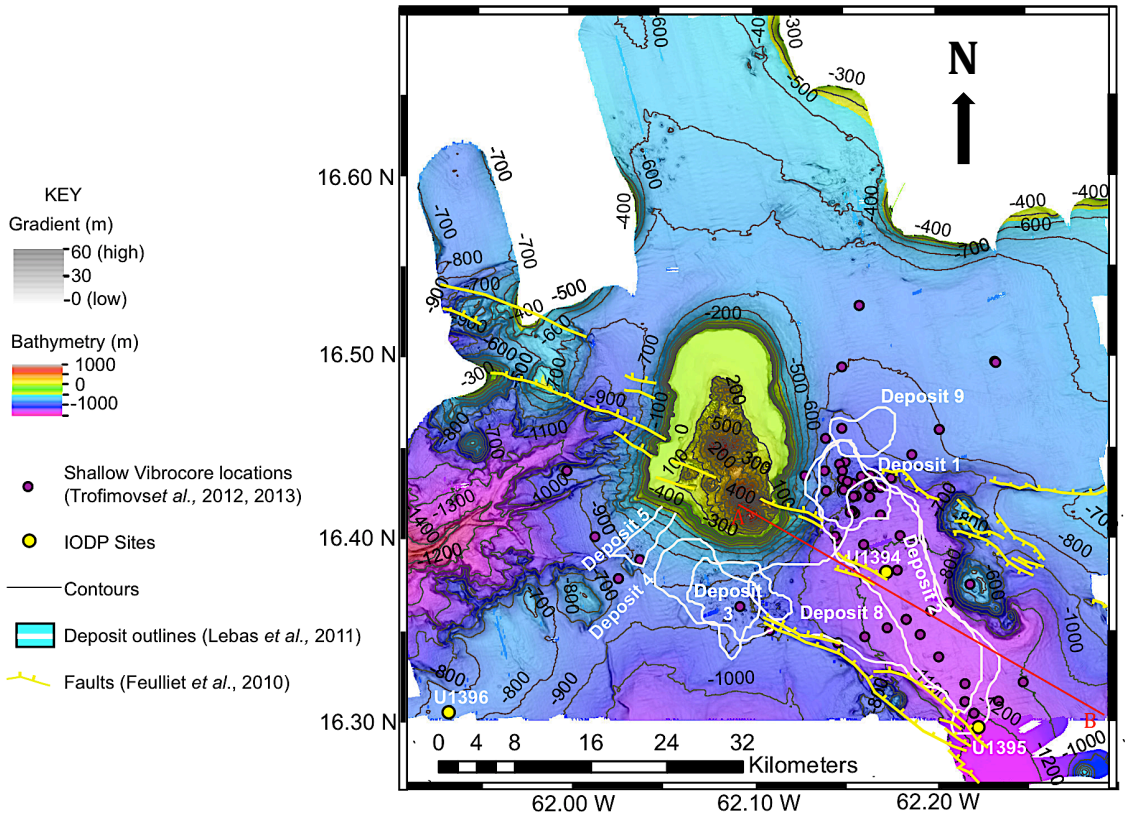

Figure 1: Topographic and bathymetric map of Montserrat and the surrounding sea floor. Also shown are the shallow vibrocore locations, the IODP drill Site locations, large landslide deposits identified using bathymetry and seismic studies, the Montserrat-Havers Fault system in yellow, and the seismic line AB used in figure 8.

Onshore deposits are more easily interpreted than offshore core sediments, as the deposits are not affected by interactions with the water column (Jutzeler *et al*., 2014, 2015). However, the onshore record is largely incomplete due to erosion. The marine cores are likely to be a more complete record of volcanic and mass wasting events (Figure 1). Here the onshore record is used to determine how eruptive styles have evolved through time (Chapter 2), but the more complete marine record is used to determine how the frequency of volcanic and mass wasting events change through time (Chapters 3 and 4).

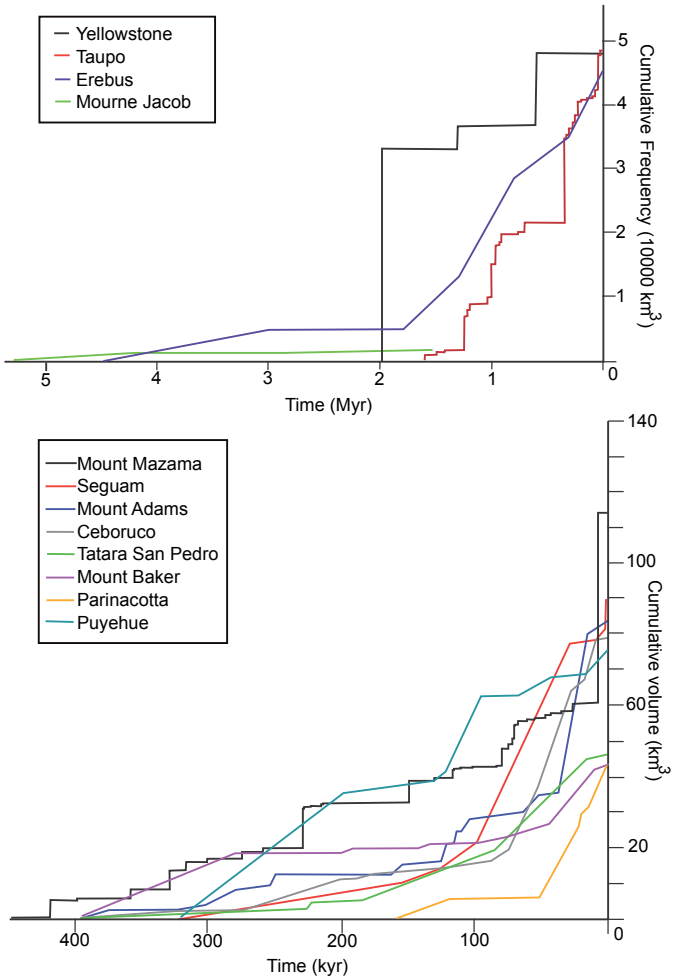

Figure 2: Adapted from Singer *et al.*, 2008 (Houghton *et al.* 1995; Bacon and Lanphere 2006; Singer *et al.* 2008; Germa *et al.* 2010), plotting time against cumulative volume of eruptive products.

Other studies of arc volcanoes such as Taupo and Santorini (Houghton, 1995; Druitt, 1989) show significant repose periods (Figure 2), variations in eruptive style and multiple mass-wasting events (Seta *et al.*, 2012; Yoshida *et al.*, 2012). However, most studies have primarily been conducted using only the subaerial deposits (Houghton, 1995; Druitt 1989), short lacustrine/ marine cores that extend <100 ka (Narcisi, 1996; Wulf *et al.*, 2002, 2004; Wutke *et al.*, 2015), or long (>12 Ma) distal cores that sample tephra from multiple volcanoes (Keller *et al.*, 1978; Carter *et al.*, 2004; Alloway *et al.*, 2005) (Figure 1). This is one of the few studies that attempts to sample a long (>1 Ma) record of both eruptive and mass-wasting deposits from a single volcanic island and will give valuable insight into how island arc volcanoes evolve.

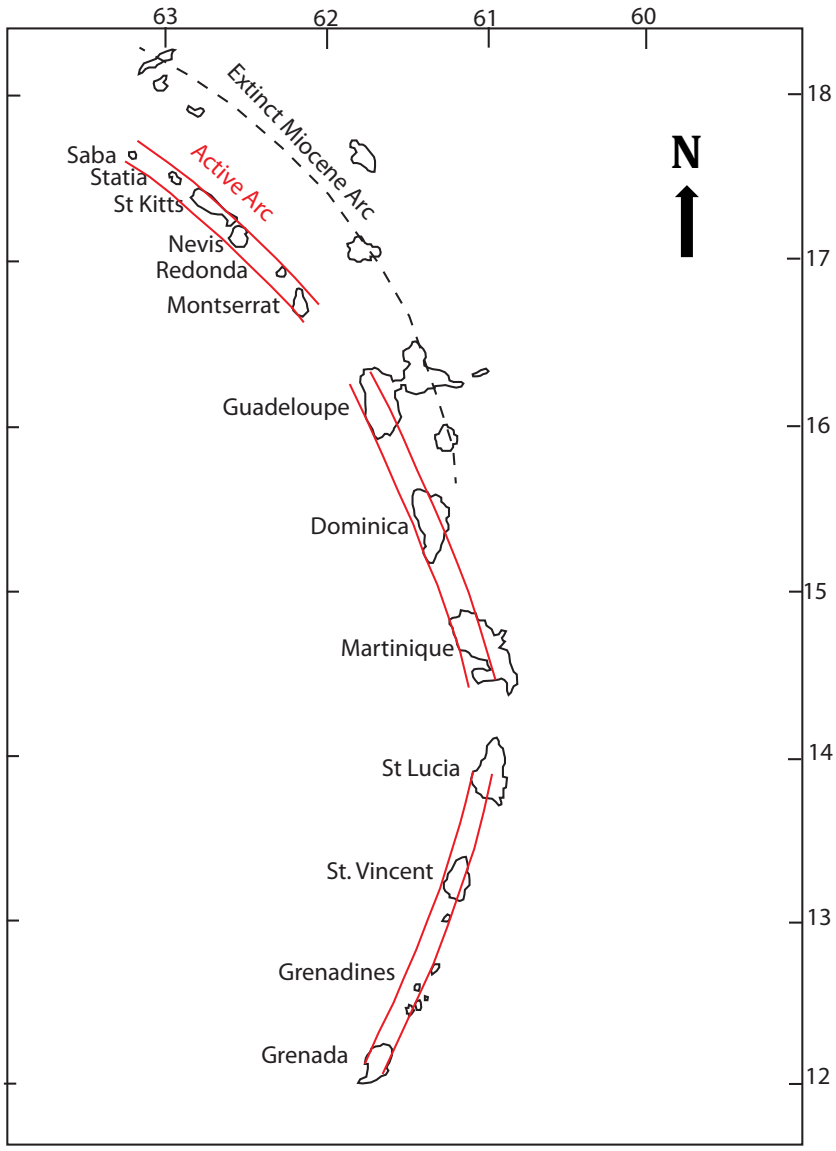

Figure 3: Map showing the location of the currently active island arc (in red), the extinct Miocene arc (dashed line), and also each of the arc segments. Latitude and longitude in degrees north and degrees west are given.

3. Geological setting

Montserrat is one of the volcanically active islands that form the 750 km long Lesser Antilles Island Arc. The island arc is created by the westward subduction of the North American plate (dipping at ~60°) beneath the Caribbean plate at a convergence rate of ~2 cm/yr (Wadge and Shepherd, 1984; Pindell and Barrett, 1990). The Lesser Antilles Arc is bifurcated from Martinique northwards (Figure 3), with a younger western arc comprising active volcanoes. The islands that form the eastern arc are older and are made up of extinct volcanoes largely covered by limestones and coral reefs; these islands are referred to as the Limestone Caribbees. The westward shift of volcanism occurred during the Miocene and has been attributed to the subduction of a buoyant aseismic ridge (Bouysse and Westercamp, 1990).

The Lesser Antilles arc has a broad, curved shape. In the north the arc strikes NNE, but in the south the arc strikes NNW (Wadge & Shepherd, 1984). The change in strike occurs at ~12° N, and is attributed to either the subducting plate being torn or to two separate plates being subducted with different vectors (Wadge and Shepherd, 1984). There are three distinct volcanic sections defined by the strike of the arc: from Saba to Montserrat, from Guadeloupe to Martinique, and from St Lucia to Grenada (Figure 3).

The Island of Montserrat is located within the northern volcanic chain and is made up from 3 main volcanic centres (Figure 4) called Silver Hills, Centre Hills, and the Soufrière Hills–South Soufrière Hills volcanic complex. Based on limited Ar–Ar dating of subaerial volcanic products, Silver Hills is thought to have been active between 1020–2580 ka, Centre Hills between 550–950 ka, and the Soufrière Hills has been active since 290 ka (Harford *et al*., 2002; Brown and Davidson *et al*., 2008). The Soufrière Hills–South Soufrière Hills volcanic complex comprises two main edifices, the northern Soufrière Hills edifice and the more southerly-located South Soufrière Hills edifice. No two volcanic centres are thought to have been active at any one time (Harford *et al*., 2002).

Volcanic activity has generally migrated southwards through time on Montserrat. This is also observed on Guadeloupe (Sampler *et al*., 2007) and suggests that the southwards migration of volcanism may be related to the movement of the Caribbean plate.

To the southeast of Montserrat is the Boulliant-Montserrat Graben (Figure 1). This is a major depositional basin where many of the recent deposits have been directed (Trofimovs *et al*., 2006). The graben is bounded by faults that are part of the extensive Montserrat-Havers fault system (Feulliet *et al*., 2010) and also the Kahouanne sea mounts in the north. This fault system is also expressed onshore on Montserrat where many of the Soufrière Hills Volcano lava domes are aligned along this fault system (Figures 1 and 4).

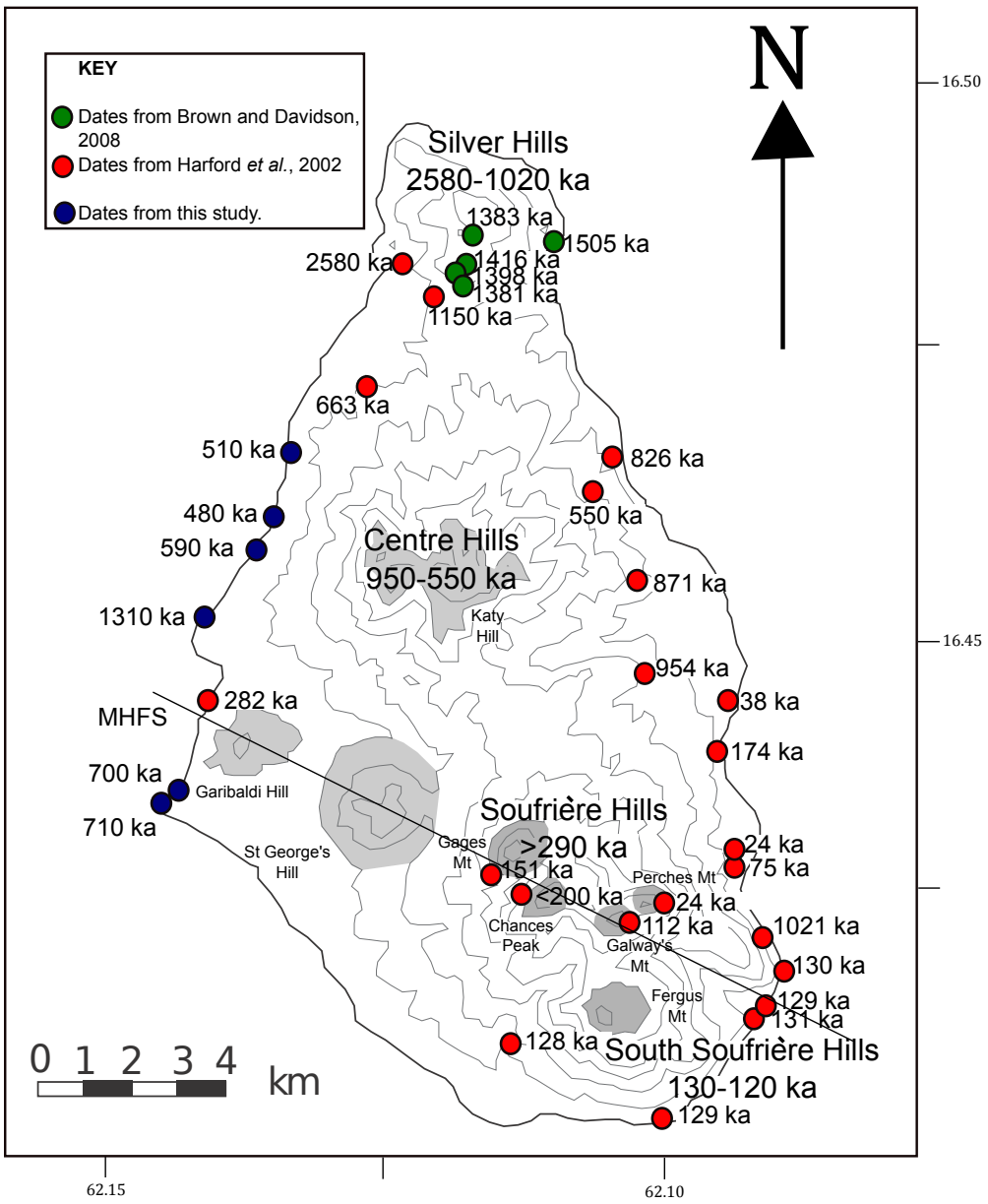

Figure 4: Ar–Ar dates and locations from the literature. Red circles are from Harford *et al.* (2002), green circles from Brown and Davidson, (2008). Also shown by grey shading are hill locations and the approximate location of the Montserrat-Havers Fault System (MHFS).

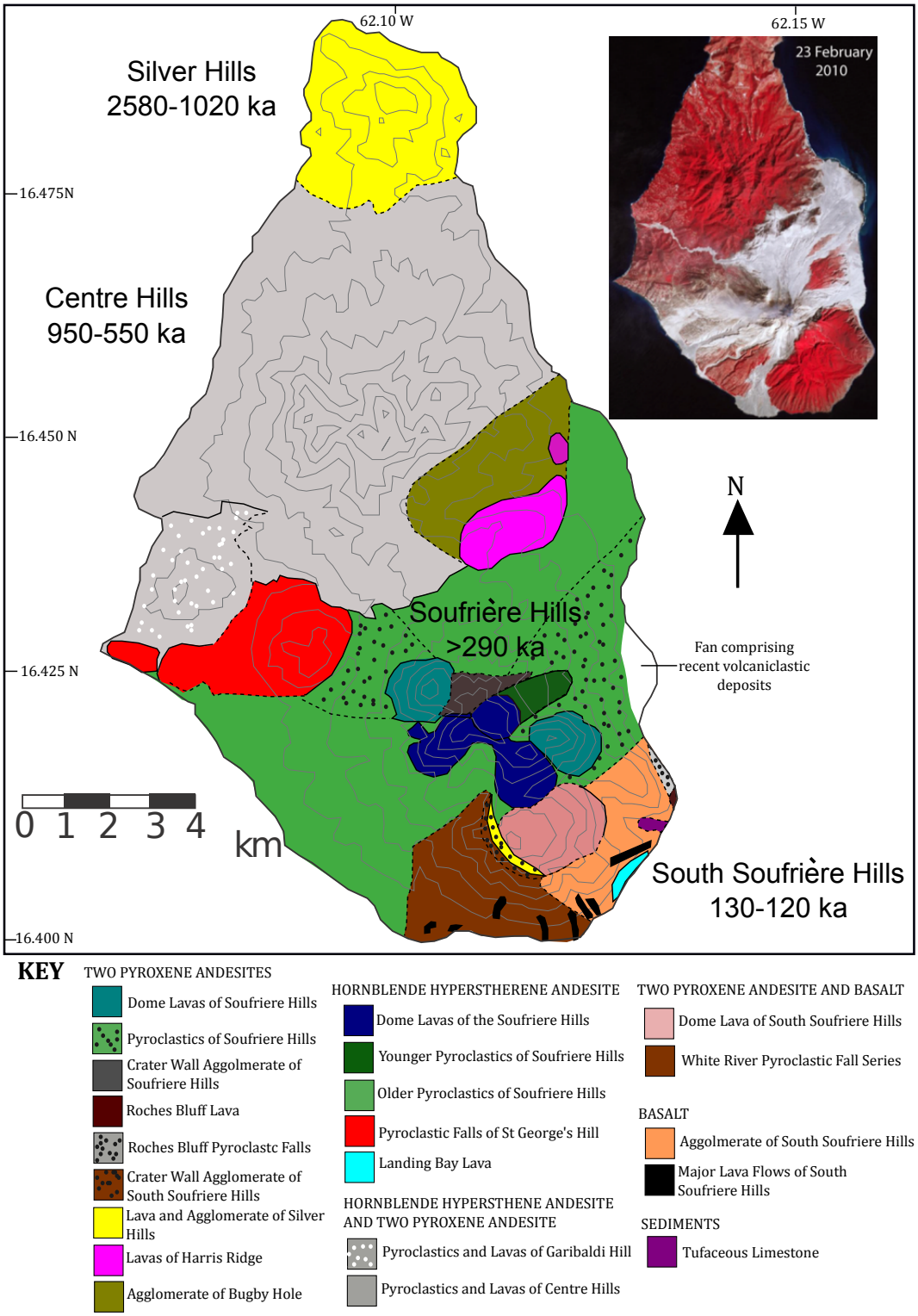

Figure 5: Geological map adapted from Rea *et al.* (1975). This figure shows the stratigraphy prior to the recent eruption. Inset is a false colour satellite image (red represents vegetation, grey volcanic deposits) and shows the distribution of recent eruptive deposits (Wadge *et al.,* 2014) (Envisat image, copyrighted by the European Space Agency).

4. Previous Work

4.1 Historical activity

Soufrière Hills has been erupting since 1995 and has led to widespread disruption on the island (Sparks and Young, 2002). The on-going eruption has been characterised by alternating periods of relative quiescence and active dome extrusion, accompanied by dome collapse events ranging in scale from a few cubic meters up to 0.2 km^3 (Sparks and Young, 2002; Kokelaar, 2002; Trofimovs *et al*., 2006; Le Friant *et al*., 2008, 2010; Wadge *et al*., 2014). Dome collapses can be large and occur with little warning (IDC 1997). In 2003 the largest recorded collapse involved 210 x 10^6 m^3 of material and generated a 0.5 m high tsunami along Guadeloupe's coast (Trofimovs *et al*., 2012).

Frequent vulcanian explosions occurred as well as pauses in activity that range from a few months to a year (Figure 6) (Kokelaar, 2002, Wadge *et al*., 2014). Eruptive activity has paused since 2010, but ground deformation and regular rock falls are observed (Wadge *et al.,* 2014). It is uncertain whether the pause signifies the end of the eruption or if activity will continue after this uncharacteristically long pause. Prior to the current eruption, the only previous documented activity were small ash-producing, explosions in the 1660s (Young *et al*., 1998; Harford *et al*., 2002; Le Friant *et al*., 2008).

The current eruption can be subdivided into 5 main phases and is summarised in figure 6. Phase 1 occurred between November 1995– March 1998. Dome building was initiated after a 4 month precursory phreatic episode. The first pyroclastic density currents (PDCs) began in March 1996 (Cole *et al*., 1998, 2002; Wadge *et al*., 2014). Dome morphology was highly variable with spines, whalebacks, shear lobes and pancakes (Watts *et al*., 2002). Vulcanian eruptions were frequent and on 17th September 1996 a large vulcanian eruption destroyed 35% of the lava dome. Three major collapses occurred in September, November and on the 26th December 1997 (Sparks *et al*., 2002; Voight *et al*., 2002; Sparks and Young *et al*., 2002) followed by an 18 month pause in lava extrusion followed that marked the

end of Phase 1. Surface activity (seismic swarms, ash venting, and small explosions) continued, and increased after the July 1998 dome collapse (Norton *et al*., 2002) and during the run up to the initiation of Phase 2.

Phase 2 Occurred between November 1999– July 2003 and involved near–continuous lava extrusion with only two short breaks of 68 days (March–May 2001) and 48 days (June–July 2002). Two large collapses occurred on the 3rd July and 20th March 2002, and 12th July 2003 (Carn *et al.,* 2004; Norton *et al*., 2002; Herd *et al*., 2005). The July 2003 collapse involved 210 X 10^6 m^3 of material, and is the largest collapse observed on Montserrat to date, and may be the largest historical dome collapse world wide (Herd *et al*, 2005). The collapse event ended with 5 vulcanian explosions that occurred at progressively longer intervals, during 12–15th July 2003. The large dome collapse marks the end of Phase 2, but earthquake swarms, ash venting events and PDCs regularly occurred between phases 2 and 3 (Wadge *et al*., 2014).

Phase 3 occurred between August 2005- April 2007 after a 3.5 month phreatic precursory phase along a NW-oriented fracture (Cole *et al*., 2014a). This phase of activity is marked by a paucity in the occurrence of explosive pulses when compared to earlier phases (Wadge *et al*., 2014). Initial dome growth was low–rate (<1 m^3s^{-1}) and asymmetric (towards the northwest). In November 2005 extrusion rate quadrupled (Ryan *et al*., 2010) and gradually increased. Dome growth direction and morphology regularly changed, in May 2006 a large collapse (97 x 10^6 m^3) occurred and lasted just 3 h (Trofimovs *et al*., 2012). This was followed by 2 eruptions that released 0.2 Tg (1 Tg= 1 x 10^{12} g) of suphur dioxide and produced a 20 km high eruption column and was the largest such event observed in the current eruption (Carn and Prata, 2010). Lava extrusion resumed 8 h after the collapse event. To the north and west of the dome two vents producing high–pressure gas had formed by August 2006, with endogenous dome grown continuing in the northeast and southwest. On the 8th January 2007 an explosion and collapse on the northwest sector of the dome occurred. Dome growth gradually diminished and had largely ceased by April 2007 (Ryan *et al*., 2010). Little surface activity occurred after cessation of dome growth, but the

Gages Wall vent continuously produced gas, sometimes at high-pressures (Cole *et al*., 2014a).

Phase 4 occurred between July 2008– January 2009. This period of dome growth was short and explosive when compared to earlier phases of growth. Dome extrusion began following an increase in volcanic tremors, ash venting and several small explosions from the Gages Wall vent (Cole *et al*., 2014a) between May–July 2008. On the 29th July 2008 an explosion from the Gages Wall vent produced a 12 km high column, following a period of increased surface activity. Dome extrusion was observed from August 2008 and on the 14th August 2008 an explosion occurred, followed by a collapse on the 25th August 2008 (Wadge *et al*., 2014). Between September to December little surface activity was detected. On the 3rd December 2008 a small dome collapse and PDC occurred and marked the start of increased seismicity. This was followed by renewed dome growth on the 10th December 2008 (Komorowski *et al*., 2010). Two pumice–producing explosions on the 11th January 2009 mark the end of Phase 4, and produced 11 km high eruption columns (Komorowski *et al*., 2010).

Phase 5 occurred between October 2009– February 2010 (Wadge *et al*., 2014). Activity began following intense seismic activity (24 VT earthquakes in 1 h) and 13 explosive episodes that produced plumes up to 6 km and minor PDCs (Cole *et al*., 2014a; Wadge *et al*., 2014). Extrusion was primarily focussed on the southwest sector from October to November. Activity decreased in November, but increased after a series of hybrid and VT earthquakes. Renewed extrusion was accompanied by a shift of the extrusion locus to the northeast. Throughout phase 5 sub-daily cycles of surface activity and seismicity were observable (Wadge *et al*., 2014). Activity shifted northwest and was followed on the 8th of January 2010 by the largest magnitude (2.7 km^3 DRE (dense rock equivalent) Vulcanian explosion of the eruption so far. Further Vulcanian eruptions occurred on the 10th and 11th January and the 5th February 2010. Dome extrusion was terminated by a large collapse on 11th February 2010 to the north of the volcano and involved 40 X 10^6 m^3 of material (Stinton *et al*., 2014b). These collapses occurred when the dome was at it's highest (1150 masl) and was followed by two

Vulcanian explosions producing 15 km high plumes (Wadge *et al.*, 2014). Post phase 5 activity has involved several ash explosions in June–July 2010, and continued fumerolic activity (Wadge *et al.*, 2014).

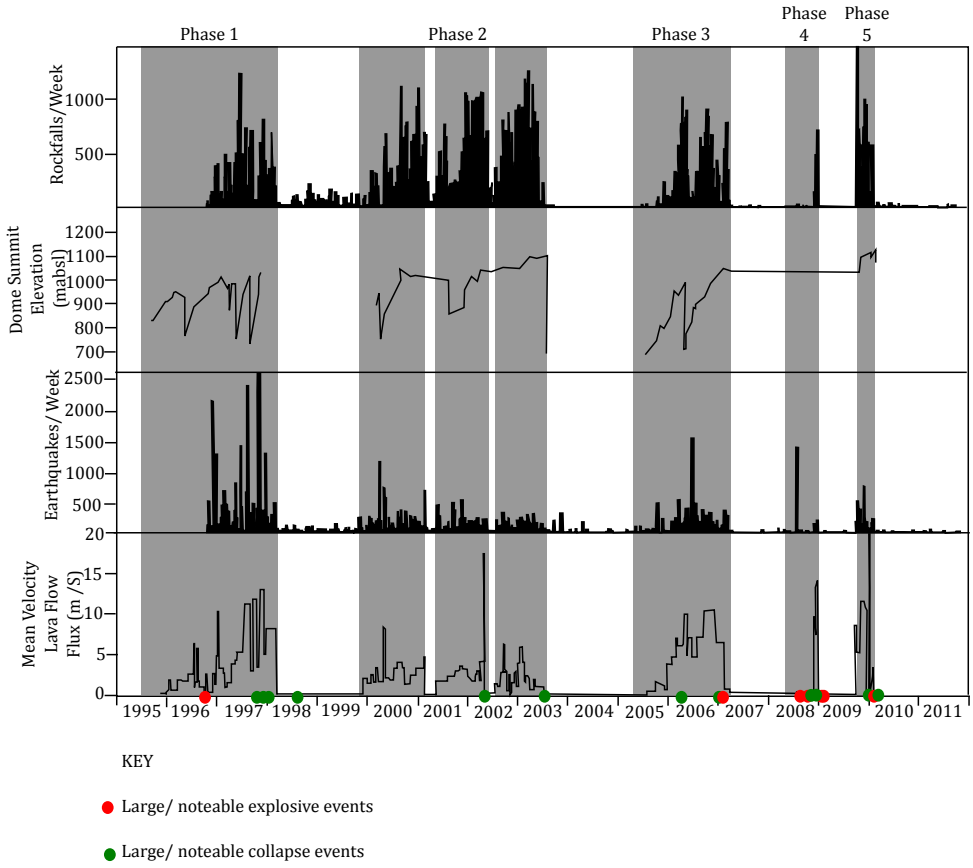

Figure 6: Figure adapted from Odbert *et al.*, 2014 and Wadge *et al.*, 2014 summarising the recent eruption of the Soufrière Hills Volcano. The figure summarises dome growth (lava flux and dome summit elevation), seismicity (earthquakes/week), and collapse events (rock falls, and large collapses shown in green).

4.2 Pre–Historical Activity

Earlier activity of Montserrat is little studied. Much of the onshore work conducted by Roobol and Smith. (1998) and Smith (2007) focused on pre–1995 eruption deposits from Soufrière Hills. Scant observations of Centre Hills and the Silver Hills subaerial stratigraphy exist within the literature (Harford *et al.*, 2002; Brown and Davidson *et al.*, 2008). Offshore, a series of shallow (<10 m)

vibrocores have been analysed (Le Friant *et al.*, 2008; Cassidy et al., 2013, 2014; Trofimovs *et al.*, 2013) (Figure 1); however, these cores are too shallow to sample the deeper buried deposits from Centre and Silver Hills.

The volcanic activity of Silver Hills is little known as the edifice is highly eroded and only the more resilient lava dome material is preserved (dated at ~1–2 Ma (Harford *et al.*, 2002; Brown and Davidson, 2008)). However, some small, isolated pumiceous deposits are preserved on–shore (Stuart Hatter personal communication), suggesting that there were explosive eruptions at Silver Hills. To the north, a mass flow deposit extending 10 km offshore can be observed and is visible in seismic reflection profiles (Kenedi *et al.*, 2010), suggesting large collapse events occurred at Silver Hills.

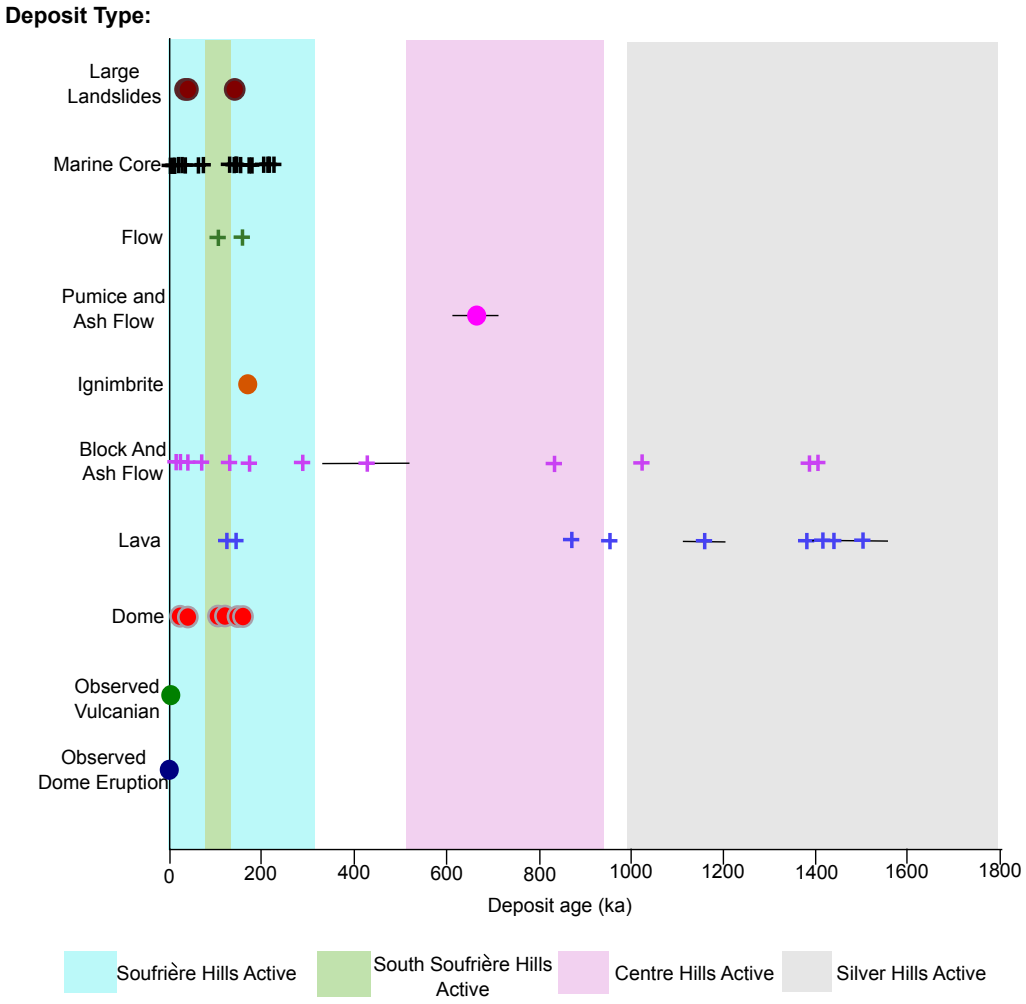

Figure 7: Review of dated event deposits from the literature. Periods of activity are based on Ar–Ar age ranges available prior to this thesis.

Onshore Centre Hills is composed of a series of lava domes and block and ash flow deposits with thick (>1 m) pumiceous sequences (Harford *et al*., 2002). This suggests that Centre Hills eruptions varied between dome building events and more sustained explosive eruptions. Onshore volcanic activity has been dated at 954–559 ka based on Ar–Ar dating of andesite lava domes (Harford *et al*., 2002). In the offshore record several large debris avalanche deposits can be observed in swath bathymetry data and seismic reflection profiles: these were previously named as Deposit 9 (954–550 ka), Deposit 4, and Deposit 8 (900 ka) (Lebas *et al*., 2011; Watt *et al*., 2012a, 2012b) (Figure 1). Deposit 8 is the largest flow deposit observed offshore of Montserrat (20 km^3). It has a run out of 31 km and covers 277 km^2 (Lebas *et al*., 2011).

The early activity of the Soufrière Hills Volcanic complex is little known. The oldest deposits dated within this age period are from Garibaldi Hill dome (Figure 4) at 282±8 ka (Harford *et al*., 2002; Le Friant *et al*., 2008). Several primary and reworked block and ash flows, PDC's and tephra fall sequences are observed and are separated by unconformities and paleosols (Smith, 2007) (Figure 5). Further eruptive and collapse events have been identified in marine cores from ~250 ka untill present (Le Friant *et al*., 2008; Cassidy *et al*., 2013, 2014; Trofimovs *et al*., 2013) and are largely represented by turbidites. Between 175–130 ka thick sequences of ignimbrites are found onshore, suggesting a period of large magnitude explosive eruptions (Smith, 2007).

A large collapse deposit (Deposit 2) dated at ~130 ka (Le Friant *et al*., 2004; Lebas *et al*., 2011a) has been associated with the end of the first phase of Soufrière Hills activity (Cassidy *et al.*, 2015). The deposit has a volume of ~8.4 km^3 and extends 30 km offshore covering an area of 190 km^2 (Watt *et al*., 2012a, 2012b). After the emplacement of Deposit 2, activity migrated to the South Soufrière Hills, (the southern most edifice of the Soufrière Hills volcanic colmplex) between ~131–128 ka (Smith, 2007; Cassidy *et al*., 2015). The shift in eruptive centre brought about a significant change in composition of eruptive deposits, from andesitic deposits to basaltic deposits (Cassidy *et al*., 2015).

Activity moved back to the Soufrière Hills edifice after the South Soufrière Hills episode, with the earliest dated deposits of the second stage of Soufrière Hills volcanism at 112± 9 ka, from Galway's Mt (dome) (Figure 4)(Harford *et al*., 2002). The onshore and offshore stratigraphic records comprise a series of andesitic lithic breccias, tuffs, thin pumiceous deposits and turbidites. The second stage of activity appears to be similar to earlier activity at Soufrière Hills.

Offshore there are three large landslide deposits that lie near the surface, and are hence interpreted to be of relatively young (likely Soufrière Hills) age, named Deposits 1, 3, and 5 (Deplus *et al*., 2001; La Friant *et al*., 2004; Lebas *et al*., 2011; Watt *et al*., 2012a, 2012b; Cassidy *et al*., 2014) (Figure 1). These large landslide deposits are identified as large hummocky deposits in bathymetry and low seismic amplitude, chaotic facies in seismic sections (Deplus *et al*., 2001; Le Friant *et al*., 2004; Watt *et al*., 2012a, 2012b). Deposit 1 has an estimated volume of ~0.5 km^3 and covers an area of 25 km^2 to the southeast of Montserrat and may be associated with the formation of the English's crater collapse scar at ~4 ka (Le Friant *et al*., 2004). Deposit 3 has an estimated volume of ~0.9 km^3 and is deposited on the near surface covering an area of ~45 km^2 (Le Friant *et al*., 2004) to the south of Montserrat. Deposit 3 has been correlated with volcaniclastic turbidites found in vibrocores to the southwest of Montserrat, a sequence of onshore lava flows from South Soufrière Hills and may be related to a collapse structure in the island shelf (Le Friant *et al*., 2004; Cassidy *et al*., 2014). Deposit 5 is dated at 8–12 ka with a volume of 0.3 km^3, and lies to the southwest of Montserrat (Le Friant *et al*., 2004; Lebas *et al*., 2011; Cassidy *et al*., 2013).

4.3 Chemistry, Mineralogy, and the Soufrière Hills plumbing structure

The whole rock, mineral, glass and volatile contents of magmas from the recent eruption of Soufrière Hills are well studied (Barclay *et al*., 1998; Devine *et al*., 1998, 2003; Rutherford *et al*., 2003; Humphreys *et al*., 2009a, 2009b, 2013; Christopher *et al*., 2014). However, there are only a few analyses of earlier Soufrière Hills deposits or eruptive products from the extinct edifices of Centre Hills and Silver Hills (Harford *et al*., 2002; Devine *et al*., 2003; Cassidy *et al*.,

2013). Based on these limited observations, deposits from Montserrat have largely been homogenous, with SiO_2 contents varying from 55–64 wt % over the past ~2.6 Ma (Harford *et al*., 2002; Zellmer *et al*., 2003a; Cassidy *et al*., 2013). The bulk of eruptive products were two pyroxene andesites. However, at ~112 ka there was a shift in the mineralogy from a hypersthene-augite andesitic assemblage to hypersthene-hornblende andesite.

In the eruptive products from the recent Soufrière Hills eruption abundant (2–12%) mafic enclaves (48–53 wt% SiO_2) can be identified and range in size from a few millimetres to decimeters in scale (Humphreys *et al*., 2009a, 2009b; Plail *et al*., 2014). Enclaves can be divided into glassy and crystalline types (Plail *et al*., 2014), and are observed in deposits from at least the past 24 ka. Temperature estimates using a clinopyroxene-orthopyrxene thermometer suggest magmas forming enclaves were between 1070–1196°C (Christopher *et al*., 2014).

Petrological studies from select units over the last ~151 ka suggest eruption deposits are derived from long-lived magmatic bodies. Estimates using a variety of geothermometers (QUILF orthopyroxene, clinopyroxene-orthopyroxene, plagioclase-liquid, hornblende-plagioclase, and clinopyroxene-melt) suggest magma resides at upper crustal pressures at temperatures of 810-880°C (Barclay *et al*.,1998; Murphy *et al*., 1998, 2000; Christopher *et al*., 2014), and is within the amphibole stability field (Barclay *et al*., 1998). Sr and Ba zonation in plagioclase phenocrysts from the recent eruption deposits suggest that the present magma body has been residing for ~320 yrs (Zellmer *et al*., 2003b). This is supported by observations of lower gas compositions in the initial deposits from the Soufrière Hills eruption (Barclay *et al*., 1998). Magmatic residence times of between 10-1200 years are estimated for other studied eruptive deposits (Zellmer *et al*., 2003b).

Phenocrysts from the recent eruptive deposits often have high-temperature overgrowths (870-1040°C), and are indicative of late heating of the magmatic reservoir. The lack of Ti diffusion gradients in high-temperature rims on Fe-Ti

oxides suggests that heating of the magmatic reservoir occurred shortly prior to eruption (time scale of days) (Rutherford *et al*., 2003). The abundant mafic enclaves (particularly the glassy enclaves) may represent the intrusion of a hotter magma into the shallow-level magma storage region causing reservoir heating and potentially inducing an eruption (Barclay *et al*., 1998, 2010; Devine *et al*., 1998, 2003; Humphreys *et al*., 2009a, 2009b; Christopher *et al*., 2014). This model is supported by geophysical evidence (seismic and ground deformation) that suggests there is a magmatic body at 5 km that is periodically recharged from a second body at 12 km depth (Elsworth *et al*., 2008).

4.4 Stratigraphy

4.4.1 Note on terminology

Montserrat is prone to a range of collapse events. We use the term *dome collapse* to refer to collapses of the lava dome, *shelf collapses* describes only the collapses of the carbonate shelf that surrounds Montserrat, and *flank collapses* describe collapse events that can incorporate a combination of dome, flank and carbonate shelf material. Flank collapses may be very large events, incorporating >1 km^3 of material. We use the term *mass-wasting events* or *landslides* to collectively refer to all types of collapse.

Mass-wasting events can result in a wide range of events and deposits. *Debris avalanche* refers to a mass transportation down slope of volcaniclastic material (hot and/ or cold) (lava blocks, ash etc), and *debris avalanche deposit* refers to the blocky, poorly sorted deposits produced at proximal locations (e.g. Trofimovs *et al*., 2006). At more distal locations turbidity currents may develop resulting in a range of turbidites. We use the term *turbidity current* for both fully turbulent and non-turbulent flows and *turbidites* to refer to their resultant deposits.

4.4.2 Event types

Three different types of event dominate the stratigraphy on Montserrat: dome eruptions, explosive eruptions, and mass–wasting events. The different event types and the deposits produced are summarised in figure 8. Dome eruptions are

made up of effusive dome emplacement events followed by dome collapses as the growing dome destabilises. The collapse of hot dome material results in rock falls or debris avalanches that often develop into pyroclastic density currents (PDC) (Loughlin *et al*., 2002; Sparks and Young, 2002). Dome collapses can range in scale from a few cubic metres to a tenth of a cubic kilometre. Dome eruptions can last for several years (e.g. the current eruption) and ancient dome eruptions are represented in the stratigraphy as packages of multiple collapse events (Figure 8).

On Montserrat both smaller magnitude explosions (Vulcanian) and larger magnitude explosions (Plinian) have been identified (Harford *et al*., 2002; Kokelaar *et al*., 2002; Wadge *et al*., 2014). Eruption plumes from explosive activity can extend up to tens of kilometers in height and often reach the stratosphere. Tephra fall out from the eruption plume forms blanketing layers of tephra fall deposits, and destabilisation of the eruption plume may result in the development of PDC's that extend radially from the volcanic edifice. In the offshore record PDCs are likely to be represented as a sequence of debris avalanche deposits and volcaniclastic turbidites (Trofimovs *et al*., 2006).

Mass-wasting events can involve up to several kilometres cubed of material. In the offshore stratigraphy, smaller dome collapse events are more likely to be monogenetic volcaniclastic deposits, whereas larger flank collapse events are more likely to be made up of a mix of bioclastic, juvenile and recycled volcanic material that are deposited as a range of density flow deposits (Lebas *et al*. 2011; Watt *et al*., 2012a). Figure 8 summarises the processes and the resultant deposits on Montserrat.

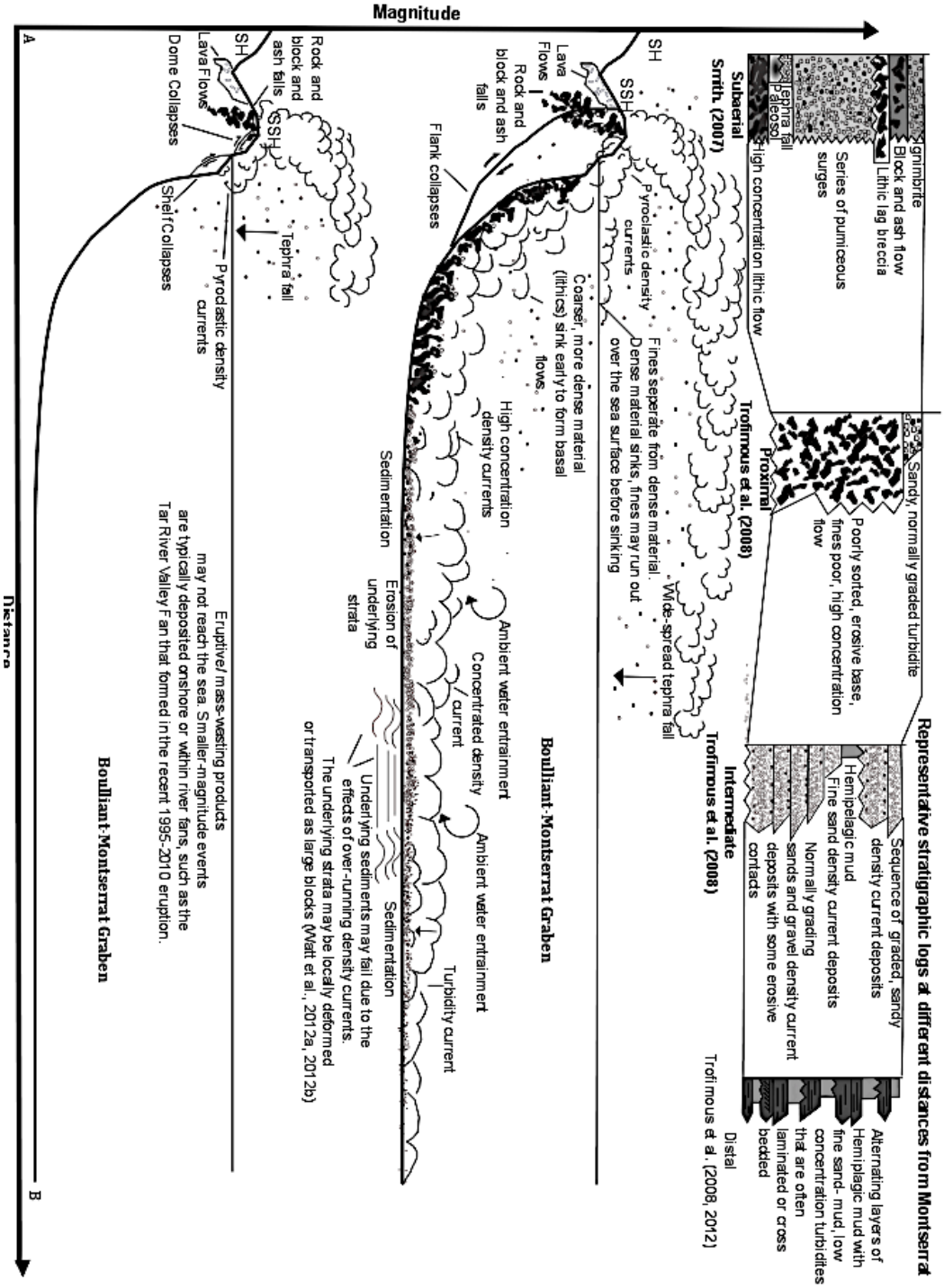

Figure 8: Summary of the processes and resultant deposits that occur on Montserrat. Topography is 2.5 vertical exaggeration of line AB on figure 1. SH is Soufrière Hills and SSH is South Soufrière Hills.

5. Summary and aims

The past 250 ka of Montserrat's volcanic history (i.e. the Soufrière Hills period) has been relatively well studied. The stratigraphy records multiple dome-forming eruptions and mass–wasting events. Some of these mass wasting events can be very large with volumes of >8 km^3 (Watt *et al.*, 2012a, 2012b). In this thesis I extend this record to >1 Ma using both onshore and offshore deposits to form one of the longest records and most comprehensive studies of the volcanic history of an island arc volcano. Chapter 2 describes the past >1 Ma of onshore stratigraphy (principally focussing on the little studied Centre Hills volcano), and describes how eruption styles have varied at Montserrat. Chapter 3 uses the stratigraphic record in Hole U1395B to identify and discuss processes that may trigger mass-wasting events (e.g. periods of elevated volcanism, sea–level change). Chapter 4 combines both the onshore–and offshore stratigraphies to form a detailed >1 Ma history of Montserrat. This compiled stratigraphy is then used to determine how the frequency, magnitude, and styles of volcanism and mass wasting evolve through time.

Chapters 2–4 are in paper style format; therefore, relevant methods are contained within each chapter. Below, each chapter is outlined briefly, highlighting the key questions that are addressed.

Chapter 2– A 1 Ma evolution of explosive volcanic activity: chronostratigraphy of the Centre Hills Volcano, Montserrat.

This chapter describes the past >1 Ma of onshore stratigraphy of Montserrat. The chapter presents new data from the Centre Hills volcano and summarises the stratigraphy of Soufrière Hills to evaluate how eruptions have changed. Key question addressed:

Qu 2.1: How does the eruptive style of Montserrat change over the past 1 Ma, and is activity at the Soufrière Hills and Centre Hills significantly different?

This chapter is based on a submission to The Journal of Volcanology and Geothermal Research.

Chapter 3– The relationship between eruptive activity, flank collapse and sea–level at volcanic islands: a long–term (>1 Ma) record offshore Montserrat, Lesser Antilles.

This chapter describes the offshore stratigraphy preserved within Hole U1395B. This Hole provides the most complete record of both mass–wasting and volcanic events of all studied IODP and onshore sites. This core is used to investigate the following key questions:

Qu 3.1: How does the submarine record at Site U1395 record volcanic activity at Montserrat?

Qu 3.2: Are mass–wasting events distributed evenly through time, or do events cluster?

Qu 3.3: What triggers mass wasting events, and do volcanism and sea–level changes facilitate mass wasting events?

This chapter is currently under review for publication in Geology, Geochemistry and Geophysics.

Chapter 4: The long–term evolution of construction and destruction processes at an island arc volcano: a 1 Ma long integrated stratigraphy for Montserrat.

This chapter aims to develop an integrated stratigraphy for Montserrat, combining the onshore and offshore stratigraphies. This includes observations from the subaerial stratigraphy (Chapter 2), the extensive shallow core data set (Le Friant *et al*., 2008; Trofimovs *et al*., 2013; Cassidy *et al*., 2013; 2014a), IODP Site U1395B (Chapter 3) and two further IODP Sites U1394 and U1396. Using this stratigraphic framework we build on the observations of Chapters 2 and 3 to determine how volcanism and mass–wasting processes have evolved on Montserrat over the past 1 Ma. We attempt to answer the following questions:

Qu 4.1: Has eruptive styles and eruptive frequency varied on Montserrat and is there a pause in volcanism during migration of activity from Centre Hills to Soufrière Hills?

Qu 4.2 Do other marine sites (IODP Sites U1394 and U1396) show similar variations in mass–wasting composition and frequency to U1395, and does mass–wasting coincide with periods of more intense volcanism?
4.3: What comprises the large landslide, Deposit 2, and what are the emplacement mechanisms?
This chapter is partly based on a data synopsis that has been accepted by IODP for publication, however further work and since been conducted and is included within this chapter.
(http://publications.iodp.org/proceedings/340/204/204_.htm). This data synopsis also forms the basis of a manuscript in preparation.

6. References

Alloway, B. V., Pillans, B. J., Carter, L., Naish, T. R., and Westgate, J. A. (2005), Onshore–offshore correlation of Pleistocene rhyolitic eruptions from New Zealand: implications for TVZ eruptive history and paleoenvironmental construction, *Quaternary Science Reviews*, 24(14), 1601–1622

Bacon, C. R. and Lanphere, M. (2006), Eruptive history and geochronology of Mount Mazama and the Crater Lake region, Oregon, *Geological Society of America Bulletin*, 118(11–12), 1331–1359

Barclay. J., Rutherford, M. J. and Caroll, M. R, (1998), Experimental phase equilibria. Constraints on pre−eruptive storage conditions of the Soufrière Hills magma, *Geophysical Research Letters*, 25, 3437–3440

Barclay, J., Herd, R. A., Edwards, B. R., Christopher, T., Kiddle, E. J., Plail, M. and Donovan, A. (2010), Caught in the act: Implications for the increasing abundance of mafic enclaves during the recent eruptive episodes of the Soufrière Hills Volcano, Montserrat, *Geophysical Research Letters*, *37*(19)

Boudon, G., Le Friant, A., Komorowski, J. C., Deplus, C. and Semet, M. P. (2007), Volcano flank instability in the Lesser Antilles Arc: Diversity of scale,

processes, and temporal recurrence, *Journal of Geophysical Research*, 112, B08205, doi:10.1029/2006JB004674

Bouysse, P. and Westercamp, D. (1990), Subduction of Atlantic aseismic ridges and Late Cenozoic evolution of the Lesser Antilles island arc, *Tectonophysics,* 175(4), 49–380

Brendryen, J., Haflidason, H. and Sejrup, H. P. (2010), Norwegian Sea tephrostratigraphy of marine isotope stages 4 and 5: Prospects and problems for tephrochronology in the North Atlantic region, *Quaternary Science Reviews*, 29(7–8), 847–864

Brown, K and Davidson, C. (2008), 40Ar/39Ar geochronology of the Silver Hills andesite, Montserrat, West Indies, B. A. Senior integrative excersize, Carelton College, Northfield, Minnesota

Brown, R. J., Civetta, L., Arienzo, I., D'Antonio, M., Moretti, R., Orsi, G., Tomlinson, E. L., Albert, P. G. and Menzies, M. A. (2014), Geochemical and isotopic insights into the assembly, evolution and disruption of a magmatic plumbing system before and after a cataclysmic caldera–collapse eruption at Ischia volcano (Italy), *Contributions to Mineralogy and Petrology*, *168*(3), 1–23

Carey, S. (1997), Influence of convective sedimentation on the formation of widespread tephra fall layers in the deep sea, *Geology*, 25(9), 839–842

Carn, S. A., Watts, R. B., Thompson, G. and Norton, G. E. (2004), Anatomy of a lava dome collapse: the 20 March 2000 event at Soufrière Hills Volcano, Montserrat, Journal of Volcanology and Geothermal Research, 131(3), 241-264

Carn, S. A. and Prata, F. J. (2010), Satellite-based constraints on explosive SO2 release from Soufrière Hills Volcano, Montserrat, *Geophysical Research Letters*, *37*(19)

Carter, L., Alloway, B., Shane, P. and Westgate, J. (2004), Deep–ocean record of major late Cenozoic rhyolitic eruptions from New Zealand, *New Zealand Journal of Geology and Geophysics*, 47(3), 481–500

Cassidy, M., Trofimovs, J., Palmer, M. R., Talling. P. J., Watt, S. F. L., Moreton, S. G. and Taylor, R. N. (2013), Timing and emplacement dynamics of newly recognised mass flow deposits at ~8–12 ka offshore Soufrière Hills volcano, Montserrat: How submarine stratigraphy can complement subaerial eruption histories, *Journal of Volcanology and Geothermal Research*, 253, 1–14, doi:10.1016/j.jvolgeores.2012.12.002

Cassidy, M., Trofimovs, J., Watt, S. F. L., Palmer, M. R., Taylor, R. N., Gernon, T. M., Talling, P. J. and Le Friant, A. (2014), Multi–stage collapse events in the South Soufrière Hills, Montserrat, as recorded in marine sediment cores, *In the eruption of Soufrière Hills Volcano, Montserrat from 2000–2010*, Edited by Wadge, G., et al., *The Geological Society Special Publications*, 39, 383–397

Cassidy. M., et al., (2015), Rapid onset of mafic magmatism facilitated by volcanic edifice collapse, *Geophysical Research Letters*, 42(12), 4778–4785

Christopher, T. E., Humphreys, M. C., Barclay, J., Genareau, K., De Angelis, S. M., Plail, M. and Donovan, A. (2014), Petrological and geochemical variation during the Soufrière Hills eruption, 1995 to 2010, *The Eruption of Soufrière Hills Volcano, Montserrat from 2000 to 2010,* Edited by Wadge, G., Robertson, R. and Voight, B, *Geological Society, London, Memoirs*, 39(1), 317–342

Cole, P. D., Calder, E. S., Druitt, T. H., Hoblitt, R., Robertson, R., Sparks, R. S. J. and Young, S. R. (1998), Pyroclastic flows generated by gravitational instability of the 1996–97 lava dome of Soufriere Hills Volcano, Montserrat, *Geophysical Research Letters*, *25*(18), 3425-3428.

Cole, P. D., Calder, E. S., Sparks, R. S. J., Clarke, A. B., Druitt, T. H., Young, S. R. and Norton, G. E. (2002), Deposits from dome–collapse and fountain–collapse pyroclastic flows at Soufrière Hills Volcano, Montserrat, *Geological Society, London, Memoirs*, 21(1), 231–262

Cole, P. D., Smith, P., Komorowski, J. C., Alfano, F., Bonadonna, C., Stinton, A. *et al*., (2014), Ash venting occurring both prior to and during lava extrusion at Soufriere Hills Volcano, Montserrat, from 2005 to 2010, *Geological Society, London, Memoirs*, *39*(1), 71-92

Crutchley, G. J., Karstens, J., Berndt, C., Talling, P. J., Watt, S. F. L, Vardy, M. E., Huhnerbach, V., Urlaub, M., Sarkar, S., Klaeschen, D., Paulatto, M., Le Friant, A., Lebas, E. and Maeno, F., (2013), Insights into the emplacement dynamics of volcanic landslides from high−resolution 3D seismic data acquired offshore Montserrat, Lesser Antillies, *Marine Geology*, 335:1−15

Deplus, C., Le Friant, A., Boudon, G., Komorowski, J. C., Villement, B., Harford, C., Segoufin, J. and Chiminee, J. L. (2001), Submarine evidence for large−scale debris avalanches in the Lesser Antillies Arc, *Earth and Planetary Science Letters*, 192, 145−157

Devine, J., *et al*., (1998), Petrologic evidence for pre−eruptive pressure−temperature conditions, and recent reheating, of andesitic magma eruption at the Soufrière Hills Volcano, Montserrat, W. I., *Geophysical Research Letters*, 25, 3669−3672

Devine, J. D., Rutherford, M. R., Norton, G. E. and Young, S. R., (2003), Magma storage region processes inferred from geochemistry of Fe−Ti oxides in andesitic magma, Soufrière Hills Volcano, Montserrat, W.I. *Journal of Petrology*, 44, 1375−1400

Druitt, T. H., Mellors, R. A., Pyle, D. M. and Sparks, R. S. J. (1989), Explosive volcanism on Santorini, Greece, *Geological Magazine*, 2; 95−126

Edmonds, M. and Herd, R. A. (2005), Inland−directed base surge generated by the explosive interaction of pyroclastic flows and seawater at Soufrière Hills volcano, Montserrat, *Geology*, 33(4), 245−248

Edmonds, M., Herd, R. A. and Strutt, M. H., (2006), Tephra deposits associated with a large lava dome collapse, Soufrière Hills Volcano, Montserrat, 12−15

July 2003, *Journal of Volcanology and Geothermal Research*, 153(3–4), 313–330

Elsworth, D., Mattioli, G., Taron, J., Voight, B. andHerd, R. (2008), Implications of magma transfer between multiple reservoirs on eruption cycling, *Science*, *322*(5899), 246-248

Feuillet, N., Leclerc, F., Tapponnier, P., Beauducel, F., Boudon, G., Le Friant, A., *et al*., (2010), Active faulting induced by slip partitioning in Montserrat and link with volcanic activity: New insights from the 2009 GWADASEIS marine cruise data, *Geophysical Research Letters*, *37*(19)

Germa, A., Quidelleur, X., Labanieh, S., Lahitte, P. and Chauvel C. (2010), The eruptive history of Morne Jacob volcano (Martinique Island, French West Indies): Geochronology, geomorphology and geochemistry of the earliest volcanism in the recent Lesser Antilles arc, *Journal of Volcanology and Geothermal Research*, 198(3–4), 297–310, doi:10.1016/j.jvolgeores.2010.09.013

Harford, C. L., Pringle, M. S., Sparks, R. S. J. and Young, S. R. (2002), The volcanic evolution of Montserrat using 40Ar/39Ar geochronology, *Geological Society, London, Memoirs,* 21, 93–113, doi: 10.1144/GSL.MEM.2002.021.01.05

Herd, R. A., Edmonds, M. and Bass, V. A, (2005), Catastrophic lava dome failure at Soufrière Hills Volcano, Montserrat, 12–13 July 2003, *Journal of Volcanology and Geothermal Research*, 148(3–4), 234–252

Houghton, B. F., Wilson, C. J. N., McWilliams, M. O., Lanphere, M. A., Weaver, S. D., Briggs, R. M. and Pringle, M. S. (1995), Volcanic Zone , New Zealand Chronology and dynamics of a large silicic magmatic system : Central Taupo Volcanic Zone, New Zealand, *Geology*, 23, 13–16, doi: 10.1130/00917613(1995)023<0013:CADOAL>2.3.CO;2

Humphreys, M. C. S., Christopher, T. and Hards, V. (2009a), Microlite transfer by disaggrega− tion of mafic inclusions following magma mixing at Soufrière

Hills volcano, Montserrat, *Contributions to Mineralogy and Petrology* 157, 609–624

Humphreys, M.C.S., Edmonds, M., Christopher, T. and Hards, V. (2009b), Chlorine variations in the magma of Soufrière Hills Volcano, Montserrat: insights from Cl in horn− blende and melt inclusions. *Geochimica et Cosmochimica Acta* 73, 5693–5708

Humphreys, M. C. S., Edmonds, M., Barclay, J., Plail, M., Parkes, D. and Christopher. T. (2013), A new method to quantify the real supply of mafic components to a hybrid andesite. *Contributions to Mineralogy and Petrology*, 165, 191–215, http://dx.doi.org/10.1007/ s00410−012−0805−x

IDC (1997) in House of Commons, Session 1997−1998, International Development Committee, First Report, together with the Proceedings of the Committee, Minister of Evidence and Appendices Montserrat (Stationery Office, London)

Jutzeler, M., Marsh, R., Carey, R. J., White, J. D. L., Talling, P. J. and Karlstrom, L. (2014), On the fate of pumice rafts formed durin the 2012 Havre submarine eruption, *Nature Communications*, 5, 3660, DOI: 10.1038/ncomms4660

Jutzeler, M., McPhie, J., Allen, S. R. and Proussevitch, A. A., (2015), Grain−size distribution of volcaniclastic rocks 2: Characterizing grain size and hydraulic sorting, *Journal of Volcanology and Geothermal Research*, 301, 191−203

Karstens, J., Crutchley, G. J., Berndt, C., Talling, P. J., Watt, S. F., Hühnerbach, V., Lebas, E., Le Friant, A. and Trofimovs, J. (2013), Emplacement of pyroclastic deposits offshore Montserrat: Insights from 3D seismic data, J*ournal of Volcanology and Geothermal Research*, 257, 1−11

Keller, J., Ryan, W. B. F., Ninkovich, D. and Altherr, R. (1978), Explosive volcanic activity in the Mediterranean over the past 200,000 yr as recorded in deep−sea sediments, *Geological Society of America Bulletin*, 89(4), 591−604

Kenedi, C. L., Sparks, R. S. J., Malin, P., Voight, B., Dean, S., Minshull, T., Paulatto, M., Peirce, C. and Shalev, E. (2010), Contrasts in morphology and deformation offshore Montserrat: New insights from the SEA-CALIPSO marine cruise data, *Geophysical Research Letters,* 37(19)

Kokelaar, B. P. (2002), Setting, chronology and consequences of the eruption of Soufrière Hills Volcano, Montserrat (1995–1999), *In the eruption of Soufrière Hills volcano, Montserrat, from 1995 to 1991,* edited by T. Druitt, and P. Kokelaar, *Geological Society Special Publications*, 21,1–43, doi: 10.1144/GSL.MEM.2002.021.01.02

Komorowski, J. C., Legendre, Y., Christopher, T., Bernstein, M., Stewart, R. *et al*., (2010), Insights into processes and deposits of hazardous vulcanian explosions at Soufrière Hills Volcano during 2008 and 2009 (Montserrat, West Indies), *Geophysical Research Letters*, *37*(19)

Kutterolf, S., Freundt, A. and Perez, W. (2008), Pacific offshore record of plinian arc volcanism in Central America: 2. Tephra volumes and erupted masses. *Geochemistry, Geophysics, Geosystems,* 9(2)

Lebas, E., Watt, S. F. L., Talling, P. J., Feuillet, N., Deplus, C., Berndt, C. and Vardy, M. (2011), Multiple widespread landslides during the long–term evolution of a volcanic island: Insights from high–resolution seismic data, Montserrat, Lesser Antilles, *Geochemistry Geophysics Geosystems*, 12(5), Q05006, doi:10.1029/2010GC003451

Le Friant, A., Boudon, G., Komorowski, J. C. and Deplus, C. (2002), L'île de la Dominique, à l'origine des avalanches de débris les plus volumineuses de l'arc des Petites Antilles, *C.R. Geosci*, 334, 235–243

Le Friant, A., Boudon, G., Deplus, C. and Villement, B. (2003), Large–scale flank collapse events during the activity of Montagne Pelée, Martinique, Lesser Antilles, *Journal of Geophysical Research*, 108 (B1), 2055, doi:10.1029/2001JB001624

Le Friant, A., Harford, C.L. and Deplus, C. (2004), Geomorphological evolution of Montserrat (West Indies): importance of flank collapse and erosional processes, *Journal of the Geological Society*, 161(1), 147–160, doi:10.1144/0016–764903–017

Le Friant, A., Lock, E. J., Hart, M. B., Boudon, G., Sparks, R. S. J., Leng, M. J., Smart, C. W., Komorowski, J. C., Deplus, C. and Fisher, J. K. (2008), Late Pleistocene tephrochronology of marine sediments adjacent to Montserrat, Lesser Antilles volcanic arc, *Journal of the Geological Society*, 165(1), 279–289, doi:10.1144/0016–76492007–019

Le Friant, A., Deplus, C. and Boudon, G. (2009), Submarine deposition of volcanicastic material from the 1995–2005 eruptions of Soufrière Hills volcano, Montserrat, *Journal of the Geological Society*, 166, 171–182, doi: 10.1144/0016–76492008–047

Le Friant, A., Deplus, C., Boudon, G., Feuliiet, N., Trofimovs, J., Komorowski, J. C., Sparks, R. S. J., Talling, P. J., Loughlin, S., Palmer, M. R. and Ryan, G. (2010), Eruption of Soufrière Hills (1995– 2009) from an offshore perspective: Insights from repeated swath bathymetry surveys, *Geophysical Research Letters*, 37, L11307, doi:10.1029/2010GL043580

Le Friant, A., Lebas, E., Clement, V., Boudon, G., Deplus, C., de Voogd B. and Bachélery, P. (2011), A new model for the evolution of la Reunion volcanic complex from complete geophysical surveys, *Geophysical Research Letters*, 38, L09312, doi:10.1029/2011GL047489

Le Friant, A., Ishizuka, O., Stroncik, N. A., Slagle, A. L., Morgan, S., Adachi, T., Aljahdali, M. and Boudon, G. (2012), Lesser Antillies Volcanism and Landslides. Implications for hazard assessment and long–term magmatic evolution of the arc, Integrated Ocean Drilling Program, *Expedition 340 preliminary report,* doi:10.2204/iodp.pr.340.2012

Le Friant, A., *et al*., (2015), Submarine record of volcanic island construction and collapse in the Lesser Antilles arc: First scientific drilling of submarine

volcanic island landslides by IODP Expedition 340, *Geochemistry, Geophysics, Geosystems*, 16, 420–442, doi:10.1002/ 2014GC005652

Lim, C., Ikehara, K. and Toyoda, K. (2008), Cryptotephra detection using high–resolution trace–element analysis of Holocene marine sediments, southwest Japan. *Geochimica et Cosmochimica Acta*, 72(20), 5022–5036

Longpré, M. A., Troll, V. R., Walter, T. R. and Hansteen, T. H. (2009), Volcanic and geochemical evolution of the Teno massif, Tenerife, Canary Islands: Some repercussions of giant landslides on ocean island magmatism, *Geochemistry, Geophysics, Geosystems*, 10(12)

Loughlin, S. C., Calder, E. S., Clarke, A., Cole, P. D., Luckett, R., Mangan, M. T. and Watts, R. B. (2002), Pyroclastic flows and surges generated by the 25 June 1997 dome collapse, Soufrière Hills Volcano, Montserrat, *Memoris of the Geological Society of London*, 21, 191–210

Murphy, M. D., Sparks, R. S. J., Barclay, J., Carroll, M. R., Lejeune, A. M., Brewer, T. *et al,*. (1998), The role of magma mixing in triggering the current eruption at the Soufriere Hills volcano, Montserrat, West Indies, *Geophysical Research Letters*, *25*(18), 3433-3436

Murphy, M. D., Sparks, R. S. J., Barclay, J., Carroll, M. R. and Brewer, T. S. (2000), Remobilization of andesite magma by intrusion of mafic magma at the Soufriere Hills Volcano, Montserrat, West Indies, *Journal of petrology*, 41(1), 21-42

Narcisi, B. (1996), Tephrochronology of a late Quaternary lacustrine record from the Monticchio maar (Vulture volcano, southern Italy), *Quaternary Science Reviews*, 15(2), 155–165

Norton, G. E., Watts, R. B., Voight, B., Mattioli, G. S., Herd, R. A., Young, S. R., *et al*., (2002), Pyroclastic flow and explosive activity at Soufrière Hills Volcano, Montserrat, during a period of virtually no magma extrusion (March 1998 to November 1999), *Geological Society, London, Memoirs*, *21*(1), 467-481

Odbert, H. M., Stewart, R. C. and Wadge, G. (2014), Cyclic phenomena at the Soufrière Hills volcano, Montserrat, *Geological Society, London, Memoirs*, *39*(1), 41-60

Pindell, J. L. and Barrett, S. F. (1990), Geological evolution of the Caribbean region: a plate tectonic perspective, *In The Caribbean Region*, Edited by Dengo. G. and Case. J. E., *The Geological Society of America*, 405–432

Plail, M., Barclay, J., Humphreys, M. C., Edmonds, M., Herd, R. A. and Christopher, T. E. (2014), Characterization of mafic enclaves in the erupted products of Soufrière Hills Volcano, Montserrat, 2009 to 2010, *Geological Society, London, Memoirs*, *39*(1), 343-360

Rea. W. J. (1975), The volcanic geology and perology of Montserrat, West Indies, *Journal of the Geological Society of London.,* 130, 341-366

Roobol, M. J., and Smith, A. L. (1998), Pyroclastic stratigraphy of the Soufrière Hills volcano, Montserrat– Implication for the present eruption, *Geophysical Research Letters*, 25 (18),3393–3396

Rutherford. M. J. and Devine, J. D. (2003), Magmatic conditions and magma ascent as indicated by hornblende phase equilibria and reactions in the 1995–2002 Soufrière Hills Magma, Journal of Petrology, 44 (8), 1433–1454

Ryan, G. A., Loughlin, S. C., James, M. R., Jones, L. D., Calder, E. S., Christopher, T. *et al*., (2010), Growth of the lava dome and extrusion rates at Soufrière Hills Volcano, Montserrat, West Indies: 2005–2008, *Geophysical Research Letters*, 37(19)

Samper, A., Quidelleur, X., Lahitte, P. and Mollex, D. (2007), Timing of effusive volcanism and collapse events within an oceanic arc island: Basse-Terre, Guadeloupe archipelago (Lesser Antilles Arc), *Earth and Planetary Science Letters*, *258*(1), 175-191

Seta, M. D. *et al*. (2012), Slope instability induced by volcano–tectonics as an additional source of hazard in active volcanic areas: The case of Ischia island (Italy), *Bulletin of Volcanology*, 74, 79–106

Singer, B. S., Jicha, B. R., Harper, M. A., Naranjo, J. A., Lara, L. E. and Moreno–Roa, H, (2008) Eruptive history, geochronology, and magmatic evolution of the Puyehue–Cordón Caulle volcanic complex, Chile, *Geological Society of America Bulletin*, 120(5–6), 599–618.

Smith, A. L., (2007), Prehistoric stratigraphy of the Soufrière Hills–South Soufrière Hills volcanic complex, Montserrat, West Indies, *The Journal of Geology*, 115:115–127

Sparks, R. S. J., Barclay, J., Calder, E. S., Herd, R. A., Komorowski, J. C., Luckett, R. *et al*., (2002), Generation of a debris avalanche and violent pyroclastic density current on 26 December (Boxing Day) 1997 at Soufriere Hills Volcano, Montserrat, *Geological Society, London, Memoirs*, *21*(1), 409-434

Sparks, R. S. J. and Young, S. R. (2002), The eruption of Soufrière Hills Volcano, Montserrat (1995–1999): overview of scientific results, *Geological Society, London, Memoirs*, 21(1), 45–69

Stinton, A. J., Cole, P. D., Odbert, H. M., Christopher, T., Avard, G. and Bernstein, M. (2014), Dome growth and valley fill during Phase 5 (8 October 2009–11 February 2010) at the Soufriere Hills Volcano, Montserrat, *Geological Society, London, Memoirs*, *39*(1), 113-131

Trofimovs, J. *et al*., (2006), Submarine pyroclastic deposits formed at the Soufrière Hills volcano, Montserrat (1995–2003): What happens when pyroclastic flows enter the ocean? *Geology*, 34(7), 549–552, doi: 10.1130/G22424.1

Trofimovs, J., Sparks, R. S. J. and Talling, P. J. (2008), Anatomy of a submarine pyroclastic flow and associated turbidity current: July 2003 dome collapse,

Soufrière Hills volcano, Montserrat, West Indies, *Sedimentology*, 55, 617–634, doi: 10.1111/j.1365–3091.2007.00914

Trofimovs, J., *et al*. (2010), Evidence for carbonate platform failure during rapid sea–level rise; ca 14 000 year old bioclastic flow deposits in the Lesser Antilles, *Sedimentology*, 57, 735–759, doi: 10.1111/j.1365–3091.2009.01117

Trofimovs, J., Foster, C., Sparks, R. S. J., Loughlin, S., Le Friant, A., Deplus, C., Porritt, L., Christopher, T., Luckett, R., Talling, P. J., Palmer, M. R. and Le Bas, T. (2012), Submarine pyroclastic deposits formed during the 20th May 2006 dome collapse of Soufrière Hills volcano, Montserrat, *Bulletin of Volcanology*, 74, 391–405, doi: 10.1007/s00445–011–0533–5

Trofimovs, J., Talling, P. J., Fisher, J. K., Hart, M. B., Sparks, R. S. J., Watt, S. F. L., Cassidy, M., Smart, C. W., Le Friant, A., Moreton, S. G. and Lang, M. J. (2013), Timing, origin and emplacement dynamics of mass flows offshore of SE Montserrat in the last 110 ka: Implications for landslide and tsunami hazards, eruption history, and volcanic island evolution, *Geochemistry, Geophysics, Geosystems*, 14(2), 385–406. doi:10.1002/ggge.20052

Voight, B., Komorowski, J. C., Norton, G. E., Belousov, A. B., Belousova, M., Boudon, G., *et al*., (2002), The 26 December (Boxing Day) 1997 sector collapse and debris avalanche at Soufriere Hills volcano, Montserrat, Memoirs of the Geological Society of London, 21, 363-408

Wadge, G. and Shepherd, J. B. (1984), Segmentation of the Lesser Antilles subduction zone, *Earth and Planetary Science Letters*, 71, 297–304

Wadge. G., Voight, B., Sparks, R. S. J., Cole, P. D., Loughlin, S. C., and Robertson, R. E. A. (2014), An overview of the eruption of Soufrière Hills Volcano, Montserrat from 2000 to 2010, *In: The Eruption of the Soufrière Hills Volcano, Montserrat from 2000–2010*, edited by G. Wadge, R. A. E.Robertson, and B. Voight, *Memoirs of the Geological Society of London*,1–4

Watt, S. F. L., *et al*., (2012a), Combinations of volcanic−flank and seafloor−sediment failure offshore Montserrat, and their implications for tsunami generation, *Earth and Planetary Science Letters*, 319(320), 228–240, doi:10.1016/j.epsl.2011.11.032

Watt, S. F. L., *et al*., (2012b), Widespread and progressive seafloor−sediment failure following volcanic debris avalanche emplacement: Landslide dynamics and timing offshore Montserrat, Lesser Antilles, *Marine Geology,* 323(325), 69–94, http://dx.doi.org/10.1016/j.margeo.2012.08.002

Watts, R. B., Herd, R. A., Sparks, R. S. J. and Young, S. R. (2002), Growth patterns and emplacement of the andesitic lava dome at Soufriere Hills Volcano, Montserrat, *Geological Society, London, Memoirs*, *21*(1), 115-152

Wulf, S., Kraml, M., Kuhn, T., Schwarz, M., Inthorn, M., Keller, J. and Halbach, P. (2002), Marine tephra from the Cape Riva eruption (22 ka) of Santorini in the Sea of Marmara, *Marine Geology*, 183(1), 131−141

Wulf, S., Kraml, M., Brauer, A., Keller, J. and Negendank, J. F. (2004), Tephrochronology of the 100 ka lacustrine sediment record of Lago Grande di Monticchio (southern Italy), *Quaternary International*, 122(1), 7−30

Wutke, K., Wulf, S., Tomlinson, E. L., Hardiman, M., Dulski, P., Luterbacher. and Brauer, A. (2015), Geochemical properties and environmental impacts of seven Campanian tephra layers deposited between 40 and 38 ka BP in the varved lake sediments of Lago Grande di Monticchio, southern Italy, *Quaternary Science Reviews*, 118, 67−83

Yoshida, H., Sugai, T. and Ohmori, H. (2012), Size−distance relationships for hummocks on volcanic rockslide− debris avalanche deposits in Japan, *Geomorphology*, 136, 76−87, doi:10.1016/j.geomorph.2011.04.044

Young, S. R., Sparks, R. S. J., Aspinall, W. P., Lynch, L. L., Miller, A. D., Robertson, R. E. and Shepherd, J. B. (1998), Overview of the eruption of Soufrière Hills

volcano, Montserrat, 18 July 1995 to December 1997, *Geophysical Research Letters*, 25(18), 3389–3392

Zellmer, G. F., Sparks, R. S. J., Hawkesworth, C. J. and Wiedenbeck, M (2003), Magma emplacement and remobilization timescales beneath Montserrat: insights from Sr and Ba profiles across plagioclase phenocrysts, *Journal of Petrology*, 44, 1413–1432

Chapter 2:

1 Ma evolution of explosive volcanic activity: chronostratigraphy of the Centre Hills Volcano, Montserrat

Abstract

Over the past 1 Ma, volcanism on Montserrat has been focused at two volcanic centres, the Soufrière Hills-South Soufrière Hills volcanic complex, and the Centre Hills volcano. The subaerial stratigraphy primarily comprises andesitic lithic breccias and tuffs that resulted from effusive, dome-forming eruptions. At the Centre Hills volcano, 24 thick (>1 m) pumiceous sequences are interlayered with the deposits of dome eruptions. These pumiceous deposits suggest that large (up to magnitude 5) explosive eruptions occurred throughout the history of the Centre Hills volcano. Such thick pumiceous sequences are rare within the stratigraphic record of the Soufrière Hills volcanic complex, and are restricted to the period ~175 to 130 ka. Eruptions on Montserrat over the past 1 Ma have consistently erupted magmas with similar bulk chemistry (52-65 % SiO_2) and mineral chemistry and petrography. This suggests that predominance towards effusive or explosive eruptive styles, and changes between these styles, was not driven by major compositional changes but instead reflected local controls on magma storage and ascent.

1. Introduction

Individual volcanoes commonly exhibit different styles of eruptive behaviour through time, with changes in parameters such as eruptive style, frequency and composition (Druitt *et al*., 1989; Ancochea *et al*., 1990; Ablay and Marti, 2000; Germa *et al*., 2011; Pioli *et al*., 2015). Variations in volcanic behaviour may reflect changes in magma genesis and the underlying volcanic plumbing system (Brown *et al*., 2014; Piloi *et al*., 2015). Therefore, reconstructing patterns in volcanic

behaviour can provide insights into the physical and chemical parameters that govern eruptive styles at a volcanic edifice and the processes that occur during the evolution of a volcanic system.

The offshore record on Montserrat (Lesser Antilles island arc) is more complete than the onshore record (Chapter 3), but discerning eruption styles from marine deposits is difficult. For example, interactions with the water column, currents, and bioturbation affect marine deposition and the preservation of primary volcanic deposits (Carter *et al*., 1995; Cassidy *et al*., 2014a; Jutzeler *et al*., 2014, 2015). Eruption style is thus more easily characterised via proximal subaerial exposures. This paper provides the first description of the onshore stratigraphy of the Centre Hills volcano and compares it with the well-described stratigraphy of Soufrière Hills volcanic complex. The combined ~1 Ma record gives insights into how and when eruptive styles change at Montserrat, and addresses whether these changes follow consistent patterns that may relate to long-lived volcanic processes (Roobol and Smith, 1976; Cortese *et al*., 1986; Druitt *et al*., 1989).

1.1 Previous work

The island of Montserrat is composed of three main volcanic centres: Silver Hills, Centre Hills, and the Soufrière Hills - South Soufrière Hills complex (comprising the Soufrière Hills edifice and the South Soufrière Hills edifice) (Figures 1 and 2). Ar-Ar dates on subaerial lavas suggest that Silver Hills was active between 2.6-1.2 Ma; Centre Hills was active between 0.95-0.55 Ma; and the Soufrière Hills volcanic complex was active from 0.29 Ma. Activity started at the Soufrière Hills edifice and briefly migrated to the South Soufrière Hills edifice between ~0.15-0.12 Ma, before returning to Soufrière Hills (Harford *et al*., 2002; Brown and Davidson, 2008). The currently active Soufrière Hills has been erupting since 1995, and was dominated by dome growth and dome-collapse events interspersed with short-lived Vulcanian pulses (Druitt and Kokelaar 2002; Wadge *et al*., 2014). Previous Ar-Ar dating is summarised in Table 1 and Figure 1.

Table 1: All previous Ar-Ar dates on Montserrat.

Sample name	Age (ka)	± Age (ka) (2σ)	Reference
SH07-B UW67A4	1383.6	40.2	Brown and Davidson, 2008
SH07-C UW67A6	1416	37.6	Brown and Davidson, 2008
SH07-D UW67A8	1398.8	40.4	Brown and Davidson, 2008
SH07-E UW67A10	1381.1	32.4	Brown and Davidson, 2008
SH07-F UW67A12	1505.4	99	Brown and Davidson, 2008
MVO144	2580	120	Harford *et al*., 2002
MVO755	1160	92	Harford *et al*., 2002
MVO135	1021	40	Harford *et al*., 2002
MVO148	954	24	Harford *et al*., 2002
MVO131	871	20	Harford *et al*., 2002
MVO831	826	24	Harford *et al*., 2002
MVO147	663	98	Harford *et al*., 2002
MVO809	550	46	Harford *et al*., 2002
MVO785	282	16	Harford *et al*., 2002
MVO819	174	6	Harford *et al*., 2002
MVO152	151	8	Harford *et al*., 2002
MVO830	129	34	Harford *et al*., 2002
MVO139	131	14	Harford *et al*., 2002
MVO791	129	28	Harford *et al*., 2002
MVO1099	128	54	Harford *et al*., 2002
18654 and	112	18	Harford *et al*., 2002
MVO777	75	20	Harford *et al*., 2002
MVO127	38	16	Harford *et al*., 2002
MVO154	24	4	Harford *et al*., 2002
MVO775	24	2	Harford *et al*., 2002

Stratigraphic studies on subaerial deposits from Soufrière Hills, and the short-lived basaltic centre of South Soufrière Hills show that most eruptive activity on Montserrat over the past ~300 ka has been dominated by lava-dome forming eruptions (Rea *et al*., 1975; Baker *et al*., 1985; Wadge and Isaacs 1988; Roobol and Smith, 1998; Smith, 2007). The stratigraphy largely comprises primary and reworked block-and-ash flows, pyroclastic density current (PDC) deposits containing semi-vesiculated (20-60 vol.%) material, and a few thin (<1 m thick) tephra fall deposits of Vulcanian origin that are interspersed within the stratigraphy (Rea *et al*., 1975; Baker *et al*., 1985; Wadge and Isaacs, 1988; Roobol and Smith, 1998; Smith, 2007).

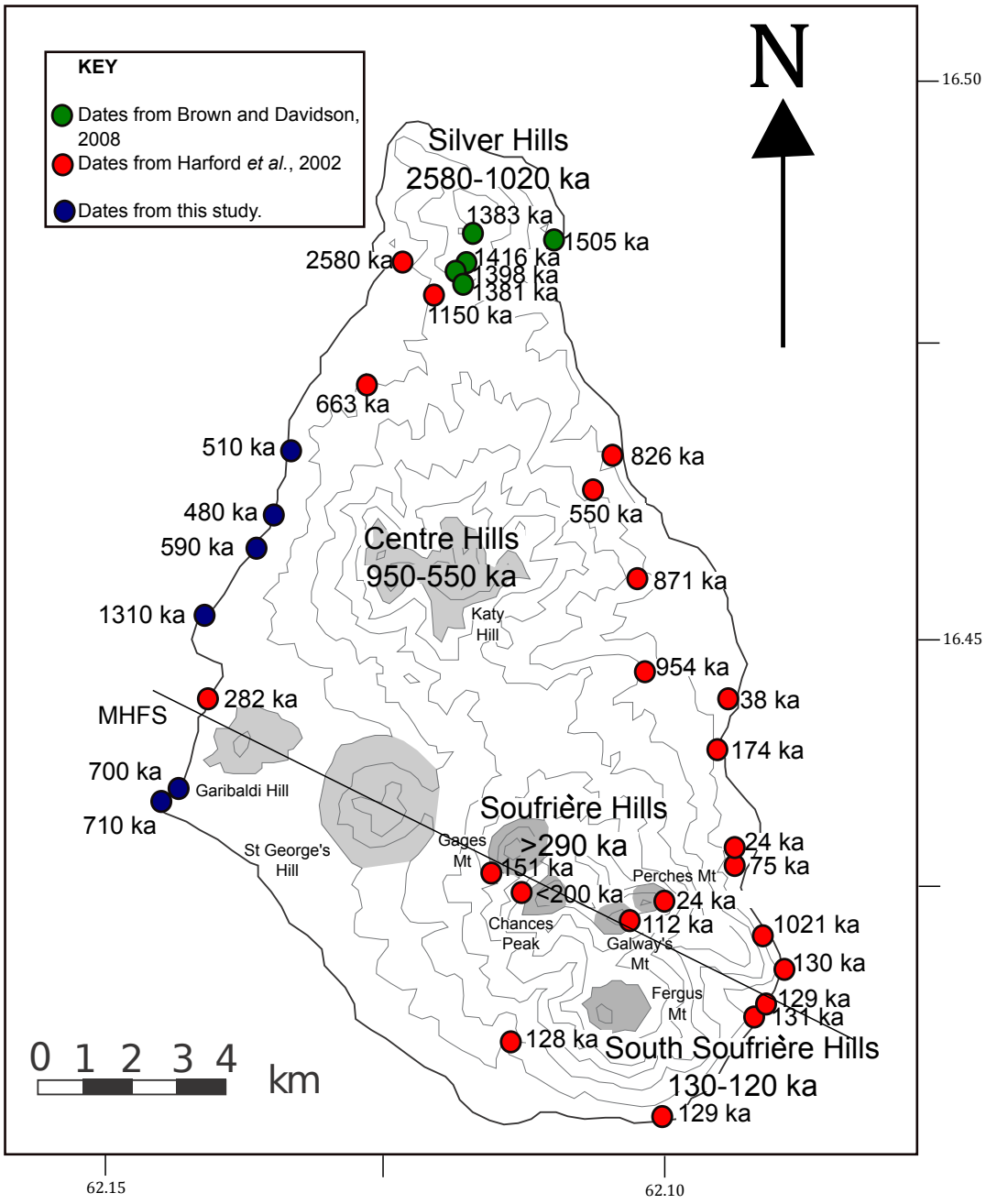

Figure 1: Ar-Ar dates (shown without error values, for clarity) and locations from the literature. Red circles are from Harford *et al*. (2002), green circles from Brown and Davidson, (2008). Also shown is the Montserrat-Havers Fault System (MHFS).

Volcanic activity at the South Soufrière –Soufrière Hills complex has been subdivided into 8 periods of activity, each lasting between 10^2 – 10^5 years (Smith, 2007; Trofimovs *et al*., 2013), and separated by the migration of activity to

different vent sites or by eruptive hiatuses of 10^2 – 10^4 years (Smith, 2007). Little work has been conducted on deposits from the extinct edifices of Centre Hills and Silver Hills, but thick (>5 m) pumice deposits occur at Woodlands Bay and are associated with Centre Hills (Harford *et al*., 2002). This suggests that larger magnitude explosive events have occurred on Montserrat than are represented by the past 300 ka of Soufrière Hills complex's stratigraphy.

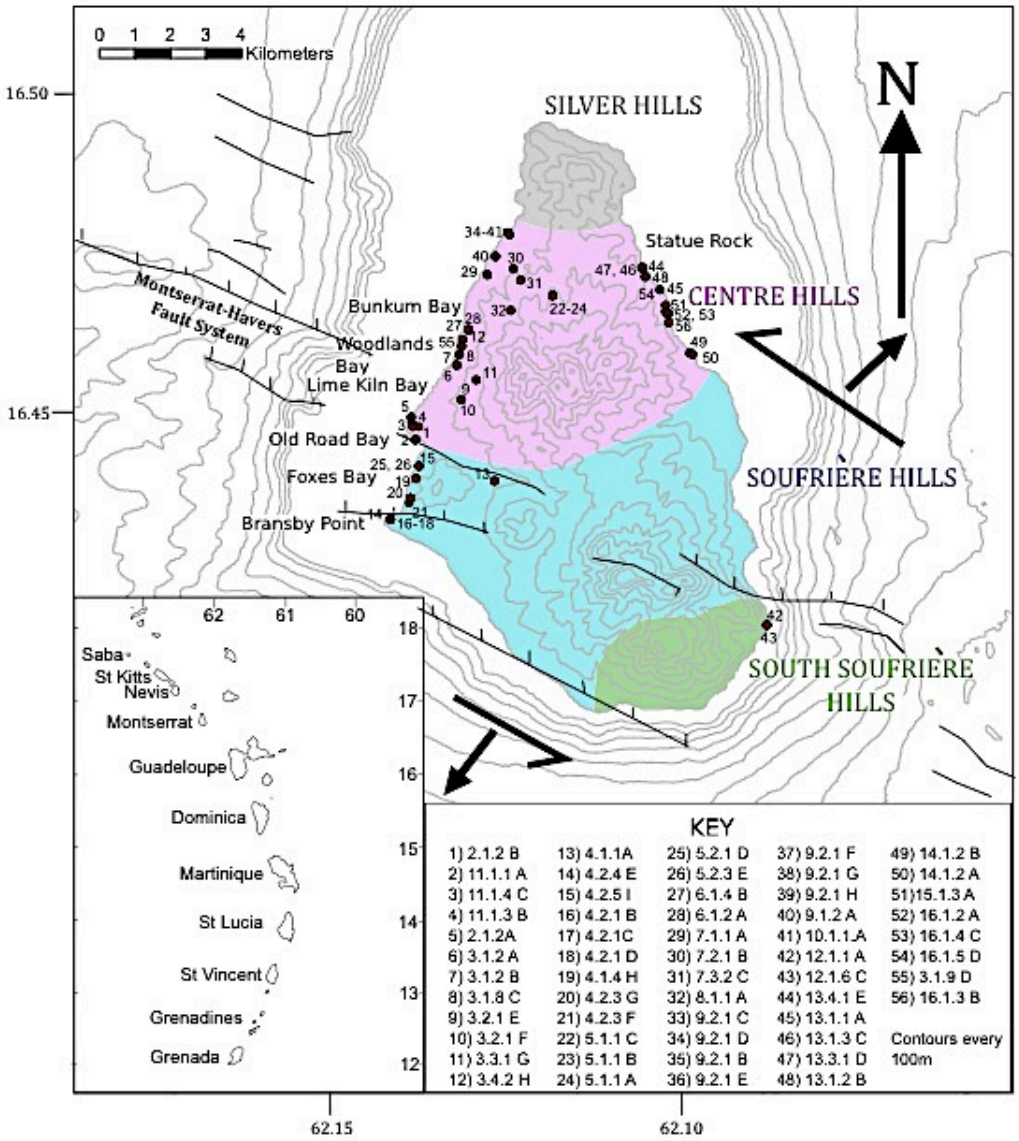

Figure 2: Map of Montserrat identifying the four main volcanic centres, based on observations from Harford *et al*, (2002). Also shown are the sample locations from fieldwork undertaken in this study. Numbers correspond to sample names, identified in the key. Samples are shown in stratigraphic logs in figures 10 and 11.

1.2 Aims

This study aims to document the major explosive periods of volcanism on Montserrat, and to determine whether this behaviour was restricted to certain evolutionary stages of the Centre Hills volcano and Soufrière Hills volcanic complexes. Explosive eruptions are particularly hazardous because large volumes of tephra can be widely dispersed (>1000 km). Explosive volcanism has harmful effects on human health, the economy and also the environment (e.g., Robock, 2000; Watt *et al*., 2009; Sammonds *et al*., 2010; Carlsen *et al*., 2012; Sigl *et al*., 2015). A better understanding of past volcanic periodicity, such as this study, may contribute towards better prediction of future eruption magnitudes and styles.

2. Methods

This study focuses on the explosive eruption deposits of Centre Hills. Deposits that appear as a continuous stratigraphic sequence that is dominated by juvenile pyroclastic material of consistent chemistry and petrography (e.g. colour, phenocryst assemblage) were grouped together to form a single eruptive unit. It is inferred that this eruptive unit was formed within the same eruption and represents one event.

Stratigraphic relationships between units are complex, as the onshore deposits are proximal facies that show strongly localised erosion and deposition controlled by topography and erosion or burial by mass wasting and normal slope erosion processes. Thus, in developing a stratigraphy of explosive deposits from Centre Hills, a combination of different methods was required. Initial correlations were made using field observations of the unit lithofacies and stratigraphic order of the deposits. Bulk chemical analyses (see below) were undertaken to test correlations of deposits, but also to chemically characterise the eruptive products of Centre Hills. Where correlations were uncertain, further

analyses on glass and mineral compositions were used to tighten stratigraphic control.

Clast	Description
Pumice	White/pale vesiculated (>50 vol. %) material. Some appear pink in colour. phenocrysts of plagioclase + hypersthene + Fe-Ti oxides ± augite ± hornblende ± quartz.
Scoria	Dark/black vesiculated (>20 vol.%) material.
Crystals	Mostly fragments of plagioclase and pyroxene.
Lithics	Grey/black/purple in colour. Very poorly vesiculated (typically <5 vol. %). Porphyritic with phenocrysts of plagioclase + hypersthene + Fe-Ti oxides + augite ± hornblende ± quartz.
Altered Lithics	Commonly red, green, yellow and white in colour. The clasts are mostly altered to clay minerals. Phenocrysts may be preserved but are often altered.

Table 2: Different volcanic clast types in Montserrat's volcaniclastic deposits

2.1 Field work

The Centre Hills volcano consists of three steep-sided hills that merge together to form the central peak of Katy Hill (Figure 2). It is thought to be the site of the main Centre Hills vent, due to the presence of lava blocks at the summit (Harford *et al*., 2002). The volcano is cut by several steep valleys, (locally referred to as ghauts), which radiate from the centre of the volcano (Figure 2). The coastal cliffs and road cuttings provide several good exposures for logging and sampling (Figures 3 and 4). Coastal cliffs typically range between 10–50 m high on the west coast, and 30–100 m high on the east coast.

Approximately 15 km of coastline (see figures 3 and 4 for example outcrops) and 8 road-cutting sites were logged around Centre Hills (Figure 2). Physical

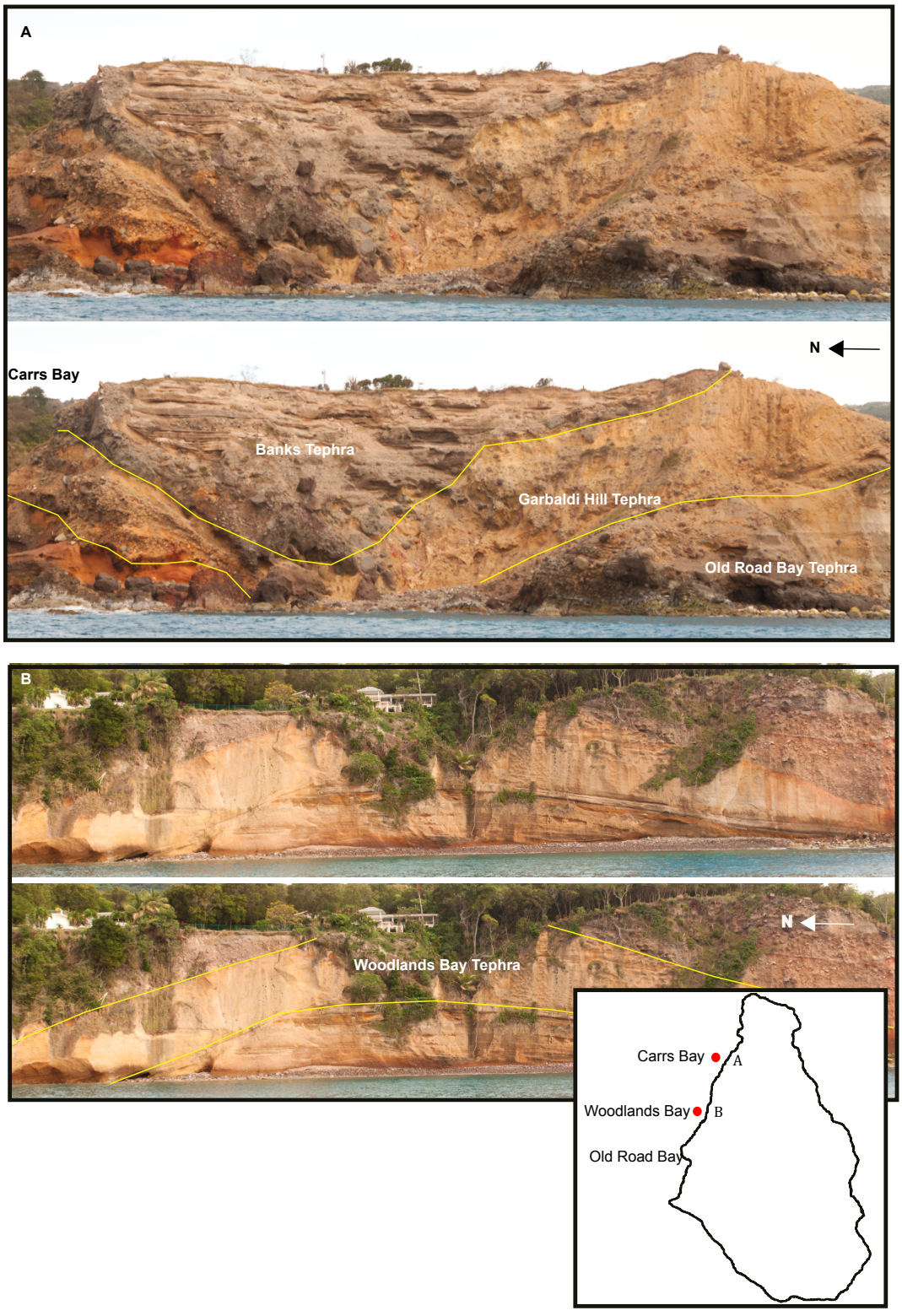

Figure 3: Pictures of coastal exposures of the NW Centre Hills. Please see inset maps for photo locations. Photos courtesy of Paul Cole.

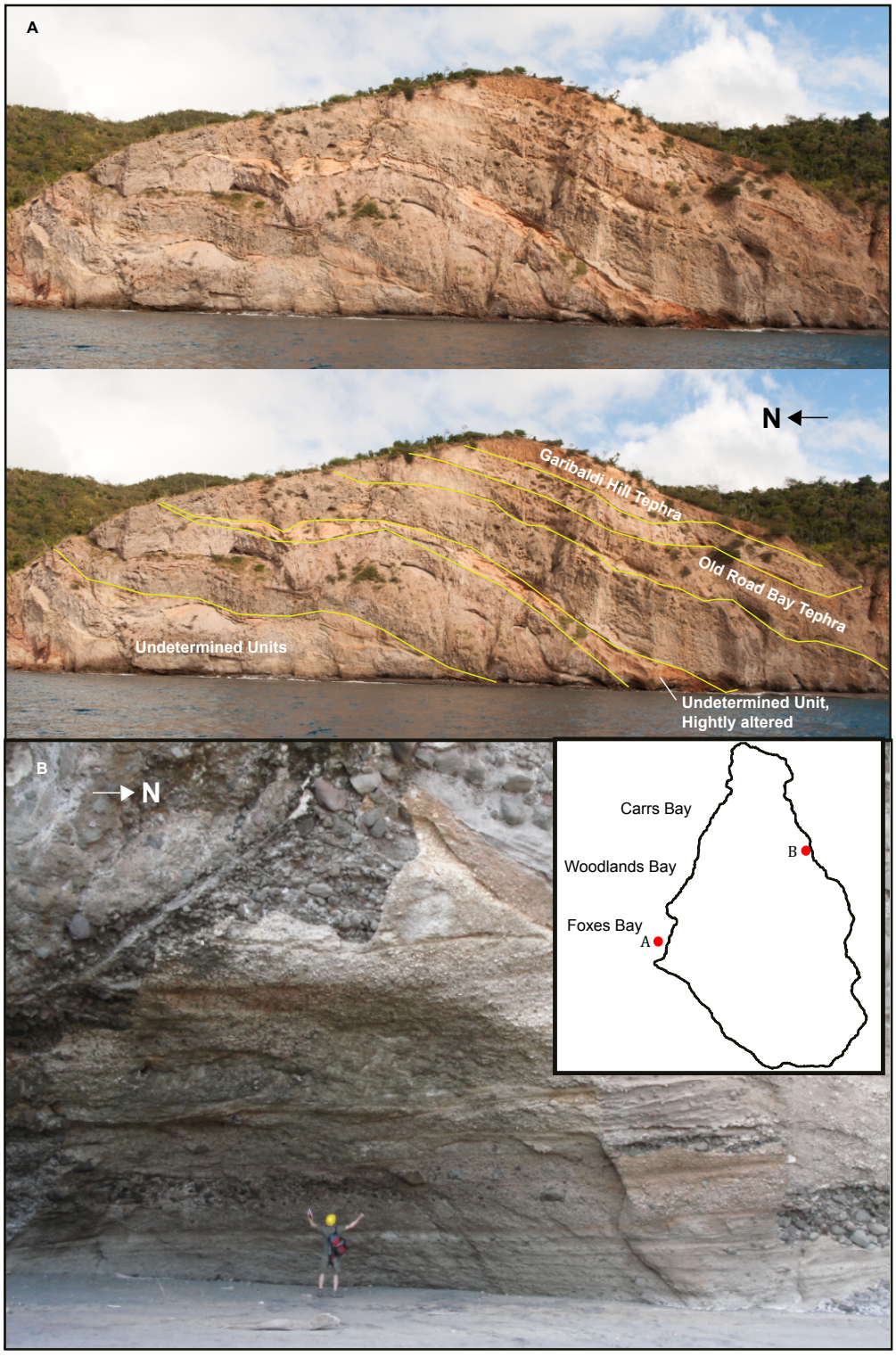

Figure 4: Photos of SW and E coastal exposures of Centre Hills pyroclastic deposits. Please see inset map for locations. Photo A courtesy of Paul Cole.

appearance, deposit structure, average and maximum grain size were noted. Average grain size was calculated by measuring the mean orthogonal axes of 5-10 visually average clasts. Maximum lithic and pumice sizes were calculated by measuring the mean of the orthogonal axes of the three largest clasts found within a 10-metre length outcrop. Samples were taken, where possible, of each unit at each outcrop.

Deposits are described using the terminology outlined by White and Houghton (2006), with the addition of the term lapillistone to represent units comprising >90% lapilli. PDC deposits are identified using criteria outlined in Branney and Kokelaar, (2002). Logged sections showed some signs of weathering (such as discolouration and clay alteration), which is expected along coastal outcrops of sequences that are aged between ~0.5-1 Ma (Harford *et al*., 2002). We cannot be certain if outcrops preserve original consolidation, therefore we do not distinguish between consolidated and non-consolidated units, ash is used only as a grain-size description (<2 mm sized grains).

2.2 Whole rock Chemistry

Lapilli-sized pumice clasts were collected from most subaerial tephra deposits mapped around Centre Hills, with some additional analyses of lithic clasts and tuff deposits. Trace element data were collected on bulk pumice clasts from each pyroclastic unit. Both ICP-MS (VG Plasmaquad PQ2 þ instrument) and XRF (Philips Magix Pro wavelength- dispersive XRF (WD-XRF)) were used to measure trace elements, and XRF to measure major elements. For bulk chemical analyses, only unaltered (i.e. showing no discolouration) material was selected. With the exception of the Angry Bird pumice, it was possible to sample relatively fresh pumice clasts in all units.

Altered (typically discoloured) material was removed. Samples were rinsed then soaked for 24 h and re-rinsed in MilliQ water to remove sea spray. Cleaned samples were dried and crushed before being ground to a fine powder using a tungsten carbide ball mill. Powder pellets and glass beads were analysed using a

Philips Magix Pro wavelength- dispersive XRF (WD-XRF) at the National Oceanography Centre (NOC), Southampton, UK. The standards used were JA-1, BCR1, and BE-N.

For ICP-MS, samples were dissolved and made into solutions with a dilution factor of 4000. The solution was made by dissolving 0.05g of powdered sample with 3% HNO_3 and 3% HF. Samples were dried and re-dissolved with ~5 g HCl and topped up to 10 g with MilliQ Water; 0.5 ml of this solution was then extracted and dried overnight. The residue was then re-dissolved, and made up to a 10 g solution with 3% HNO_3 solution with 5 ppm of indium and rhenium. Samples were measured using inductively coupled plasma-mass spectrometry (ICP-MS) at the NOC on a VG Plasmaquad PQ2 þ instrument. Precision for all elements is generally better than 2%, except for Ni and Cs where precision is better than 6% RSD (Appendix Table 1).

2.3 Mineral and glass compositions

Mineral and glass chemistry were analysed in juvenile clasts from all units. For mineral chemistry a Leo 1450VP scanning electron microscope (SEM) with an Oxford Instruments X-Act 10mm^2 area silicone drift detector and energy dispersive spectroscopy was used at the NOC. Beam current was 10 nA with an analysis time of 180 seconds. An iron haematite standard and a clinopyroxene crystal were repeatedly measured to check for instrument drift and for calibration. All analyses were then normalized to 100 wt.% anhydrous compositions. Standard deviation of results is generally < 0.4 wt.% (raw data and precision (standard deviation) are in the Appendix- Tables 2-5).

Glass chemistry was analysed using a Cameca SX100 microprobe at the Department of Earth Sciences, University of Bristol. A beam current of 4 nA was used with a beam diameter of 5 μm and an analysis time of 3 minutes. Multiple analyses were made on each sample, and any with totals <95 wt.% were discarded. Pumice clasts from several locations were analysed to test correlations (raw data is in Appendices- Table 6, standard deviation are in Appendix Table 6).

2.4 Ar-Ar dating

Samples were crushed using a jaw crusher and then wet sieved and left to dry overnight. Plagioclase crystals were separated from sieved fractions of 125–250 μm and 250–500 μm using a model LB-1 Frantz magnetic separator.

Samples and neutron flux monitors were placed in copper foil packets and stacked in quartz tubes. The sample package was irradiated for 2.0 hours in the Oregon State University reactor, Cd-shielded facility. Gas was extracted from samples using either an all-metal resistively-heated furnace or a mid-infrared (10.6 μm) CO_2 laser. Liberated argon was then purified of active gases (e.g., CO_2, H_2O, H_2, N_2, CH_4) using three Zr-Ti-Al getters; one at 16°C and two at 400°C. Data were collected on a GVi instruments ARGUS V multi-collector mass spectrometer using a variable sensitivity Faraday collector array in static collection mode. The reader is directed to Harford *et al.* (2002) for full details of this approach. The Ar-Ar dates have relatively large errors, with 2 σ errors < ± 0.2 Ma. The high error is due to the low K content of Montserrat's eruptive products (Figure 4).

3. Results

This work has identified 24 pumice-bearing deposits from explosive eruptions on Montserrat within the age span of Centre Hills volcanism. Many of these units are poorly exposed, but 11 of these units are laterally extensive and can be correlated between sites, and form the basis of a stratigraphic framework. One unit is likely to be associated with Silver Hills activity, and is also described below. Names for units have been assigned based on their type locality, and their characteristics are described in Tables 2 and 3 and in *Section 4.3*.

On the west coast, the oldest deposit is a poorly exposed pyroclastic unit, South Lime Kiln Bay tephra, which may be associated with Silver Hills activity. To the southwest, five extensive units (Old Road Bay tephra, Garibaldi Hill tephra, Bransby Point tephra, Old Road Bay tuff, and Foxes Bay tephra) overlie the South

Lime Kiln Bay tephra. To the north of the west coast three younger and more extensive units can be identified (the Bunkum Bay tephra, Woodlands Bay tephra, and the Attic tephra). On the east coast four extensive units are identifiable. The oldest is the Angry Bird tephra followed by the Bramble tephra, the Old Road Bay tephra, and the Statue Rock tephra. The South Lime Kiln Bay tephra may also crop out on the west coast, but the stratigraphic relationships are unclear due to poor unit preservation. The only unit with extensive outcrops on both the east and west coasts is the Old Road Bay tephra. The typical mineral assemblage of all these units is hypersthene + augite/low Fe diopside + plagioclase ± quartz with estimated crystallinities of 20-50 vol.%, based on both pumice and lithic clasts. The Attic tephra is mineralogically distinct and comprises hypersthene + hornblende + plagioclase + quartz.

On the basis of stratigraphic relationships, age and geochemistry, the deposits described are inferred to be derived from the Centre Hills volcano. Along the coastline, the thickest pumice-rich units are found east and west of Katy Hill (summit of the Centre Hills Volcano) (Figure 1). These thin north and southwards along the coastline, consistent with a Centre Hills provenance (assuming a vent site at Katy Hill). Cassidy *et al*. (2012) show that rocks erupted from the Centre Hills and Silver Hills volcanoes have distinctive low Ba/La ratios compared to the Soufrière Hills-South Soufrière Hills volcanic complex. Most samples in this study plot within the Centre-Silver Hills Ba/La field defined by Cassidy *et al*. (2012) (Figure 5). Deposits erupted from the Silver Hills volcano are unlikely to be well represented, due to burial by the younger Centre Hill products. All dated units in this study fall within the age range of Centre Hills volcanism documented by Harford *et al*. (2002), with exception of the oldest dated unit the South Lime Kiln Bay tephra (> 1 Ma), which crops out within a faulted block, and may originate from Silver Hills.

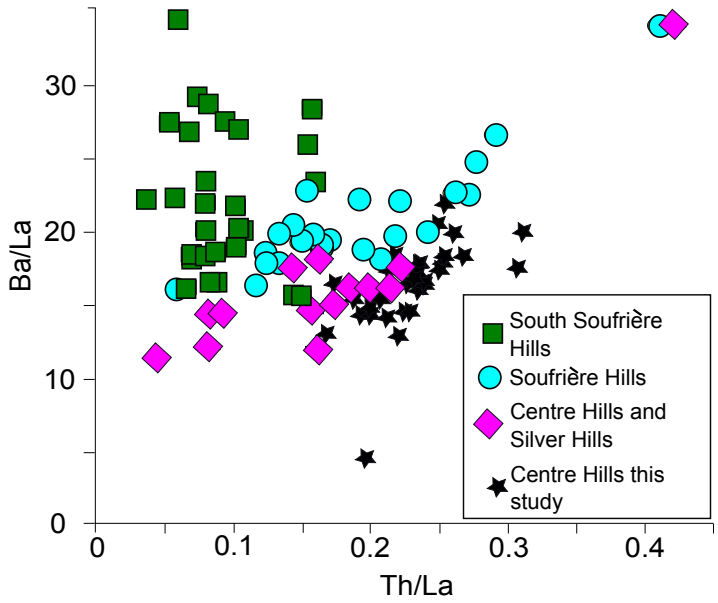

Figure 5: Ba/La and Th/La for samples from South Soufrière Hills, Soufrière Hills, Centre Hills and Silver Hills demonstrating that Centre Hills and Silver Hills have distinct ratios from Soufrière Hills and South Soufrière Hills. The figure is adapted from Cassidy *et al*. (2012) and plots both data from this study and previous studies (downloaded from the GEOROC database http://georoc.mpch-mainz.gwdg.de/georoc/).

3.1 Unit chemistry and mineralogy

Figures 6 to 10 plot the bulk rock, mineral and glass chemistry of different units as correlated from field stratigraphy. The chemistry of the explosive eruption products analysed here are broadly similar, but some have a distinct chemical composition that aids their stratigraphic correlation. Importantly, the studied eruptive units appear largely compositionally homogenous.

	Whole rock analyses						Glass analyses		Clinopyroxene rims					
Unit	**Nd (ppm)**	**Y (ppm)**	**Dy (ppm)**	**Sc (ppm)**	**Si/Ca**	**Si/Na**	**TiO_2 %**	**K_2O**	**Fe_2O_3 %**	**Al_2O_3 %**	**MgO %**	**Samples**	**Type Locality GR**	**Type Locality description**
Attic Tephra	11.7-12.6	15.27-17.06	2.29-2.53	9.10-12.71	11.32-11.93	18.44-20.35	0.17-0.28	1.10-2.19				8.1.1A, 3.3.1G, 3.2.1I+E, 3.2.1F, 3.1.8C	16.75413, 62.22226	White, metre scale tuffs rich in pelletal grains. Cross bedding and coarse ash - medium lapilli sized pumice clasts can be found.
Woodlands Tephra	12.82-15.65	21.82-31.08	3.21-4.62	11.43-13.42	9.33-9.67	17.23-19.12	0.30-0.35	1.62-1.76	21.74-22.65	0.84-1.13	21.86-22.85	5.1.1C, 5.1.1A, 5.1.1B, 10.1.1A, 3.1.2A+B,	16.76298, 62.22343	A sequence of metre scale pumice lapillistones. Pumices are yellow and are typically medium-coarse lapilli in size. Some thin (decimetre scale) interleaving lapilli-ash and ash beds are found.
Bunkum Bay Tephra	12.17-12.24	15.98-18.01	2.49-2.94	7.88-12.77	10.06	16.87	0.14-0.47	0.15-2.21	21.94-23.30	0.74-1.42	21.61-22.48	6.1.4B, 6.1.2A, 3.4.2H	16.77193, 62.22037	A sequence of overlapping channels that alternate between a pumice clast rich lapilli ash and tuffs. Tuffs often have accreationary lapilli and an orange colour.
Foxes Tephra	15.64	28.05	4.14	13.24					21.74-22.64	0.95-1.12	21.86-22.85	4.2.5I, 4.2.2E	16.72365, 62.24035	The unit outcrops as a ~4 m thick lapillistone that fines and thins to an ash northwards. Clasts are primarily pumicious >90%
Statue Rock Tephra	13.81	27.29	3.95	12.08	8.44	17.25						13.4.1E. 13.3.1D	16.78158, 62.17855	A sequence of pumice rich lapilli-ash with 50-10 cm thick bedding, which is picked out by varying clast size. Pumice lapilli rich lenses and andesite lapilli rich lenses occur throughout the unit. Fresh outcrops are pale beige to white in colour. Weathered surfaces are more yellow.
Old Road Bay Tuff	11.09	17.38	2.61	13.33								2.1.2B	16.74559, 62.23432	A 60 cm thick tuff. The lower 15 cm and the top 5 cm of the unit is pink, the middle of the tuff is grey.
Bransby Point Tephra	8.99	15.97	2.63	19.94	6.1	19.15	0.15-0.2	2.48-2.65	23.37-23.55	1.07-1.19	21.12-21.26	BP	16.72365, 62.24035	The unit comprises of 2 thick beds (~1 m) of pumiceous lapillistone that are each capped by a thin (~10 cm) tuff. The upper lapillistone and ash beds are pink in colour the lower lapillistone and ash are white.

Garibaldi Hill Tephra	13.98-14.72	24.97-26.51	3.74-3.94	10.85-12.99	8.77	18.19	0.3-0.36	1.34-1.66				4.1.4H, 5.2.3E, 11.1.3B, 9.2.1C, 9.2.1D, 7.1.1A	16.72899, 62.23521	A sequence of pumice rich lapilli-ash units with pumice lapilli rich lenses and lithic clast rich lenses. Beds are metre scale in thickness. The unit is capped by a 70 cm thick, well-sorted pumiceous lapillistone.
Bramble Tephra	11.99-13.20	19.40-22.39	3.05-3.41	11.50-13.03	9.64	18.91			23.38p 24.61	0.62-0.9	20.90-21.41	14.1.2B, 15.1.3A, 16.1.4C	16.77051, 62.16901	A series of metre scale lapilli ash with fine-medium lapilli sized, rounded pumice clasts (~30%) within a yellow, coarse ash matrix (~70%). The unit is capped by 1.5 m thick ash-breccia that has block sized rip up clasts.
Old Road Bay Tephra	11.37-12.14	19.55-21.72	2.97-3.32	10.24-15.16	8.63-9.02	17.19-17.41	0.16-0.34	0.76-1.73				13.1.1A. 11.1.1A, 4.2.3G, 9.2.1F, 9.2.1G, 9.2.1H	16.74559, 62.23432	A lapilli-ash with medium lapilli-sized pumice clasts and a medium to coarse orange ash matrix. Lenses of pumice lapillistone and andesite lapillistone present, with some localised andesite breccia.
Angry Bird Tephra	18.38	34.8	5.57	37.26	7.06	21.26			20.73-22.91	1.13-1.60	21.93-23.69	14.1.2.A, 13.1.2B	16.77051, 62.16901	A sequence of metre-scale, normally graded pumice rich lapilli stones that grade into a pink ash. Pumice clasts are white with a flattened shape, most glass has altered to clays. Lithic breccia lenses can be found interleaving lapillistone beds. Underlying is a >4 m thick porphyritic lava flow, that has a purple colour.
South Lime Kiln Bay Tephra	16.42	33.89	4.83	11.57	9.41	18.13	0.26-0.36	1.22-1.63				11.1.4C	16.74799, 62.23473	A medium lapillistone with some more ash rich horizons. The unit is made up of 10-90% buff pumice clasts, 10-80% lithic clasts, and 10-90% medium-coarse ash. Clasts are typically 1-2 cm in size, but clasts up to 15 cm are found.

Table 3: Summary of chemistry and lithology of the pumiceous units identified around Centre Hills

Sample	Unit	SiO_2	TiO_2	Al_2O_3	Fe_2O_3	MnO	MgO	CaO	K_2O	Na_2O	P_2O_5	Mg#
3.1.8C	Attic	65.39	0.42	16.72	5.13	0.14	1.99	5.77	1.12	3.22	0.11	43.49
8.1.1A	Attic	65.36	0.41	16.37	5.32	0.16	2.13	5.49	1.10	3.54	0.12	44.19
3.1.2 A	Woodlands	62.27	0.54	17.77	6.23	0.15	2.38	6.44	0.91	3.26	0.05	43.08
5.1.1B	Woodlands	61.33	0.61	17.64	6.88	0.16	2.51	6.57	0.91	3.29	0.10	41.88
3.4.2H	Bunkum Bay	62.87	0.46	17.56	5.58	0.14	2.30	6.25	1.04	3.73	0.09	44.91
13.4.1E	Statue Rock	58.66	0.59	19.38	7.68	0.18	2.46	6.95	0.60	3.40	0.10	38.85
BP 1	Bransby Point	61.60	0.53	17.65	6.79	0.16	2.24	6.77	0.90	3.26	0.13	39.50
BP 2	Bransby Point	59.14	0.53	17.45	7.02	0.18	2.87	7.07	0.87	4.34	0.15	44.74
7.1.1A	Garibaldi Hill	60.90	0.55	18.81	6.65	0.15	2.48	6.34	0.83	3.22	0.06	42.49
5.2.3 E	Garibaldi Hill	60.98	0.56	17.51	6.98	0.18	2.52	6.96	0.80	3.35	0.16	41.73
15.1.3A	Bramble	62.27	0.54	17.74	6.22	0.15	2.36	6.46	0.91	3.29	0.05	42.94
4.2.3G	Old Road Bay	61.04	0.56	17.76	6.60	0.17	2.52	6.78	0.86	3.55	0.17	43.01
9.2.1 G	Old Road Bay	59.86	0.57	19.15	6.69	0.15	2.45	6.93	0.70	3.44	0.07	42.02
13.1.1 A	Old Road Bay	60.91	0.54	17.64	6.71	0.17	2.59	6.96	0.85	3.50	0.14	43.29
13.1.2 B	Angry Bird	52.30	0.84	21.29	10.42	0.32	4.59	7.41	0.24	2.46	0.13	46.61
11.1.4C	South Lime Kiln Bay	61.98	0.51	17.43	6.43	0.18	2.53	6.58	0.78	3.42	0.15	43.82
9.1.2 A	Unnamed	62.13	0.51	17.87	6.00	0.17	2.25	6.48	0.92	3.60	0.08	42.65
2.1.2 A	Unnamed	59.22	0.56	19.02	7.40	0.19	2.62	6.75	0.72	3.40	0.11	41.24
7.3.2C	Unnamed	61.94	0.53	17.90	6.06	0.15	2.28	6.77	0.91	3.36	0.11	42.72
5.2.1 D	Unnamed	58.27	0.86	15.30	9.45	0.21	4.99	7.14	1.16	2.44	0.17	51.12
9.2.1 E	Unnamed	58.21	0.68	19.38	9.32	0.17	2.99	5.89	0.28	3.00	0.09	38.82
12.1.4 B	Unnamed	56.80	0.72	18.67	7.42	0.14	3.45	8.54	0.90	3.23	0.11	47.95
16.1.2 A	Unnamed	60.19	0.52	17.86	6.52	0.16	2.56	6.83	0.84	4.38	0.14	43.69

Table 4: Whole rock major element data from XRF (wt.%).

Sample	Unit	Y	Sr	Ta	Nb	La	Ce	Pr	Nd	Sm	Eu	Dy	Ho	Er	Tm	Yb	Lu	Hf	Th
3.2.1F	Attic	15.28	253.8	0.349	3.166	11.55	22.86	3.026	11.71	2.395	0.817	2.304	0.504	1.511	0.243	1.692	0.281	2.09	2.869
8.1.1A	Attic	16.05	256.9	0.614	3.501	12.85	26.72	3.26	12.5	2.519	0.811	2.369	0.515	1.552	0.252	1.808	0.303	2.243	3.325
3.1.8C	Attic	17.05	277.8	0.412	3.289	12.66	26.48	3.236	12.59	2.625	0.83	2.518	0.545	1.628	0.261	1.843	0.311	3.097	3.921
10.1.1 A	Woodlands	22.36	241.1	0.441	3.361	10.84	22.96	3.138	12.87	2.933	0.961	3.323	0.73	2.206	0.361	2.593	0.429	3.399	3.339
3.1.2 A	Woodlands	21.83	251.5	0.3	2.985	10.77	22.73	3.05	12.83	2.924	0.932	3.215	0.695	2.103	0.338	2.381	0.385	3.305	2.878
5.1.1B	Woodlands	21.07	250.8	0.38	3.04	10.87	24.32	3.105	12.75	2.904	0.935	3.197	0.692	2.086	0.334	2.338	0.38	3.03	2.75
5.1.1A	Woodlands	21.66	239.4	0.291	3.087	10.53	23.12	3.09	12.87	2.989	0.935	3.307	0.727	2.148	0.347	2.435	0.401	2.867	2.46
3.4.2H	Bunkum Bay	15.99	249	0.713	2.72	11.04	21.19	3.078	12.23	2.587	0.809	2.501	0.525	1.529	0.243	1.717	0.274	1.855	2.606
6.1.2 A	Bunkum Bay	18	216.8	0.304	2.928	9.446	20.74	2.918	12.18	2.734	0.83	2.934	0.628	1.879	0.297	2.089	0.338	2.566	2.003
4.2.5I	Foxes Bay	28.05	260.7	0.357	3.352	12.34	27.04	3.71	15.64	3.643	1.101	4.144	0.919	2.729	0.436	3.052	0.491	3.31	2.941
13.4.1E	Statue Rock	27.29	235.3	0.297	2.808	9.906	21.56	3.21	13.81	3.306	1.063	3.954	0.861	2.599	0.404	2.736	0.45	2.885	2.187
2.1.2B	Old Road Bay tuff	17.38	284.3	0.357	2.64	10.2	22.04	2.753	11.09	2.458	0.849	2.611	0.57	1.692	0.276	1.889	0.305	1.927	2.214
9.2.1 C	Garibaldi Hill	25.91	235.5	0.528	3.17	11.61	24.36	3.542	14.77	3.467	0.997	3.823	0.836	2.515	0.404	2.828	0.46	3.009	2.693
7.1.1A	Garibaldi Hill	24.55	238.7	1.684	3.132	12.21	23.49	3.544	15.08	3.42	1.018	3.696	0.806	2.388	0.383	2.699	0.439	3.04	2.754
4.1.4H	Garibaldi Hill	24.98	271.4	0.337	3.08	10.47	24.18	3.272	13.9	3.353	1.059	3.88	0.843	2.534	0.401	2.832	0.452	2.838	2.098
5.2.3 E	Garibaldi Hill	25.01	278.8	1.312	3.095	11.34	25.48	3.373	14.23	3.362	1.089	3.754	0.824	2.478	0.393	2.701	0.438	3.235	2.465
11.1.3 B	Garibaldi Hill	26.5	261.8	0.29	2.713	12.61	24.58	3.483	14.71	3.308	1.006	3.927	0.856	2.542	0.402	2.77	0.439	2.655	2.357

15.1.3A	Bramble	22.31	246.8	0.335	2.725	10.1	22.67	3.113	13.19	3.064	0.955	3.404	0.727	2.187	0.352	2.417	0.389	2.651	2.033
16.1.4C	Bramble	19.41	256.1	0.943	2.605	9.011	20.2	2.855	12.23	2.875	0.936	3.016	0.64	1.906	0.306	2.104	0.337	2.387	1.744
14.1.2 B	Bramble	20.38	211.6	0.473	2.7	9.841	21.9	2.886	12	2.741	0.84	3.056	0.667	2.009	0.324	2.223	0.352	2.673	2.31
9.2.1 H	Old Road Bay	21.71	244.4	0.269	2.431	9.483	20.34	2.886	12.13	2.906	0.87	3.303	0.709	2.116	0.332	2.305	0.37	2.568	2.15
9.2.1F	Old Road Bay	20.25	257.2	0.268	2.805	9.332	21.27	2.808	12.13	2.9	0.968	3.172	0.678	2.02	0.327	2.279	0.36	2.866	2.09
9.2.1 G	Old Road Bay	20.97	301	0.27	2.865	8.883	19.99	2.639	11.38	2.821	0.969	3.219	0.711	2.126	0.347	2.431	0.393	3.077	2.213
11.1.1A	Old Road Bay	19.56	220.9	0.414	2.684	10.12	22.28	2.835	11.64	2.645	0.839	2.975	0.64	1.934	0.312	2.192	0.354	2.73	2.536
4.2.3G	Old Road Bay	20.35	233	1.315	2.721	8.985	20.67	2.789	11.95	2.841	0.912	3.306	0.706	2.139	0.343	2.393	0.387	2.04	1.569
13.1.2 B	Angry Bird	34.8	236.7	0.549	3.751	15.06	26.34	4.322	18.38	4.592	1.407	5.567	1.175	3.43	0.536	3.686	0.576	3.285	2.971
11.1.4C	South Lime Kiln Bay	33.89	262.8	0.284	2.944	10.64	24.43	3.606	16.42	4.157	1.189	4.828	1.036	3.104	0.482	3.296	0.517	2.885	2.202
9.1.2 A	Unnamed	31.07	236.9	0.351	3.001	11.1	23.33	3.822	17.43	4.261	1.223	4.613	1.023	3.181	0.525	3.794	0.639	2.871	2.577
7.3.2C	Unnamed	29.41	232.9	0.406	2.954	15.09	23.41	4.51	19.57	4.34	1.282	4.352	0.953	2.768	0.442	3.011	0.483	2.63	2.505
12.1.6C	Unnamed	18.39	226.7	0.441	2.823	8.002	17.36	2.299	9.956	2.408	0.88	2.832	0.614	1.851	0.296	2.098	0.337	2.804	2.058
16.1.5D	Unnamed	20.69	223.6	0.237	2.526	9.436	20.74	2.952	12.72	2.94	0.895	3.169	0.677	1.997	0.328	2.224	0.357	2.424	1.866
2.1.2 A	Unnamed	20.73	282.8	0.306	2.834	9.032	20.96	2.894	12.7	2.999	1.057	3.231	0.692	2.062	0.329	2.26	0.37	2.812	1.93
4.2.3F	Unnamed	21.97	273.1	1.25	2.493	9.313	21.21	2.907	12.66	3.143	1.004	3.502	0.741	2.224	0.346	2.335	0.364	2.484	1.899
16.1.2 A	Unnamed	16.3	196.6	0.22	2.315	7.361	16.85	2.247	9.385	2.245	0.738	2.522	0.545	1.669	0.262	1.848	0.305	2.093	1.534
9.2.1 E	Unnamed	16.27	224.3	0.354	2.858	7.178	19.18	2.408	10.34	2.492	1.131	2.69	0.56	1.647	0.262	1.861	0.299	2.274	1.818
12.1.1A	Unnamed	16.08	326.7	0.321	1.531	6.008	13.24	1.778	7.862	2.082	0.771	2.7	0.569	1.612	0.24	1.594	0.242	1.18	1.242

Table 5: Whole rock trace element chemistry from ICP-MS (ppm, BP data is from Cassidy *et al.*, 2012)

3.1.1 Major elements

Bulk pumice samples from all units span 52.8-65.4 wt.% SiO_2, and are mostly andesitic, with tholeiitic and medium K-series trends (<1 wt.% K_2O) (Figure 6, Table 4). Whole rock major elements plotted against silica content lie on well-defined fractionation trends; thus, much of the observed chemical variation can be attributed to fractional crystallisation processes (Figure 6). The compositions analysed here are similar to previously reported data from lavas from both Centre Hills (52.8- 60.8 wt.% SiO_2) and Soufrière Hills (53.7-63.8 wt.% SiO_2) (Zellmer *et al*., 2003; Cassidy *et al*., 2012;). There is no apparent temporal variation in major element compositions (Figure 7), except for a general trend towards more potassic compositions in younger units (Figure 7). Low Al_2O_3 (<17 wt.%) is only found in the dacitic samples (the Attic tephra) (Figure 7). The Angry Bird tephra has a distinctive, mafic composition (~52 wt.% SiO_2), with MgO > 4.5 wt.% (Figure 6). This magma composition is unusual for a widely distributed pumiceous fall deposit. The Attic tephra is the only dacitic unit identified in this study, with low MgO (~ 2 wt.%) and CaO (<6 wt.%) contents (Figure 6).

The Bransby Point tephra is thickest (~2 m) to the south of Centre Hills. This could suggest that the unit may not be from Centre Hills, but from a more southerly vent site, perhaps associated with magmatic activity in the uplifted region around Garibaldi Hill. Nevertheless, the Bransby Point Pb-isotope composition is consistent with a Centre Hills origin, which supports a direct relationship with the Centre Hills magmatic system (Cassidy *et al*., 2012). Ar-Ar ages show that the unit is older than Soufrière Hills Complex, and the wide shelf around this southwest corner of Montserrat (Le Friant *et al*., 2004) indicates that this part of the island is similar in age to Centre Hills, even though it lies far to the south. This suggests that vent sites of Centre-Hills age may have existed in the southern part of Montserrat, but may now be buried by younger Soufrière Hills deposits.

Subtle differences in CaO and Na_2O contents can help distinguish individual units (Table 4, Figure 6). For example, the Woodlands Bay tephra, Statue Rock tephra, Garibaldi Hill tephra, and Old Road Bay tephra are compositionally similar, but

the Woodlands Bay tephra has a lower CaO content, and the Old Road Bay tephra and Statue Rock tephra have higher Na_2O contents (Figure 6). These differences likely reflect the degree of plagioclase fractionation, a major phenocryst phase in the Centre Hills eruptive products.

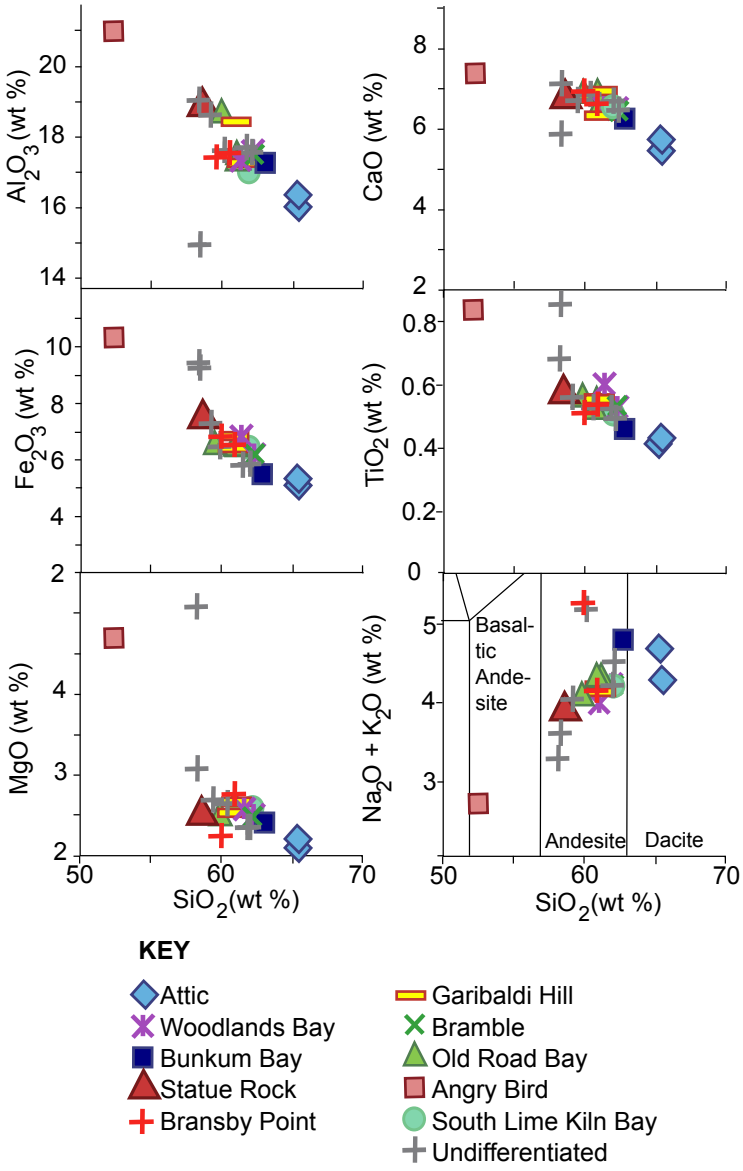

Figure 6: Whole rock major element compositions plotted against silica for selected pumice samples from Centre Hills. Most units have similar compositions and plot along a fractional crystallisation trend. Bottom right is a TAS plot.

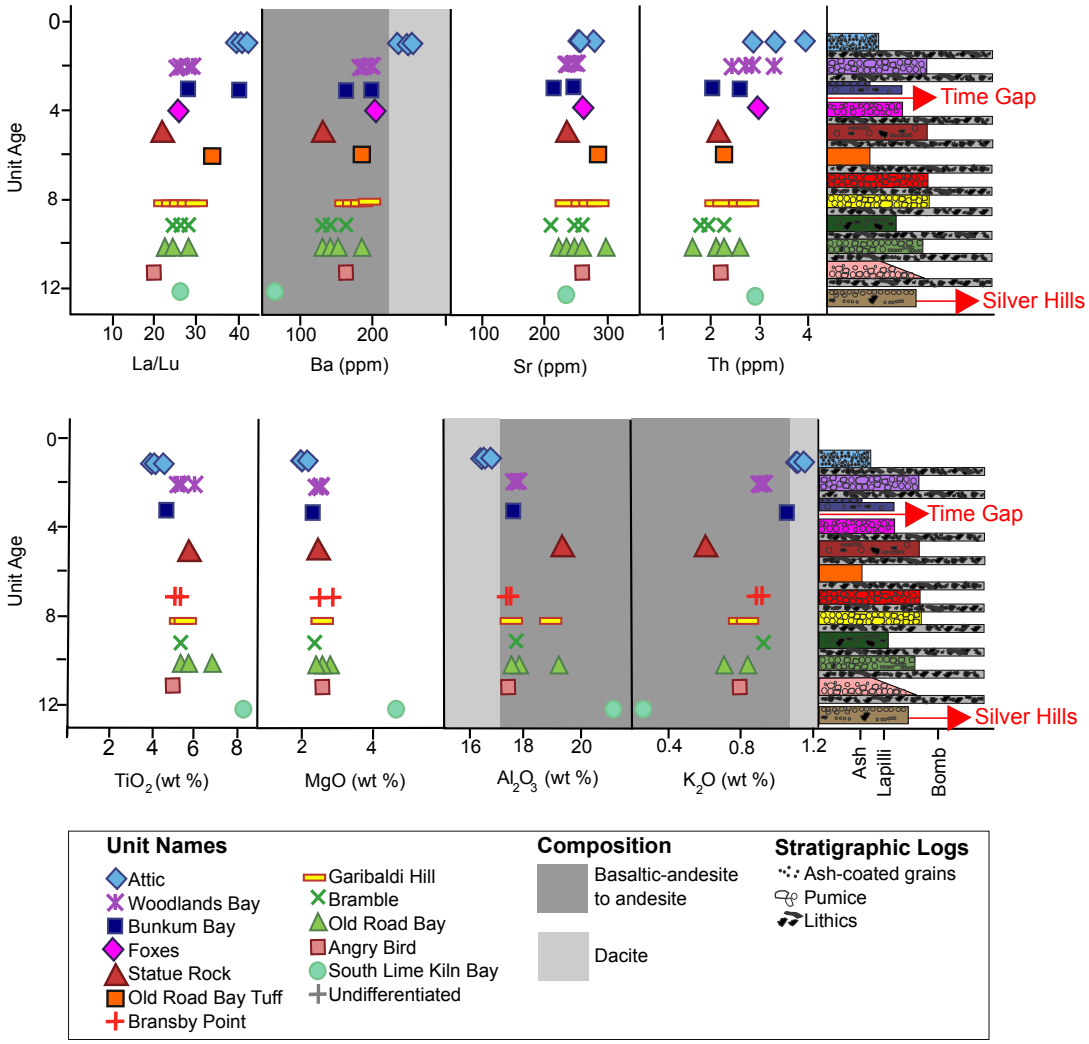

Figure 7: Comparisons of a range of element concentrations with relative unit age (oldest unit has relative unit age of 12). Upper panel are whole rock trace elements, lower panel are whole rock major elements. Also shown to the right of each panel is a summary stratigraphic log.

3.1.2 Trace elements

Whole rock trace element compositions of Centre Hills units show more inter-unit variation than major element compositions and are useful for distinguishing

units (Figure 8). Nd and Y are particularly useful in this regard (Figure 8, Table 5). For example the Bunkum Bay and Attic tephras are distinguished from the rest of Centre Hills deposits by a higher Nd enrichment relative to Y (Figure 8).

Some temporal variation in trace element chemistry across the Centre Hills units is observed (Figure 7). Younger eruptive products are depleted in HREEs (heavy rare earth elements), resulting in higher La/Lu ratios (Figure 7), and enriched in HFSEs (high field-strength elements) such as Th (Figure 7). LILE (large ion lithophile elements) concentrations are similar across all Centre Hills deposits, with higher Ba in more evolved (e.g. Attic dacite) units (Figure 7).

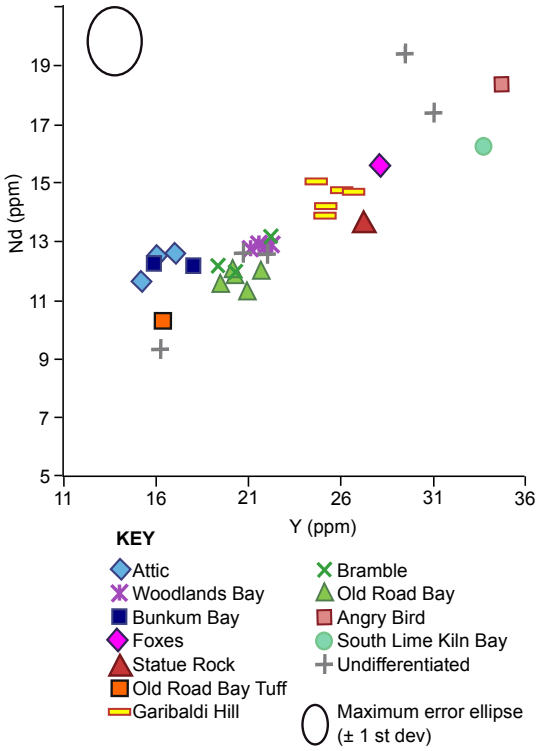

Figure 8: Whole rock trace element data for selected pumice and tuff samples from Centre Hills. Most units have similar trace element compositions, however units have distinct Nd/Y compositions.

3.1.3 Mineral and glass chemistry

The pre-eruptive state of a magma reservoir and the conditions during ascent are likely to vary between eruptions, even for stable volcanic systems, and may impose slight variations in bulk magma chemistry between eruptions. These

small chemical differences are useful for spatial correlation of explosive eruption deposits. Groundmass glass chemistry is widely used for this purpose (Lowe, 2011; Tomlinson *et al.*, 2014), but glass chemistry may also vary within an individual eruption due to crystallisation during magma ascent (Blundy and Cashman, 2001). Late stage diffusive re-equilibration of compatible elements such as Fe or Na can also result in complications when identifying eruption deposits using glass chemistry. Thus, in analysing matrix glass, we focus on less compatible elements such as TiO_2 and K_2O.

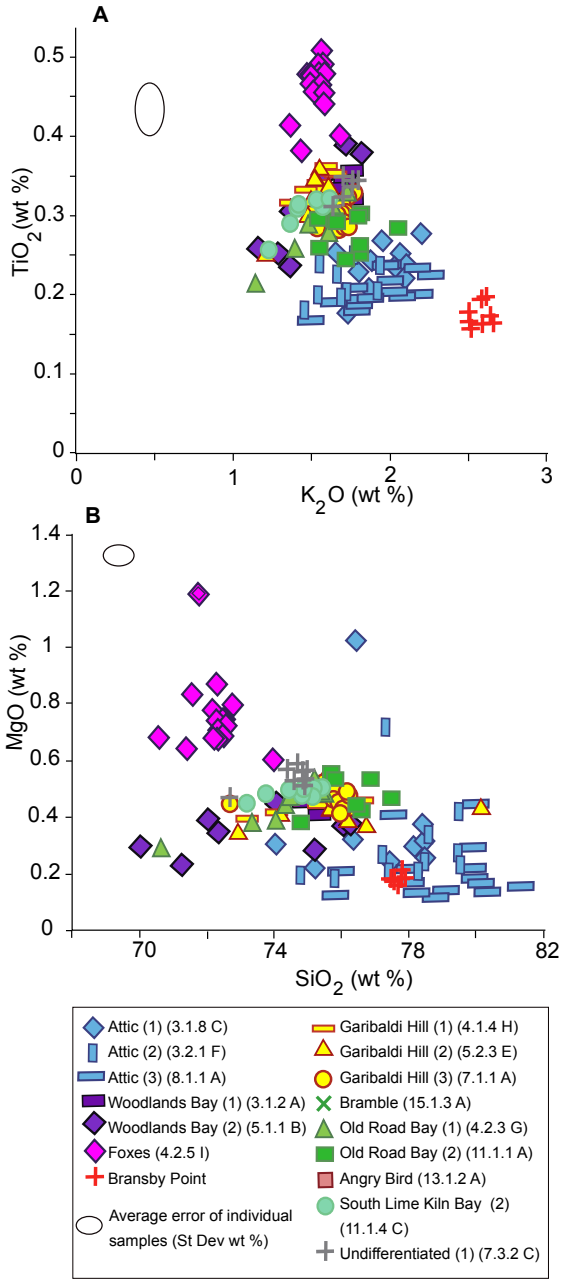

Figure 9: Major element glass composition of pyroclastic units from Centre Hills, measured using EMP. Figures A and B show small compositional differences in glass composition between units.

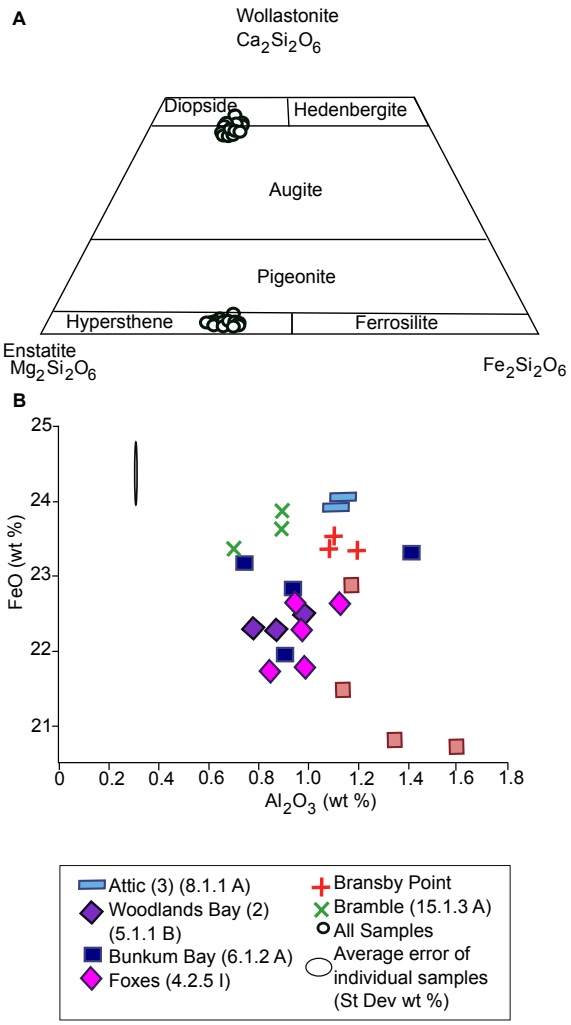

Figure 10: Major element analyses of pyroxene using EMP analyses. 10A is a ternary diagram of pyroxene showing a population of orthopyroxene and clinopyroxene phenocrysts. Chemistry of pyroxene crystals is broadly similar between units. 10B shows the chemistry of the rims of clinopyroxene phenocrysts. Some units have phenocrysts of clinopyroxene with rims of distinct chemistry.

K_2O concentrations can be affected by weathering, but we used only pristine samples with no visible signs of weathering. Samples typically formed tightly clustered K_2O compositions (Figure 9), suggesting little secondary alteration (weathering), with the exception of the Bunkum Bay tephra (this unit is therefore excluded from glass-compositional plots).

Glass compositions are similar across all units (70-80 wt.% SiO_2), with small differences in TiO_2, K_2O and MgO (Figure 9). The Garibaldi Hill tephra, Woodlands tephra, Foxes tephra, Ashoks tephra, and Old Road Bay tephra cannot easily be distinguished (Figure 9), although the Foxes tephra has slightly higher TiO_2 (0.47 wt.%) contents. The Attic tephra has higher SiO_2 (78 wt.%) and K_2O (~2 wt.%) and a lower TiO_2 (0.2 wt.%) content than many other units. The Bransby Point tephra is also distinctive in having a high K_2O content (~2.5 wt.%; Figure 9).

Phenocrysts are compositionally similar within all of the analysed units and occupy narrow compositional ranges. Orthopyroxenes are all Fe-rich hypersthene. Their cores have $Fs_{33-38}En_{59-65}Wo_{1-5}$ (n=30) compositions, whereas their rims have $Fs_{34-38}En_{60-64}Wo_{1-2}$ (n=29) compositions (Figure 10a). Clinopyroxenes are mostly Fe Diopside or high Ca Augite with core compositions of $Fs_{15-18}En_{39-41}Wo_{43-44}$ (n=32), with rims of $Fs_{15-18}En_{38-41}Wo_{43-47}$ (n=27) (Figure 8a). Plagioclase compositions range from An_{77-91} (n=34) in cores to An_{79-94} (n=28) in rims. No significant compositional zoning is observable in pyroxene phenocrysts from the units analysed. Plagioclase phenocrysts are varied and complex, exhibiting oscillatory, normal and reverse zoning. The Attic tephra is the only unit to contain amphibole instead of augite. Amphiboles have Al♯ 0-0.01 ($Al♯= [Al]^6/Al^{Total}$) (n=14) and are classified as magnesiohornblende.

Orthopyroxene crystals show trace variations in chemistry between the major stratigraphic units from Centre Hills (Figure 10b). Between units, variations in Al_2O_3 and Fe_2O_3 (0.1wt.% and 1 wt.% respectively) are observable in orthopyroxene rims, and are useful for identifying individual eruptive units, particularly distinguishing the Bramble tephra from Woodlands Bay tephra. The Attic and Bramble tephra units have higher FeO/Al_2O_3 ratios than the other analysed units (Figure 10b).

Pre-eruptive magma storage temperatures have been estimated using amphibole, orthopyroxene-liquid, clinopyroxene-liquid, and plagioclase-liquid geothermobarometry based on phenocryst and glass compositions (Ridolfi *et al.*, 2010; Putirka *et al.*, 2003, 2005, 2008). Different geothermometers have been

used, depending on the phases present, and results of different methods cannot necessarily be directly compared. For the Attic tephra, amphibole geothermometry indicates temperatures of 812-852°C (n=10). Higher temperatures are derived from an orthopyroxene-melt geothermometer for the South Lime Kiln Bay tephra (947-1080°C (n=13)) (note that orthopyroxene rims could not be used for any other units, because they did not pass a melt equilibrium test based on $Kd_{(Fe-Mg)}$). Clinopyroxene-melt geothermometers (conducted on rims that pass the $Kd_{(Fe-Mg)}$ equilibrium test) indicate a broad temperature range between 894-1022°C (n=7), using Putirka *et al*. (1996) pressure independent equations. Slightly higher temperatures are produced from plagioclase-melt geothermometers (1003-1032°C; n=17) (only plagioclase rims that passed the $Kd_{(Ab-An)}$ equilibrium test) (Putirka *et al*., 2005).

3.2 Ages

The Angry Bird tephra is stratigraphically the oldest unit studied here, but the unit is mostly altered to clays and is thus unsuitable for Ar-Ar dating. The oldest dated pyroclastic unit is the South Lime Kiln Bay tephra at 1.31 ± 0.21 Ma (Figure 11; all errors quoted at 2σ level); this age overlaps with activity at Silver Hills (Harford *et al*., 2002), and Silver Hills is thus a potential source for the unit. The next oldest pyroclastic deposits are found at Garibaldi Hill and Bransby Point with Ar-Ar ages of ~0.7 Ma (Figures 11 and 12). Stratigraphic relationships on the west coast suggest that the youngest deposits are found further north (Figure 12) and are dated at ~0.5 Ma (Figure 11). On the east coast, stratigraphic relationships indicate the youngest pyroclastic deposits outcrop at Statue Rock (Figure 13).

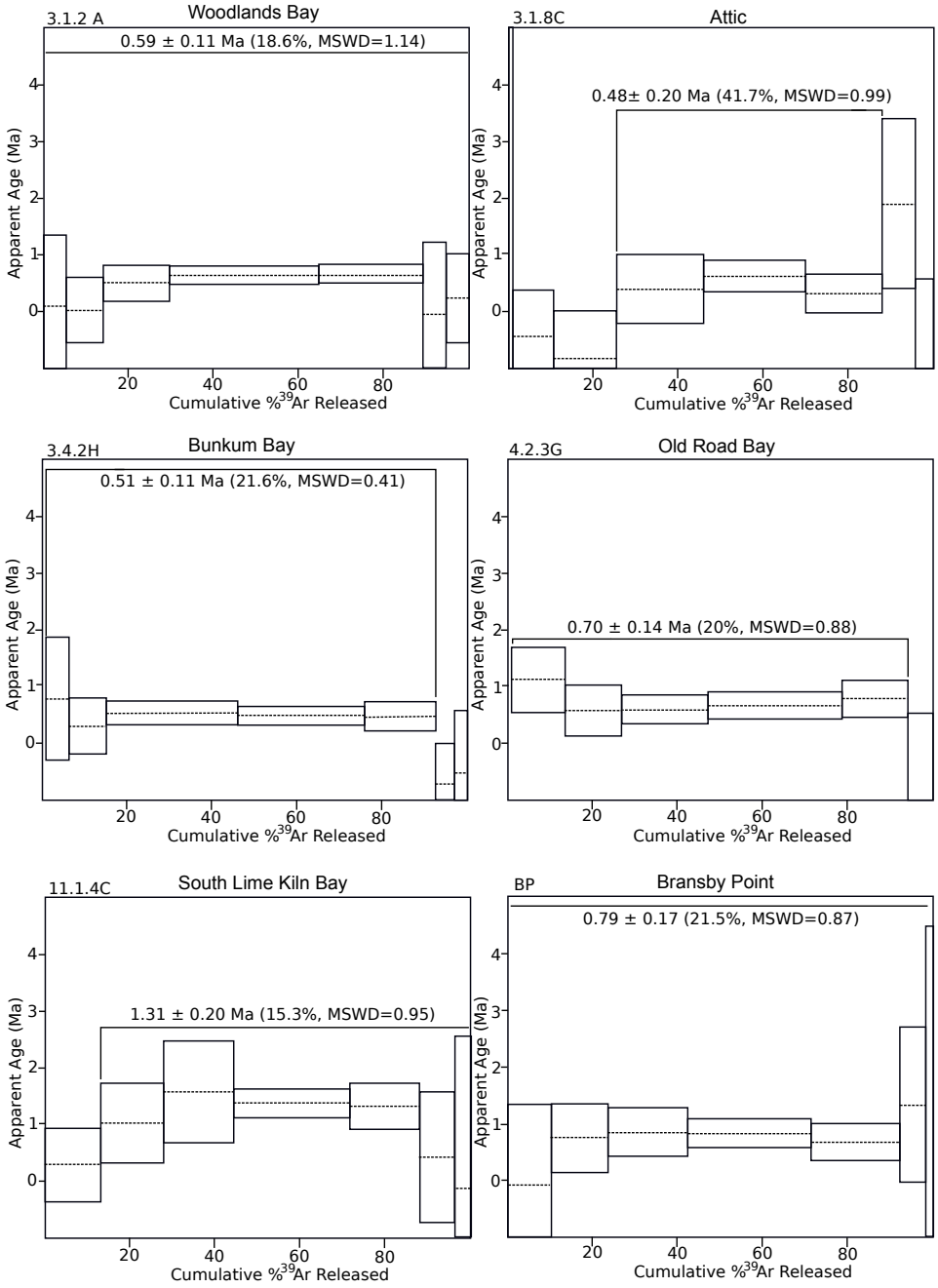

Figure 11: Ar-Ar plateau of apparent age plotted against cumulative percentage of Ar released. Dashed lines show mean apparent age and solid lines show errors to 2 σ. Data used to estimate ages are shown above.

Within error, the dates are consistent with the stratigraphic order of the units, but suggest that some units are closely spaced in time. For example, the Bransby Point tephra is stratigraphically above the Old Road Bay tephra, but dated at 0.79 ± 0.13 Ma, whereas the Old Road Bay tephra is dated at 0.7 ± 0.14 Ma (Figures 11 and 12). The ages are within error suggesting similar ages for the two deposits. This study provides ages for Centre Hills deposits from 0.8 ± 0.2 Ma to ~0.48 ± 0.2 Ma, consistent with previous dates obtained by Harford *et al*. (2002; ~0.98 Ma to ~0.52 Ma).

3.3 Stratigraphy

The stratigraphy of Centre Hills is composed of thick (up to 15 m) pyroclastic-rich sequences preserved between sequences (often >10 m thick) of dense andesite lithic breccias (Figures 12 and 13). Units to the northeast and southwest of the Centre Hills are laterally continuous across a few hundred metres. To the west, northwest and southeast, units are not as laterally continuous, because channels filled with lithic breccias truncate the pyroclastic units through erosive discordances. Eleven pyroclastic units are identifiable across Centre Hills (Figures 12 and 13) and have been confirmed as separate units by geochemical and age data (Figures 6-11) (see Sections 4.1 and 4.2 above). Other pumiceous units occur (Figures 12 and 13), but these cannot be correlated across the island due to their poor preservation and limited outcrop.

We describe each of the 11 main pyroclastic units in approximate stratigraphic order (noting the age for directly dated units), and we also describe the oldest observed unit, which may be from Silver Hills. For more detailed lithofacies descriptions we refer the reader to Table 6.

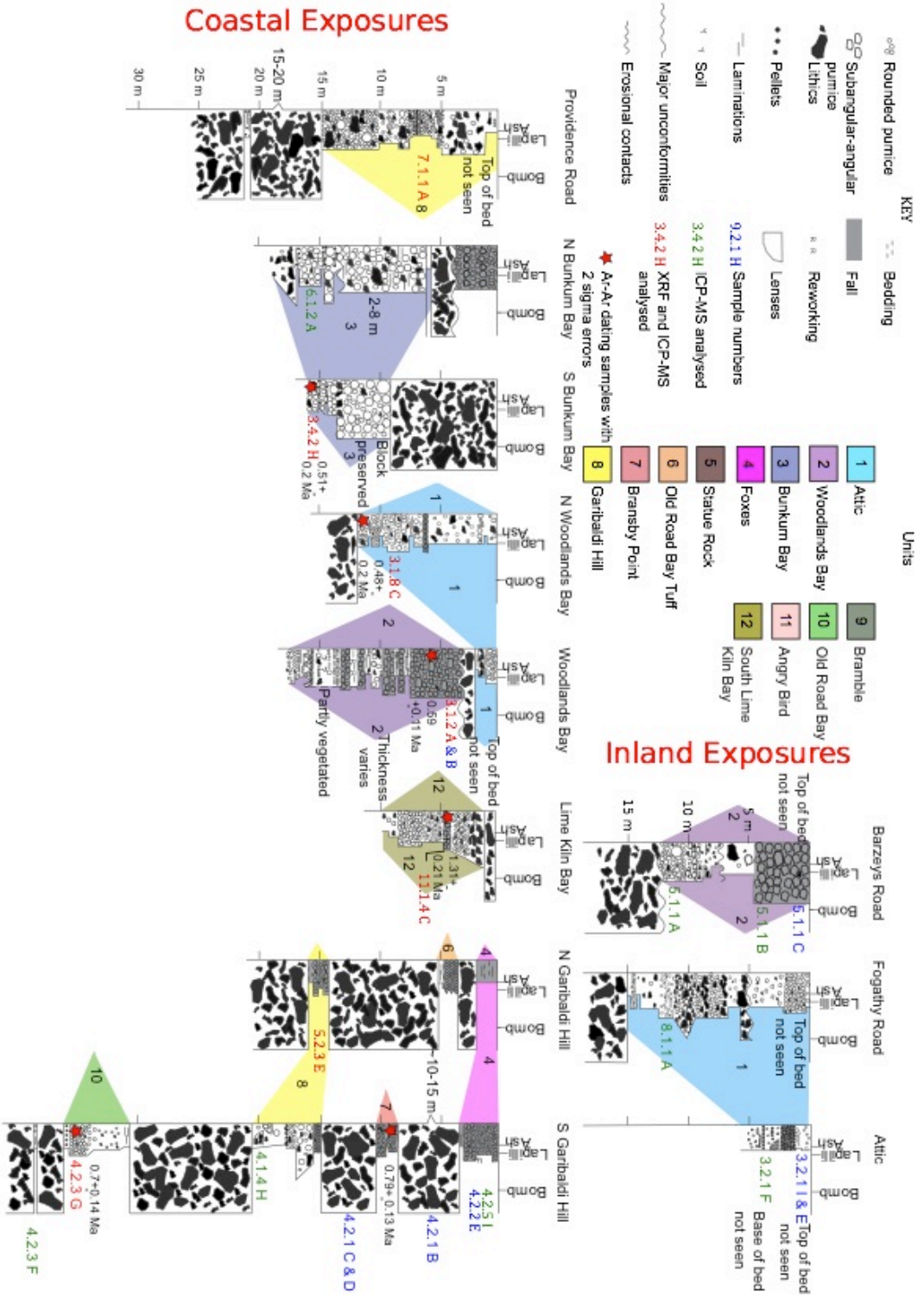

Figure 12: Stratigraphy for the W coast of Montserrat. Varying the density of the clast symbols shows composition and concentration of each unit. Colours and numbers indicate possible correlations.

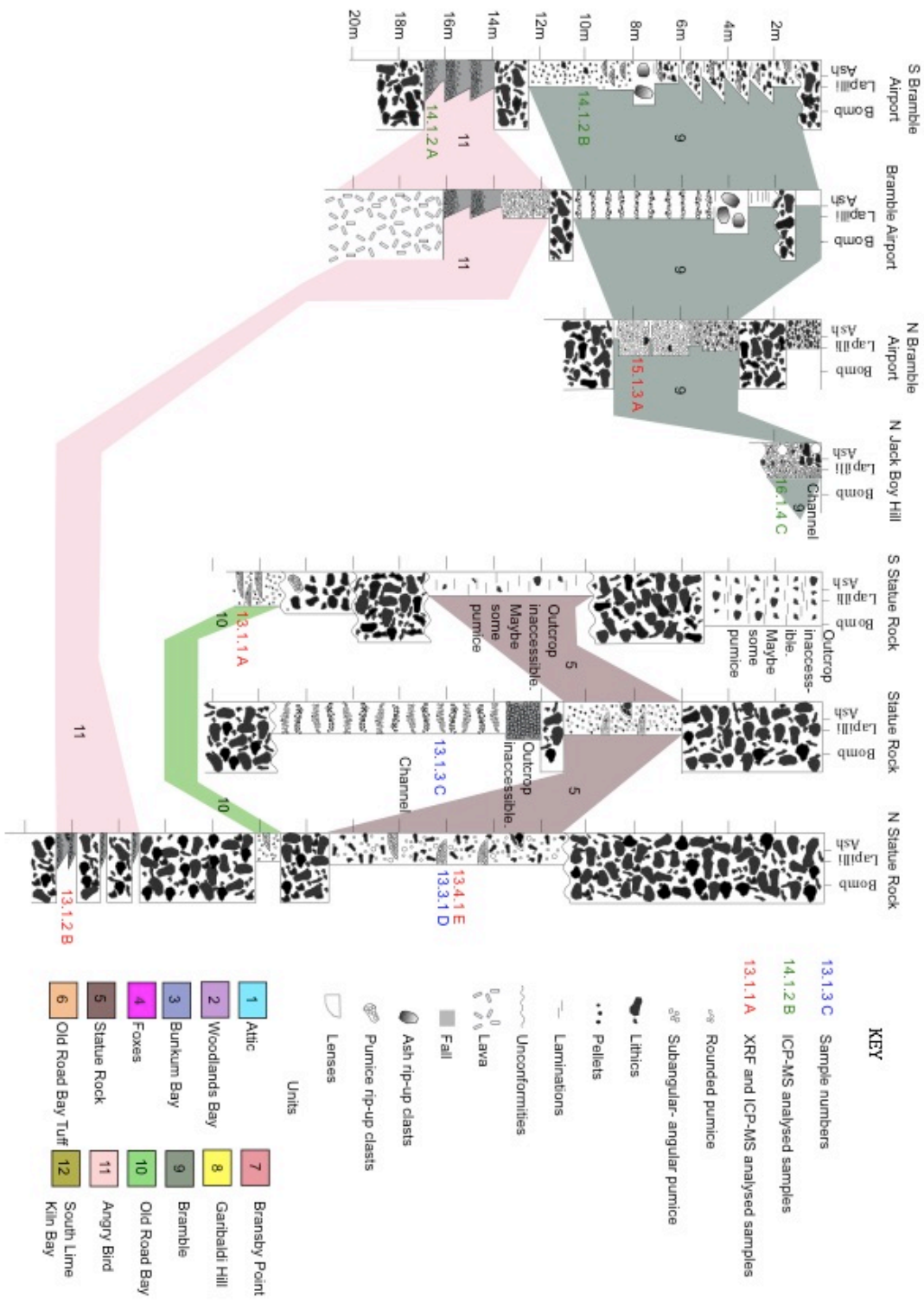

Figure 13: Stratigraphy for the W coast of Montserrat. Varying the density of the clast symbols shows composition and concentration of each unit. Colours and numbers indicate possible correlations.

Facies	Lateral variation	Log site name (figures 12 and 13) and grid reference.	Sample names	Lithofacies		Thickness, grading and large-scale features	Clast and Lithology	Primary/ reworked	Interpretation
					West Coast				
Attic Tephra	Laterally continuous as road cut by the Attic café	Attic; N 16.75413; E 62.22226	3.2.1 I and E	Cross-bedded tuff	Upper	1.2 m, massive, with cross-bedded base.	Moderately sorted deposit; subangular-subrounded pumice clasts; composed of 90 vol.% of 2 mm pumice and ash coated grains; pumice clasts up to 1 cm and lithic clasts up to 3 cm; lower part of the subunit contains fewer larger clasts (coarse-tail reverse sorting).	Primary; thick unit and homogeneity of deposit composition.	Low concentration PDC deposit. Presence of sedimentary structures.
				Tuff	Middle	2 m, massive	Well-sorted; contains >90 vol.% of 2 mm pumice and ash-coated clasts.	Primary; thick unit and homogeneity of the deposit composition.	Low-moderate concentration PDC deposit as the unit is well sorted, but there is no development of sedimentary structures. Wet due to ash sticking and coating clasts
			3.2.1 F	Massive lapilli-tuff	Lower	3 m, dm-bedded	Moderately to poorly sorted deposit; variable amounts of pumice clasts, lithic clasts, ash-coated grains, and ash; clasts 2-5 mm in size; single-clast-thick pumice horizons; fewer ash-coated grains at the base of the subunit.	Primary; thick unit.	Moderate concentration PDC deposit due to the development of some 1 clast thick pumice horizons
Woodlands Bay Tephra	Laterally continuous, can be traced along coastal cliffs on the west coast for ~500 m	Woodlands Bay; N 16.76298; E 62.22343	3.1.2 A and B	Bedded lapillistone	Upper	5 m, dm-bedded	Moderately sorted; angular; comprises >95 vol.% pumice clasts (4.5 cm, max 18 cm), and <5 vol.% grey lithic clasts (max 5 cm), and <1 vol.% matrix.	Primary; thick unit and homogeneity of the deposit composition.	Tephra Fall as the unit is moderately sorted, angular and comprises mainly pumice clasts (>90 vol.%).

				Interbedded lapillistone and lapilli-tuff	Middle	7 m, dm-m bedded	Alternating between tuff rich and pumice rich units. Tuff rich units: poor-moderately sorted; subangular; comprises up to 60 vol.% pumice clasts, 10-20% lithic clasts and <40 vol.% ash matrix; clasts are typically 1 cm. Pumice lenses and single clast thick pumice horizons are found. Pumice rich: Moderately sorted, angular; comprise 70-90 vol.% pumice clasts (2-4 cm, max 11 cm), 30 vol.% lithic clasts, and 10 vol.% ash.	Primary; thickness of deposit and abundance of pumice (70-90% throughout the whole unit).	Tephra fall interleaved with moderately concentrated, moderately cohesive PDC deposits due to poor-moderate sorting and relatively high (up to 40 vol.%) ash content. Some fall units maybe reworked by subsequent density currents.
				Lapilli-tuff	Lower	4.5 m, dm-m bedded	Well-poorly sorted, angular-subangular; comprising 20-90 vol.% pumice clasts, 10-50 vol.% lithic clasts and 10-90 vol.% ash; clasts are typically 1-2 cm in size; some pumice lenses are observed.	Primary or reworked; heterogeneous clast compositions.	High concentration PDC deposits or reworked units.
Bunkum Bay Tephra	Outcrops in small pockets (<50 m), but often appears as channelised sequences	N Bunkum Bay; N 16.77193; E 62.22037	6.1.2 A	Lapilli-tuff	Upper	7 m, massive, discordant basal contact.	Poorly-sorted, polymict; composition uncertain as outcrop was inaccessible.	Primary or reworked; heterogeneous clast compositions.	High concentration, cohesive PDC deposits, or reworked material as the unit is poorly sorted with heterogeneous clasts.
				Interbedded lapilli-tuff and tuff channels	Lower	0-7m, channelised deposits.	Alternating units of tuff and lapilli-tuff. Tuff units: moderate-well sorted, laminated with accreationary lapilli-rich (3 mm) and pumice-rich horizons (up to 2 cm in size); 50 vol.% crystal rich (20 vol.%) medium tuff. Lapilli-ash horizons: Poorly-sorted, angular; comprises 65-90 vol.% pumice clasts (5 cm), 5-15 vol.% grey and altered lithic clasts, and <5-20 vol.% coarse crystal rich grey ash	Primary; thick unit and abundance of pumice.	Alternating high and low concentration PDC deposits, or high concentration PDC deposits followed by finer deposits from the waning flow. This would explain alternation between well-sorted, laminated deposits to poorly- sorted deposits. Accretionary lapilli suggestive of a wet depositional environment.

Foxes Tephra	Outcrops on one isolated cliff section andos traceable for ~50 m	S Garibaldi Hill; N 16.72365; E 62.24035	4.2.5 I and 4.2.2 E	Lapillistone	Upper	3 m, massive to dm-bedded.	Well-sorted, angular; comprising >90 vol.% pumice clasts (2-5 mm in size), <1 vol% lithic clasts, and <10 vol.% ash.	Primary; thick unit and abundance of pumice.	Tephra fall as the deposits are well-sorted angular and comprise mainly pumice.
				Tuff	Lower	20 cm, laminated.	Well-sorted, pink, medium ash.	Primary; ash content and homogeneity.	Tephra fall or low concentration PDC deposits as deposits are well-sorted.
Old Road Bay Tuff	Largely traceable from Old Road Bay to Lime Kiln Bay, thinning towards Lime Kiln Bay	N Garibaldi Hill; N 16.73722; E 62.23302		Bedded lapilli-Tuff	Upper	1 m, cm-bedded.	Alternating unit between yellow ash and 1 clast thick pumice layers; well sorted, subangular.	Primary; thick unit that appears compositionally similar.	Tephra fall from pulsed eruption or low concentration density current.
				Tuff	Lower	50 cm, dm-bedded	Top and base are grey, middle is yellow; well sorted, laminated tuff.	Primary; lateral continuity and thick unit.	Tephra fall as units are laterally continuous and well-sorted.
Bransby Point Tephra	Laterally continuous for ~3 km around Bransby Point towards Plymouth	S Garibaldi Hill; N 16.72365; E 62.24035	Mike BP	Massive lapillistone	Upper	1 m, massive	Well-sorted, angular; comprises >90 vol.% of pink coloured pumice clasts (max 4.5 cm), 5 vol.% grey and pink lithic clasts (max 2.5 cm), and 5 vol.% pink ash; discontinuous 1 cm thick ash horizons; top of unit is a ~5 cm thick ash	Primary; lateral continuity and thick unit.	Tephra fall as deposits are well sorted, angular and with a high proportion of tephra deposits
				Massive lapillistone	Lower	1 m, dm-bedded	Well-sorted, angular; comprises >95 vol.% white pumice clasts (max 5 cm), 5 vol.% grey and pink lithic clasts, and <1 vol.% white fine-medium ash; unit is capped by a thin (<10 cm) pink ash.	Primary; lateral continuity and thick unit.	Tephra fall as deposits are well sorted, angular and with a high proportion of tephra deposits

Garibaldi Hill Tephra	Laterally continuous, thickening southwards. Around Garibaldi Hill the unit is tilted	S Garibaldi Hill; N 16.72899 E 62.23521	4.1.4 H	Lapillistone	Upper	50 cm, massive.	Well-sorted, angular; comprises 95 vol.% yellow pumice clasts (max 4 cm), 5 vol.% lithic clasts, and <1 vol.% yellow medium ash.	Primary; thick unit and abundance of pumice.	Tephra fall as deposits are well sorted, angular and with a high proportion of tephra deposits
				Normally graded lapilli-tuff	Lower	5 m, normally graded	Poorly-sorted, subangular-rounded; comprising 50- 80 vol.% pumice clasts (max 12 cm), 5-20 vol.% lithics, and <5- 45 vol.% ash; lithic rich and pumice rich lenses.	Primary; thick unit.	High concentration PDC deposits due to poor-sorting and lack of sedimentary structures. Some subunits may have been cohesive currents given high (>30 vol%) ash contents.
Old Road Bay Tephra	The only unit that outcrops on both the east and west coasts of Montserrat. Unit thickness is variable	S. Garibaldi Hill; N 16.72899; E 62.23521	4.2.3 G	Lapilli-tuff	Upper	3.5 m. massive and normally graded	Moderately-poorly sorted, rounded; comprises 50 vol.% yellow pumice clasts and lithic clasts (difficult to distinguish due to weathering), and 50 vol.% coarse ash.	Primary; thick unit	High concentration PDC deposits as units are poorly sorted, heterogeneous and clasts are rounded.
				Lapillistone	Lower	1.5 m, massive with normally graded top	Moderately sorted, rounded; comprises >90 vol.% yellow pumice clasts (max 7cm), and <10 vol.% white ash.	Primary; unit thickness and a high proportion of pumice (>90 vol.%)	Remobilised tephra fall, or low concentration PDC deposits as deposits are well sorted, homogenous, but clasts are rounded.
				Lapilli-tuff	Middle	<1 m, laminated	Alternating tuff and lapilli; tuff layers are laminated; lapilli bands are more pumice rich at the top of the unit.	Primary; unit thickness.	Tephra fall from pulsed eruption, or series of low-medium concentration PDC deposits s as the deposits are well-sorted.

Lime Kiln Bay Tephra	Only outcrops within a small, downward faulted block	Lime Kiln Bay; N 16.74799; E 62.23473	11.1.4 C	Lapillistone	Upper	>2 m reversely graded	Poorly-sorted, subangular- subrounded; comprises 15-85 vol.% pumice clasts (2cm, max 5 cm), 5-75 vol.% grey, black and purple lithic clasts, and 10 vol.% buff ash. Lithic clast concentration and size increases towards the top.	Primary; The base of the unit has a high proportion of tephra and appears compositionally homogenous, the top of the unit maybe reworked as the deposits decreases in homogeneity.	Lithic-rich, high concentration PDC deposits reworking an underlying tephra fall sequence. The base of the unit is well sorted and primarily comprises pumice, but the upper parts of the unit are increasingly lithic rich, and sorting decreases.
				Lapillistone	Middle	4 m, massive	Sequence of units that have moderate-poor sorting of subangular- subrounded clasts; comprises 75->95 vol.% pumice clasts (2 cm, max 15 cm), 5-10 vol.% assorted lithic clasts and <1-20 vol.% ash.	Primary; unit thickness.	Sequence of tephra fall and high concentration PDC deposits, generating alternating facies of well and poorly-sorted units with subangular-subrounded clasts.
				Lapilli-tuff	Lower	>1 m, massive	Poor-moderately sorted, subangular; comprises 5-30 vol.% pumice clasts (2 cm), 10-40 vol.% assorted lithic clasts (3 cm, max 15 cm), and 60-90 vol.% coarse crystal rich (30. vol%) red ash; fine-grained fiamme (carbonised material).	Primary; presence of carbonaceous material.	Cohesive, high concentration PDC deposits due to poor-moderate sorting, lack of sedimentary structures and high ash contents.
						East Coast			
Statue Rock Tephra	Laterally traceable along the length of the cliff section that forms Statue rock	N Statue Rock; N 16.78158; E 62.17855	13.4.1 E and 13.3.1 D	Lapilli-tuff		10 m, cross-bedded, low-angled bedding, imbrication	Poorly sorted, rounded; comprises 30 vol.% pumice clasts (3 cm), 30 vol.% grey and black lithic clasts (7 cm, max ~1 m) and 40 vol.% coarse ash (ash is made up of ~30 vol.% pyroxene and plagioclase crystals); lithic clast rich lenses and pumice clast rich lenses.	Largely reworked unit; abundance of coarse lithic clasts.	Sequence of high concentration, cohesive PDC deposits due to poor-sorting, lack of sedimentary structures and high ash contents

Bramble Tephra	Outcrops in small (<50 m) pockets	S. Bramble Airport; N 16.76603; E 62.16407	14.1.2 B	Lapilli-tuff		12 m, massive and reversely graded	Poorly-sorted, angular-rounded clast containing units; comprises 5-30 vol.% pumice clasts (1-5 cm in size), 30-50 vol.% lithic clasts, and 40-85 vol.% of grey or orange medium-coarse crystal rich (<30 vol.%) ash; 30-50 cm sized rip up clasts of laminated ash.	Largely reworked unit; abundance of coarse lithic clasts.	Sequence of high concentration, cohesive PDC deposits due to poor-sorting, lack of sedimentary structures and high ash contents
Angry Bird Tephra	Traceable along much of the east coast, but towards the south the unit outcrops in small (<50 m) blocks	Bramble Airport; N 16.77051; E 62.16901		Lapillistone	Upper	4.5 m, massive and normally graded	Moderately-well sorted, angular-subangular; comprises 85 vol.% white pumice (1 cm, max 3 cm) (flattened and altered to clays), 5 vol.% grey and red lithics, and 10 vol.% pink coarse crystal rich (50 vol. %) ash.	Primary; thick unit and high proportion of tephra (85 vol.%)	Tephra fall as units are well-sorted, homogenous, and clasts are angular.
				Lava	Lower	>4 m, massive	Porphyritic lava comprising 35 vol.% plagioclase, 15 vol.% pyroxene, and 50 vol.% pink-purple glass.	Primary; The outcrop appears in-situ as the unit is laterally continuous with no evidence of remobilisation	Lava flow.

Table 6: Description of lithofacies and interpretations of deposit emplacement for the main correlated pumiceous units around Centre Hills.

South Lime Kiln Bay tephra 1.31 ± 0.2 Ma

The South Lime Kiln Bay tephra crops out within a faulted block at Lime Kiln Bay (southwest of Katy Hills) (Figure 14a). The unit is dominantly a medium grained lapillistone including tuff-rich intervals with decimetre to meter scale bedding. The unit comprises 10-90 vol.% pumice clasts, 10-80 vol.% lithic clasts, and 10-90 vol.% medium-coarse ash. This unit is older than other units found to the southwest of Katy Hills and its age overlaps with previous dates for activity at Silver Hills (Harford *et al*., 2002) (Figure 15). The unit may therefore be of Silver Hills origin. Deposits from Silver Hills cannot easily be distinguished from those from Centre Hills based on geochemical indicators (Figure 3) (Cassidy *et al*., 2012).

Angry Bird tephra and lava flow > 1 Ma.

The Angry Bird eruption deposits crop out only on the east coast of Montserrat near Bramble Airport, and around Statue Rock. The Angry Bird tephra is stratigraphically below the Old Road Bay tephra on the east coast and comprises four ~1 m thick lapillistone beds that grade upwards into a medium ash that are interlayered with ~1 m thick lithic breccia lenses. The appearance of the Angry Bird tephra is distinct with a pink coloured medium ash matrix (10 vol.%), flattened white pumice class (85 vol.%) 1-2 cm in size, and 1 cm lithic clasts (5 vol.%) (Figure 16). The glass within the unit is chiefly devitrified to indiscernible clay minerals. A >4 m thick porphyritic lava (Figure 14a) is present at the base of the unit at Bramble Airport. The contact between the lava flow and overlying pumiceous deposits is sharp and apparently conformable, with an absence of interleaving material, thus suggesting that the two deposits were emplaced close in time.

Clay alteration makes accurate determination of whole rock chemistry difficult for this unit. For example, mobile elements such as Ba (67 ppm) have concentrations much lower than the Centre Hills average (175 ppm), which are likely due to secondary chemical alteration processes.

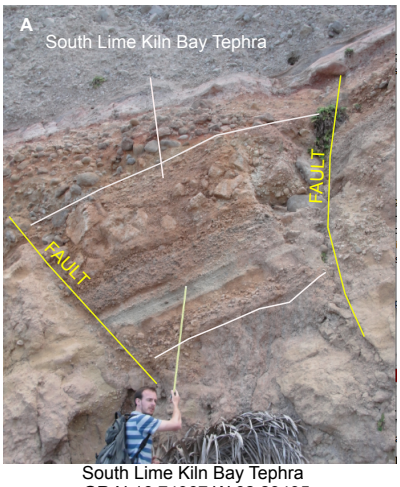

South Lime Kiln Bay Tephra
GR N 16.74967 W 62.23495

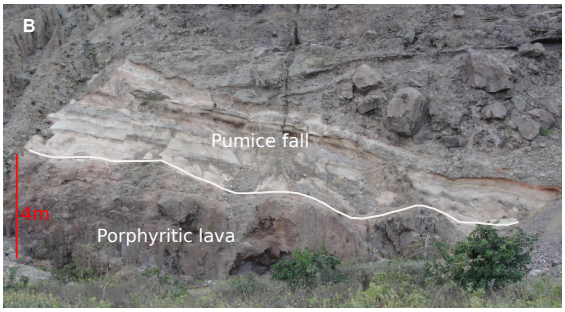

Angry Bird Tephra
GR N 16.77051, W 62.16901

Old Road Bay Tephra
GR N 16.74735 W 62.23485

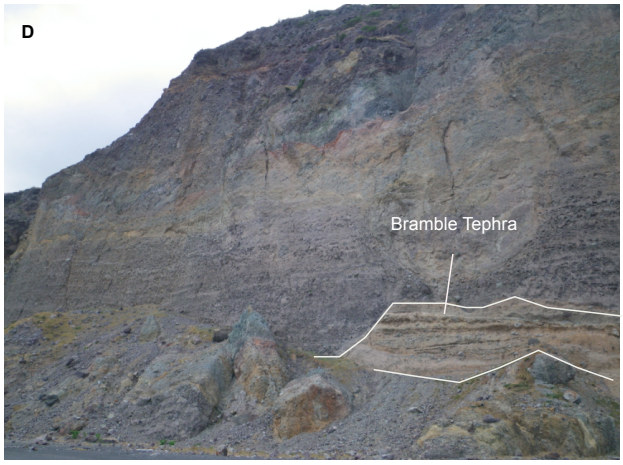

Bramble Tephra
GR N 16.77605 W 62.16952

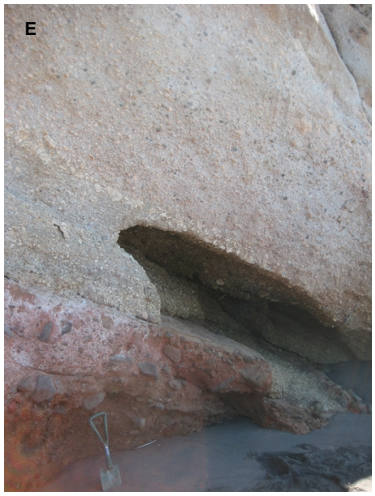

Garibaldi Hill Tephra
GR N 16.74967 W 62.23495

Bransby Point Tephra
GR N 16.72365, W 62.24035

Figure 14: Photos of the oldest units described. 14A shows the faulted block containing the South Lime Kiln Bay tephra. 14b shows the Angry Bird tephra and lava flow. 14C shows the Old Road Bay tephra. 14D shows a preserved block of the Bramble tephra. 14 E and F show the Garibaldi Hill and Bransby Point tephra respectively.

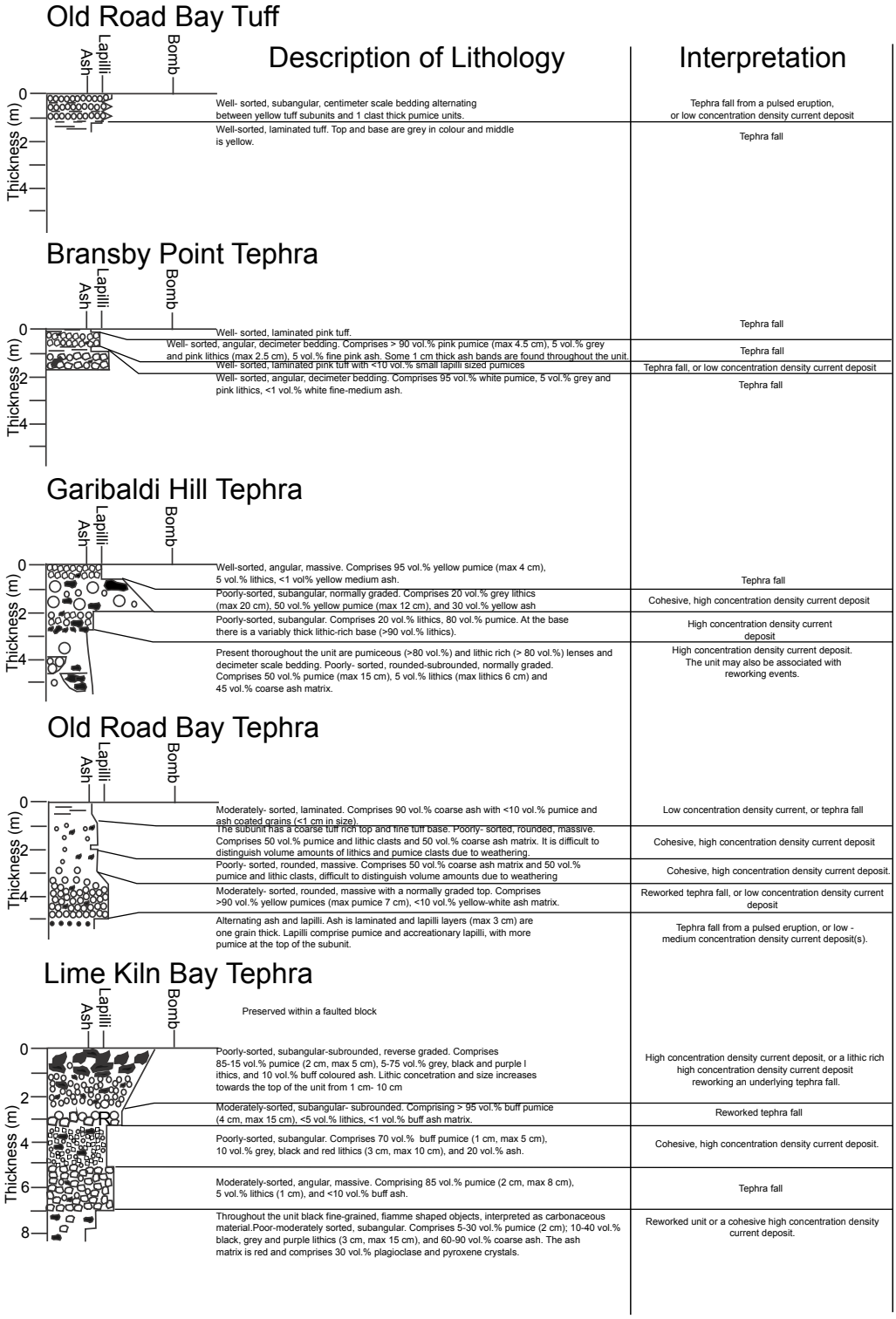

Figure 15: Stratigraphic logs and descriptions of units on the oldest units on the W coast of Montserrat.

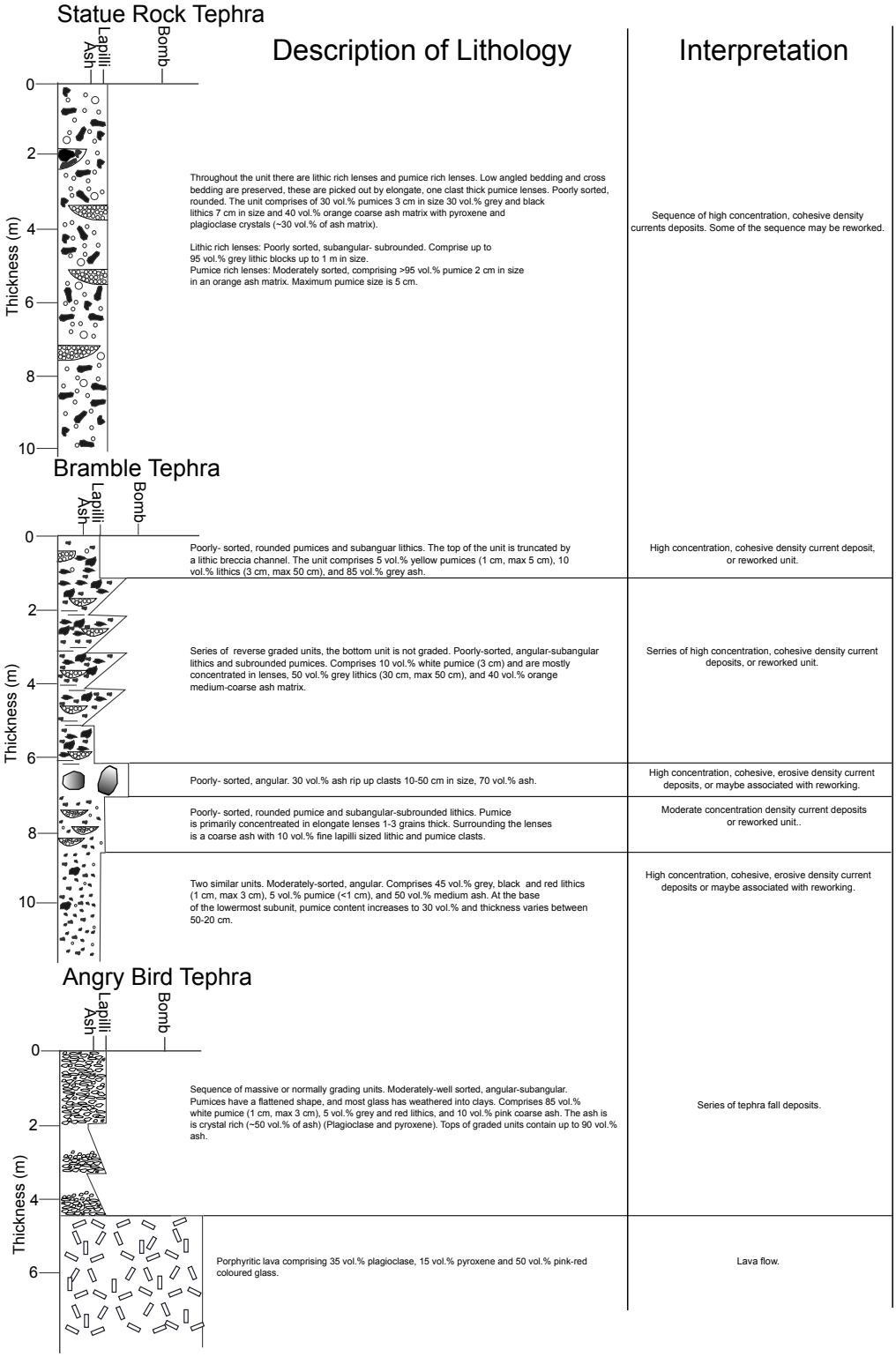

Figure 16: Stratigraphic logs and descriptions of units on the E coast of Montserrat.

Old Road Bay tephra 0.7 ± 0.14 Ma

The Old Road Bay tephra is extensive and found on both the east and west coasts of Centre Hills (Figures 12 and 13). Reworked pumice fall deposits and low angle bedding occur locally at the base of the unit. The unit comprises a series of pumice-rich (up to 80 vol.%) lapilli-tuff deposits with lenses of lapillistone and discontinuous tuff horizons (Figures 14c and 15). The pumice clasts are buff coloured and the cement weathers to a pink-orange colour (14c). It is one of oldest units on the west coast.

Bramble tephra

The Bramble tephra is poorly preserved on the east coast in small (~10 m laterally) pockets within massive andesitic breccias (>10 m thick) (Figure 14d). The Bramble tephra is composed of a series of lapilli-tuff deposits with pumice clasts concentrated in bands or thin, elongate lenses. At Bramble airport, there is a distinctive bed that contains block-sized rip-up clasts of laminated tuff (Figures 13 and 16).

Garibaldi Hill tephra

The Garibaldi Hill tephra is a tephra fall deposit to the southwest of Centre Hills that thins northwards into a laminated grey tuff with a pink tuff top. Channelised lapilli-tuff deposits occur locally. It is composed of alternating pumice-rich (>95 vol.%) lapillistone and tuff beds (Figures 12, 14e, and 15).

Bransby Point tephra 0.79 ± 0.13 Ma

The Bransby Point tephra is laterally continuous and is traceable for >3 km. The unit crops out to the southwest of Centre Hills at Bransby Point and Foxes Bay (Figure 12), and thins northwards. This outcrop pattern is consistent with a more southerly vent site to the Katy Hill vent site The Bransby Point tephra consists of two 1 m thick lapillistone beds (90 vol.% pumice) that are both capped by 2-10 cm of medium-fine ash beds (Figures 14f and 15). The lower lapillistone bed is white, and the upper is pink.

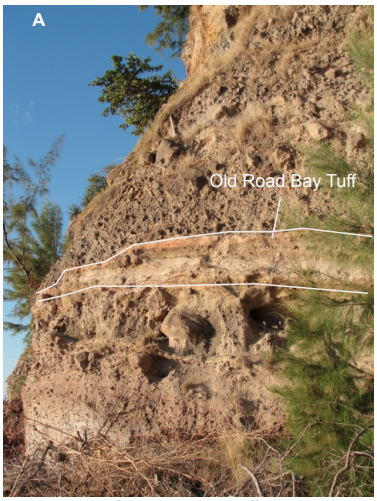

Old Road Bay Tuff
GR N 16.74967 W 62.23495

Statue Rock Tephra
GR N 16.78850 W 62.17641

Foxes Tephra
GR N 16.72785 W 62.238470

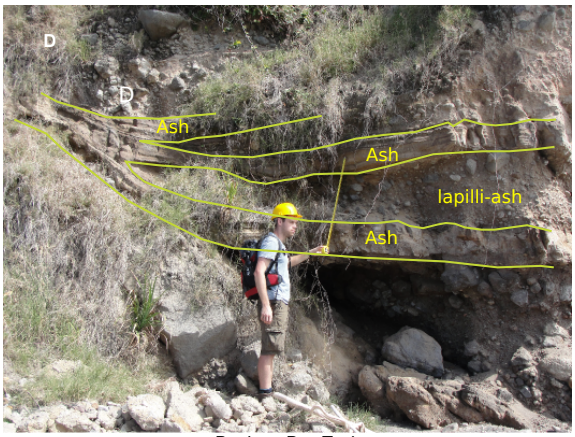

Bunkum Bay Tephra
GR N 16.77357 W 62.22002

Woodlands Tephra
GR N 16.76298 W 62.22343

Attic Tephra
GR N 16.75413 W 62.22226

Figure 17: Pictures of the youngest described units. 17a shows the pink and grey tuffs of the Old Road Bay tuff, 17b is the outcrop of the Statue Rock tephra, 17c is a cliff section of the Foxes tephra, 17d shows channels found from the Bunkum Bay tephra, 17e shows a lapilli stone from the Woodlands tephra, and 17f shows accreationary lapilli found in the Attic tephra.

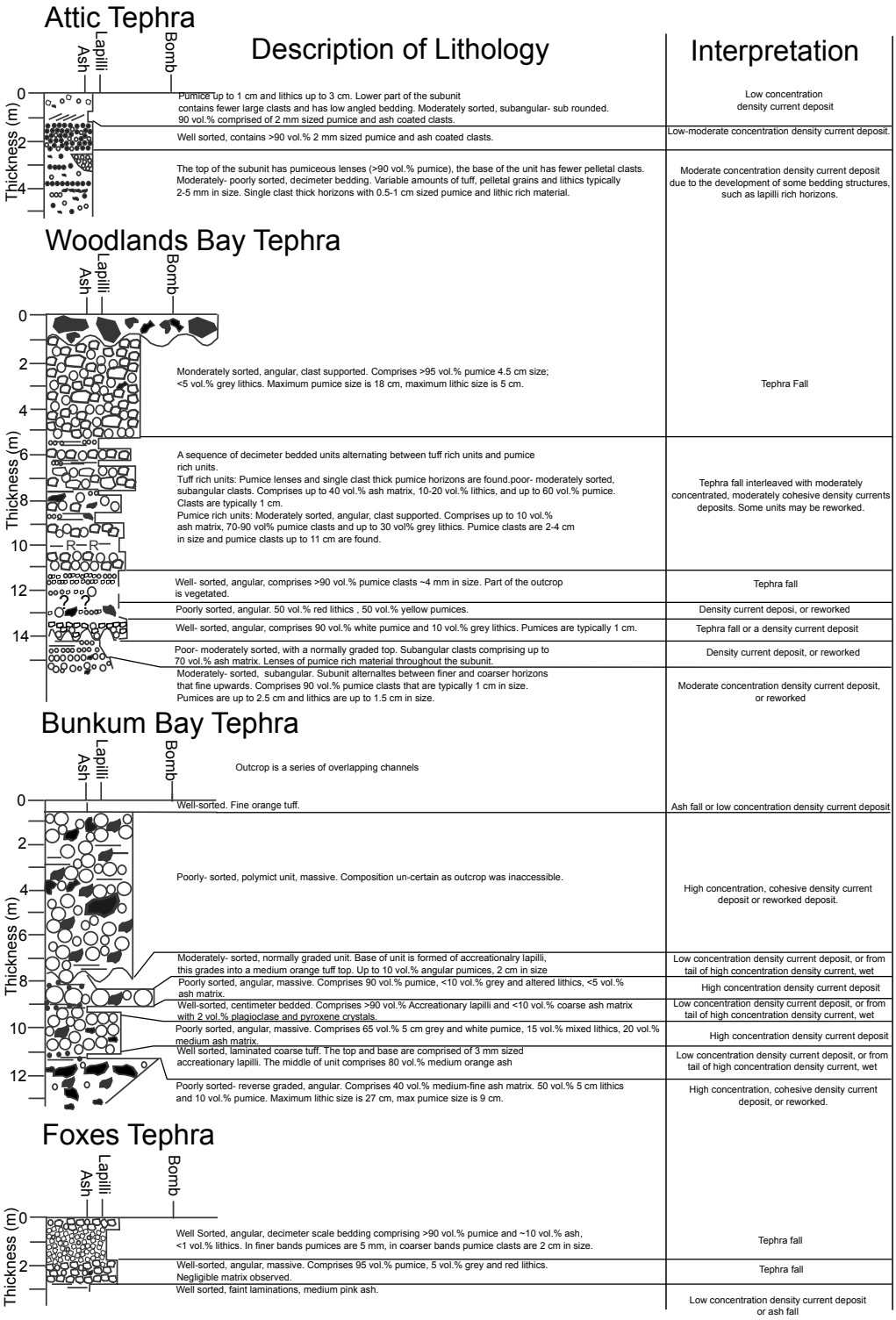

Figure 18: Stratigraphic logs and descriptions of the youngest units found along the W coast of Montserrat.

Old Road Bay tuff

The unit outcrops along the southwest coast from Garibaldi Hill to Lime Kiln Bay. It has a maximum preserved thickness of 60 cm at Garibaldi Hill. This is a distinctive marker bed with 2 or 3 centimeter-decimeter thick beds of grey and yellow tuff (Figure 15 and 17a).

Statue Rock tephra

The unit crops out on the west coast at Statue Rock and can be traced along the cliff section for ~1 km. The unit is laterally variable, with multiple channels (Figures 17b and 16). The Statue Rock tephra is predominantly a lapilli-tuff, with localised lenses of breccia-tuff. The unit is made up of yellow ash matrix 60 vol.% with subordinate pumice clasts (up to 10 cm; 30 vol.%) and lithic clasts (up to 50 cm; 10 vol.%) clasts.

Foxes tephra

The unit crops out only on the southwest coastline of Montserrat (Figure 12). The Foxes tephra is composed of metre-scale, pumice rich (>95 vol.%) lapillistone that fine northwards into tuff units (Figures 12, 17c and 18). Within the unit are variations in grain size.

Bunkum Bay tephra 0.51 ± 0.2 Ma

Bunkum Bay tephra only crops out at Bunkum Bay as a series of overlapping channels of alternating lapilli-tuff and tuff beds (Figures 17d and 18). Low-angle bedding and reverse grading can be seen (Figures 12 and 17c). The lapilli-tuff beds are up to 3 m thick and contain between 10-90 vol.% pumice clasts, 10-80 vol.% lithic clasts, and up to 50 vol.% ash. The tuff beds have a distinctive orange-brown colour with abundant accretionary lapilli.

Woodlands Bay tephra, 0.59 ± 0.11 Ma

The unit is laterally extensive and outcrops along the majority of the west coast of Centre Hills. The Woodlands Bay tephra comprises thick (up to 5 m), well-sorted lapillistone beds with locally-reworked horizons in between (Figures 12, 17e, and 18) and localised cross bedding and pumiceous lenses are found. The unit is one

of the coarsest and thickest deposits from Centre Hills with 95 vol.% pumice clasts, and 5 vol.% lithic clasts. Pumice is buff in colour and 4-5 cm in size (max size 20 cm). The thick pumiceous lapillistone beds suggest the Woodlands Bay eruption was a large magnitude event that produced large volumes of pyroclastic material (Table 7).

Attic tephra 0.48 ± 0.2 Ma

The Attic tephra is best exposed inland as a sequence of white, metre scale fine-lapilli tuffs that have abundant pelletal grains (Figures 12, 17f, and 18). The fine-lapilli tuffs are variably cross-bedded, and planar laminated. Locally exposed in road sections beneath the fine-lapilli tuffs is a 2 m thick medium-coarse lapilli-tuff with lenses of coarse lapillistone.

The Attic tephra is the youngest primary pumiceous unit from Centre Hills and is the most chemically evolved (dacitic) (Figure 6). Furthermore, the Attic tephra is the only unit to contain a hornblende- hypersthene mineral assemblage.

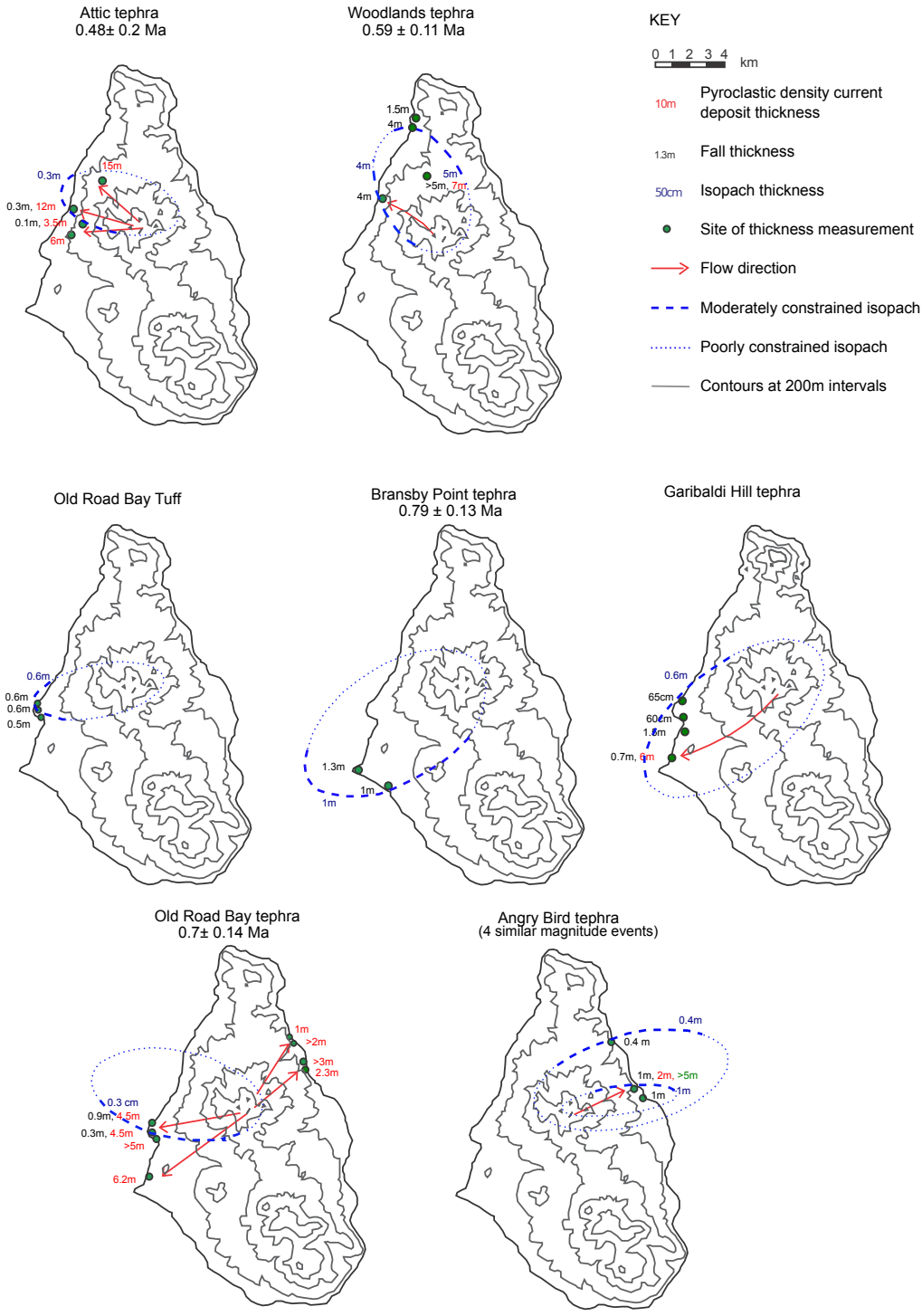

Figure 19: Isopachs constructed for major fall deposits found from Centre Hills. Fall unit thicknesses used in constructing isopachs are shown in black text with location shown by green circles. Flow deposit thicknesses are shown in red, with flow directions shown by red arrows. Vent site is assumed to be Katy Hill as no other vent sites from Centre Hills have been identified.

3.4 Eruption Parameters

Partial isopachs were constructed for tephra fall units that could be correlated across multiple sites (Figure 16), using maximum measured fall deposit thicknesses (Figure 16). Constraints are generally poor due to limited subaerial exposure. Katy Hill was assumed as the vent location for all eruptions, although as noted above, the Bransby Point tephra may be derived from a more southerly vent site. Isopach areas were estimated by visually fitting an ellipse to the available data, but uncertainties are large due to poor constraints on isopach width (Figure 16).

Minimum fall deposit volumes (V_{min}) were estimated using:

$$V_{min} = 3.7AT \quad (1)$$

where A= area of isopach, and T= thickness of isopach (Pyle, 1999). Tephra fall deposit volumes calculated range between 0.02 km^3 to 0.43 km^3 (Table 7). Legros *et al*. (2000) show that 70% of results are underestimated by at least a factor of 2 using this method. Several of these eruptions, as shown in figure 19, produced thick PDC deposits, with thicknesses exceeding 10 m at distances of several kilometres from the vent. Such deposits may be greater in volume than the fall deposit component.

Unit	Isopach thickness (m)	Area of isopach (km^2)	Deposit volume (km^3)
Attic	0.3	20	0.02
Woodlands	4	29	0.43
Old Road Bay	0.6	19	0.04
Bransby Point	1	63	0.23
Garibaldi Hill	0.6	62	0.14
Old Road Bay	0.3	30	0.03
Angry Bird	1	49	0.18
Angry Bird	0.4	49	0.07

Table 7: Estimation of fall deposit volume using a minimum volume estimate by Pyle, (1999) method.

Proximal thickness of fall deposits from the 1980 Mt St Helens eruption and the Quizapu 1932 eruption are similar to proximal thicknesses of fall deposits seen at Centre Hills (Carey and Sigurdsson, 1982; Hildreth and Drake, 1992; Bonadonna *et al*., 1998). The Mt St Helens event had an eruption volume of 2-3km^3 and the Quizapu eruption had an eruption volume of 9.52 km^3 (Hildreth & Drake ,1992). This suggests that the eruption magnitude estimates made here on the Centre Hills deposits are likey to be a significant underestimation, several of these eruptions may have had magnitudes in the range of 4-5 (see Pyle, 2000).

4. Discussion

Here the past 1 Ma of activity at Montserrat is discussed, using both observations from this and previous studies (Rea, 1975; Roobol and Smith, 1998; Smith, 2007; Cassidy *et al*., 2012) (Figures 20 and 21). Activity at the Centre Hills volcano is then compared to activity at the Soufrière Hills volcanic complex to determine if eruption style varied between the volcanic centres.

It is important to note that the Centre Hills subaerial deposits described in this study and the subaerial deposits of the Soufrière Hills volcanic complex are likely to be biased towards the largest magnitude events. Many smaller events are unlikely to be preserved due to their small spatial extent and volume. This is a common caveat when working with the geological record and has been highlighted on recent work as part of the LaMEVE (large magnitude explosive volcanic eruption) database initiative (Brown S. K. *et al.*, 2014).

4.1 History of eruptive activity at Montserrat since 1 Ma

Volcanic activity on Montserrat over the past 1 Ma has been subdivided into 6 episodes in this study based on onshore observations from this and previous studies (Roobol and Smith, 1998; Smith, 2007) (Figure 17). The divisions mark an absence of subaerial eruption related products, a change in eruptive vent, or a change in eruptive style. Below, each episode of activity is described. The oldest unit described in this work (South Lime Kiln Bay tephra) is not included, as this is

not extensively correlated and it may originate from Silver Hills, or from the transitional period between the end of Silver Hills' activity and the onset of Centre Hills activity.

Vent locations are difficult to determine from the Centre Hills deposits due to the poor preservation of proximal deposits and dense vegetation. However, using unit thickness of fall deposits two vent locations are hypothesised. Katy Hills form the summit of the Centre Hills edifice and are thought to be vent sites. This is supported by the observation of lava blocks near the summit of Katy Hills. The youngest pyroclastic deposits from this study are thickest to the east and west of Katy Hills, consistent with a Katy Hills vent location. Earlier deposits from Centre Hill are thickest further south, between Lime Kiln Bay and Bransby Point. This may suggest that there was an earlier, more southerly located Centre Hills vent that has since been covered by more recent deposits (Figure 20), or the thicker deposits to the south may reflect a change in prevailing wind direction. Vent locations of the Soufrière Hills complex are still well preserved and are more easily identifiable (Figure 1 and 20).

Centre Hills Episode 1, 0.92 -~ 0.56 Ma

Several deposits dated ~0.7 Ma are well preserved on-land and are best exposed on the southwest and on the east coasts of Montserrat. This period is represented on-land by 8 main pumiceous units that are interlayered with andesite lithic breccias (Figures 12 and 13). Other pumiceous units are present, but are only locally preserved (See Appendix Figure 1). This period appears to represent a major stage of Centre Hills volcanism, and the production of large explosive eruptions of evolved magma suggests a mature volcanic system. The earlier stages of this system have little subaerial exposures, except perhaps in the aforementioned stratigraphy on the northeast coast (Angry Bird tephra and associated lava and breccia stratigraphy).

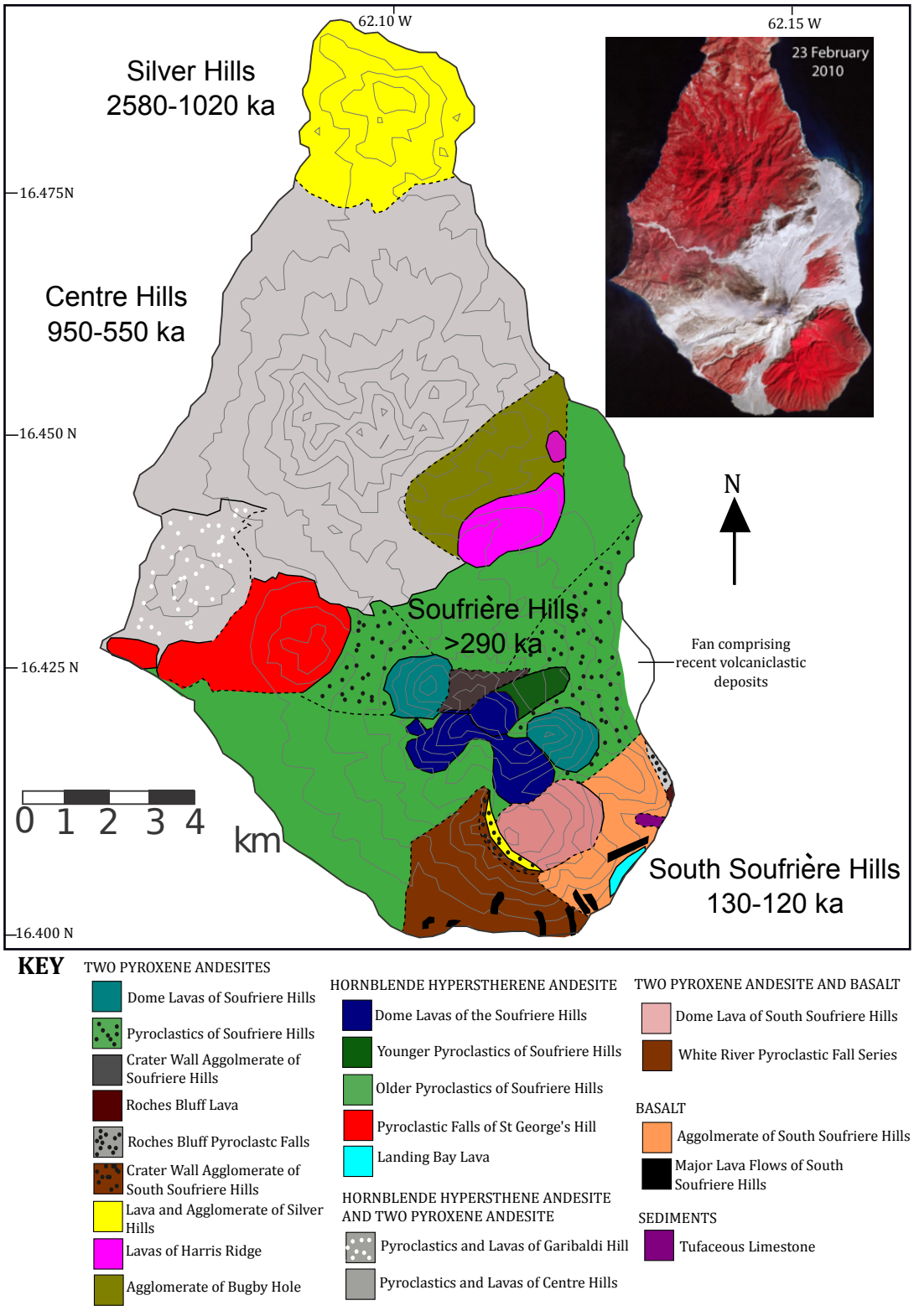

Figure 20: Geological map of Montserrat. Adapted from Rea 1975. This figure shows the stratigraphy prior to the recent eruption. Inset is a false colour satellite image (red represents vegetation, grey volcanic deposits) and shows the distribution of recent eruptive deposits (Wadge *et al.,* 2014).

Centre Hills Episode 2, ~0.71 - 0.38 Ma

Onshore, 3 main pumiceous deposits represent a later stage of Centre Hills activity after an apparent pause in major explosive volcanism of ~100 ka (based on our interpretation of the subaerial volcanic stratigraphy). These deposits thicken to the E of Centre Hills (Figure 12), which is consistent with a vent location at Katy Hills. The Woodlands Bay tephra is chiefly composed of fall deposits (>5 m in thickness <4 km from vent) (Figures 12, 17e, and 18), and is indicative of large-magnitude explosive activity (magnitude 5, >0.43 km^3 is estimated in this study, but this is likely to be a large underestimation). The youngest known pumiceous deposit, the Attic tephra, is geochemically the most evolved, and is the only pyroclastic unit that is a hypersthene-hornblende dacite from Centre Hills. The Attic tephra is the only unit that has thick (5 m) tuff dominated sequences (Figures 12 and 17f).

Soufrière Hills Episode 1, >0.3- 0.175 Ma

Between 0.45-0.38 Ma, activity ceased at Centre Hills and moved south to Soufrière Hills (Smith *et al*., 2007; Chapter 3). It is uncertain if both Soufrière and Centre Hills were active at the same time. Onshore, little outcrop is preserved of early Soufrière Hills activity; only a few deposits from lava dome-forming eruptionsare found on Garibaldi, Richmond and St Georges Hills (Smith, 2007).

Soufrière Hills Episode 2, 0.175-~0.13 Ma

Eruptions during 0.175-0.13 Ma emplaced PDC deposits as well as a 1 m thick pumice fall deposit (Smith, 2007) (Figure 21). This is the only evidence of large-magnitude explosive activity known to be associated with Soufrière Hills activity.

South Soufrière Hills Episode 1, 0.13-0.12 Ma

At ~0.13 Ma, activity shifted further south to South Soufrière Hills. Basaltic scoria deposits dominate the onshore stratigraphy, with interbedded basaltic lava flows and andesite lithic breccias (Figure 21), which are indicative of explosive and effusive activity (Smith, 2007; Cassidy *et al*., 2014b).

Soufrière Hills Episode 3, <112 ka

Activity returns to Soufrière Hills and is dominated by andesite lithic breccias from lava dome-forming eruptions (Figure 21) (Roobol and Smith, 1998; Smith, 2007).

4.2 Comparison to Soufrière Hills

The onshore stratigraphy of Soufrière Hills and South Soufrière Hills edifices have been previously studied in detail both prior to and during the 1995-2010 eruption (Rea *et al*., 1975; Baker *et al*., 1985; Wadge and Isaacs, 1988; Roobol and Smith, 1998; Smith *et al*., 2007). The flanks of the Soufrière Hills edifice are primarily composed of dense to poorly-vesiculated andesitic lithic breccias with thin (~10 cm), localised interbedding of pumiceous material. The andesitic lithic breccias were deposited by block-and-ash flows and surges associated with lava dome-forming eruptions, whilst the pumiceous layers are representative of short-lived explosive eruptions (Wadge and Isaacs, 1988; Roobol and Smith, 1998; Smith, 2007). The flanks of the South Soufrière Hills edifice are similar to the Soufrière Hills edifice, but more basaltic material is found (Roobol and Smith, 1998).

On the northeast flank of the Soufrière Hills edifice, pumice lapilli and tuff fall deposits up to 1.5 m thick, and pumiceous surge deposits up to 2 m thick from Soufrière Hills Episode 2 are represented (Roobol and Smith, 1998; Smith, 2007). These are the only pumiceous deposits that are representative of sustained explosive activity at the Soufrière Hills complex.

The eruption deposits of the Soufrière- South Soufrière Hills complex differ markedly from the eruption deposits of Centre Hills. Thick (>1 m) pumiceous deposits from sustained explosive eruptions were common in the stratigraphy of Centre Hills, but are confined to early eruptive activity at Soufrière Hills (episode 2). Activity at Centre Hills appears to have had more regular, larger magnitude explosive eruptions than the Soufrière Hills complex.

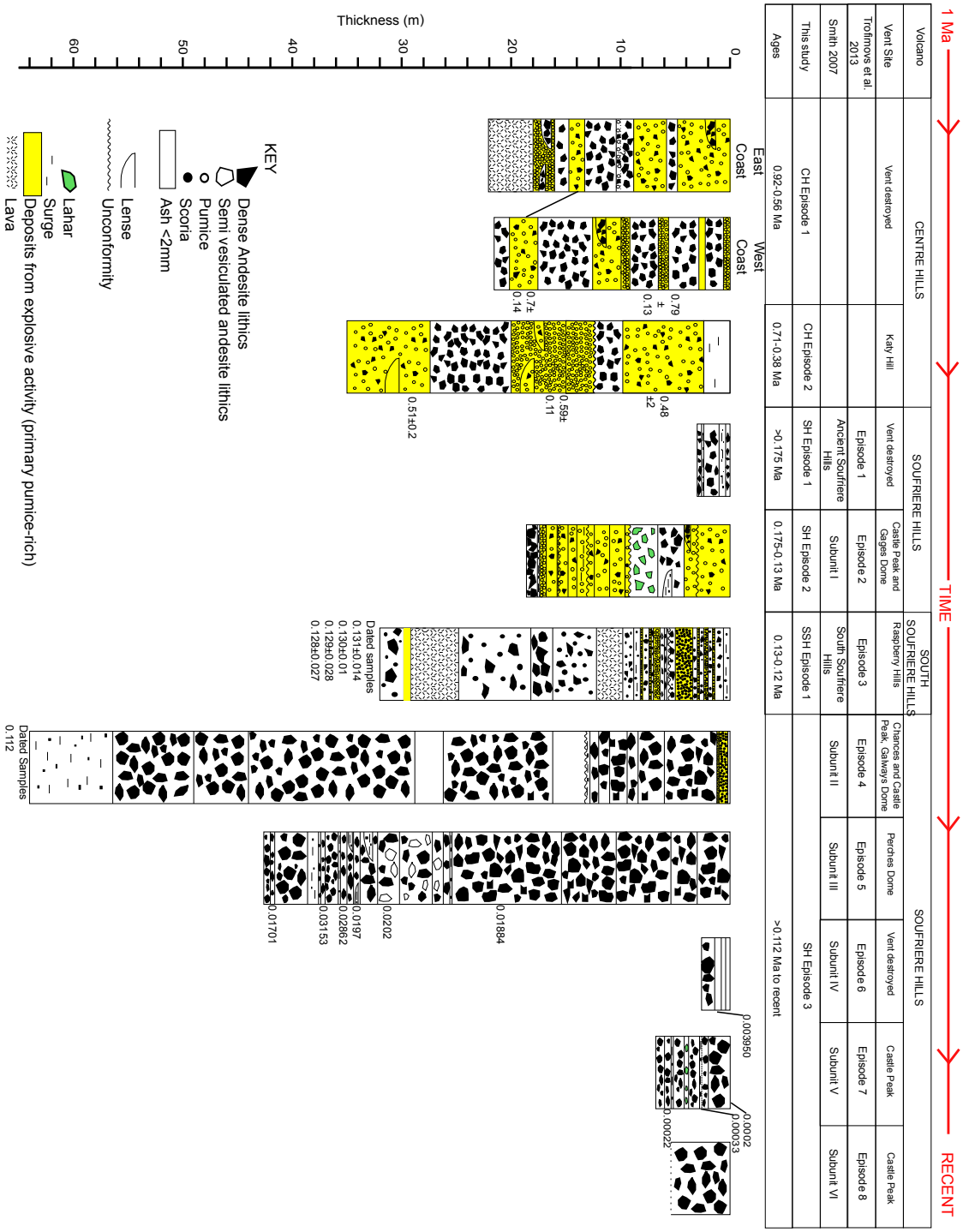

Figure 21: Summary of onshore stratigraphy of Centre Hills, Soufrière Hills, and South Soufrière Hills. Episodes of activity defined in this study are shown, with stratigraphic logs of representative on-land deposits. Scales are approximate and logs are primarily representative of deposits found at

the distal margins of the subaerial edifice. Also shown are episodes of activity defined previously by Smith (2007) and Trofimovs *et al.* (2013). Data from Smith, (2007) are used in conjunction with data from this study.

The Centre Hills Volcano appears to have been a larger edifice than the Soufrière Hills volcanic complex. Earlier stratigraphic work suggested that the formation of Bransby point was related to activity of the Soufrière Hills volcanic complex (see Figure 2 (Harford *et al*., 2002)). However, recent observations and geochemical evidence (such as Pb isotopes (Cassidy *et al*., 2012) and Ba/La (Figure 5)) show that these deposits are associated with the Centre Hills magmatic system. The Soufrière Hills volcanic complex covers an approximate area of 80 km^2, whereas the Centre Hills volcano may have covered >100 km^2.

4.2.1 Geochemistry and mineralogy

Magmas from the recent eruption of Soufrière Hills are well studied (Barclay *et al*., 1998; Devine *et al*., 1998, 2003; Rutherford *et al*., 2014; Humphreys *et al*., 2009a, 2009b, 2013; Plail *et al*., 2014; Cristopher *et al*., 2014), but less petrological work has been conducted on earlier Soufrière Hills complex's deposits (Zellmer *et al*., 2003; Devine *et al*., 2003; Cassidy *et al*., 2012) or magmas from effusive (dome-forming) eruptions at Centre Hills (Harford *et al*., 2002; Cassidy *et al*., 2012). Consequently we primarily compare results from the Centre Hills volcano and the Soufrière Hills edifice. Effusive eruption deposits (lithic breccia units) from the recent eruption are similar both physically, and in their mineralogy and chemistry, to older lithic-dominated deposits from Centre Hills and the Soufrière Hills complex, suggesting that this style of volcanism has characterised eruptions throughout the last 1 Ma on Montserrat.

Both Centre Hills and the Soufrière Hills edifice produced two-pyroxene andesites with relatively homogenous compositions over long time periods. At the Soufrière Hills edifice, silica contents typically vary between 55-64 wt.% SiO_2 and MgO contents vary between 2-5 wt.% (Zellmer *et al*., 2003; Cassidy *et al*., 2012; Humphreys *et al*., 2009a; Christopher *et al*., 2014), with mafic enclave

compositions varying between 49-56 wt.% SiO_2 (Humphreys *et al*., 2009a). This is similar to compositions seen at Centre Hills from this and previous studies where SiO_2 compositions vary between 52-65 wt.%, and MgO varies between 2-5 wt.% (Figure 6) (Cassidy *et al*., 2012).

Trace element compositions are similar between the Soufrière Hills edifice and Centre Hills and MREE and HREE produce the characteristic trough-shaped patterns related to MREE removal by crystallising amphibole (Figure 22), supporting an interpretation of comparable magma-genetic processes between the two systems (cf. Cassidy *et al*., 2012).

At ~110 ka the mineralogy of the Soufrière Hills edifice changed from erupting two-pyroxene andesite to dominantly erupting hypersthene-hornblende andesite (Harford *et al*., 2002), with no change in bulk compositions. In this study, Centre Hills appears to have a similar mineralogical transition towards the final stages of activity at the volcano, with the youngest explosive eruption, the Attic tephra, having a hypersthene-hornblende assemblage. However, unlike at Soufrière Hills, this mineralogical change is accompanied by a chemical change, since the Attic tephra is the most chemically evolved unit (dacite). The presence of amphibole in the Attic tephra may therefore reflect cooling of the magma reservoir, promoting amphibole stability (hornblende is unstable at T >~880°C and upper crustal pressures at Montserrat (Barclay *et al*., 1998; Devine *et al*., 2003)).

Phenocryst compositions broadly overlap from both studied Centre Hills and Soufrière Hills edifices' samples. Eruption temperatures from Soufrière Hills have only been estimated for the recent eruption, and it is difficult to draw any conclusions on long-term differences between the two volcanic centres. However, based on limited plagioclase and phenocryst compositions, estimated storage temperatures of magmas feeding explosive eruptions at Centre Hills appear hotter (900-1000° C) than stored magmas feeding the recent Soufrière Hills eruption (based on Fe-Ti oxide temperature estimates of ~870° C; Christopher *et al.*, 2014).

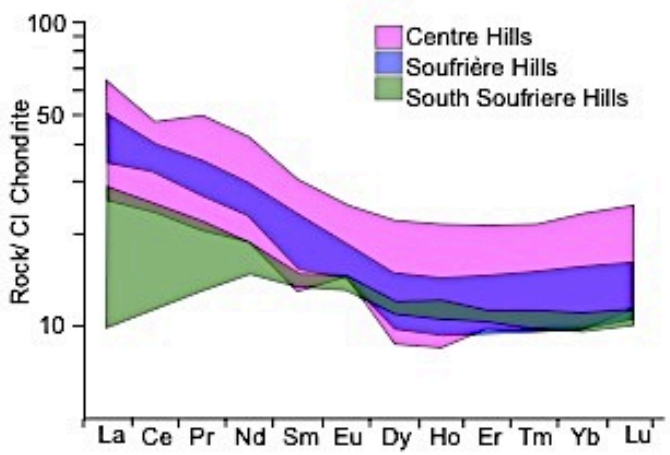

Figure 22: REE spider plot comparing the different centres active on Montserrat over the past 1 Ma. The figure is adapted from Zellmer *et al.*, (2003) to include data from this study.

The youngest (<24 ka; older units have not been studied) products of the Soufrière Hills complex show a notable difference in the abundance and composition of enclaves from the explosive Centre Hills deposits. At Soufrière Hills, mafic enclaves can be found preserved within lithic and pumice clasts and make up 1-12 vol % of recent (1995-2010) eruptive products (Murphy *et al.*, 1998, Barclay *et al.*, 2010, Plail *et al.*, 2014). These enclaves vary in size from sub-millimeter to decimetre scale (Wadge and Isaacs, 1988; Murphy, 1998) and are thought to represent late-stage intrusion of mafic magma into the upper crustal storage region, resulting in mingling and localised heating (Barclay *et al.*, 1998; Devine *et al.*, 1998; Murphy *et al.*, 1998, 2000; Couch *et al.*, 2001; Rutherford *et al.*, 2003; Humphreys *et al.*, 2009a, 2009b). Within the Centre Hills units no evidence of this process and no mafic enclaves were found; all enclaves have a similar mineralogy to the rest of the Centre Hills deposits, suggesting that there is unlikely to be late injection of mafic magma onto the Centre Hills magmatic reservoir.

4.2.2 Potential causes for regular, larger-magnitude explosive activity at Centre Hills

The products of effusive, lava-dome forming eruptions (including reworked material) comprise the bulk of both Centre Hills and the Soufrière Hills volcanic complex (Figure 21). Along with the broad similarities in magma composition, it is suggested that the processes driving volcanism at both volcanoes were similar, but Centre Hills was also prone to large, sustained-explosive events over several hundred thousand years of its history. In contrast, such explosive eruptions are confined to early activity at the Soufrière Hills volcanic complex. A number of factors influence magma explosivity, including melt composition, gas content, magma viscosity, temperature, crustal thickness, and vent and conduit geometries (Wilson *et al*., 1980; Scandone *et al*., 2007; Koleszar *et al*., 2012; Nguyen *et al*., 2014). Identifying a particular cause of the difference in behaviour between the two volcanoes is therefore difficult. It is not known if pre-eruptive volatile contents or magma viscosities were different between the two edifices, as these parameters are not well constrained at Montserrat. Detailed volatile studies have only been conducted on recent eruption deposits from the Soufrière Hills complex (Barclay *et al*., 1998, 2010; Hammoya *et al*., 1998; Young *et al*., 1998; Oppenheimer *et al*, 2002; Devine *et al*., 2003; Humphreys *et al*., 2009a, 2009b; Christopher *et al*., 2010; Edmonds *et al*., 2001; 2010; 2014). The difference in enclave content, noted above, may mark a significant difference in the typical eruption triggering process and the temperature and viscosity of ascending magma, but such an inference remains speculative without further investigation.

Increased surface loading has been suggested as a driver towards more explosive eruptions of more evolved magmas, by reducing the permeability of the edifice (higher pressures can cause fractures and pore spaces to close up) (Taisne and Jaupart, 2008) or by supressing magma ascent (increased confining stresses due to load can suppress magma transport) (Pinel and Jaupart, 2000, 2003, 2004; Caricchi *et al.,* 2014), but our observations do not support a systematic trend of this type. Explosive eruptions are observed throughout the history of Centre Hills (i.e. they do not show an increased prevalence with age or edifice growth), and confined to the earlier stages of Soufrière Hills Complex (when the edifice may

have been smaller). There is, however, some general evidence that the Centre Hills edifice was larger than the Soufrière Hills complex, with subaerial deposits covering ~100 km^2, in contrast to ~80 km^2 at the Soufrière Hills volcanic complex.

5. Conclusions

This study greatly enhances our knowledge of the eruption sequence on Montserrat, allowing more precise time constraints on volcanic episodes. The last 1 Ma of Montserrat's activity has been subdivided into 6 episodes of volcanic activity, chiefly represented by andesitic breccias and PDC deposits. Centre Hills stratigraphy is composed of thick (up to 15 m thick) pumiceous units interlayered within andesitic breccias. There are 24 identifiable pumiceous units, including 11 correlatable units that crop out across Montserrat. One pumiceous unit has also been described that may be derived from Silver Hills.

The occurrence of multiple pumiceous deposits implies that there were repeated sustained explosive eruptions throughout the lifetime of Centre Hills. Minimum volume estimates suggest eruption magnitudes up to 5, with the largest eruption being the Woodlands Bay pumice. Andesitic breccias, lava flows (such as in the interlayered Angry Bird pumice), and remnant lava domes indicate that effusive dome-forming eruptions were also common throughout the activity of Centre Hills.

Comparison of the Soufrière Hills volcanic complex and the Centre Hills stratigraphies shows that activity at Montserrat over the past ~1 Ma has consistently involved regular dome-forming eruptions. Magma compositions show little variation in major (52-65 wt.% SiO_2, 2-5 wt.% MgO) and trace element chemistry throughout this period, suggesting long-term stability in conditions driving both magma generation and upper crustal storage conditions. However, at Centre Hills there is a significantly greater propensity towards explosive volcanism, which occurred throughout its history. This contrasts with a marked absence of explosive volcanism at Soufrière Hills, except in the period 175 - 130

ka, and suggests that local controls on pre-eruptive dynamics have a strong influence on eruption style. Small differences in viscosity or volatile content may potentially be associated with lower permeability beneath the Centre Hills edifice (perhaps associated with more coherent and less weathered lava bodies within the shallow edifice) that may inhibit gas loss. Or differences in the prevailing eruption trigger, where there is a common occurrence of mafic enclaves (heating of magma and reduction of viscosity) at the Soufrière Hills complex that contrasts strongly with an absence of such enclaves in the explosive Centre Hills products.

6. References

Ablay, G. J. and Marti, J. (2000), Stratigraphy, structure and volcanic evolution of the Pico-Teide Viejo formation, Tenerife, Canary Islands, *Journal of Volcanology and Geothermal Research,* 103(1-4), 183–208

Ancochea, E., Fuster, J. M., Ibarrola, E., Cendrero, A., Coello, J., Hernan, F., Cantagrel, J. M. and Jamond, C. (1990), Evolution of the island of Tenerife (Canary Islands) in the light of new K-Ar data, *Journal of Volcanology and Geothermal Research*, 44, 231-249, doi: 0377-0273/90/$03.50

Baker, P. E. (1985), Volcanic hazards on St Kitts and Montserrat, West Indies, *Journal of the geological Society of London* 142: 279-295

Barclay, J., Rutherford, M. J. and Caroll, M. R. (1998), Experimental phase equilibria constraints on pre-eruptive storage conditions of the Soufrière Hills magma, *Geophysical Research Letters,* 25, 3437-3440

Barclay, J., Herd, R. A., Edwards, B. R., Chrisopher, T., Kiddle, E. J., Plail, M. and Donovan, A. (2010), Caught in the act: Implications for the increasing abundance of mafic enclaves during the recent eruptive episodes of the Soufrière Hills Volcano, Montserrat, *Geophysical Research Letters,* 37, L00E09, doi:10.1029/2010GL042509

Blundy, J. and Cashman, K. (2001), Ascent-driven crystallisation of dacite magmas at Mount St Helens, 1980-1986, *Contributions to Mineralogy and Petrology*, 140(6), 631-650

Bonadonna, C., Ernst, G.G.J. and Sparks, R.S.J. (1998), Thickness variations and volume estimates of tephra fall deposits : the importance of particle Reynolds number, C, 174–187

Bonadonna, C. and Houghton, B. F. (2005), Total grain-size distribution and volume of tephra-fall deposits, *Bulletin of Volcanology*, 67, 441–456, doi:10.1007/s00445-004-0386-2

Branney, M. J. and Kokelaar, B. P. (2002), Pyroclastic density currents and the sedimentation of ignimbrites (book), *Geological Society of London*

Brown, K and Davidson, C. (2008), 40Ar/39Ar geochronology of the Silver Hills andesite, Montserrat, West Indies, B. A. Senior integrative excersize, Carelton College, Northfield, Minnesota Carey, S., 1997, Influence of convective sedimentation on the formation of widespread tephra fall layers in the deep sea

Brown, R. J., Civetta, L., Arienzo, I., D'Antonio, M., Moretti, R., Orsi, G., Tomlinson, E. L., Albert, P. G. and Menzies, M. A. (2014), Geochemical and isotopic insights into the assembly, evolution and disruption of a magmatic plumbing system before and after a cataclysmic caldera-collapse eruption at Ischia volcano (Italy), *Contributions to Mineralogy and Petrology*, *168*(3), 1-23

Brown, S. K., Crosweller, H. S., Sparks, R. S. J., Cottrell, E., Deligne, N. I., Guerrero, N. O. et al., (2014), Characterisation of the Quaternary eruption record: analysis of the Large Magnitude Explosive Volcanic Eruptions (LaMEVE) database, *Journal of Applied Volcanology*, *3*(1), 1-22

Carey, N. and Sigurdsson, H. (1982), Influence of Particle Aggregation on Deposition of Distal Tephra from the May 18, 1980, Eruption of Mount St Helens. *Journal of Geophysical Research*, 87(2), 7061–7072

Caricchi, L., Annen, C., Blundy, J., Simpson, G. and Pinel, V. (2014), Frequency and magnitude of volcanic eruptions controlled by magma injection and buoyancy, *Nature Geoscience*, *7*(2), 126-130

Carlsen, H. K., Gislason, T., Benediktsdottir, B., Kolbeinsson, T. B., Hauksdottir, A., Thorsteinsson, T. and Briem, H. (2012), A survey of early health effects of the Eyjafjallajökull 2010 eruption in Iceland: a population-based study, *Public health, BMJ Open*, 2, e000343, doi:10.1136/bmjopen-2011-000343

Carter, L., Nelson, C. S., Neil, H. L. and Froggatt, P. C. (1995), Correlation, dispersal, and preservation of the Kawakawa Tephra and other late Quaternary tephra layers in the Southwest Pacific Ocean, *New Zealand Journal of Geology and Geophysics*, *38*(1), 29-46

Cassidy, M., Taylor, R. N., Palmer, M. R., Cooper, R. J., Stenlake, C. and Trofimovs, J., (2012), Tracking the magmatic evolution of island arc volcanism: Insights from a high-precision Pb isotope record of Montserrat, Lesser Antilles, *Geology, Geochemistry, Geophysics,* 13(5), 1525-2027, doi:10.1029/2012GC004064

Cassidy, M., Watt, S. F. L., Palmer, M. R., Trofimovs, J., Symons, W., Maclachlan, S. E. and Stinton, A. J. (2014a), Construction of volcanic records from marine sediment cores: A review and case study (Montserrat, West Indies), *Earth-Science Reviews*, 138:137–155

Cassidy, M., Trofimovs, J., Watt, S. F. L., Palmer, M. R., Taylor, R. N., Gernon, T. M., Talling, P. J. and Le Friant, A. (2014b), Multi-stage collapse events in the South Soufrière Hills, Montserrat, as recorded in marine sediment cores, *In The eruption of Soufriére Hills Volcano, Montserrat from 2000-2010,* edited by Wadge, G., *et al*., 2014, *The Geological Society Special Publications*, 39:383-397

Christopher. T., Edmonds, M., Humphreys, M. and Herd, R. A. (2010), Volcanic gas emissions from Soufrière Hills Volcano, Montserrat 1995–2009, with

implications for mafic magma supply and degassing, *Geophysical Research Letters,* 37(19)

Christopher, T. E., Humphreys, M. C., Barclay, J., Genareau, K., De Angelis, S. M., Plail, M. and Donovan, A. (2014), Petrological and geochemical variation during the Soufrière Hills eruption, 1995 to 2010*, In The Eruption of Soufrière Hills Volcano, Montserrat from 2000 to 2010,* edited by Wadge, G., Robertson, R. and Voight, B., *Geological Society, London, Memoirs,* 39(1), 317-342

Cole, P. D., Calder, E. S., Sparks, R. S. J., Clarke, A. B., Druitt, T. H., Young, S. R., Herd, R. A., Harford, C. L. and Norton, G. E. (2002), Deposits from dome-collapse and fountain-collapse pyroclastic flows at Soufrière Hills volcano, Montserrat, *Geological Society, London, Memoirs*, 21:231-262, doi: 10.1144/GSL.MEM.2002.021.01.11

Cortese, M., Frazzetta, G. and La Volpe, L. (1986), Volcanic history of Lipari (Aeolian islands, Italy) during the last 10,000 years, *Journal of Volcanology and Geothermal Research,* 27, 117-133

Couch, S., Sparks, R. S. J. and Carroll, M. R. (2001), Mineral disequilibrium in lavas explained by convective self-mixing in open magmachamber, *Nature*, 411, 1037–1039

Coussens, M. F., *et al* Submitted. On the relationship between eruptive activity, flank collapse and sea-level at volcanic islands: a long-term (>1 Ma) record offshore Montserrat, Lesser Antilles

Crutchley, G. J., Karstens, J., Berndt, C., Talling, P. J., Watt, S. F. L., Vardy, M. E., Huhnerbach, V., Urlaub, M., Sarkar, S., Klaeschen, D., Paulatto, M., Le Friant, A., Lebas, E. and Maeno, F. (2013), Insights into the emplacement dynamics of volcanic landslides from high-resolution 3D seismic data acquired offshore Montserrat, Lesser Antillies, *Marine Geology,* 335:1-15

Devine, J., Murphy, M. D., Rutherford, M. J., *et al*. (1998), Petrologic evidence for pre-eruptive pressure-temperature conditions, and recent reheating, of andesitic magma eruption at the Soufrière Hills Volcano, Montserrat, W. T., *Geophysical Research Letters,* 25, 3669-3672

Devine, J. D., Rutherford, M. R., Norton, G. E. and Young, S. R. (2003), Magma storage region processes inferred from geochemistry of Fe–Ti oxides in andesitic magma, Soufrière Hills Volcano, Montserrat, W.I., *Journal of Petrology*, 44, 1375–1400

Druitt, T. H., Mellors, R. A., Pyle, D. M. and Sparks, R. S. J. (1989), Explosive volcanism on Santorini, Greece, *Geological Magazine,* 2; 95-126

Druitt, T.H., and Kokelaar, B.P. (2002), The eruption of Soufrière Hills Volcano, Montserrat, from 1995 to 1999, *Memoirs of the Geological Society of London*, 21:45–69

Edmonds, M., Pyle, D. and Oppenheimer, C. (2001), A model for degassing at the Soufrière Hills Volcano, Montserrat, West Indies, based on geochemical evidence, *Earth and Planetary Science Letters*, 186, 159–173

Edmonds, M., Pyle, D. M. and Oppenheimer, C. (2002), HCl emissions at Soufrière Hills Volcano, Montserrat, West Indies, during a second phase of dome building, November 1999 to September 2000, *Bulletin of Volcanology*, 64, 21 – 30

Edmonds, M., Aiuppa, A. *et al*. (2010), Excess volatiles supplied by mingling of mafic magma at an andesite arc volcano, *Geochemistry, Geophysics, Geosystems*, 11, Q04005

Edmonds, M., Humphreys, M. C. S. *et al*. (2014), Pre-eruptive vapour and its role in controlling eruption style and longevity at Soufrière Hills Volcano, *In The Eruption of Soufrière Hills Volcano, Montserrat from 2000 to 2010,*

edited by Wadge, G., Robertson, R. and Voight, B., *Geological Society, London, Memoirs*, 39, 291 – 315, doi. org/10.1144/M39.16

Germa. A., Quidelleur, X., Lahitte, P., Labanieh, S. and Chauvel, C. (2011), The K-Ar Cassignol-Gillot technique applied to wester Martinique lavas: A record of Lesser Antilles arc activity from 2 Ma to Mount Pelee volcanism, *Quaternary Geology,* 6, 341-355

Hammouya, G., Allard, P., Jean-Baptiste, P., Parello, F., Semet, M. P. and Young, S. R. (1998), Pre- and syn-eruptive geochemistry of volcanic gases from Soufrière Hills Volcano, Montserrat, West Indies, *Geophysical Research Letters*, 25, 3685–3688

Harford, C. L. Pringle, M. S., Sparks, R. S. J. and Young, S. R. (2002), The volcanic evolution of Montserrat using 40Ar/39Ar geochronology *Geological Society, London, Memoirs*, 21:93–113, doi: 10.1144/GSL.MEM.2002.021.01.05

Hildreth, W. and Drake, R. (1992), Volcfin Quizapu , Chilean Andes, *Bulletin of Volcanology*, 54, 93–125

Humphreys, M. C. S., Christopher, T. and Hards, V. (2009a), Microlite transfer by disaggregation of mafic inclusions following magma mixing at Soufrière Hills volcano, Montserrat, *Contributions to Mineralogy and Petrology,* 157, 609–624

Humphreys, M. C. S., Edmonds, M., Christopher, T. and Hards, V. (2009b), Chlorine variations in the magma of Soufrière Hills Volcano, Montserrat: insights from Cl in hornblende and melt inclusions, *Geochimica et Cosmochimica Acta* 73, 5693–5708

Humphreys, M. C. S., Edmonds, M., Barclay, J., Plail, M., Parkes, D. and Christopher, T. (2013), A new method to quantify the real supply of mafic components to a hybrid andesite, *Contributions to Mineralogy and Petrology,* 165, 191 – 215

Jutzeler, M., Marsh, R., Carey, R. J., White, J. D. L., Talling, P. J. and Karlstrom, L.(2014), On the fate of pumice rafts formed durin the 2012 Havre submarine eruption, *Nature Communications,* 5: 3660, doi 10.1038/ncomms4660

Jutzeler, M., McPhie, J., Allen, S. R. and Proussevitch, A. A. (2015), Grain-size distribution of volcaniclastic rocks 2: Characterizing grain size and hydraulic sorting, *Journal of Volcanology and Geothermal Research,* 301: 191-203

Koleszar. A. M., Kent, A. J. R., Wallace, P. J. and Scott, W. E. (2012), Controls on long-tern low explosivity at andesitic arc volcanoes: insights from Mount Hood, Oregon, *Journal of Volcanology and Geothermal Research,* 219-220, 1-14

Legros, M., Elliott, B. R., Rittner, M. N., Weertman, J. R. and Hemker, K. J. (2000), Microsample tensile testing of nanocrystalline metals, *Philosophical magazine A*, *80*(4), 1017-1026

Le Friant, A., Harford, C. L. and Deplus, C. (2004), Geomorphological evolution of Montserrat (West Indies): importance of flank collapse and erosional processes*, Journal of the Geological Society*, 161(1), 147–160, doi:10.1144/0016-764903-017

Lowe. D. J. (2011), Tephrochronology and its application: A review, *Quaternary Geology,* 6, 107-153

Murphy, M.D., *et al*. (1998), The role of magma mixing in triggering the current eruption at the Soufrière Hills volcano, Montserrat, West Indies, *Geophysical Research Letters,* 25 (18), 3433–3436

Murphy, M. D., Sparks, R. S. J., Barclay, J., Carroll, M. R. and Brewer, T. S. (2000), Remobilization of andesite magma by intrusion of mafic magma at the Soufrière Hills Volcano, Montserrat, West Indies, *Journal of petrology* 41 (1), 21-42

Nguyen. C. T., Gonnermann, H. M. and Houghton, B. F. (2014), Explosive to effusive transition during the largest volcanic eruption of the 20th century (Novarupta 1912, Alaska), *Geology,* 42, 703-706

Oppenheimer, C., Edmonds M., Francis, P. and Burton, M. (2002), Variation in HCl/SO2 gas ratios observed by Fourier transform spectroscopy at Soufrière Hills Volcano, Montserrat, *In The Eruption of SoufrièreHills Volcano, Montserrat, from 1995 to 1999,* Edited by Druitt, T.H. and Kokelaar, B. P., *Geological Society, London, Memoirs*, 21, 621–639

Pinel, V. and Jaupart, C. (2000), The effect of edifice load on magma ascent beneath a volcano, *Philosophical Transactions of the Royal Society of London A: Mathematical, Physical and Engineering Sciences,* 358(1770), 1515-1532

Pinel, V. and Jaupart, C. (2003), Magma chamber behavior beneath a volcanic edifice, *Journal of Geophysical Research,* 108(B2)

Pinel, V. and Jaupart, C. (2004), Magma storage and horizontal dyke injection beneath a volcanic edifice, *Earth and Planetary Science Letters,* 221(1), 245-262

Pioli, L., Scalisi, L., Costantini, L., Di Muro, A., Bonadonna, C. and Clavero, J. (2015), Explosive style, magma degassing and evolution in the Chaimilla eruption, Villarrica volcano, Southern Andes, *Bulletin of Volcanology*, *77*(11), 1-14

Plail. M., Barclay, J., Humphreys, M. C. S., Edmonds, M., Herd, R. A., and Christopher, T. E. (2014), Characterization of mafic enclaves in the erupted products of Soufrière Hills Volcano, Montserrat, 2009 to 2010, *In The Eruption of Soufière Hills Volcano, Montserrat from 2000 to 2010,* edited by Wadge. G., Robertson. R. E. A., and Voight. B., *The Geological Society of London,* 39, 343-360

Putirka, K., Johnson, M., Kinzler, R., Longhi, J. and Walker, D. (1996), Thermobarometry of mafic igneous rocks based on clinopyroxene-liquid

equilibria, 0–30 kbar, *Contributions to Mineralogy and Petrology*, 123(1), 92-108

Putirka, K. D., Mikaelian, H., Ryerson, F. and Shaw, H. (2003), New clinopyroxene-liquid thermobarometers for maric, evolved, and volatile-bearing lava compositions, with applications to lavas from Tibet and the Snake River Plain, Idaho, *American Mineralogist,* 88, 1542-1554

Putirka, K. D. (2005), Mantle potential temperatures at Hawaii, Iceland, and the mid-ocean ridge system, as inferred from olivine phenocrysts: evidence for thermally driven mantle plumes, *Geochemistry, Geophysics, Geosystems,* 6, 5, doi:10.1029/ 2005GC000915

Putirka, K. D. (2008), Thermometers and barometers for volcanic systems, *In Minerals, Inclusions, and Volcanic Processes,* Edited by Putirka, K. D. and Tepley, F. J. I,. *Mineralogical Society of America*, 61–120

Pyle, D. M. (1999), Widely dispersed Quaternary tephra in Africa. *Global and Planetary Change* 21,95–112

Pyle, D. M. (2000), Sizes of volcanic eruptions. *In Encyclopedia of Volcanoes*, 1, 263-269

Rea, W. J. (1975), The volcanic geology and petrology of Montserrat, West Indies, *Journal of the geological Society of London,* 130,341-366

Ridolfi, F., Renzulli, A. and Puerini, M. (2010), Stability and chemical equilibrium of amphibole in calc-alkaline magmas: an overview, new thermobarometric formulations and application to subduction-related volcanoes, *Contributions to Mineralogy and Petrology*, 160, 45-66

Robock, A. (2000), Volcanic eruptions and climate, *Reviews of Geophysics*, *38*(2), 191-219.

Roobol, M. J. and Smith, A. L. (1976), Mount Pelée, Martinique: a pattern of

alternating eruptive styles. *Geology*, *4*(9), 521-524

Roobol, M. J., Smith A. L. and Wright, J. V. (1987), Lithic breccias in pyroclastic flow depositson St. Kitts, West Indies, *Bulletin of Volcanology,* 49, 694-707

Roobol, M. J. and Smith, A. L., (1998), Pyroclastic stratigraphy of the Soufrière Hills volcano, Montserrat- Implication for the present eruption, *Geophysical Research Letters*, 25 (18),3393-3396

Rosi. M., Vezzoli, L., Castelenzano, A. and Grico, G. (1999), Plinian pumice fall deposit of the Campainian Ignimbrite eruption (Phlegraean Fields, Italy), *Journal of Volcanology and Geothermal Research,* 91, 179-198

Rutherford. M. J. and Devine, J. D. (2003), Magmatic conditions and magma ascents indicated by hornblende phase equilibria and reactions in the 1995-2002 Soufrière Hills Magma, *Journal of Petrology,* 44 (8), 1433-1454

Sammonds, P., McGuire, W. and Edwards, S. (2010), Volcanic Hazard from Iceland: Analysis and Implications of the Eyjafjallajökull Eruption, *UCL Institute for Risk and Disaster Reduction, London.* Available at: www.ucl.ac.uk/rdr/publications/irdr-special-reports/iceland

Scandone, R., Cashman, K. V. and Malone, S. D. (2007), Magma supply, magma ascent and the style of volcanic eruptions, *Earth and Planetary Science Letters,* 253, 513–529

Sigl, M., Winstrup, M., McConnell, J. R., Welten, K. C., Plunkett, G., Ludlow, F., Büntgen, U., Caffee, M., Chellman, .N, Dahl-Jensen, D. and Fischer, H. (2015), Timing and climate forcing of volcanic eruptions for the past 2,500 years, *Nature,* 523, 543-549

Smith, A. L., (2007), Prehistoric stratigraphy of the Soufrière Hills-South Soufrière Hills volcanic complex, Montserrat, West Indies, *The Journal of Geology,* 115:115-127

Taisne, B and Jaupart, C. (2008), Magma degassing and intermittent lava dome growth, *Geophysical Research Letters,* 35, L20310

Tomlinson, E. L., Albert, P. G., Wulf, S., Brown, R. J., Smith, V. C., Keller, J., Orsi, G., Bourne, A. J. and Menzies, M. A. (2014). Age and geochemistry of tephra layers from Ischia, Italy: constraints from proximal-distal correlations with Lago Grande di Monticchio, *Journal of Volcanology and Geothermal Research*, *287*, 22-39

Trofimovs, J., Talling, P. J., Fisher, J. K., Hart, M. B., Sparks, R. S. J., Watt, S. F. L., Cassidy, M., Smart, C. W., Le Friant, A., Moreton S. G. and Lang, M. J. (2013), Timing, origin and emplacement dynamics of mass flows offshore of SE Montserrat in the last 110 ka: Implications for landslide and tsunami hazards, eruption history, and volcanic island evolution, *Geochemistry, Geophysics, Geosystems*, 14(2),385–406, doi:10.1002/ggge.20052

Wadge, G. and Isaacs, M. C. (1988), Mapping the volcanic hazards from Soufrière Hills volcano, Montserrat, West Indies using an image processor, *Journal of the geological Society of London,* 145: 541-551

Wadge. G., Voight, B., Sparks, R. S. J., Cole, P. D., Loughlin, S. C. and Robertson, R. E. A. (2014), An overview of the eruption of Soufrière Hills Volcano, Montserrat from 2000 to 2010, *In The Eruption of the Soufrière Hills Volcano, Montserrat from 2000–2010*, edited by G. Wadge, Robertson, R. A. E. and Voight, B., *Geological Society of London*, 1–39

Watson, I. M., Oppenheimer, C. *et al*. (2001), The relationship between degassing and ground deformation at Soufrie`re Hills Volcano, Montserrat, *Journal of Volcanology and Geothermal Research*, 98, 117 – 126

Watt, S. F., Pyle, D. M., Mather, T. A., Martin, R. S. and Matthews, N. E. (2009), Fallout and distribution of volcanic ash over Argentina following the May 2008 explosive eruption of Chaitén, Chile, *Journal of Geophysical Research: Solid Earth (1978–2012)*, *114*(B4)

White. J. D. L. and Houghton, B. F. (2006), Primary volcaniclastic rocks, *Geology,* 34, 677-680, doi: 10.1130/G22346.1

Wilson, L., Sparks, R. S. J. and Walker, G. P. L. (1980), Explosive volcanic eruptions—IV. The control of magma properties and conduit geometry on eruption column behaviour, *Geophysical Journal of the Royal Astronomical Society,* 63 (1), 117–148

Young, S. R., Francis P.W., *et al*. (1998), Monitoring SO_2 emissions at the Soufrière Hills Volcano: implications for changes in eruptive conditions, *Geophysical Research Letters*, 25, 3681–3684

Zellmer, G. F., Sparks. R. S. J., Hawkesworth, C. J. and Wiedenbeck, M. (2003), Magma emplacement and remobilization timescales beneath Montserrat: insights from Sr and Ba profiles across plagioclase phenocrysts*, Journal of Petrology*, 44, 1413–14

Chapter 3:

The relationship between eruptive activity, flank collapse and sea-level at volcanic islands: a long-term (>1 Ma) record offshore of Montserrat, Lesser Antilles

Abstract

Hole U1395B, drilled southeast of Montserrat during Integrated Ocean Drilling Program Expedition 340, provides a long (>1 Ma) and detailed record of eruptive and mass-wasting events (>130 events). This record can be used to explore the temporal evolution in volcanic activity and mass-wasting at an arc volcano. Analysis of tephra fall and volcaniclastic turbidite deposits in the drill cores highlights three heightened periods of volcanic activity on the island of Montserrat, which occurred at ~930 ka to ~900 ka, ~810 ka to ~760 ka, and ~190 ka to ~120 ka. The analysis also shows that the three temporally well-constrained large flank collapses (>0.3 km^3) on Montserrat occurred during rapid sea-level rise (>5 m/ka) and coincide with periods of relatively elevated volcanic activity. Available age data from other island arc volcanoes shows that most well dated flank collapses from island arc volcanoes coincide with periods of rapid sea-level rise. In contrast, large landslides at ocean island volcanoes show no correlation with eustatic sea-level change, however we emphasise this is based on a limited, low resolution data set. We infer that rapid sea-level rise may potentially contribute to collapse processes at island arc volcanoes, but not in larger ocean-island settings. This contrast in the link between island stability and sea-level may be due to differences in scale, topography, tectonic structures and rock composition between island arc volcanoes and ocean island volcanoes.

1. Introduction

Volcanic islands in arc settings grow and decay through eruptions, mass-wasting and erosion. Rates of growth vary over time at a volcanic island (Houghton *et al*., 1995; Singer *et al*., 2008; Germa *et al*., 2010), and island arc activity is punctuated by collapse events of different volumes (Ablay and Marti, 2000; Cole *et al*., 2002; Trofimovs *et al*., 2013). As a volcanic island grows, the volcanic edifices and surrounding island flanks become increasingly unstable, resulting in partial collapses. Mass-wasting events at volcanic islands are geohazards due to their inundation (Siebert, 1984; Watt, *et al*., 2012a, 2012b), and their potential to generate tsunamis (Ward and Day, 2003). It is important, therefore, to investigate the frequency of mass-wasting events and eruptive activity at a volcanic island, and to compare the ages of collapses to potential external triggers (e.g. eustatic sea-level change) so that we can better understand the controls on volcano growth and destruction.

Here collapses of lava dome material are referred to as *dome collapses*, collapses of carbonate shelf material are referred to as *shelf collapses*, and collapses involving flank material, or a combination of dome and shelf material are referred to as *flank collapses*. Flank collapses may be very large and involve several cubic kilometres of material (e.g. the Icod landslide (Hunt *et al.,* 2014). *Mass-wasting* or *landslides* are used as collective terms for the different types of collapse event.

Landslides can generate a wide range of different events and deposits. *Debris avalanches refer* to a mass transportation down slope of volcaniclastic material (hot and/ or cold) (lava blocks, ash etc), and *debris avalanche deposits* refers to the resultant chaotic, blocky deposits produced at proximal locations. Landslides may also generate a range of density currents that are represented in the geological record as a variety of density current deposits. In this study we refer to all density current deposits as *turbidites*, regardless of whether the deposits were generated from fully turbulent or non turbulent flows.

Triggers of large-scale mass-wasting events (>0.3 km^3) on volcanic islands are poorly understood, but it has been proposed that their frequency may be affected by earthquake frequency and magnitude, rainfall intensity, eustatic sea-level changes, and edifice growth, (McGuire *et al*., 1997; Wang *et al.,* 2003; Masson *et al*., 2006; Marques *et al.,* 2008; Quidelleur *et al*., 2008; Hunt *et al*., 2013, 2014).

Landslides are frequently observed during or shortly after earthquakes (e.g. Keefer *et al.,* 2000, 1984; Sato *et al*., 2007), and the frequency and magnitude of landslides are related to the magnitude of the earthquake and distance from the earthquake hypocentre (Keefer *et al*., 2000). Mass-wasting events have also been shown to coincide with periods of more intense rainfall (e.g. increased landslide occurrence during the North Atlantic Oscillation in the Azores (Marques *et al.,* 2008; Zizere *et al.,* 2015); lahar generation in the Belham river valley, Montserrat (Barclay *et al.,* 2007)). During rainfall, pore pressures increase and may result in slope failure if pore pressures reduce the slopes' effective confining stress sufficiently (Wang *et al.,* 2003). Collating earthquake records (such as the JPGH/ MIDAS catalogues) and accurate rainfall records beyond historical accounts is difficult. However, methods such as dating exposure of fault planes, pseudotachylite formation and generation of fault gouge material (Kralik *et al.,* 1987; Plaumbo *et al.,* 2004; Sherlock *et al.,* 2004) may perhaps be used to construct pre-historical earthquake records, and speleothem records may provide useful insight into past rainfall intensity (Yadava *et al.,* 1999; Hu *et al.,* 2008).

Constructing records of eustatic sea-level change is simpler with the use of oxygen isotope analyses of microfossils (e.g. Miller *et al.,* 2005), but studies of eustatic sea-level change and volcanic flank collapses have been hampered due to difficulties in acquiring sufficient and accurate dates for landslide events. Such studies have typically relied on incomplete information from onshore observations of collapse structures or deposits, and/or been restricted to relatively recent events recorded in shallow (<6 m) marine cores and seismic profiles (McMurtry *et al*., 2004a, 2004b; Boudon *et al*., 2007; Trofimovs *et al*., 2013). Consequently, very few volcanic island landslide events have been dated

precisely over time periods that are long enough to include multiple sea-level cycles (see global database in *sections 5.4.1 and 5.4.2*) (Longpré *et al*., 2011; Cassidy *et al*., 2012; Trofimovs *et al*., 2013; Hunt *et al*., 2013).

In 2012, IODP Expedition 340 was the first successful expedition to drill through large-scale (>0.3 km^3) offshore volcanic landslide deposits (Le Friant *et al*., 2012). Three sites were drilled, Sites U1394, U1395, and U1396. Holes drilled at site U1394 (10 km SE of Montserrat) sample mass-wasting and eruptive deposits over the past <400 ka (Chapter 4), Holes drilled at Site U1395B (25 km SE Montserrat) sample >1 Ma of mass-wasting and eruptive deposits; and holes drilled at Site U1396 (35 km SW of Montserrat) sample >4 Ma (Chapter 4) of tephra fall deposits due to the site location on a topographic high. Here Site U1395 is studied as the Holes capture a long (>1 Ma) record of both eruptive and mass-wasting related deposits. Hole U1395B is used, as this hole had the most complete core recovery. It is >120 m in length, and provides an opportunity to study a long and detailed record of sedimentological processes around an island arc volcano.

The record in this hole of marine volcaniclastic deposits (both turbidites and marine tephra fall deposits) is used as a proxy for volcanic activity at Montserrat. This approach is based on studies of marine deposits associated with the 1995-2010 eruption on Montserrat. The multiple dome collapses and explosive eruptions have generated a complex and widespread sequence of volcaniclastic tubidites offshore (Kokelaar, 2002; Trofimovs *et al*., 2006). However, not all of the volcaniclastic turbidites present within core U1395B result directly from volcanic activity on-land; later reworking and resedimentation of onshore volcanic deposits may also produce volcaniclastic turbidites. However, most resedimentation of volcanic material occurs shortly after an eruptive event (Collins and Dune, 1986; Major *et al.,* 2000).

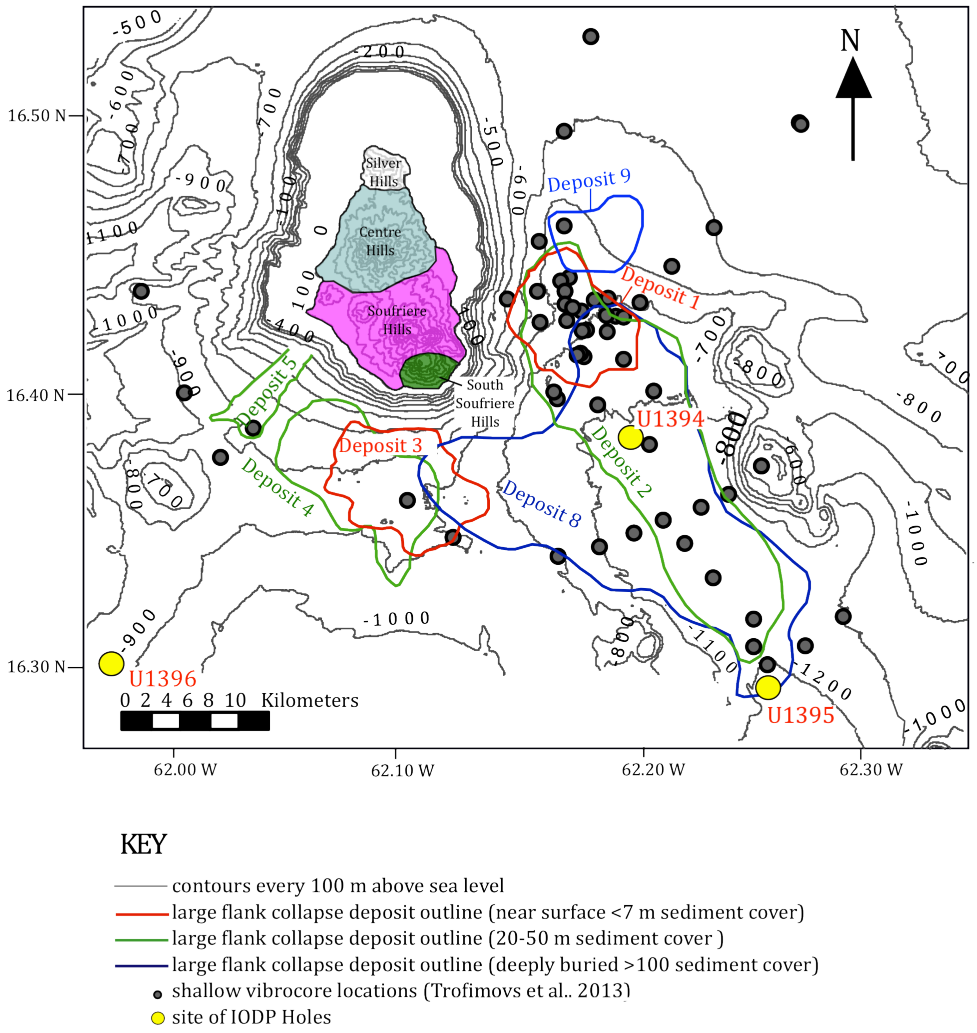

Figure 1. Topographic and bathymetric map of Montserrat showing site of U1395B and large debris avalanche flows (Le Friant *et al.*, 2004; Boudon *et al.*, 2007; Lebas *et al.*, 2011; Watt *et al.*, 2012a, 2012b).

Here we investigate if mass-wasting is affected by sea-level change or intensity of volcanic activity over the past 1 Ma, through the identification and dating of volcaniclastic deposits from Hole U1395B. This period encompasses a sufficient number of volcanic cycles and eustatic sea-level changes to allow for statistically robust hypothesis testing. It is shown that most of the major collapse events around Montserrat occurred during periods of volcanism and rapidly rising sea-level. We therefore go on to explore whether other volcanic islands (island arcs and intraplate ocean islands) show similar relationships between landslide ages

and sea level, whilst noting that the ages of many of these landslide have considerable uncertainties.

2. Study Area: Introduction to Montserrat

Montserrat is an island arc volcano located in the Lesser Antilles (Figure 1). It last erupted between 1995-2010, devastating the city of Plymouth and substantially affecting the island economy (Kokelaar *et al*., 2002; Wadge *et al*., 2014). The eruptions involved multiple collapse events of the active lava dome, which generated pyroclastic flows, block and ash flows and Vulcanian explosions. The largest dome collapse (0.21 km^3) occurred in 2003 and generated a 0.5 m high tsunami on the neighbouring island of Guadeloupe (Trofimovs *et al*., 2012). Bathymetric mapping has since identified much larger landslide deposits offshore of Montserrat with volumes of 0.3-20 km^3 (Deplus *et al*., 2001; Boudon *et al*., 2007; Lebas *et al*., 2011; Watt *et al*., 2012a, 2012b). Such large landslides have a much higher tsunami generation potential, and thus represent a more significant hazard than events associated with the recent eruptions.

Subaerial dating of eruptive deposits on Montserrat suggests that the Centre Hills Volcano and the Soufrière Hills- South Soufrière Hills volcanic complex were active over the past 1 Ma. Centre Hills activity is dated between 990-550 ka (Harford *et al*., 2002) followed by an apparent pause in volcanism untill 290 ka (Harford *et al*., 2002). Since ~290 ka activity has been focussed at the andesitic Soufrière Hills volcano, except for a brief interlude of basaltic volcanism at around ~130 ka, which formed the South Soufrière Hills (Figure 1). The apparent gap in volcanism from 550 ka to 290 ka is not clear in the marine cores, and the currently available subaerial ages may thus reflect a limited stratigraphy represented by on-land exposures (due to burial, erosion and incomplete exposure of the volcanic centres).

The offshore eruption and landslide record around Montserrat has been studied in detail (Deplus *et al*., 2001; Trofimovs *et al*., 2006, 2010, 2012, 2013; Boudon *et*

al., 2007; Lebas *et al*., 2011; Le Friant *et al*., 2010, 2015; Cassidy *et al*., 2012, 2014). To the southeast and southwest of Montserrat is an extensive shallow core (<6 m) data set (Figure 1). These >80 cores contain hemipelagic sediment and numerous volcaniclastic and bioclastic turbidites from eruption and landslide deposits emplaced during the last ~110 ka (Le Friant *et al*., 2009; Trofimovs *et al*., 2010, 2012, 2013; Cassidy *et al*., 2012, 2014). Swath bathymetry and 2D and 3D seismic data have revealed seven large landslide deposits, dating back to the time of Centre Hills volcanism (Figure 1). These large landslide deposits comprise both materials from the volcanic edifice, the carbonate shelf, and seafloor hemipelagic mud (Trofimovs *et al*., 2013).

It is important to recognise that any study based on a single sampling site will introduce some sampling bias in the record of eruptive and collapse events. The Volcanic activity at Montserrat is typified by dome-forming eruptions with durations of months to years, interspersed with moderate-sized explosive eruptions, as exemplified by the 1995-2010 eruption episode (Kokelaar, 2002; Wadge *et al*., 2014). Such eruptions form complex volcaniclastic sequences offshore that are generated by multiple pyroclastic density currents and tephra fall events distributed radially from the volcanic edifice (Trofimovs *et al*., 2006, 2013; Le Friant *et al*., 2015).

Hole U1395B is located ~25 km southeast of Montserrat, hence it is only likely to sample mass flows that entered the ocean to the east and south of Montserrat. While some individual event deposits may therefore not be recorded within Hole U1395B, extended eruptive episodes are still likely to be represented, because any one eruptive event is likely to produce multiple mass flow and tephra fall deposits, with the mass flows, in particular, travelling in a range of directions. For example, the 2003 collapse event (0.1 km^3) deposited a ~20 cm thick volcaniclastic turbidite at site U1395B (Trofimovs *et al*., 2008), but small Vulcanian eruptions that occurred throughout the 1995-2010 eruption are not represented within Hole U1395B (Kokelaar, 2002; Wadge *et al*., 2014).

Hole U1395B is only likely to sample a small proportion of the tephra fall events, as dispersal depends on wind direction and the magnitude of the eruption. Prevailing wind directions in the troposphere and upper stratosphere are predominantly from the east, and prevailing wind directions in the lower stratosphere are from the west, based on historical data from 1956 to present (Radiosonde wind dataset on Guadeloupe). Tephra fall deposits may therefore be subject to a spatial sampling bias, with many eruption plumes transported to the west and potentially leaving no record at the location of U1395B. However, large explosive eruptions, which can involve multiple phases and generate pyroclastic density currents and consequently offshore turbidites, may be represented at the core site (such as the recent eruption, which has involved multiple phases). Since we are interested simply in event timing, rather than magnitude or style, this single core is likely to provide a relatively comprehensive record of eruptions at Montserrat.

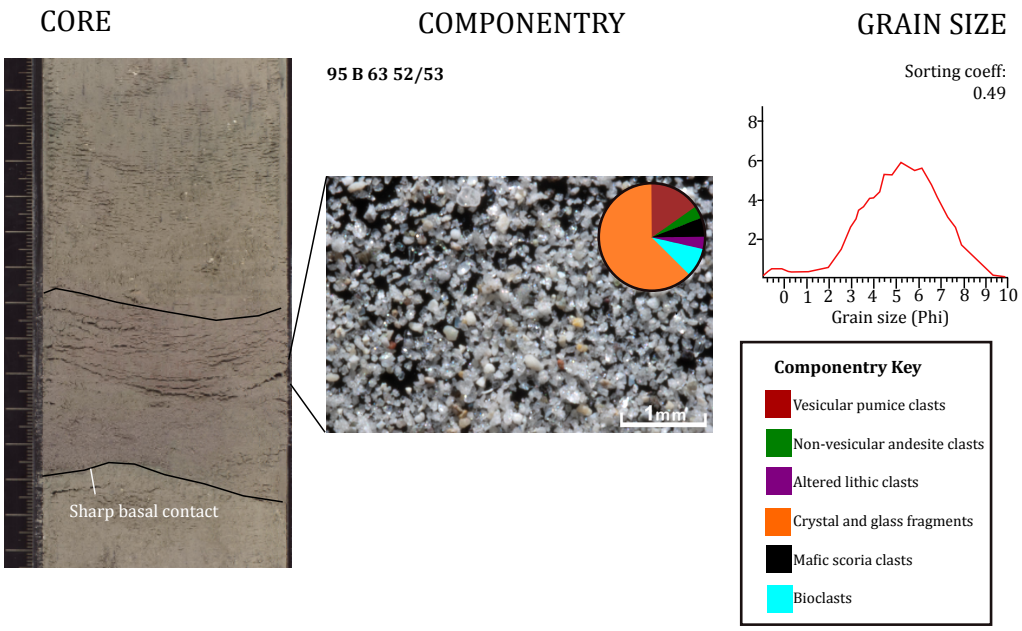

Figure 2: Fall deposit in Hole U1395B. To the left is a core photo with millimetre and centimetre marks, in the middle is a photo of material >63 µm. Composition is given by the pie chart in the top right of the photo. Far right is the grain size distribution from analysing laser grain size analyses on un-sieved samples. Also shown are calculated Folk and Ward sorting coefficients.

3. Methods

3.1. Event deposit identification

We have defined five facies at Site U1395: hemipelagic mud, bioclastic turbidites, mixed bioclastic-volcaniclastic turbidites, volcaniclastic turbidites, and tephra fall deposits (Figures 2 to 6). Hemipelagic mud is mostly composed of carbonate and detrital clay with abundant interspersed foraminifera. The volcaniclastic turbidite and tephra fall deposits are less easily distinguished from each other, as both can comprise normally graded sand and silt (Trofimovs *et al*., 2013). Their discrimination requires grain size and component analysis to identify the type of event deposit (Cassidy *et al*., 2012, 2015a).

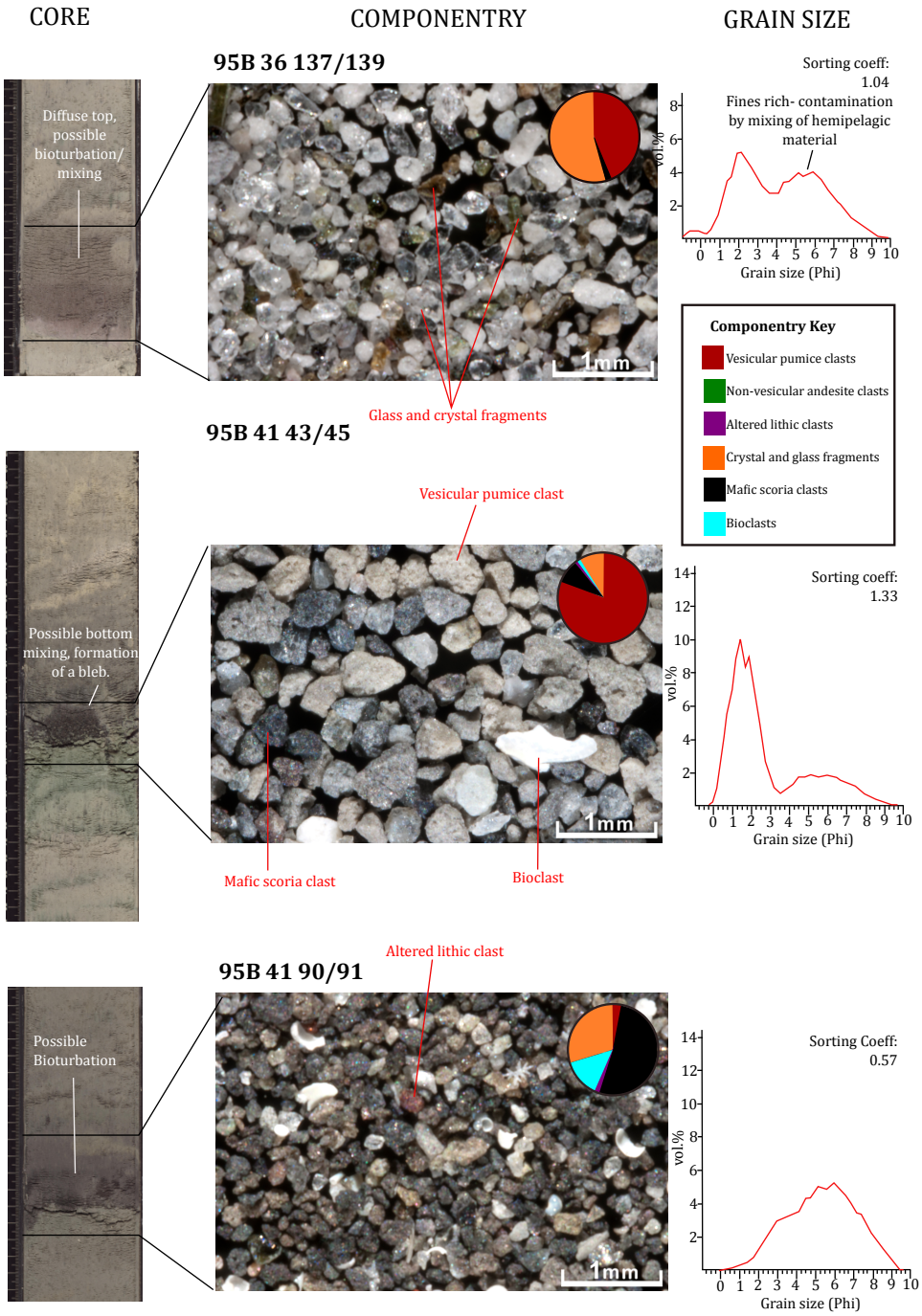

Figure 3: Fall deposits in Hole U1395B where all tephra fall show evidence for bioturbation and/or bottom mixing. To the left are core photos with millimetre and centimetre marks, in the middle are photos of material >63 µm. Composition is given by the pie charts in the top right of each photo and different clast types are labelled. Far right is the grain size distribution from laser grain size analyses of un-sieved samples. Also shown are calculated Folk and Ward sorting coefficients.

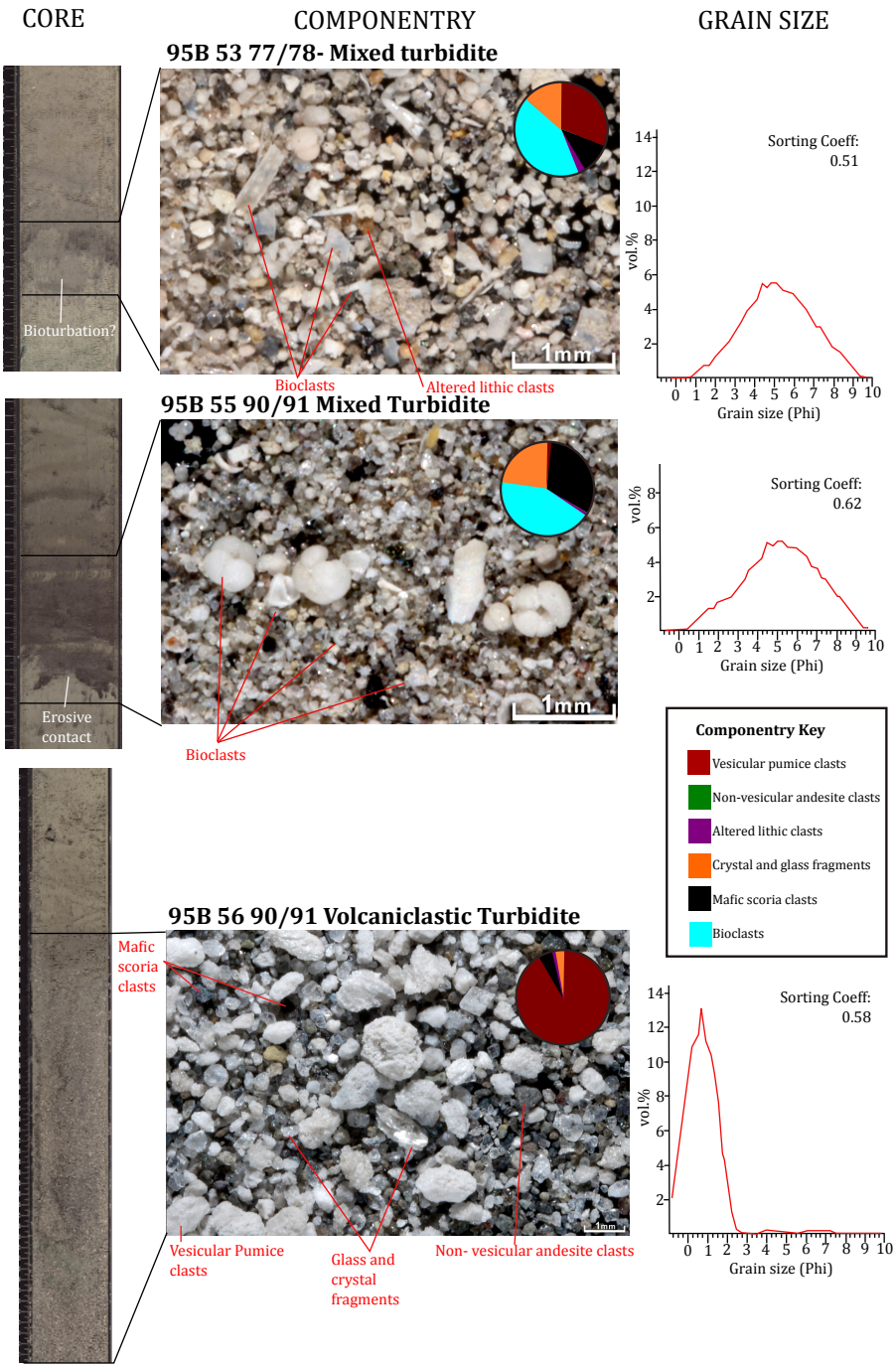

Figure 4: Turbidite deposits in Hole U1395B. To the left are core photos with millimetre and centimetre marks, in the middle are photos of material >63 µm. Composition is given by the pie charts in the top right of each photo and different clast types are labelled. Far right is the grain size distribution from laser grain size analyses on un-sieved samples. Also shown are calculated Folk and Ward sorting coefficients.

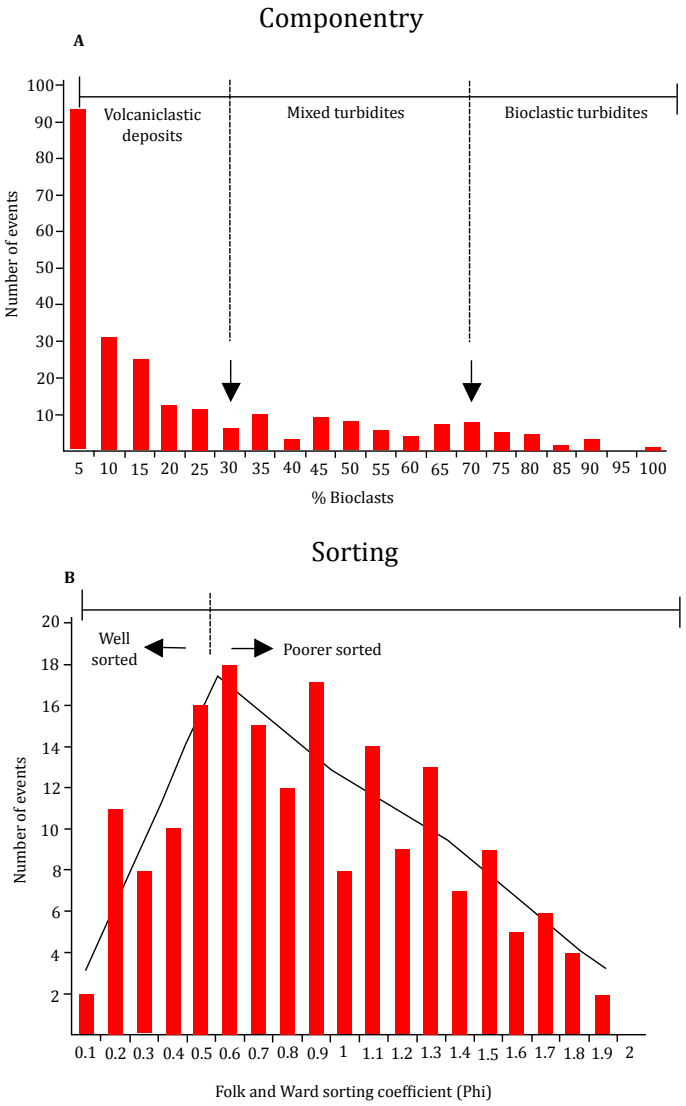

Figure 5: Histograms of bioclastic content of all analysed deposits (top) and all calculated Folk and Ward Sorting Coefficents (phi) (bottom). Also shown on both histograms are the unit classification boundaries used in this study. It is noted that there are no clear breaks in composition or sorting.

Tephra fall layers were defined in this study as having <30% bioclasts, a Folk and Ward (1957) sorting coefficient of <0.5 phi (where grainsize (phi) = - $\log_2$ (grainsize (mm)) (analyses conducted on particles from -1 to 10 phi), and a thickness of <20 cm (Figures 2 to 4). No clear clusters in composition or sorting are identifiable (Figure 5), but there appears to be a decrease in events at 30% bioclasts, and at a peak in the sorting coefficient at 0.5 phi. Tephra fall deposits

are well sorted by density due to settling through the water column and they are dominated by volcanic clasts. Hole U1395B is ~25 km away from Montserrat, where tephra fall deposits from moderate-sized explosive eruptions, even downwind, are likely to be on the order of a few centimetres thick; consequently, thick (>20 cm) deposits are unlikely to be tephra fall layers (Figure 6). Thin tephra fall layers are commonly mixed with hemipelagic material, through bioturbation, bottom current reworking, or contamination during sampling, and which artificially increase the bioclast contents and sorting coefficients of the tephra fall. We have thus defined tephra fall layers as comprising up to 30% bioclast content to allow for post-depositional mixing, and take into account any evidence of bioturbation or sediment mixing seen in the core (Figure 3).

Volcaniclastic turbidites are deposits of erosive flows that may entrain bioclastic material and previously deposited volcaniclastic sediments. Therefore, although some parts of a volcaniclastic turbidite can be well-sorted, they are generally less well-sorted than tephra fall deposits. Volcaniclastic turbidites are defined here as comprising <30% bioclasts, with a Folk and Ward (1957) sorting coefficient >0.5 (phi). Mixed turbidites are defined as having 30-70% bioclasts. Bioclastic turbidites are defined as containing > 70% bioclasts.

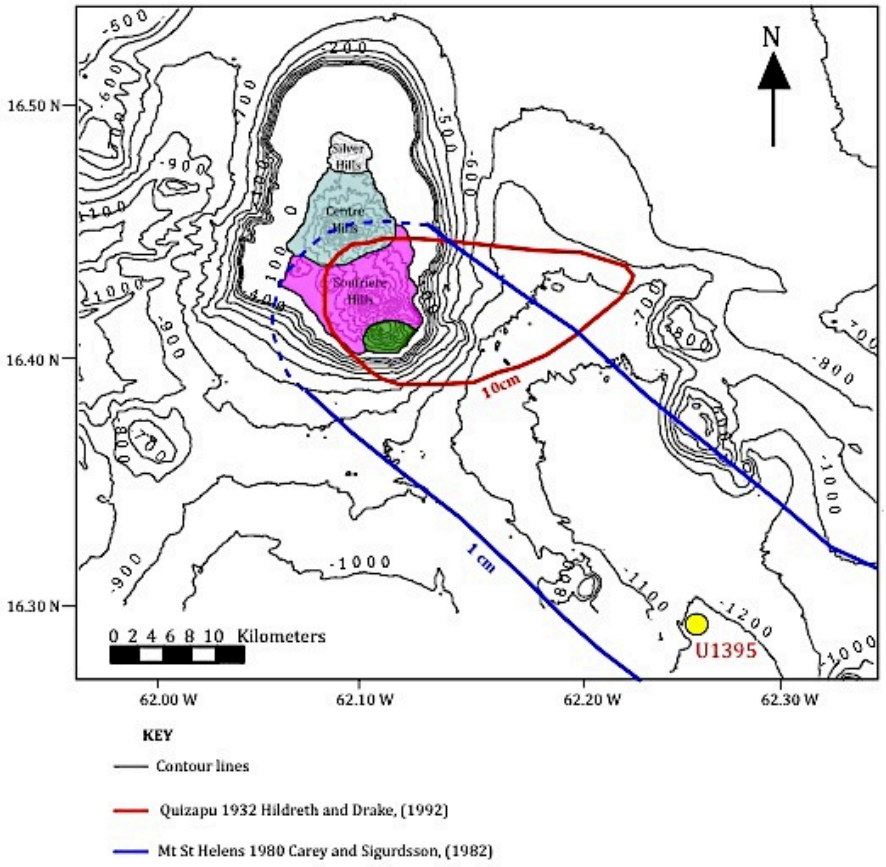

Figure 6: Shows isopachs constructed for the Quizapu 1932 eruption (Hildreth and Drake, 1992), and the Mt St Helens 1980 eruption (Carey and Sigurdsson, 1982) projected onto a bathymetric map of Montserrat. Also shown is the IODP Site U1395 in yellow. The Quizapu 1932 eruption and the Mt St Helens 1980 eruption have proximal tephra fall deposit thicknesses similar to the thickest tephra fall deposits found on Montserrat (Woodlands Tephra, Chapter 2). This diagram suggests that tephra fall thicknesses of even the largest eruptions at Montserrat are unlikely to exceed thicknesses greater than 20 cm at IODP Site U1395.

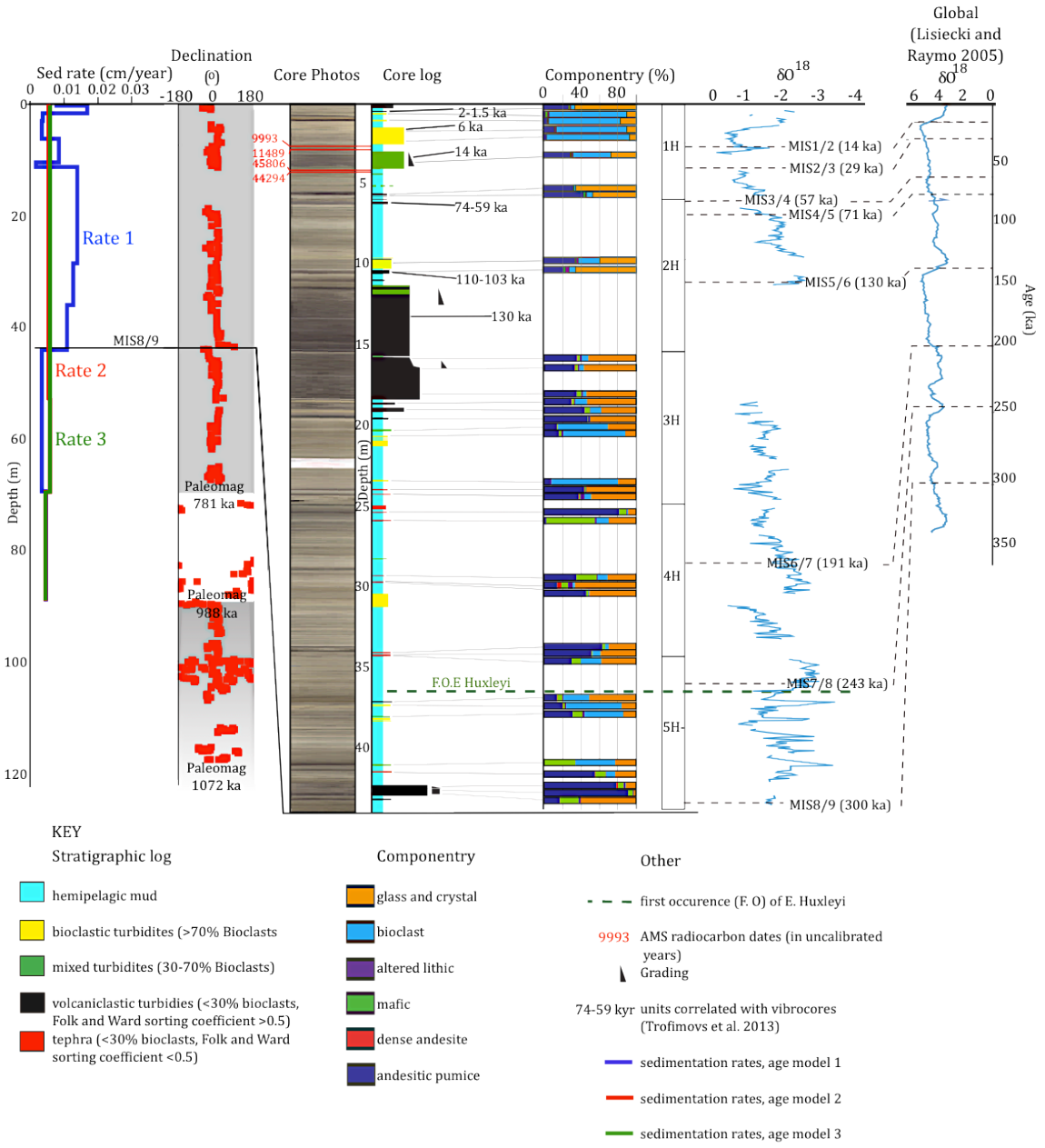

Figure 7: Upper 44 m of Hole U1395B including core log and photos; calculated sedimentation rates for age model 1; NRM declination data from shipboard measurements; section of stratigraphic core photos and log; sample of componentry data; oxygen isotopes from this study and the global oxygen isotope curve from Lisiecki and Raymo (2005). For full componentry data and stratigraphic log of Hole U1395B see appendix table 10 and appendix figures 2 and 3.

Grain size measurements using laser-diffraction analyses were carried out using a Malvern Master-sizer 2000 particle size analyser, which can measure grain sizes between 0.2–2000 μm. To disperse grains, 25 ml of reverse osmosis water with 0.05% sodium hexametaphosphate dispersant was added to 1 cm^3 of sample and left overnight on a shaking table. Samples were analysed in triplicate and accuracy was monitored using standard size particles (32 and 125 μm) (as in Hunt *et al*., (2013)).

Componentry analysis was conducted on sieved fractions >63 μm and <250 μm material from all volcanic-rich units and some bioclastic-rich units. For each sample, approximately 400 grains were point-counted using an area counting method. Componentry classes follow Le Friant *et al*., (2008) and Cassidy *et al*., (2015a): 1) vesicular pumice clasts; 2) non-vesicular andesite; 3) altered lithic clasts; 4) crystal and glass fragments; 5) mafic scoria clasts; and 6) bioclasts. Grainsize and componentry data are summarised in appendix tables 9 and 10, respectively (Figures 2-5).

3.2. Dating Hole U1395B

The core from U1395B was dated using a combination of oxygen isotope stratigraphy, biostratigraphy, AMS radiocarbon dating, and the shipboard paleomagnetic reversal records. This work was a combined effort between D. Wall-Palmer and myself. Higher resolution dating was carried out on the upper 40 m of Hole U1395B using oxygen isotope stratigraphy of the hemipelagic mud (Figure 7). Twenty *Globigerinoides ruber* specimens between 250-355 μm in size were picked and analysed from each hemipelagic sample. Samples were 7 cm apart and analysed at Plymouth University on an Isoprime Instruments continuous flow mass spectrometer with a Gilson Multiflow carbonate auto-sampler. Oxygen Isotope values are given as deviations in the isotope ratios ($^{18}O/^{16}O$) per mil (‰), using the VPDB scale (Appendix Table 11).

Allocation number	Publica-tion code	Sample identi-fier	$\delta^{13}C_{VPDB}$ ‰ ± 0.1	Carbon content (% by wt.)	^{14}C Enrich-ment (% modern)	+/- 1σ (% modern)	Conventional Radiocarbon Age (years BP)	+/- 1σ (radio carbon yrs BP)	Stratigra-phic position (cm)
1721.0513	SUERC-46961	1H2W-108-110	1.1	10.9	28.82	0.13	9993	37	258-260
1721.0513	SUERC-46962	1H2W-115-117	1.1	10.8	23.93	0.12	11489	40	265-267
1721.0513	SUERC-46965	1H3W-109-111	1.2	11.4	0.33	0.06	45806	1463	409-411
1721.0513	SUERC-46966	1H3W-116-118	1.0	11.3	0.40	0.06	44294	1208	416-418

Table 1: AMS carbon dates from core U1395.

To limit the ambiguity of identifying marine isotope stages, biostratigraphic boundaries and AMS radiocarbon dates (for sediments <50 ka) were used (Table 1).

Calcareous nannofossils in the <63 μm material from hemipelagic samples were analysed using scanning electron microscopy (SEM), employing the calcareous nannofossil zonation of Kameo and Bralower (2000) for the Caribbean Sea. Sediment was fixed to metal stubs using a thin layer of spray adhesive, then sputter coated with gold. The first occurrence of *Emiliania huxleyi* (250 ka) was found at 36.74 m, close to the MIS 7/8 boundary (243 ka). This work was undertaken by D. Wall-Palmer. The first occurrence of *E. huxleyi* has also been identified across the MIS 7/8 transition in Hole U1396C (Wall-Palmer *et al*., 2014) and CAR-MON 2 (Le Friant *et al*., 2008) (Figure 7).

New AMS dates were obtained in this study from four samples in the upper 4 m of Hole U1395B (aged <57 ka), in addition to the radiocarbon AMS dates reported by Trofimovs *et al*., (2013). Approximately 1000 pristine tests of white *Globgerinoides ruber* (Figure 8) >150 μm in size were picked (~17 mg) and then sonically cleaned. I prepared the samples and D. Wall-Palmer picked the samples. The new samples were located beneath two of the largest turbidites (Figure 7). Radiocarbon dates were measured at Scottish Universities Environmental

Research Council (SUERC) laboratory using their in-house protocol (Trofimovs *et al*., 2013).

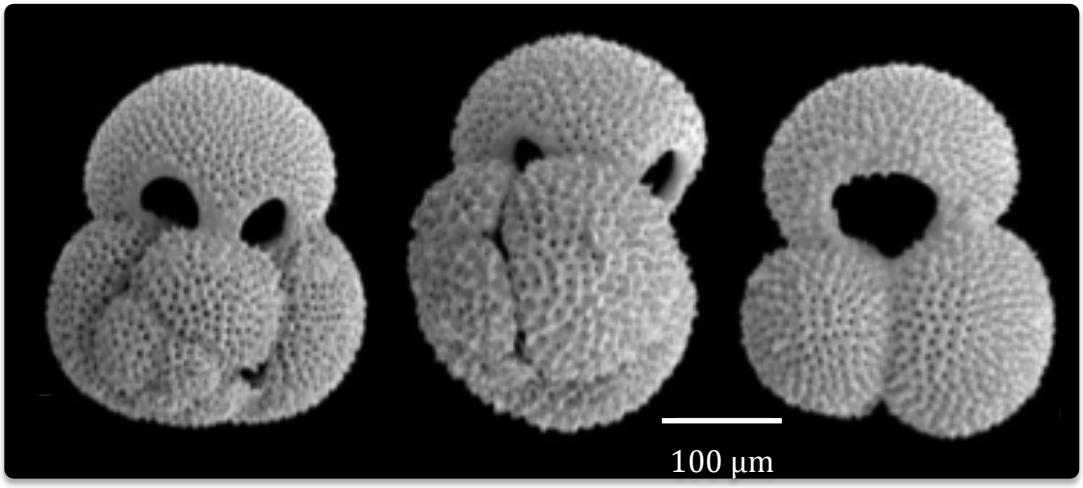

Figure 8: Scanning electron photograph of *Globgerinoides ruber,* which was picked for oxygen isotope work and AMS dating (Wall-Palmer *et al*., 2014)

Paleomagnetic reversals were determined on board during Expedition 340 as 180° changes in declination (after azimuthal correction). Associated changes in inclination after demagnetization of the natural remnant magnetization (NRM) in a field of 20 mT (to remove the coring overprint) were also recorded (see Hatfield *et al*., (2013) for details). Here we report ages based on the geomagnetic polarity timescale (GPTS) of Ogg *et al*., (2012) instead of the GPTS of Cande and Kent (1995) as was reported on board of the ship. Two paleomagnetic reversals occur at 781 ka (6.3% error) and 988 ka (11.3% error) in core U1395B (Cande and Kent 1992a, 1992b; Ogg *et al*., 2012), with a possible third reversal at the base of the core at 1072 ka (11.3% error) (Cande and Kent 1992; Ogg *et al*., 2012).

Figure 9: Correlations of the top of core U1395B with shallow cores based on componentry and oxygen isotope data (Le Friant *et al.*, 2008; Cassidy *et al.*, 2012, 2014; Ogg *et al.*, 2012; Trofimovs *et al.*, 2013; Wall-Palmer *et al.*, 2014).

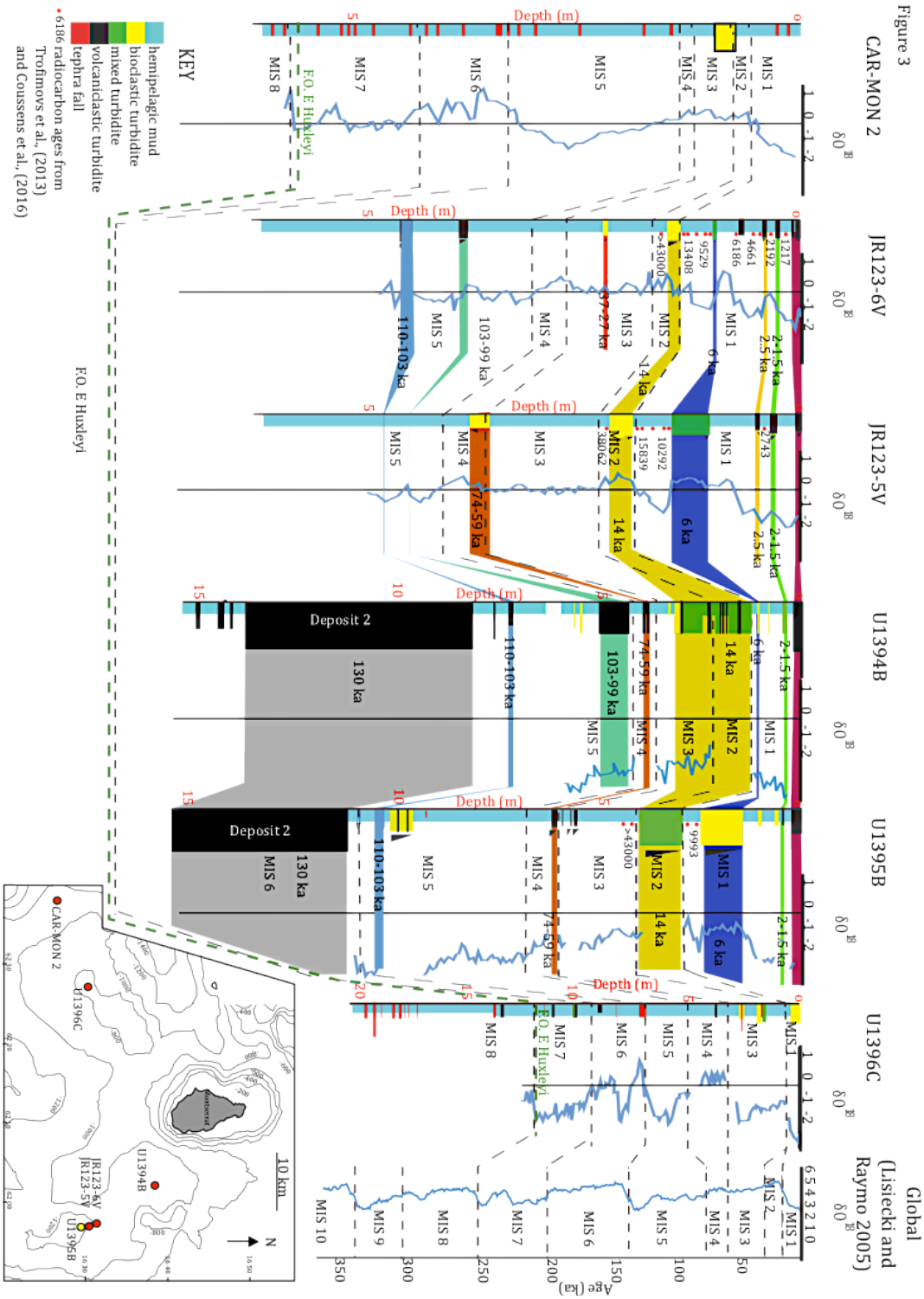

The 781 ka reversal is obscured by a volcaniclastic turbidite and coring disturbance at 68.5-71 m (Figure 7). The coring disturbance occurs primarily within the volcaniclastic turbidite. The reversal is likely to have occurred shortly prior to the emplacement of the volcaniclastic turbidite, thus obscuring the reversal through erosion of hemipleagic mud. Here we take the base of the volcaniclastic turbidite as 781 ka. The MIS 8/9 (300 ka) boundary is interpreted to occur at ~44 m, suggesting that sedimentation rates decreases with depth in the core. The 988 ka reversal occurred between 88.3-89.9 m, with a mid point at 89.1 m (Figure 7). The 1072 ka reversal may be present at the base of Hole U1395B (Figure 7) but this is less certain due to poor sample recovery at the base of the core.

Data from Hole U1395B were also compared and correlated to previously studied cores around Montserrat (Figure 9). These cores include JR123-5V, JR123- 6V, CAR-MON 2, and Hole U1396C (Figure 9). JR123-5V and JR123-6V are part of an extensive vibrocore data set that has been used to compile a comprehensive stratigraphy of Montserrat over the past 110 ka (Trofimovs *et al*., 2013). The vibrocore data set includes over 80 <6 m long cores with 40 accelerator mass spectrometry (AMS) radiocarbon dates (Figure 9). JR123-5V and JR123-6V are located 1-2 km north of Site U1395, and some units within core U1395B can be correlated to units found in JR123-5V and JR123-6V by age (Figure 9). CAR-MON 2 is a piston core collected in 2002, which extends 5.75 m and was taken ~55 km to the southwest of Montserrat (Figure 9) (Le Friant *et al*., 2008). Site U1396C is situated ~33 km southwest of Montserrat (Figure 9) and was collected during IODP Expedition 340 (Wall-Palmer *et al*., 2014; Chapter 4).

4. Results

Hole U1395B is 127.51 m long and is made up of 62.6% hemipelagic mud, 24.4% volcaniclastic deposits, 9% mixed turbidites and 4% bioclastic deposits, by deposit thickness. The core comprises 18 bioclastic turbidites, 52 tephra fall deposits, 27 mixed turbidites, and 41 volcaniclastic turbidites. Core recovery is

good (>90%), with only one occurrence of basal flow-in coring disturbance over the studied core length at the bottom of Core U1395B-2H, followed by probable fall-in at the top of Core Section U1395B-3H (Jutzeler *et al*., 2014).

4.1. Age Models

Unit ages have been estimated by calculating hemipelagic sedimentation rates between dated horizons, assuming constant rates of sedimentation between dated horizons. However, developing accurate age models for marine cores is difficult due to the effects of erosion (commonly at the base of turbidites), short-term fluctuations in sediment supply, and the sometimes ambiguous identification of marine isotope stages. We therefore include three age models to help capture these uncertainties, and their implications.

Age models can be affected by erosion. In the upper 5 m of U1395B ~88 cm of hemipelagic sediment is estimated to have been eroded by the 12-14 ka turbidite (Trofimovs *et al*., 2013), indicating that the effects of erosion at Site U1395B may be significant. Erosion rates in the upper 10 m of U1395B are well constrained by a combination of AMS dates from this study, and correlation with well-dated units (40 AMS dates) in the shallow vibrocore dataset (Trofimovs *et al*., 2013). Below the threshold for AMS radiocarbon dating (>10 m in Hole U1395B) the effects of erosion by turbidites cannot be accurately constrained at site U1395B, potentially leading to inaccuracies in age models. It is plausible that most turbidity currents are erosive, removing underlying hemipelagic mud and event deposits from the stratigraphy and meaning that the apparent sedimentation rate is likely to be lower than the true sedimentation rate. However, we expect this to be a systematic error that affects the whole core, rather than something that introduces bias to specific time periods.

Dating cores using oxygen isotopes may also lead to age model inaccuracies due to the difficulty in identifying marine isotope stages (MIS). Oxygen isotopes from Hole U1395B have been compared to the Lisiecki and Raymo (2005) curve; however, local environmental factors (e.g. amount and species of biota, oxygen

supply) may affect the magnitude of isotope fluctuations, and also erosion may remove parts of the isotope record, resulting in the misidentification of MIS boundaries. Any inaccuracies in the age models will affect the reliability of unit ages assigned to individual events, and thus affect subsequent analysis of the dataset.

Assuming that the average total erosion beneath turbidites is on the order of centimetres, and assuming that marine isotope boundaries have been correctly constrained within a few centimetres, the event dating errors are likely to be on the order of 10^2-10^5 years. This is a similar magnitude to stratigraphic gaps (i.e. sections of missing stratigraphy) identified in other cores around Montserrat, including instances where >30 ka of stratigraphy has been removed by turbidite erosion (JR 123-5-V and Hole U1396C) (Trofimovs *et al*., 2013; Wall-Palmer *et al*., 2014). Age uncertainties on this order are likely to affect the entire sequence. In order to assess how sensitive our event-frequency analysis is to dating errors of this magnitude, we conduct the same analysis with three different age models. Age Model 1, described below, uses all age constraints (i.e. MIS boundaries, palaeomagnetic reversals etc.) but is also potentially more sensitive to the effects of erosion, producing a record with several apparent fluctuations in sedimentation rate. Age Models 2 and 3 use fewer age constraints, resulting in a smoother estimate of long-term sedimentation rate that may be more geologically realistic. Individual unit ages derived from the three age models may vary by up to 10^5 years. By using all three age models within subsequent analyses, we can test how robust our results are to these uncertainties.

Age Model 1: Age Model 1 uses 11 dated horizons, and is the best-constrained age model. This includes dated horizons derived from correlations to units described by Trofimovs *et al*. (2013), identification of MIS boundaries, and identification of paleomagnetic reversals. The 2-1.5 ka, 6 ka, 14 ka, 74-59 ka, 110-103 ka, and 130 ka deposits from Trofimovs *et al*. (2013) and Cassidy *et al*. (2015b) have been correlated to units in U1395B. Unit ages of 1.75 ka, 6 ka, 14 ka, 66.5 ka, 107 ka, and 130 ka in Hole U1395B at core depths of 0.49 m, 2.52 m, 3.98 m, 6.26 m, 10.47 m, and 18.49 m respectively were used in Age Model 1. Using oxygen

isotope analysis 3 MIS boundaries were identified and used. These are MIS boundaries 6/7 (191 ka), 7/8 (243 ka) and 8/9 (300 ka) at core depths of 28.31 m, 35.93 m, and 43.84 m respectively (Lisiecki and Raymo, 2005). Finally, two paleomagnetic reversal dates of 781 ka, and 988 ka, at depths of 63.06 m, and 89.08 m are used in Age Model 1.

Using Age Model 1, the calculated sedimentation rates in the upper 300 ka of Hole U1395B fluctuate between 2 to 17 cm/ka, and encompass the range of hemipelagic sedimentation rates (5 to 10 cm/ka) previously determined in the area by Reid *et al*. (1996). Sedimentation rates are likely to appear higher in Hole U1395B than in the marine cores in Reid *et al*. (1996), as Hole U1395B is more proximal to Montserrat. The greater variability in apparent accumulation rates determined from Age Model 1 (particularly for the lower sedimentation rates) likely reflects the effects of turbidite erosion. Sedimentation rates in Age Model 1 between 300-988 ka are relatively constant at 3.2-9 cm/ka. The reduction in variability of sedimentation rates further down the core likely reflects the fact that there are fewer dated horizons deeper in Hole U1395B, resulting in a smoother apparent sedimentation rate.

Age Models 2 and 3: Age Model 2 uses Deposit 2 as a boundary at 130 ka (Figure 7; Cassidy *et al*., (2015b)) at 18.49 m, and the paleomagnetic dates of 781 ka, and 988 ka, at depths of 63.06 m, and 89.08 m respectively. Age Model 3 uses only the two paleomagnetic dates. Using Age Models 2 and 3, estimated sedimentation rates are less variable throughout the core with long-term rates of 4-8 cm/ka.

4.2. Event frequency offshore Montserrat

Events are not distributed regularly through time in core U1395B, but appear to cluster within specific time periods (Figure 10). To better understand this long-term variation in event timing we conduct a moving sum, where the number of events are summed every 50 ka, at 10 ka increments. Observations do not change when using bins of 30 ka and 100 ka (see Figures 10-13). To be conservative, we classify periods of increased frequency as periods where all three age models

show that the frequency of event deposits is above the mean 90% confidence interval of the moving sum data (Figure 11). Periods of reduced activity are defined as periods where all three age models show that event frequency is below 1 standard deviation from the mean (mean- standard deviation). In Hole U1395B, all age models show an increased frequency of all event deposits (above the 90% confidence interval of 8.44 events in 50 ka) between ~120 ka to ~170 ka. In age models 1-3, periods of relative quiescence last of the order of 10^4- 10^5 ka.

There are three periods where the frequency of volcaniclastic deposits (volcanic turbidites and tephra fall) is greater than the mean 90% confidence interval. These are ~930 ka to ~900 ka; ~810 ka to ~760 ka; and ~190 ka to ~120 ka. Tephra fall deposits result from explosive eruptions, and volcaniclastic turbidites are associated with dome/flank collapse (including lava-dome collapse) and pyroclastic density currents entering the sea. We interpret periods with a higher frequency of both tephra fall and volcaniclastic turbidites as representing episodes of elevated eruptive activity at Montserrat. However, some volcaniclastic turbidites from flank collapses may occur during periods of volcanic quiescence (Figure 11).

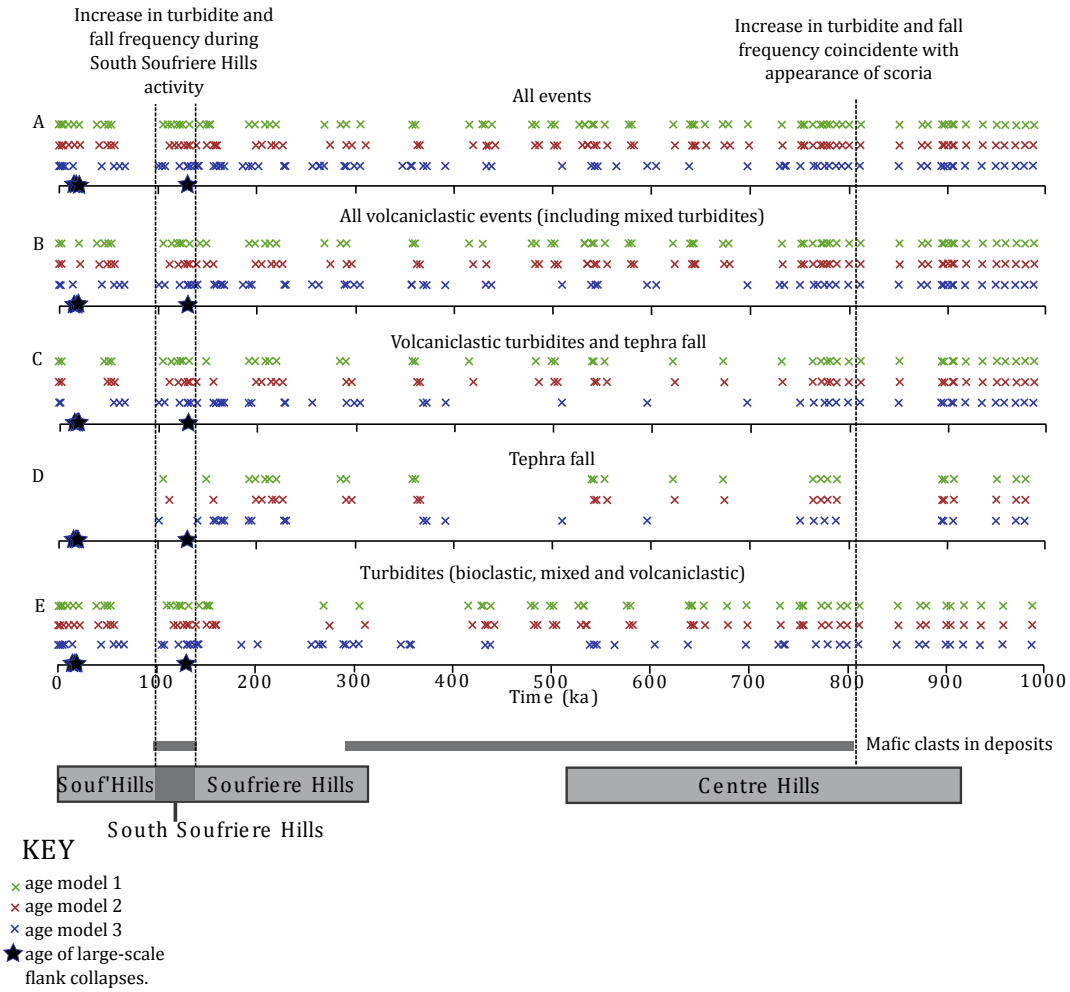

Figure 10: Timing of (a) all events, (b) volcaniclastic events (tephra fall and turbidite deposits; including mixed composition turbidites), (c) volcaniclastic events (tephra fall and volcaniclastic turbidite), (d) tephra fall deposits, and (e) all turbidites at Montserrat. In each case, three different age models are shown. Age model 1 (green) uses oxygen isotope data, biostratigraphic data, AMS dates, and paleomagnetic dates. Age model 2 (red) uses Deposit 2 as a boundary at 130 ka (Figure 2), and the paleomagnetic intervals. Age model 3 (blue) uses only the paleomagnetic data. Clustering of events in all age models can be seen at ~950-860 ka, 810-750 ka, 200-100 ka and from ~50 ka, on Montserrat. There is an absence of prolonged pauses in activity. Thin grey lines show occurrence of scoria within core U1395B, the thick grey line shows known extents of activity at volcanic centres on Montserrat based on limited subaerial dating (Harford *et al.*, 2002).

The periods of heightened volcanic activity show a general correlation with changes in the style of eruptions at Montserrat (Figures 4 and 5). The ~810 to ~760 ka period coincides with the appearance of basaltic scoria within Hole U1395B. The ~190 ka to ~120 ka period coincides broadly with the onset of activity at South Soufrière Hills volcano (Harford *et al*., 2002).

To test if there is any correlation between sea-level and turbidite frequency we use a linear model (LM), generalised linear model (GLM), and proportional hazards model (PHM) after binning the data into 10 ka intervals. For similar examples see Hunt *et al*., (2014) and Clare *et al*., (2016). Unit ages are given in appendix table 12 and test results are given in Table 2.

Statistical analyses are conducted on all three age models in order to test the sensitivity of results to dating errors and to determine if results are artefacts of the specific age model used. By comparing results from the three age models the effects of age uncertainty can be better understood. We pose the null hypothesis that turbidite frequency is not correlated with sea-level, and P-values < 0.05 allow us to reject this hypothesis. Table 2 shows that using age model 1 does not show significance in any statistical tests, but using age models 2 and 3 shows significance in all three statistical tests. However, the correlation coefficient for LM is very low (0.002, 0.085, and 0.077 for age models 1-3 respectively). Low correlation coefficients for age models 2 and 3 indicate that while there may be a broad correlation between sea-level and turbidite frequency, the variation means that the scatter about that trend is very wide. Grouping together of turbidites from eruptive and collapse activity, effects of data binning, or genuine natural noise, may cause this broad scatter. Therefore we conclude that all three age models are in agreement and show that there is little to no correlation between sea-level and turbidite frequency. Dating errors are unlikely to affect this observation due to the consistency of this result across all three age models.

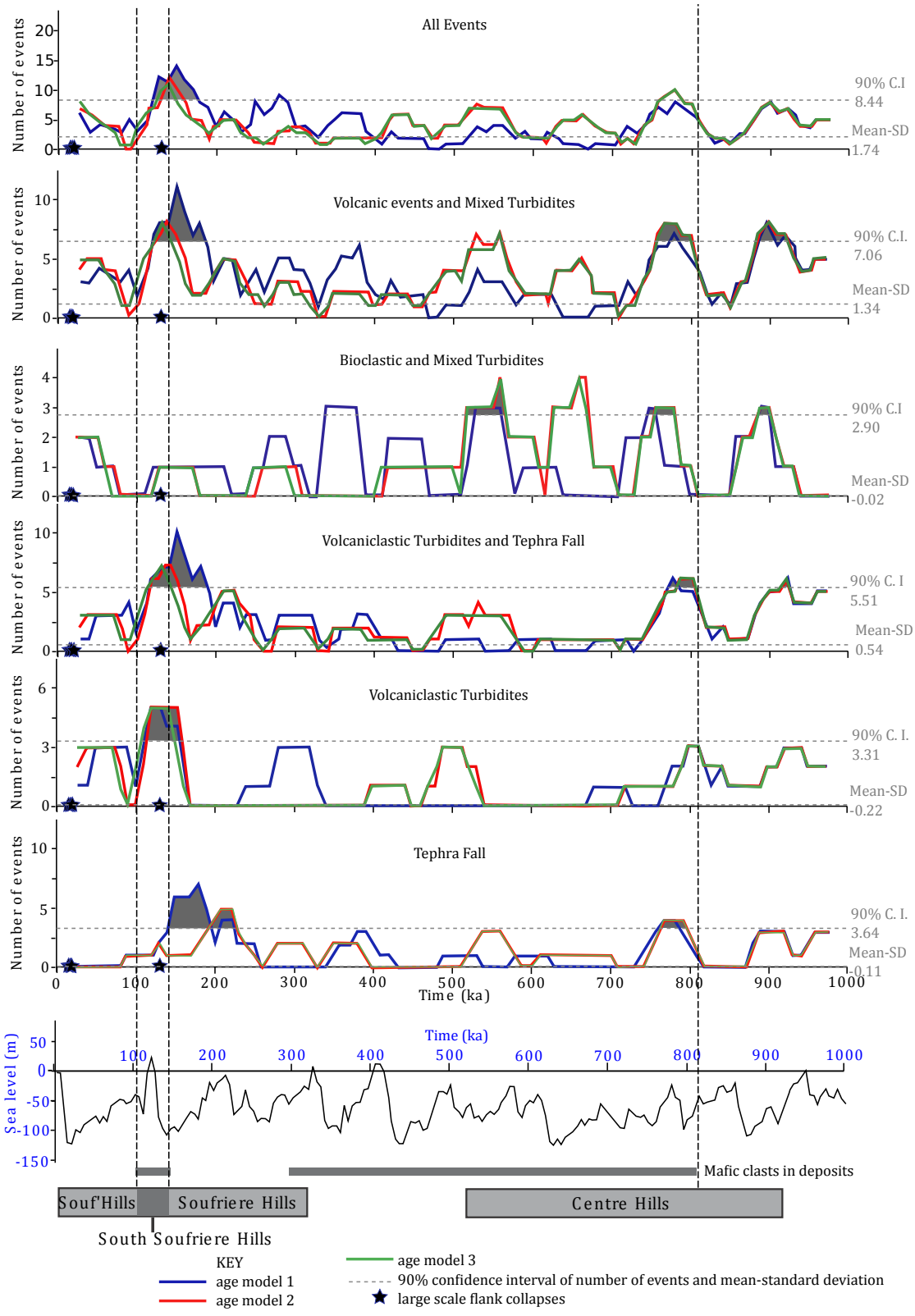
All Events
Number of events
90% C.I
8.44
Mean-SD
1.74
Volcanic events and Mixed Turbidites
90% C.I.
7.06
Mean-SD
1.34
Bioclastic and Mixed Turbidites
90% C.I
2.90
Mean-SD
-0.02
Volcaniclastic Turbidites and Tephra Fall
90% C. I
5.51
Mean-SD
0.54
Volcaniclastic Turbidites
90% C. I.
3.31
Mean-SD
-0.22
Tephra Fall
90% C. I.
3.64
Mean-SD
-0.11
Time (ka)
Sea level (m)
Mafic clasts in deposits
Souf'Hills
Soufriere Hills
Centre Hills
South Soufriere Hills
KEY
age model 1
age model 2
age model 3
90% confidence interval of number of events and mean-standard deviation
large scale flank collapses

Figure 11: Number of events within 50 ka (centred on window, at 10 ka increments). Peaks correspond to clusters in Figure 10. Age model 1 (green) uses oxygen isotope data, biostratigraphic data, AMS dates, and paleomagnetic dates. Age model 2 (red) uses Deposit 2 as a boundary at 130 ka (Figure 2), and the paleomagnetic intervals. Age model 3 (blue) uses only the paleomagnetic data. Peaks in event frequency occur at ~930 ka to ~900 ka, ~810 ka to ~760 ka, and ~190 ka to ~120 ka. Periods when event frequency is above the 90% confidence interval in all age models are shaded in grey. The black line is the Miller *et al*., (2005) sea-level curve in meters from present day sea-level. Thin grey lines show occurrence of mafic scoria within Hole U1395B, the thick grey line shows known extents of activity at volcanic centres on Montserrat based on limited subaerial dating (Harford *et al*., 2002). There is a peak in event frequency that coincides with the appearance of mafic scoria in Hole U1395B and all large flank collapses occur during periods of rapid sea-level rise.

	Age Model 1	Age Model 2	Age Model 3
Linear model	0.0898	*0.00176*	*0.00285*
Generalised linear model	0.083407	*0.00138*	*0.00696*
Proportional hazards model	0.106	*0.00219*	*0.00942*

Table 2: Results of linear statistical tests for turbidite frequency and sea-level correlations. Italicised values show when statistical tests are significant, (ie when the null hypothesis can be rejected).

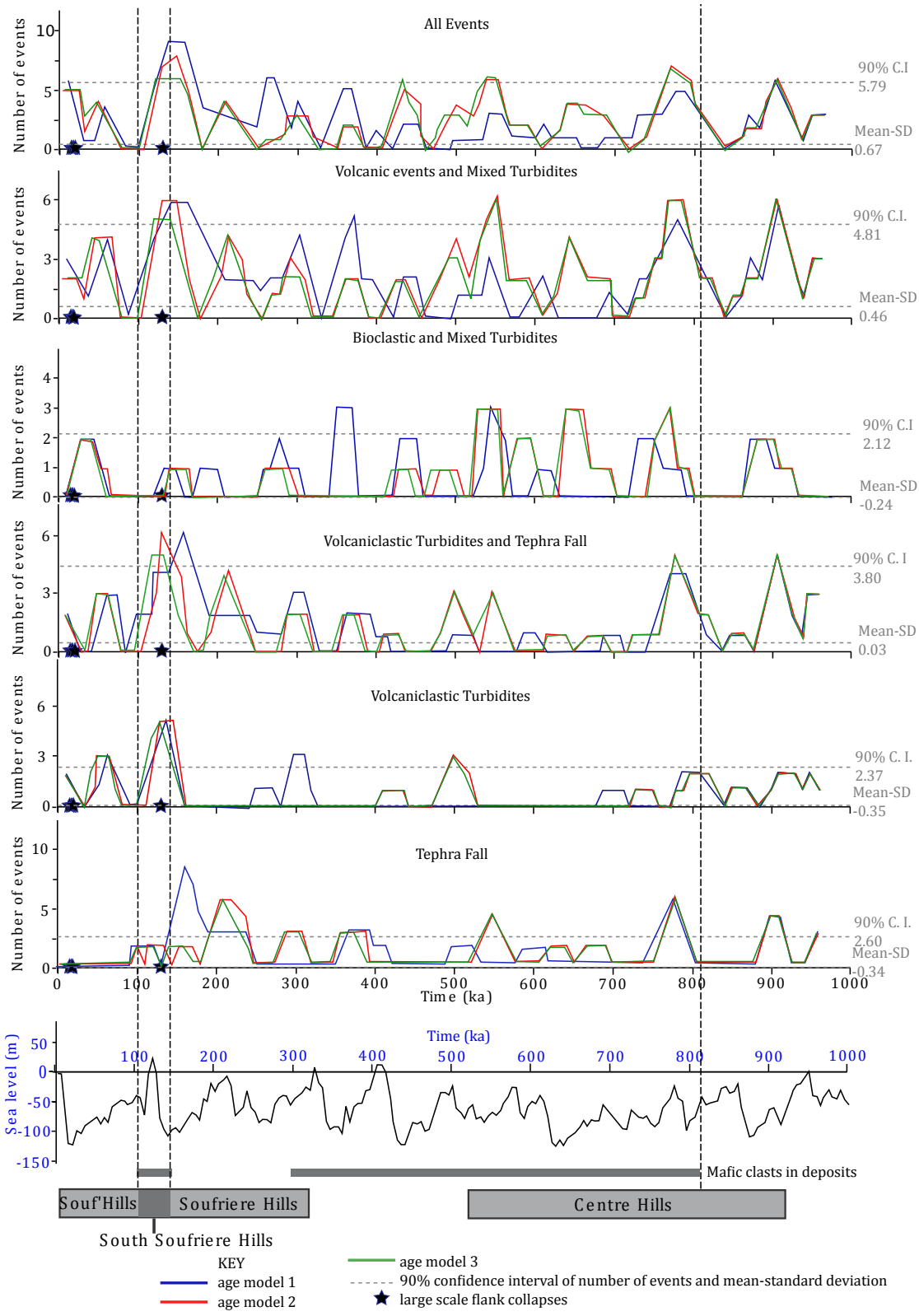
All Events
90% C.I
5.79
Mean-SD
0.67
Volcanic events and Mixed Turbidites
90% C.I.
4.81
Mean-SD
0.46
Bioclastic and Mixed Turbidites
90% C.I
2.12
Mean-SD
-0.24
Volcaniclastic Turbidites and Tephra Fall
90% C. I
3.80
Mean-SD
0.03
Volcaniclastic Turbidites
90% C. I.
2.37
Mean-SD
-0.35
Tephra Fall
90% C. I.
2.60
Mean-SD
-0.34
Number of events
Time (ka)
Sea level (m)
Mafic clasts in deposits
Souf'Hills
Soufriere Hills
Centre Hills
South Soufriere Hills
KEY
age model 1
age model 2
age model 3
90% confidence interval of number of events and mean-standard deviation
large scale flank collapses

Figure 12. Similar to Figure 11, but this figure shows the number of events within 30 ka (centred on window, at 10 ka increments). Age model 1 (green) uses oxygen isotope data, biostratigraphic data, AMS dates, and paleomagnetic dates. Age model 2 (red) uses Deposit 2 as a boundary at 130 ka (Figure 2), and the paleomagnetic intervals. Age model 3 (blue) uses only the paleomagnetic data. Peaks in event frequency are similar to figure 11 (that uses bin widths of 50 ka). The black line is the Miller *et al*. [2005] sea-level curve in meters from present day sea-level. Thin grey lines show occurrence of mafic scoria within Hole U1395B, the thick grey line shows known extents of activity at volcanic centres on Montserrat based on limited subaerial dating [Harford *et al*., 2002]. There is a peak in event frequency that coincides with the appearance of mafic scoria in Hole U1395B and all large flank collapses occur during periods of rapid sea-level rise.

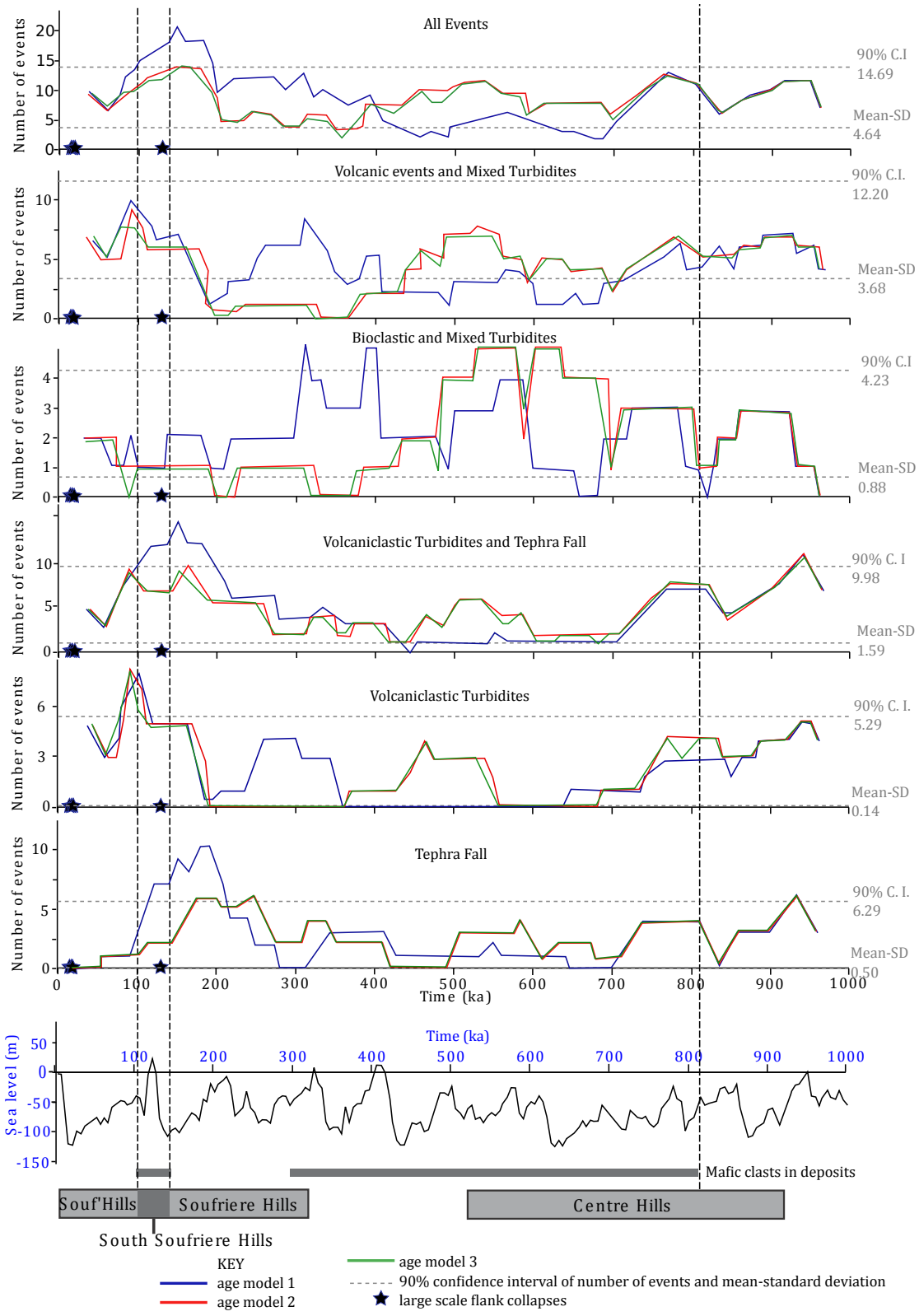
All Events
90% C.I
14.69
Mean-SD
4.64
Volcanic events and Mixed Turbidites
90% C.I.
12.20
Mean-SD
3.68
Bioclastic and Mixed Turbidites
90% C.I
4.23
Mean-SD
0.88
Volcaniclastic Turbidites and Tephra Fall
90% C. I
9.98
Mean-SD
1.59
Volcaniclastic Turbidites
90% C. I.
5.29
Mean-SD
0.14
Tephra Fall
90% C. I.
6.29
Mean-SD
0.50
Number of events
Time (ka)
Sea level (m)
Mafic clasts in deposits
Souf'Hills
Soufriere Hills
Centre Hills
South Soufriere Hills
KEY
age model 1
age model 2
age model 3
90% confidence interval of number of events and mean-standard deviation
large scale flank collapses

Figure 13: Similar to Figure 11, but this figure shows the number of events within 100 ka (centred on window, at 10 ka increments). Age model 1 (green) uses oxygen isotope data, biostratigraphic data, AMS dates, and paleomagnetic dates. Age model 2 (red) uses Deposit 2 as a boundary at 130 ka (Figure 2), and the paleomagnetic intervals. Age model 3 (blue) uses only the paleomagnetic data. Peaks in event frequency are similar to figure 11 (that uses bin widths of 50 ka). The black line is the Miller *et al*. [2005] sea-level curve in meters from present day sea-level. Thin grey lines show occurrence of mafic scoria within Hole U1395B, the thick grey line shows known extents of activity at volcanic centres on Montserrat based on limited subaerial dating [Harford *et al*., 2002]. There is a peak in event frequency that coincides with the appearance of mafic scoria in Hole U1395B and all large flank collapses occur during periods of rapid sea-level rise.

Although there appears to be no correlation between turbidite frequency and sea-level, all three of Montserrat's dated larger landslide deposits (Deposits 1 and 5, 8-14 ka and Deposit 2, 130 ka) occurred during periods of rapid sea-level rise (>5 m/ka) (Figure 11). Larger landslide deposits, associated with large-scale flank collapses, are more easily distinguishable (due to the large volumes of material involved) from other eruption-related deposits, unlike turbidites.

5. Discussion

5.1. How does the submarine record relate to subaerial activity?

Montserrat is part of an active island arc with numerous active volcanoes nearby that also generate tephra fall deposits and turbidites. Site U1395B is situated ~35 km downwind (northwest) of Guadeloupe (Radiosonde wind data) and some tephra fall layers from Guadeloupe may be recorded in Hole U1395B. Eruptive products from Guadeloupe can be distinguished using lead isotopes because Guadeloupe magmas have a higher radiogenic lead component (Cassidy *et al*.,

2012). Coussens *et al*. (2016) (Chapter 4) show that most tephra layers recorded within Hole U1395 B are from Montserrat. The presence of turbidites derived from Guadeloupe within Hole U1395B can be ruled out because over the past 1 Ma (Samper *et al*., 2007), volcanic activity occurred in the southeast of Guadeloupe at Grande Découverte Soufrière and this produced landslides that have mostly travelled westwards into a canyon system (Samper *et al*., 2007). We thus assume that most visible turbidite layers are from Montserrat.

Limited ^{40}Ar-^{39}Ar dating of onshore samples from Montserrat suggests that volcanism occurred at Centre Hills between ~990–550 ka (Harford *et al*., 2002) followed by a long pause in activity until ~290 ka, when activity began at Soufrière Hills. At ~130 ka there was a brief period (~10 ka) of eruptive activity at the new volcanic centre, South Soufrière Hills, after which activity migrated back to the Soufrière Hills. All age models for Hole U1395B (Figures 10-13) show several periods of reduced volcaniclastic turbidite deposition and tephra fall frequency lasting 10^4-10^5 ka. The duration of this reduced activity is smaller than the pauses of activity shown in the on-land record (>10^5 ka). The longer pauses in activity deduced from the terrestrial record are likely to be an artefact of limited dating, exposure and erosion of the subaerial record. This indicates that the offshore stratigraphy provides a higher resolution record that can be used to investigate temporal patterns in volcanic activity in greater detail.

Trofimovs *et al*. (2006) showed that 90 vol.% of the erupted products from the current eruption of Montserrat had been deposited offshore, supporting our inference that the submarine record is likely to provide a more complete archive of events than the subaerial record. However, deposition in marine settings involves complex transitions between subaerial and submarine transport processes. Thus, although the offshore stratigraphy records more volcanic events than the subaerial record, offshore facies may not provide a truly representative record of a particular type of eruption.

5.2. How does the frequency of collapses relate to volcanism?

Increases in the frequency of tephra fall deposits above the mean 90% confidence interval (3.64 events in 50 ka) indicate that there was more explosive volcanic activity between ~800 ka to ~760 ka, and ~230 ka to ~140 ka (Figure 5). Turbidite frequency also increases during these periods, but not all observed increases are above the mean 90% confidence interval (Figure 5). These observations are consistent for all age models used, suggesting that these periods of increased volcanism and turbidite frequency are unlikely to be age model artefacts. During periods of effusive volcanic activity (i.e. the lava-dome forming eruptions that typify much of Montserrat's volcanism), there is a greater rate of edifice growth and an increase in the number of volcano-tectonic earthquakes and explosive eruptions. As the lava dome grows, it becomes less stable, and may result in collapse. All three temporally well-constrained large landslide deposits occurred when Montserrat experienced periods of relatively heightened volcanic activity (Figures 4 and 5).

Bioclastic turbidites show another increase in frequency at ~560 ka to ~500 ka suggesting that other factors may be important in triggering or priming carbonate shelf collapse (Figure 5), such as sea-level change or large earthquakes.

5.3. How does the frequency of collapses at Montserrat relate to sea-level?

Turbidite frequency may not coincide with eustatic sea-level changes (in all age models), but all three of the well-dated large-scale flank collapses (>0.3 km^3) from Montserrat (Deposits 1, 2 and 5) occur during periods of rapid (>5 m/ka) global sea-level rise (Figure 5) (Miller *et al.*, 2005). Deposits 1 and 5 (dated between 14-8 ka) coincide with rapid sea-level rise at 15 ka to 5 ka, from 60 m to 1.6 m below present day sea-level (Figure 5). Deposit 2 is dated at 130 ka, which coincides with a second period of rapid sea-level rise at 130 ka to 120 ka (Figure 5).

5.4. Large-scale flank collapse: constructing a global landslide record.

The data suggest that large-scale flank collapses on Montserrat occurred during rapid sea-level rise, suggesting that sea-level changes may trigger large-scale collapses. To investigate if this is replicated more widely, we have compiled a global data set of landslide ages at volcanic islands over the past 1 Ma (building on the compilation by Quidelleur *et al*., (2008)). The compiled global data set has 26 reasonably-constrained ages from volcanic islands (errors <±22.5 ka) (Quidelleur *et al*., 2008; McMurtry *et al*., 2004a, 2004b; Boudon *et al*., 2007; Lebas *et al*., 2011; Hunt *et al*., 2013, 2014), comprising 11 from ocean islands and 15 from island arcs (Tables 3 and 4). These sample sets are relatively small, and we therefore limit our analysis in Section 5.5.

For a valid statistical analysis of global landslide frequency, the sample set must be relatively large. Many landslides have large age uncertainties, and if age errors are too large (i.e., on the order of sea-level cycles) then relationships between sea level, volcanism, and landslides cannot be determined (Pope *et al*., 2015). Our age-uncertainty criterion of <± 22.5 ka has been selected on this basis, because it provides a large enough dataset, with age errors that are a similar order of magnitude to the periodicity of sea-level cycles (10^3-10^4 yrs).

5.4.1 Ocean islands

For the ocean island data set 11 well-dated large landslide events are included. Dating of each deposit is summarised in table 3. These include some of the largest observed collapse events, including the Orotava landslide that has an estimated volume of 1000 km^3 (Masson *et al.,* 2000) and the Tahiti North slide that has a volume of 800 km^3 (Clouard *et al.,* 2000). Given the large volumes and also the subaerial landslide scars commonly observed (e.g. the Orotava, Icod, El Golfo Valleys); many of these landslides are likely to have been flank collapse events involving both subaerial and submarine flank material (Clouard *et al.,* 2000; Longpre *et al*., 2011; Hunt *et al.,* 2013, 2014).

Most of the ocean island database comprises large landslides from the Canary Islands (8 landslides), with one landslide from the Cape Varde archipelago (Fogo) (McMurty *et al*., 1999, 2004b), one landslide from Hawaii (Alika 2) (McMurty *et al*, 1999), and one landslide from South Pacific (Tahiti North) (Clouard *et al*., 2000; Hildenbrand *et al*., 2004, 2006). Many more landslides are observed offshore, but few are well dated, for example at least 68 large volume landslides have been identified offshore Hawaii with volumes up to 5000 km^3 (Moore *et al*., 1984, 1994).

Flank collapse name	Country/ Island	Age (ka)	Volume (km^3)	Material dated	References	Letter in Figure 8
Canary	Canary Islands, El Heirro	10 to 20	400.00	Offshore a prominent turbidite (turbidite B) was first dated at 13-17 ka by Weaver *et al*., (1992) and then later dated by Hunt *et al*., (2013) at ~15 ± 5 ka using biostratigraphy of surrounding hemipelagic material. Turbidite B is correlated with the Canary landslide, as suggested by Carraceado *et al*., (1999)	Weaver *et al*., 1992; Carracedo *et al*., 1999; Hunt *et al*., 2013	a
El Golfo	Canary Islands, El Heirro	65-75	150.00	Onshore the El Golfo landslide scar has a maximum age constraint of 87± 8 ka and a minimum age constraint of 39 ± 13 ka, based on ^{40}Ar/^{39}Ar dating material that predates and in-fills the collapse scar respectively. Turbidite D1 is dated at 70 ± 5 ka and is consistent with an El Golfo origin. Here we preferentially use the dates of the turbidite.	Weaver *et al*., 1992; Longpre *et al*., 2011; Hunt *et al*., 2013	b
Las Playas 2	Canary Islands, El Heirro	141-179	> 30	Las Playas 2 is dated between 176 ± 3 ka to 145 ± 4 ka based on K-Ar dating of the youngest incised deposits and oldest crater filling deposits.	(Guillou *et al*., 1996; Gee *et al*., 2001)	c
El Julan	Canary Islands, El Heirro	545-555	130.00	turbidite P in the Madiera abyssam plain has been correlated to the El Julan turbidite. The age of turbidite P is 550 ± 5 ka	Hunt *et al*., 2013	d
Cumbre Nueva	Canary Islands, La Palma	529-574	95.00	The maximum age constraint comes from dating the Camino Ermita de La Pena 566±8 ka (K-Ar) and the minimum age constraint is from dating the Bejenado volcano 537±8 ka (K-Ar) (Guillou *et al*., 1998, 2001). Hunt *et al* (2013) also date the Cumbre Nueva slide by correlating the landslide with turbidite N in the Madeira abyssal plain using biostratigraphy (480±5 ka). Here we preferentially use the subaerial dates as the turbidite may have been generated from a different landslide from La Palma as many large landslides on La Palma are largely unstudied (Acosta *et al*. ,2003).	Costa *et al*. [2014]	e

Icod	Canary Islands, Tenerife	160-170	320)	Volcanic material infilling the Icod Valley has been dated at 118±3 and 110± 4 ka, providing minimum age constraints . Maximum age constrains come from dating material from the Upper Canadas series, which are thought to have formed shortly prior to the formation of Las Canadas and the Icod valley. K-Ar ages of 170-130 ka. More recently Hunt *et al*., (2013) correlates turbidite G in the Madeira abyssal plain with the Icod landslide, and obtains the biostratigraphic age of 165±5 ka for the Icod landslide. Here we use the age of turbidite G	Ancochea *et al*., 1990; Wynn *et al*., 2002; Carraceado *et al*., 2007; Hunt *et al*., 2013, 2014	f
Orotava	Canary Islands, Tenerife	525-566	1000.00	The minimum age constraint is from the oldest infilling lava flow, which was sampled during a drilling campaign, and dates at 534±9. The maximum age constraint comes from sampling the youngest lavas that are intersected by the landslide scar and dates at 558±8 ka . The subaerial dates agree well with submarine dates obtained by Hunt *et al*., (2013). Turbidite MO found in the Madeira abyssal plain is correlated with the Orotova landslide deposit and is dated using biostratigraphy at 540±5 ka.	Watts and Masson 1995; Masson *et al*., 2002; Boulestreix *et al*., 2013; Hunt *et al*. 2013	g
Guimar	Canary Islands, Tenerife	840-860	120.00	K-Ar dates of lavas in the landslide scar wall give a maximum age constraint of 840±30 ka (Ancochea *et al*., 1990). Tsunami deposits on the northwest coast of Gran Canaria associated with the Guimar landslide yield ages of 1.75 Ma to 32 ka. More recently Hunt *et al*., (2013) correlates turbidite Z in the Madeira abyssal basin with the Guimar landslide deposit. Using biostratigraphic ages of overlying and underlying hemipelagic material turbidite Z is 850±10 ka. Here we use the age of turbidite Z.	Krastel *et al*., 2001	h
Fogo	Cape Verde	66-80	160.00	The offshore deposit correlates with a (>10 km) collapse scar. On the neighbouring island of Santiago tsunamigenic deposits are found on the islands northern tip. Large fields of boulders and chaotic conglomerates are "plastered" against the lower cliff slopes. Such deposits are likely to he associated with the Fogo collapse event (Ramalho *et al*., 2015). 3He dating of the top surface of these tsunamic deposits suggest the landslide age is 73±7 ka (Ramalho *et al*., 2015).	McMurty *et al*. [1999]; McMurty *et al*. [2004b]	i
Alika 2	Hawaii	122-132	>0.5	Planktonic forams within the Alika 2 deposit were dated using oxygen isotope stratigraphy and suggest the Alika 2 deposit is 127±5 ka (McMurty *et al*., 1999)	McMurty *et al*. [1999]	j
Tahiti North	Tahitian Archipelago	870-850	800.00	Earliest infilling products in the northern scar have K-Ar dates of 851±11 ka. Dyking took place up to ~ 0.87 Ma, and is thought to have triggered the collapse, thus collapse is likely to have occurred inbetween 0.87-0.85 Ma.	Clouard *et al*., [2000]; Hildenbrand *et al*., [2004, 2006].	k

Table 3: Summarising well-dated landslides from ocean islands.

5.4.2 Island Arc Landslides

The island arc landslide database comprises 15 events and landslide ages are summarised in table 4. Volumes of the island arc landslides are generally smaller than observed from the ocean island database, with volumes typically <10 km^3. Many of the large landslides are likely to have been derived from dome collapse events or flank collapse events. Examples of dome collapse deposits may include the Carmichaël and Carbet landslide deposits. The onshore deposits largely comprise volcaniclastic material and very little material is found offshore (Boudon *et al.,* 1984, 2007). Estimated volumes of 0.30 and 0.5 km^3 respectively (Boudon *et al.,* 1984, 2007) are similar to volume estimates of dome collapse events observed in the recent eruption on Montserrat (where the largest dome collapse had a volume of 0.2 km^3 (Trofimovs *et al.,* 2006)). Flank collapse events may include the La Soufriere event on Dominica (Le Friant *et al*., 2002; Boudon *et al*., 2007) and the Ritter island collapse in Papua New Guinea (Cooke, 1981; Ward and Day, 2003). Megablocks (Scotts head) are observed in the subaerial stratigraphy of the La Soufriere event (Le Friant *et al*., 2002), and the flank collapse of Ritter Island was observed by eye witnesses (Cooke, 1981; Ward and Day, 2003).

Dating errors are generally much smaller (often <10 ka) than for the ocean island dataset, but 13 of the events occurred within the past 20 ka. Only one event occurred prior to the most recent rapid sea level rise (Figure 14) (Montserrat's Deposit 2 dated at ~ 130 ka). Most of the landslides included within the data base are from the Lesser Antilles Island Arc (8 landslides) (e.g. Boudon *et al*., 2007), 5 landslides have included from the Campanian Island Arc (Vezzoli, 1986; Seta *et al*., 2012), 1 from the Japanese Arc (Usu) (Moriya, 2003), and 1 from the Bismarck Island Arc (Ritter Island) (Ward and Day, 2003).

Flank collapse name	Country/ Island	Age (ka)	Volume (km^3)	Material dated	References	Letter in Figure 8
Carmichaël	Guadeloupe	11.5-6.9	0.30	Uncarbonised wood found within the landslide deposit yields C14 ages of 8400 ±1500 to 11270±185 BP	Boudon *et al.*, 1984, 2007	l
Carbet	Guadeloupe	3.5-2.8	0.50	Uncarbonised wood found within the landslide deposit yielded C14 dates between 2800-3450 BP	Boudon *et al.*, 1984, 2007; Jerime 1979, Paterne 1980; Daigun 1981; Daigun *et al.*, 1981	m
La Soufrière	Dominica	6.7-2.3	6 to 7	The lower bound age constraint is from C14 dating on carbonaceous material found within a pyroclastic flow deposit from the Plat-Pays volcano dated at 6600±50 ka. An upper bound comes from a tephra fall out that overlies the Scotts head mega block (within this landslide deposit). C14 dates from carbonate materialin the fall deposit is 2380± 75 ka.	Le Friant *et al.*, 2002; Boudon *et al.*, 2007	n
South	Ischia, Italy	3-2.4	1.50	C14 dating plantonic forams within the hemipelagic material above and below the submarine landslide deposit (DF1) 3-2.4 ka.	de Alteriis *et al.*, 2010, 2014	o
Piettre Rosse	Ischia, Italy	40-2.4	>0.3	The lower bound date is given be the age of the underlying Citara Formation ~40 ka, and the upper bound is given by the overlying Falanga DAD (400 BC).	Vezzoli 1988, Buchner 1986; Seta *et al.*, 2012	p
Falanga	Ischia, Italy	2.40	>0.3	The Falanga deposit is dated to 400 BC based on historical chronicles	Buchner 1986; Seta *et al.*, 2012	q
Casamicciola (NDDe)	Ischia, Italy	2.80	>0.3	The Casamicciola deposit is dated at < 800 BC as it overlies the Punta La Scrofa Tuff dated at <800 BC. This is included in the database as the date errors are <±10 ka.	de Vita *et al.*, 2010; Seta *et al.*, 2012	r
NDDw	Ischia, Italy	<10 ka		Within the seismic stratigraphy a reflective horizon is observed beneath the landslide. This reflective horizon has been correlated with the onshore Zaro lava flow dated at 6±2 ka and 9±1 ka using K-Ar dating, thus the landslide is < 10 ka.	Vezzoli *et al.*, de Aleriis and Violante, 2009; Seta *et al.*, 2012	s
D2 or the St Pierre event	Martinique	26.4-23.6	13.00	The upper bound date is given by U-Th disequilibrium dating of material intersected/outside the D2 structure yield ages of 37±4 ka (Mont Calebasse lava dome) and 25±1 ka (Mourne Plumé lava dome). The lower bound age, 25000±1040 years, is given by a C14 charcoal age from a scoria flow deposit that infills the structure.	Vincent *et al.*, 1989; Le Friant *et al.*, 2003	t
D3 or Rivière Sèche event	Martinique	9.8-8	2.00	The Aileron lava dome (summit part of Montagne Pelée) is intersected by the D3 structure and is dated at 9.7±0.5 ka, and provides an upper age limit. The Sans nom lava dome infills the D3 structure and is dated at 9±1 ka	Le Friant *et al.*, 2003; Boudon *et al.*, 2007	u
Usu	Hokkaido, Japan	7 to 8	1 to 2	The Zenkoji collapse occurred ~7000-8000 years ago, based on subaerial dating. We have included this event within the database as the dates are within the ±10 ka age uncertainty limit, given that Usu is	Moriya, 2003 (in Japanese); Soya *et al.*, 2007; Yoshida *et al.*, 2012	v

				<20000 years old.		
Ritter	Papua New Guinea	0.10	5.00	Eye witness account	Cooke 1981; Ward and Day 2003	w
Deposit 1	Montserrat	14 to 11	1.80	C^{14} and oxygen isotope dating on overlying and underlying hemipelagite	Trofimovs *et al*. [2013]; Watt *et al*. [2012a], [2012b]; Le Friant *et al*. [2004]; Lebas *et al*. [2011]	x
Deposit 2	Montserrat	146-112	9.00	C^{14} and oxygen isotope dating on overlying and underlying hemipelagite= 0.123 Ma. Onland dating of SSHs deposits 0.129±0.017 Ma to 0.131±0.007 Ma. And K-Ar dating of lithics in turbidite	Harford *et al*. [2002]; Le Friant *et al*. [2004]; Lebas *et al*. [2011]; Watt *et al*. [2012a], [2012b]; Crutchley *et al*. [2013]	y
Deposit 5	Montserrat	12 to 8	0.30	C^{14} of surrounding hemipelgic	Cassidy *et al*. [2012b]; Le Friant *et al*. [2004]; Lebas *et al*. [2011]	z

Table 4: Summary of well-dated landslides from arc islands

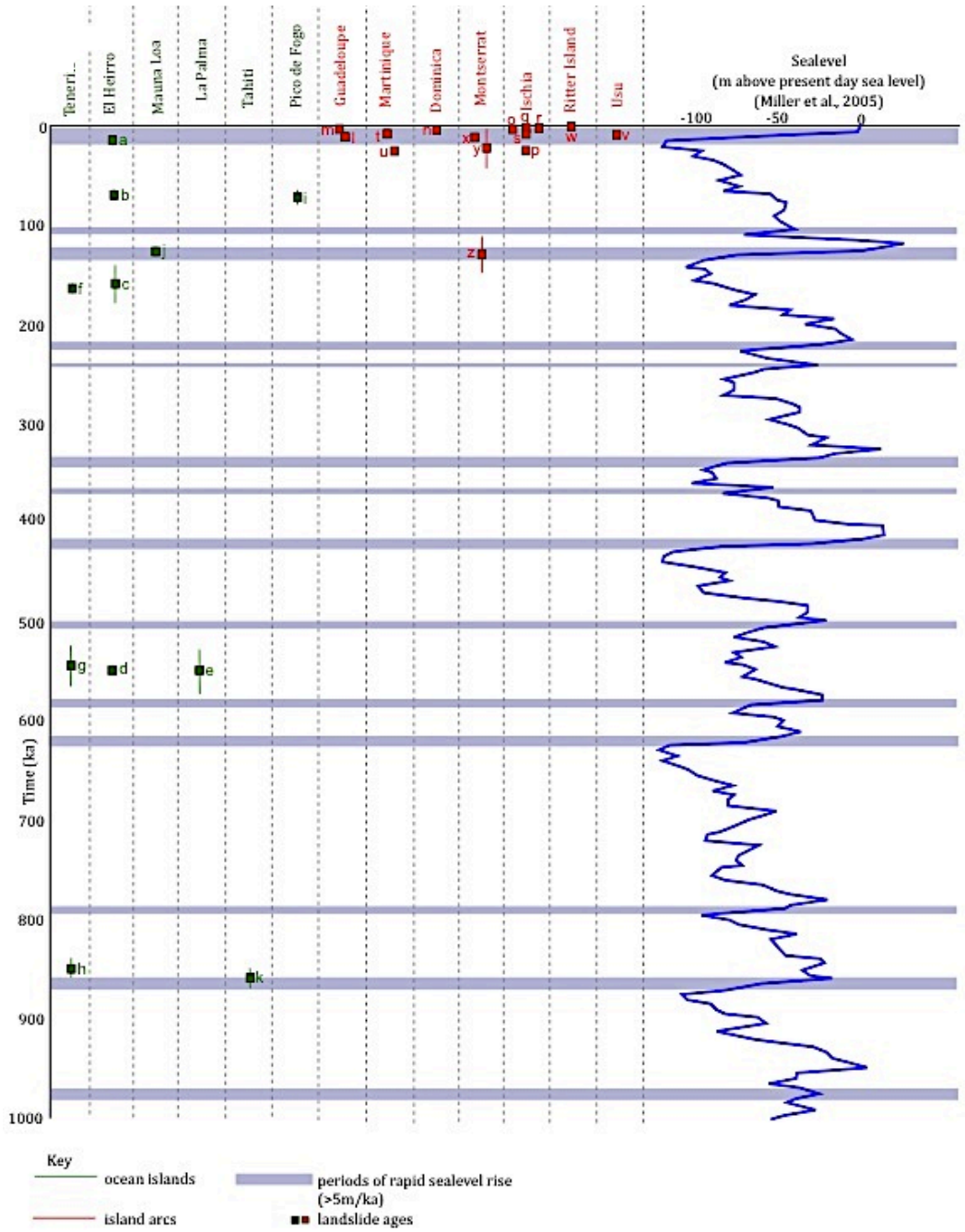

Figure 14: Diagram summarising the age of large (>0.3 km3) landslides around volcanic islands and sea-level. The sea-level curve used is that of Miller *et al.*, [2005]. Events considered have date errors of <50 ka. Periods of rapid sea-level rise (>5m/ka) are highlighted in blue. Vertical bars show landslide ages with horizontal bars showing errors of individual measurements. Squares give landslide ages with small age errors. Ocean island landslides are shown in green, and island arc landslides are shown in red. Letters identify individual landslides and correspond to letters in Tables 3 and 4.

Dating landslide deposits is challenging, as most material is emplaced offshore in poorly accessible, deep marine settings, and comprises chaotic mixtures of material (such as debris avalanche deposits). Direct dating of material within landslides only provides maximum age constraints of landslide emplacement, unless material such as trees or marine material can be identified and dated. Indirect dating of material overlying and underlying landslide deposits, or dating of subaerial landslide scars can result in large age gaps. Consequently the global landslide database is sparse with a bias towards younger deposits, and dominated by a very few well-studied regions (e.g. Ischia, Lesser Antilles), where several events have been dated. Even in other regions where numerous events have been identified (e.g. Aleutian Islands; Coombs *et al*. (2007)), very few events are dated, and so are excluded from our dataset.

5.5. Large-scale flank collapse and sea-level: comparison to global records

Using the global compilation we ascertain if landslides at other island volcanoes also coincide with periods of more rapid sea-level rise. Box and whisker plots in figure 15 show that landslide occurrences at island arc volcanoes are skewed towards periods of more rapid sea-level rise. In contrast, at ocean islands the distribution of event timing shows no clear correlation with specific regimes of sea level (Figure 15), and suggest that the effects of rapid sea-level rises at island arc and ocean island settings are different.

The global data set of landslide ages is small, and it is thus difficult to test the strength of the observed correlation between event timing and sea level change at island arc volcanoes, and if island arc flanks and ocean island flanks respond differently to the rate of sea-level change. Furthermore the island arc database is largely biased towards recent landslide events (<20 ka), which coincides with periods of rapid sea-level rise. The apparent skew of island arc landslides occurring during periods of rapid sea-level rise could also be due to a record bias towards younger deposits as opposed to rapid sea-level rise triggering landslides.

Other studies have also correlated sealevel with the occurrence of landslides, but there is contradictory evidence (Carracedo *et al.*, 2001; McMurty *et al.*, 2004b; Quidelleur *et al.*, 2008; Hunt *et al.*, 2013, 2014). Quidelleur *et al.* (2008) and Carracedo *et al.* (2001) suggest landslides occur at glacial terminations. In Contrast, McMurty *et al.* (2004b) suggest that landslides coincide with high sealevel stands. Masson *et al.*, 2002 observed four Canarian landslides coinciding with marine isotope stage boundaries and two landslides coinciding with high sealevel stands, consequently results are inconclusive.

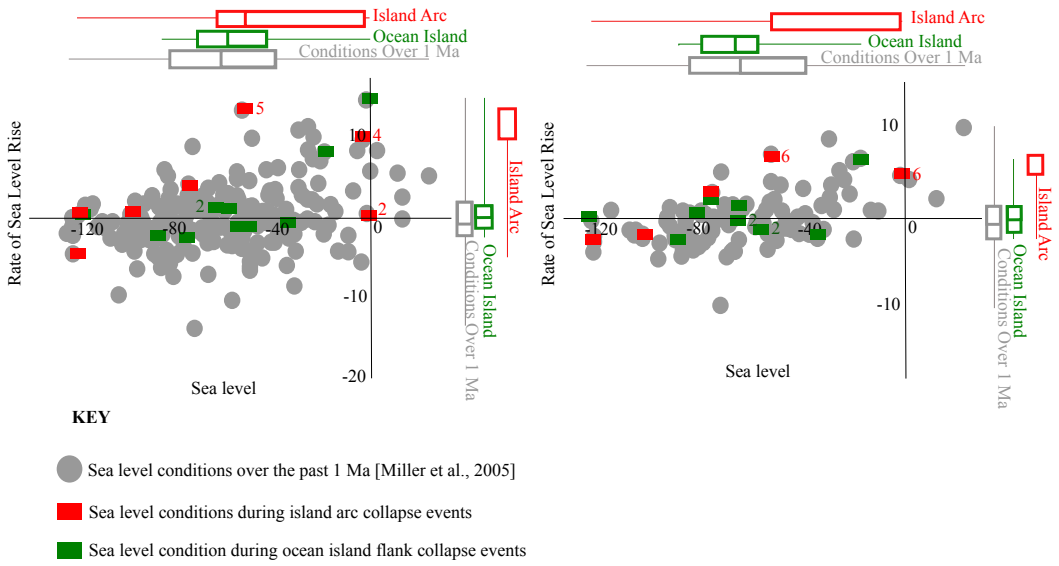

Figure 15: Comparison of sea level conditions with those at the time of documented landslides (Tables 3 and 4) using data in 5 ka bins (A, left) and in 10 ka bins (B, right). Grey solid circles indicate the full range of conditions over the past 1 Ma at which no landslides were recorded. Annotated box and whisker plots indicate the spread of each data set, with boxes showing 25%, 50% and 75% of the data, whiskers showing the minimum and maximum. Numbers next to data points show the number of overlapping data points. A general skew of landslides occurring at rapid sea-level rises can be seen in the box and whisker plots.

It is also important to consider that other factors may also influence the generation of landslides, such as tectonic activity (Sato *et al.*, 2007; Keefer *et al.*, 2000), rainfall (Marques *et al*, 2008) or volcanic activity (Hunt *et al.*, 2013, 2014).

Landslides are often coincident with large earthquakes, for example a 0.05 km^3 turbidite was generated offshore Tahiti during the January 2010 earthquake (McHugh *et al.,* 2011), and the turbidite occurrence in the Okinawa Trough (south of Taiwan) has been correlated with the occurrence of large magnitude earthquakes (Huh *et al.,* 2014). This study also shows that periods of increased frequency of turbidite occurrence coincide with periods of increased volcanic activity (section 5.2). Consequently, investigating a single landslide trigger is too simplistic an approach, as it is probable that landslides are triggered by the interplay of a variety of different triggers.

It is worth briefly considering the processes by which sea level rise may increase the likelihood of flank collapse at island-arc volcanoes. A ~100 m rise in sea level potentially enhances both dyke ascent (and hence volcanism) and fault movement in island-arc settings (cf. Nakada and Yokose, 1992), although the relationship between volcanism and sea level change may be complex (McGuire *et al*., 1997) and is incompletely understood. An incipient instability within a volcanic edifice may move closer to a critical failure point due either to direct stress increases associated with sea-level rise, possibly combined with other factors. These may include enhanced erosion and modification of the groundwater system associated with rapid sea-level change. Although the consequence of sea-level rise on groundwater may depend on local factors, pore-pressure increases within hydrothermal systems have been suggested as a cause of edifice collapse (Elsworth and Voight, 1995; Day, 1996; Reid, 2004).

Our results suggest that these factors may be less significant in ocean-island settings, but the reason for this is as yet unclear. Structurally, ocean islands are likely to have more stable flanks than island arcs, with a broader profile and lower slope gradients, and are also much larger (Watt *et al*., 2014), yet the presence of widespread landslide deposits around many ocean islands indicates that they are still prone to catastrophic flank failure.

6. Conclusions

When compared to the subaerial stratigraphic record, volcaniclastic layers within IODP Hole U1395B provide a more complete record of volcanism on Montserrat. We found that periods of reduced event frequency (interpreted as periods of volcanic quiescence) on Montserrat lasting of the order 10^4– 10^5 ka, substantially shorter than apparent gaps in the subaerial record. The pauses in activity suggested by the subaerial record are likely to be a manifestation of poor preservation and burial of onshore stratigraphy, coupled with the predominantly offshore deposition of volcanic products. The marine record reveals that three periods of heightened volcanic activity at Montserrat occurred at ~930 ka to ~900 ka, ~810ka to ~760 ka, and ~190 ka to ~120 ka. A notable increase in event frequency at ~810 ka to ~760 ka coincides with the appearance of mafic scoria in Hole U1395B.

All three of the well-dated large-scale flank collapses at Montserrat (Deposits 1,2 and 5) occur during periods of relatively elevated volcanic activity. Volcanism at Montserrat preconditions the volcanoes to collapse by loading of lava and volcaniclastic material on the flanks of the volcanoes. These flank collapses also occur during periods of rapid sea-level rise. This pattern may be replicated within a global data set for island-arc volcanoes, but not for the global ocean island landslide data set. However, we caution that many landslide ages have significant age uncertainties, the dataset is small, and the island arc database is biased towards younger deposits. The reasons for this difference remain unclear, but may reflect a greater susceptibility of the steeper, more lithologically diverse flanks of island-arc volcanoes to rapid sea-level changes, relative to ocean islands.

7. References

Ablay, G. J. and Marti J. (2000), Stratigraphy, structure, and volcanic evolution of the Pico Teide-Pico Viejo formation, Tenerife, Canary Islands, *Journal of Volcanology and Geothermal Research, 103*, 175-208

Alteris de, G., Insinga, D. D., Morabito, S., Morra, V., Chiocci, F. L.,Terrasi, F., Lubritto, C., Di Benedetto, C. and Pazzaneses, M. (2010), Age of submarine debris avalanches and tephrostratigraphy offshore Ischia Island, Tyrrhenian Sea, Italy, *Marine Geology*, 278, 1-18, doi:10.1016/j.margeo.2010.08.004

Ancochea, E., Fuster, J. M., Ibarrola, E., Cendrero, A., Coello, J., Hernan, F., Cantagrel, J. M. and Jamond, C. (1990), Evolution of the island of Tenerife (Canary Islands) in the light of new K-Ar data, *Journal of Volcanology and Geothermal Research*, 44, 231-249, doi: 0377-0273/90/$03.50

Barclay, J., Alexander, J., and Sušnik, J. (2007), Rainfall-induced lahars in the Belham valley, Montserrat, West Indies, *Journal of the Geological Society*, *164*(4), 815-827

Boudon, G., Semet, M. P. and Vincent, P. M. (1984), Flank failure–directed blast eruption at Soufrière, Guadeloupe, French West Indies: A 3,000-yr-old Mt. St. Helens?, *Geology*, *12*(6), 350-353

Boudon, G., Semet, M. P. and Vincent, P. M. (1987), Magma and hydrothermally driven sector collapses: The 3100 and 11,500 y. BP eruptions of la Grande Decouverte (la Soufrière) volcano, Guadeloupe, French West Indies, *Journal of volcanology and geothermal research*, *33*(4), 317-323

Boudon, G., Le Friant, A., Komorowski, J. C., Deplus, C. and Semet, M. P. (2007), Volcano flank instability in the Lesser Antilles Arc: Diversity of scale, processes, and temporal recurrence, *Journal of Geophysical Research, 112*, B08205, doi:10.1029/2006JB004674

Boulesteix. T., Hildenbrand, A., Gillot, P-Y. and Soler, V. (2011), Eruptive response of oceanic islands to giant landslides: New insights from the geomorphologic evolution of the Teide–Pico Viejo volcanic complex (Tenerife, Canary), *Geomorphology, 138,61-73*

Buchner, G. (1986), Eruzioni vulcaniche e fenomeni vulcano-tettonici di età preistorica e storica nell' isola di Ischia, *In Tremblements de terre, éruptions volcaniques et vie des hommes dans la Campanie antique, vol, 7,* edited by C. Albore-Livadie, *Publishe by Centre Jean Bérard*, Napoli, 145–188

Cande, S.C. and Kent, D. V. (1992a), A new geomagnetic polarity time scale for the Late Cretaceous and Cenozoic, *Journal of Geophysical Research* 97, 13917-13951

Cande, S.C. and Kent, D. V. (1992b), Ultrahigh resolution of marine magnetic anomaly profiles: A record of continuous paleointensity variations?, *Journal of Geophysical Research* 97, 15075-15083

Cande, S.C. and Kent, D. V. (1995), Revised calibration of the geomagnetic polarity timescale for the Late Cretaceous and Cenozoic, *Journal of Geophysical Research, 100(B4),* 6093-6095

Capra, L., Borselli, L., Varley, N., Gavilanes-Ruiz, J. C., Norini, G., Sarocchi, D. *et al* (2010), Rainfall-triggered lahars at Volcán de Colima, Mexico: Surface hydro-repellency as initiation process, *Journal of Volcanology and Geothermal Research*, *189*(1), 105-117

Carey, N. and Sigurdsson, H. (1982), Influence of Particle Aggregation on Deposition of Distal Tephra from the May 18, 1980, Eruption of Mount St Helens. *Journal of Geophysical Research*, 87(2), 7061–7072

Carracedo, J. C. (1999), Growth, structure, instability and collapse of Canarian volcanoes and comparisons with Hawaiian volcanoes, *Journal of Volcanology and Geothermal Research,* 94(1), 1–19.

Cassidy, M., Trofimovs, J., Palmer, M. R., Talling, P. J., Watt, S. F. L., Moreton, S. G. and Taylor, R. N. (2012), Timing and emplacement dynamics of newly recognised mass flow deposits at ~8-12 ka offshore Soufrière Hills volcano, Montserrat: How submarine stratigraphy can complement subaerial

eruption histories, *Journal of Volcanology and Geothermal Research, 253,* 1–14, doi:10.1016/j.jvolgeores.2012.12.002

Cassidy, M., Trofimovs, J., Watt, S. F. L., Palmer, M. R., Taylor, R. N., Gernon, T. M., Talling, P.J. and Le Friant, A. (2014), Multi-stage collapse events in the South Soufrière Hills, Montserrat, as recorded in marine sediment cores, *In the eruption of Soufrière Hills Volcano, Montserrat from 2000-2010,* Edited by G. Wadge, G., *et al*., *The Geological Society Special Publications*, *39*, 383-397

Cassidy, M., Watt, S. F. L., Palmer, M. R., Trofimovs, J., Symons, W., Maclachlan, S. E. and Stinton, A. J. (2015a), Construction of volcanic records from marine sediment cores: A review and case study (Montserrat, West Indies), *Earth-Science Reviews, 138*, 137–155, doi:10.1016/j.earscirev.2014.08.008

Cassidy. M., *et al*., (2015b), Rapid onset of mafic magmatism facilitated by volcanic edifice collapse, *Geophysical Research Letters, 42(12),* 4778-4785

Clare, M. A, Talling, P. J., Challenor, P. H. and Hunt, J. E. (2016). Tempo and triggering of large submarine landslides - Statsitical analysis for hazard assessment. In Submarine Mass Movements and Their Consequences, edited by G. Lamarche *et al*., . Springer, 41, 509-517

Cole, P. D., Calder, E. S., Sparks, R. S. J., Clarke, A. B., Druitt, T. H., Young, S. R. and Norton, G. E. (2002), Deposits from dome-collapse and fountain-collapse pyroclastic flows at Soufrière Hills Volcano, Montserrat, G*eological Society, London, Memoirs,* 21(1), 231-262

Collins, B. D. and Dunne, T. (1986), Erosion of tephra from the 1980 eruption of Mount St. Helens, *Geological Society of America Bulletin*, *97*(7), 896-905

Cooke, R.J.S. (1981), Eruptive history of the volcano at Ritter Is- land, in Cooke–Ravian Volume of Volcanological Papers, *In Geological Survey of Papua New Guinea Memoir*, edited by R. W. Johnson, 10, 115-123

Coombs. M. L., White, S. M. and Scholl, D. W. (2007), Massive edifice failure at Aleutian arc volcanoes, *Earth and Planetary Science Letters,* 256, 403-418

Coussens M, *et al*., (2016), Synthesis: stratigraphy and age control for IODP Sites U1394, U1395, and U1396 offshore Montserrat in the Lesser Antilles. *In Proceedings of the Integrated Ocean Drilling Program,* principal investiagators A. Le Friant, O. Ishizuka, N. A. Stroncik, Volume 340

Crutchley, G. J., Karstens, J., Berndt, C., Talling, P. J., Watt, S. F. L., Vardy, M. E., Huhnerbach, V., Urlaub, M., Sarkar, S., Klaeschen, D., Paulatto, M., Le Friant, A., Lebas, E. and Maeno, F. (2013), Insights into the emplacement dynamics of volcanic landslides from high-resolution 3D seismic data acquired offshore Montserrat, Lesser Antillies, *Marine Geology, 335*,1-15, doi:10.1016/j.margeo.2012.10.004

Dagain, J. (1981), La mise en place du massif volcanique Madaleine—Soufrière, Basse-Terre de Guadeloupe, Antilles [3rd cycle thesis]: Orsay, France, Université Paris Sud

Dagain, J., M. Paterne, and Westercamp. D (1981), La mise en place du massif Madeleine-Soufrière, *Basse-Terre de Guadeloupe, Antilles: Académie des Sciences, Comptes Rendus*, 11 (292), 921-926

Day, S. J. (1996), Hydrothermal pore fluid pressure and the stability of porous, permeable volcanoes. *In Volcano Instability on the Earth and Other Planets*, edited by W. J. McGuire, A. P. Jones, *Geological Society Special Publication*, 110, 77-93

De Alteriis, G. and Violante, C. (2009), Catastrophic landslides off Ischia volcanic island (Italy) during prehistory, *Geological Society, London, Special Publications*, 322(1), 73-104

De Alteris, G., Insinga, D. D., Morabito, S., Morra, V., Chiocci, F. L., Terrasi, F., Lubritto, C., Di Benedetto, C. and Pazzaneses, M. (2010), Age of submarine

debris avalanches and tephrostratigraphy offshore Ischia Island, Tyrrhenian Sea, Italy, *Marine Geology*, 278, 1-18, doi:10.1016/j.margeo.2010.08.004

Deplus, C., Le Friant, A., Boudon, G., Komorowski, J. C., Villement, B., Harford, C., Segoufin, J. and Chiminee, J. L. (2001), Submarine evidence for large-scale debris avalanches in the Lesser Antillies Arc, *Earth and Planetary Science Letters, 192,* 145-157

De Vita, S., Sansivero, F., Orsi, G., Marotta, E. and Piochi, M. (2010), Volcanological and structural evolution of the Ischia resurgent caldera (Italy) over the past 10 ky, *Geological Society of America Special Papers,* 464, 193-239

Elsworth. D and Voight, B. (1995), Dike intrusion as a trigger for large earthquakes and the failure of volcano flanks, *Journal of Geophysical Research*, 100, 6005-6024

Folk, R. L. and Ward, W. C. (1957), Brazos River bar: a study in the significance of grain size parameters, *Journal of Sedimentary Petrology, 27,* 3-26

Gee, M. J. R., Masson, D. G., Watts, A. B. and Allen, P. A. (2001), The Saharan Debris Flow: an insight into the mechanics of long runout debris flows, *Sedimentology*, 46, 317-335

Gee, M. J. R., Watts, A. B., Masson, D. G. and Mitchell, N. C. (2001), Landslides and the evolution of El Hierro in the Canary Islands, *Marine Geology*, 177, 271-293

Germa, A., Quidelleur, X., Labanieh, S., Lahitte, P. and Chauvel, C. (2010), The eruptive history of Morne Jacob volcano (Martinique Island, French West Indies): Geochronology, geomorphology and geochemistry of the earliest volcanism in the recent Lesser Antilles arc, *Journal of Volcanology and Geothermal Research, 198(3-4),* 297–310, doi:10.1016/j.jvolgeores.2010.09.013

Germa. A., Quidelleur, X., Lahitte, P., Labanieh, S., and Chauvel, C. (2011), The K-Ar Cassignol-Gillot technique applied to wester Martinique lavas: A record of

Lesser Antilles arc activity from 2 Ma to Mount Pelee volcanism, *Quaternary Geology*, 6, 341-355

Green, S. B. (1991), How many subjects does it take to do a regression analysis? *In Multivariate Behavioral Research*, 26, 499-510.

Guillou, H., Carracedo, J. C., Torrado, F. P. and Badiola, E. R. (1996), K-Ar ages and magnetic stratigraphy of a hotspot-induced, fast grown oceanic island: El Hierro, Canary Islands, *Journal of Volcanology and Geothermal Research*, 73(1), 141-155

Guillou, H., Carracedo, J. C. and Day, S. J. (1998), Dating of the upper Pleistocene–Holocene volcanic activity of La Palma using the unspiked K–Ar technique, *Journal of Volcanology and Geothermal Research*, 86(1), 137-149

Guillou, H., Carracedo, J. C. and Duncan, R. A. (2001), K–Ar, 40 Ar–39 Ar ages and magnetostratigraphy of Brunhes and Matuyama lava sequences from La Palma Island, *Journal of Volcanology and Geothermal Research*, 106(3), 175-194

Hatfield. R. and Expedition 340 Scientists (2013), Paleomagnetism in methods, *In Proceedings of IODP, 340: Tokyo (Integrated Ocean Drilling Program Management International, Inc.),* Edited by A. Le Friant, O. Ishizuka, N. A. Stroncik, and the Expedition 340 Scientists, doi:10.2204/ iodp.proc.340.102.2013

Harford, C. L., Pringle, M. S., Sparks, R. S. J. and Young, S. R. (2002), The volcanic evolution of Montserrat using Ar-Ar geochronology, *Geological Society, London, Memoirs*, *21*, 93–113, doi: 10.1144/GSL.MEM.2002.021.01.05

Hildenbrand. A., Gillot. P-Y., Le Roy. I. (2004). Volcano-tectonic and geochemical evolution of an oceanic intra-plate volcano: Tahiti-Nui (French Polynesia), *Earth and Planetary Science Letters*, 217, 349-365

Hildreth, W. and Drake, R. (1992), Volcfin Quizapu , Chilean Andes, *Bulletin of Volcanology*, 54, 93–125

Houghton, B. F., Wilson, C. J. N., McWilliams, M. O., Lanphere, M. A., Weaver, S. D., Briggs, R. M. and Pringle, M. S. (1995), Volcanic Zone , New Zealand Chronology and dynamics of a large silicic magmatic system : Central Taupo Volcanic Zone , New Zealand, *Geology, 23*, 13–16, doi: 10.1130/00917613(1995)023<0013:CADOAL>2.3.CO;2

Hu, C., Henderson, G. M., Huang, J., Xie, S., Sun, Y. and Johnson, K. R. (2008), Quantification of Holocene Asian monsoon rainfall from spatially separated cave records, *Earth and Planetary Science Letters*, *266*(3), 221-232

Huh, C. A., Su, C. C., Liang, W. T. and Ling, C. Y. (2004), Linkages between turbidites in the southern Okinawa Trough and submarine earthquakes, *Geophysical Research Letters*, *31*(12)

Hunt, J. E., Wynn, R. B., Talling P. J. and Masson, D. G. (2013), Turbidite record of frequency and source of large volume (>100 km^3) Canary Island landslides in the last 1.5 Ma: Implications for landslide triggers and geohazards, *Geochemistry, Geophysics, Geosystems*, *14(7)*, 2100–2123, doi: 10.1002/ggge.20139

Hunt, J. E., Talling, P. J., Clare, M., Jarvis, I. and Wynn, R. B. (2014), Long-term (17 Ma) turbidite record of the timing and frequency of large flank collapses of the Canary Islands, *Geochemistry, Geophysics, Geosystems, 15,*3322–3345, doi: 10.1002/2014GC005232

Jutzeler, M., White, J. D. L., Talling, P. J., McCanta, M., Morgan, S., Le Friant, A. and Ishizuka, O. (2014), Coring disturbances in IODP poston cores with implication for offshore record of volcanic events and the Missoula megafloods *Geochemistry, Geophysics, Geosystems,* 3572-3590, doi: 10.1002/2014GC005447

Kameo, K. and Bralower, T. J. (1998), Neogene calcareous nannofossil biostratigraphy of sites 998, 999, and 1000, Caribbean Sea, *Proceedings of the Ocean Drilling Program, Scientifc Results*, *165*,3–17

Keefer, D. K. (1984), Landslides caused by earthquakes, *Geological Society of America Bulletin*, 95(4), 406-421

Keefer, D. K. (2000), Statistical analysis of an earthquake-induced landslide distribution—the 1989 Loma Prieta, California event, *Engineering geology*, *58*(3), 231-249

Kokelaar, B. P. (2002), Setting, chronology and consequences of the eruption of Soufrière Hills Volcano, Montserrat (1995-1999). I*n the eruption of Soufrière Hills volcano, Montserrat, from 1995 to 1991*, edited by T. Druitt, and P. Kokelaar, *Geological Society Special Publications, 21*,1–43, doi: 10.1144/GSL.MEM.2002.021.01.02

Kralik, M., Klima, K. and Riedmüller, G. (1987).,Dating fault gouges, *Nature*, *327*(6120), 315-317

Krastel, S., Schmincke, H. U., Jacobs, C. L., Rihm, R., Le Bas, T. P., and Alibés, B. (2001), Submarine landslides around the Canary Islands, *Journal of Geophysical Research*, 106 (B3), 3977-3997, doi: 2000JB900413. 0148-0227/01/2000 JB900413$09.00

Lebas, E., Watt, S. F. L., Talling, P. J., Feuillet, N., Deplus, C., Berndt, C. and Vardy, M. (2011), Multiple widespread landslides during the long-term evolution of a volcanic island: Insights from high-resolution seismic data, Montserrat, Lesser Antilles, *Geochemistry Geophysics Geosystems*, *12(5)*, Q05006, doi:10.1029/2010GC003451

Le Friant, A., Boudon, G., Komorowski, J.-C., Deplus, C. (2002), L'île de la Dominique, à l'origine des avalanches de débris les plus volumineuses de l'arc des Petites Antilles, *C.R. Geosci*, 334, 235–243

Le Friant, A., Boudon, G., Deplus, C. and Villement, B. (2003), Large-scale flank collapse events during the activity of Montagne Pelée, Martinique, Lesser Antilles, *Journal of Geophysical Research, 108 (B1)*, 2055, doi:10.1029/2001JB001624

Le Friant, A., Lock, E. J., Hart, M. B., Boudon, G., Sparks, R. S. J., Leng, M. J., Smart, C. W., Komorowski, J. C., Deplus, C. and Fisher, J. K. (2008), Late Pleistocene tephrochronology of marine sediments adjacent to Montserrat, Lesser Antilles volcanic arc, *Journal of the Geological Society*, *165(1)*, 279–289, doi:10.1144/0016-76492007-019

Le Friant, A., Deplus, C. and Boudon, G. (2009), Submarine deposition of volcanicastic material from the 1995-2005 eruptions of Soufrière Hills volcano, Montserrat, *Journal of the Geological Society, 166*, 171-182, doi: 10.1144/0016-76492008-047

Le Friant, A., Deplus, C., Boudon, G., Feuliiet, N., Trofimovs, J., Komorowski, J. C., Sparks, R. S. J., Talling, P. J., Loughlin, S., Palmer, M. R. and Ryan, G. (2010), Eruption of Soufrière Hills (1995- 2009) from an offshore perspective: Insights from repeated swath bathymetry surveys, *Geophysical research letters*, *37*, L11307, doi:10.1029/2010GL043580

Le Friant, A., Lebas, E., Clement, V., Boudon, G., Deplus, C., de Voogd, B. and Bachélery, P. (2011), A new model for the evolution of la Reunion volcanic complex from complete geophysical surveys, *Geophysical Research Letters, 38,* L09312, doi:10.1029/2011GL047489

Le Friant, A., Ishizuka, O., Stroncik, N. A., Slagle, A. L., Morgan, S., Adachi, T., Aljahdali, M. and Boudon, G. (2012), Lesser Antillies Volcanism and Landslides. Implications for hazard assessment and long-term magmatic evolution of the arc, *Integrated Ocean Drilling Program, Expedition 340 preliminary report,* doi:10.2204/iodp.pr.340.2012

Le Friant, A., *et al*., (2015), Submarine record of volcanic island construction and collapse in the Lesser Antilles arc: First scientific drilling of submarine volcanic island landslides by IODP Expedition 340, *Geochemistry, Geophysics, Geosystems, 16*, 420–442, doi:10.1002/ 2014GC005652

Lehmann, E. L. and D'Abrera, H. J. (2006), Nonparametrics: statistical methods based on ranks, *Springer,* 464, New York

Lénat, J, F., Boivin, P., Deniel, C., Gillot, P. Y., Bachèlery, P., and Fournaise 2 Team (2009), Age and nature of deposits on the submarine flanks of Piton de la Fournaise (Reunion Island), *Journal of Volcanology and Geothermal Research*, 184, 199–207

Lisiecki, L. E. and Raymo, M. E. (2005), A Pliocene-Pleistocene stack of 57 globally distributed benthic $\delta^{18}O$ records, *Paleoceanography*, *20*,1–17, doi:10.1029/2004PA001071

Longpré, M. A., Chadwick, J. P., Wijbrans, J. and Iping, R. (2011), Age of the El Golfo debris avalanche, El Hierro (Canary Islands): New constraints from laser and furnace $^{40}Ar/^{39}Ar$ dating, *Journal of Volcanology and Geothermal Research, 203*, 76-80, doi:10.1016/j.jvolgeores.2011.04.002

Major, J. J., Pierson, T. C., Dinehart, R. L. and Costa, J. E. (2000), Sediment yield following severe volcanic disturbance—a two-decade perspective from Mount St. Helens, *Geology*, *28*(9), 819-822

Marques, R., Zêzere, J., Trigo, R., Gaspar, J. and Trigo, I. (2008), Rainfall patterns and critical values associated with landslides in Povoação County (São Miguel Island, Azores): relationships with the North Atlantic Oscillation. *Hydrological processes*, *22*(4), 478

Masson, D. G., (1996), Catastrphic collapse of the volcanic island of Hierro 15 ka ago and the history of landslides in the Canary islands, *Geology*, 24 (3), 231-234

Masson, D. G., Watts, A. B., Gee, M. J. R., Urgeles, R., Mitchell, N. C., Le Bas, T. P., and Canals, M. (2002), Slope failures on the flanks of the western Canary Islands, *Earth Science Reviews, 57*, 1-35, PII: S0012-8252Ž01.00069-1

Masson, D. G., Harbitz, C. B., Wynn, R. B., Pedersen, G. and Lovholt, F. (2006), Submarine landslides: processes, triggers and hazard prediction, *Philosophical Transactions of the Royal Society, 364*, 2009-2039, doi:10.1098/rsta.2006.1810

Masson, D. G., Le Bas, T. P., Grevemeyer, I. and Weinrebe, W. (2008), Flank collapse and large-scale landsliding in the Cape Verde Islands, off West Africa, *Geochemistry, Geophysics, Geosystems*, 9(7)

McCann, W. R. (2006), Estimating the threat of tsunamogenic earthquakes and earthquake induced-landslide tsunami in the Caribbean, *World Scientific Publishing, Singapore,* 43-65

McGuire, W. J, Howarth, R. J., Firth, C. R., Solow, A. R., Pullen, A. D., Saunders, S. J., Stewart, I. S., and Vita-Finzi, C. (1997), Correlation between rate of sea-level change and frequency of explosive volcanism in the Mediterranean, *Nature,* 389, 473 - 477.

McHugh, C. M., Seeber, L., Braudy, N., Cormier, M. H., Davis, M. B., Diebold, J. B, et al., (2011) Offshore sedimentary effects of the 12 January 2010 Haiti earthquake, *Geology*, *39*(8), 723-726

McMurty, G. M., Herrero-Bervera, E., Cremer, M. D., Smith, J. R., Resig, J., Sherman, C. and Torresan, M. E. (1999), Stratigraphic constraints on the timing and emplacement of the Alika 2 giant Hawaiian submarine landslide, *Journal of Volcanology and Geothermal Research*, 94, 35-58

McMurtry, G. M., Watts, P., Fryer, G. J., Smith, J. R. and Imamura, F. (2004a), Giant landslides, mega-tsunamis, and paleo-sea level in the Hawaiian Islands, *Marine Geology*, 203,219–233, doi:10.1016/S0025-3227(03)00306-2

McMurtry, G. M., Fryer, G. J., Tappin, D. R., Wilkinson, I. P., Williams, M., Fietzke, J., Garbe-Schoenberg, D. and Watts, P. (2004b), Megatsunami deposits on Kohala volcano, Hawaii, from flank collapse of Mauna Loa, *Geology*, 32(9),741–744, doi: 10.1130/G20642.1

Miller, K. G., Kominz, M. A., Browning, J. V., Wright, J. D., Mountain, G. S., Katz, M. E., Sugarman, P. J., Cramer, B. S., Christie-Blick, N. and Pekar, S. F. (2005), The Phanerozoic Record of Global Sea-Level Change, *Science, 310*, 1293-1298, doi: 10.1126/science.1116412

Moore, J. G., Clague, D. A., Holcomb, R. T., Lipman, P. W., Normark, W. R. and Torresan, M. E. (1989), Prodigious submarine landslides on the Hawaiian Ridge, *Journal of Geophysical Research: Solid Earth,* 94(B12), 17465-17484

Moore, J. G., Clague, D. A., Holcomb, R. T., Lipman, P. W., Normark, W. R. and Teorresan, M. E. (1992), Prodigious submarine landslides on the Hawaiian Ridge, *Journal of Geophysical Research*, 94(89), 17465-17484

Moore, J. G. and Holcomb, R. T. (1994), Giant Hawaiian lantslides, *Earth and Planetary Science Letters*, 22, 119–144

Moriya, I. (2003), Toya Caldera, *In Regional geomorphology of the Japanese islands,* Edited by T. Koaze, M. Nogami, Y. Ono, and K. Hirakawa, *University of Tokyo Press,* 2, 281–288

Nakada, M. and Yokose, H. (1992), Ice age as a trigger of active quaternary volcanism and tectonism, *Tectonophysics,* 212, 321-329

Oehler, J. F. (2005), Les déstabilisations de flanc des volcans de l'Ile de La Réunion. Mise en évidence, implications et origines. PhD Thesis, Univ. Blaise Pascal, Clermont- Ferrand

Oehler, J. F., Lénat, J. F. and Labazuy, P. (2008), Growth and collapse of the Reunion Island volcanoes, *Bulletin of Volcanology,* 70, 717–742, doi: 10.1007/s00445-007-0163-0

Ogg, J. G. (2012), Geomagnetic Polarity Time Scale. *In: The Geologic Time Scale 2012*, Edited by F. M. Gradstein, J. G. Ogg, M. D. Schmitz and G. M. Ogg, *Elsevier Publishing*, 85-114

Paterne, M. (1980), Chronologie des éruptions ré- centes du massif de la Soufrière (Guadeloupe— Petites Antilles). Essai de comparaison des périodes d'activité volcanique de quelques grandes régions volcaniques [3rd cycle thesis]: Bordeaux, France, Université de Bordeaux

Palumbo, L., Benedetti, L., Bourlès, D., Cinque, A. and Finkel, R. (2004), Slip history of the Magnola fault (Apennines, Central Italy) from 36 Cl surface exposure dating: evidence for strong earthquakes over the Holocene, *Earth and Planetary Science Letters*, *225*(1), 163-176

Pope, E. L., Talling, P. J., Urlaub, M., Hunt, J. E., Clare, M. A. and Challenor, P. (2015), Are large submarine landslides temporally random or do uncertainties in available age constraints make it impossible to tell?, *Marine Geology*, *369*, 19-33

Quidelleur, X., Hildenbrand, A. and Samper, A. (2008), Causal link between Quaternary paleoclimatic changes and volcanic islands evolution, *Geophysical Research Letters*, *35*, 1–5, doi:10.1029/2007GL031849

Radiosonde data downloaded from http://www1.ncdc.noaa.gov/pub/data/igra/ from directory data-por/, Download file for Le Reuzet station in Guadeloupe, code GP, numeric code 78897

Ramalho, R. S., Winckler, G., Madeira, J., Helffrich, G. R., Hipólito, A., Quartau, R. and Schaefer, J. M. (2015), Hazard potential of volcanic flank collapses raised by new megatsunami evidence, *Science advances*, 1(9), e1500456

Reid, R.P., Carey, S. N. and Ross, D. R. (1996), Geological Society of America Bulletin Late Quaternary sedimentation in the Lesser Antilles island arc Late Quaternary sedimentation in the Lesser Antilles island arc, *Geological society of America Bulletin, 108*, 78-100, doi: 10.1130/0016-7606(1996)108<0078:LQSITL>2.3.CO;2

Reid, M.E. (2004), Massive collapse of volcano edifices triggered by hydrothermal pressurization, *Geology,* 32, 373-376

Samper, A., Quidelleur, X., Lahitte, P. and Mollex, D. (2007), Timing of effusive volcanism and collapse events within an oceanic arc island: Basse-Terre, Guadeloupe archipelago (Lesser Antilles Arc), *Earth and Planetary Science Letters, 258*, 175-191, doi:10.1016/j.epsl.2007.03.030

Samper. A., Quidelleur. X., Boudon. G., Le Friant., A., Komorowski. J. C. (2008), Radiometric dating of three large volume flank collapses in the Lesser Antilles Arc, *Journal of Volcanology and Geothermal Research*, 176, 485-492

Sato, H. P., Hasegawa, H., Fujiwara, S., Tobita, M., Koarai, M., Une, H. and Iwahashi, J. (2007), Interpretation of landslide distribution triggered by the 2005 Northern Pakistan earthquake using SPOT 5 imagery, *Landslides*, *4*(2), 113-122

Seta, M. D. *et al*., (2012), Slope instability induced by volcano-tectonics as an additional source of hazard in active volcanic areas: The case of Ischia island (Italy), *Bulletin of Volcanology*, 74, 79–106

Sherlock, S. C., Watts, L. M., Holdsworth, R. E. and Roberts, D. (2004), Dating fault reactivation by Ar/Ar laserprobe: an alternative view of apparently cogenetic mylonite–pseudotachylite assemblages, *Journal of the Geological Society*, *161*(3), 335-338

Siebert, L. (1984), Large volcanic debris avalanches: characteristics of source areas, de- posits, and associated eruptions, *Journal of Volcanology and Geothermal Research*, 22, 163–197

Singer, B. S., Jicha, B. R., Harper, M. A., Naranjo, J. A., Lara, L. E. and Moreno-Roa, H. (2008), Eruptive history, geochronology, and magmatic evolution of the Puyehue-Cordón Caulle volcanic complex, Chile, *Geological Society of America Bulletin, 120 (5/6)*, 599-618, doi: 10.1130/B26276.1

Soya, T., Katsui, Y., Niida, K., Sakai, K. and Tomiya, A. (2007), Geologic map of Usu volcano, 2nd edition, Geological Map of Volcanoes (2), Geological Survey of Japan, The National Institute of Advanced Industrial Science and Technology, Tsukuba

Stillman, C. J. (1999), Giant Miocene landslides and the evolution of Fuerteventura, Canary Islands, *Journal of Volcanological and Geothermal Research,* 94(1-4), 89–104.

Trofimovs, J. *et al*., (2006), Submarine pyroclastic deposits formed at the Soufrière Hills volcano, Montserrat (1995–2003): What happens when pyroclastic flows enter the ocean? *Geology*, *34(7)*, 549-552, doi: 10.1130/G22424.1

Trofimovs, J., Sparks, R. S. J. and Talling, P. J. (2008), Anatomy of a submarine pyroclastic flow and associated turbidity current: July 2003 dome collapse, Soufrière Hills volcano, Montserrat, West Indies, *Sedimentology*, *55*, 617-634, doi: 10.1111/j.1365-3091.2007.00914

Trofimovs, J., Fisher, J. K., MacDonald, H. A., Talling, P. J., Sparks, R. S. J., Hart, M. B., Smart, C. W., Boudon, G., Deplus, C., Komorowski, J. C., Le Friant, A., Moreton, S.G and Leg, M. J. (2010), Evidence for carbonate platform failure during rapid sea-level rise; ca 14 000 year old bioclastic flow deposits in the Lesser Antilles. *Sedimentology*, *57*, 735-759, doi: 10.1111/j.1365-3091.2009.01117

Trofimovs, J., Foster, C., Sparks, R. S. J., Loughlin, S., Le Friant, A., Deplus, C., Porritt, L., Christopher, T., Luckett, R., Talling, P. J., Palmer, M. R., and Le Bas, T. (2012), Submarine pyroclastic deposits formed during the 20th May 2006 dome collapse of Soufrière Hills volcano, Montserrat, *Bulletin of Volcanology, 74*, 391-405, doi: 10.1007/s00445-011-0533-5

Trofimovs, J., Talling, P. J. Fisher, J. K., Hart, M. B., Sparks, R. S. J., Watt, S. F. L., Cassidy, M., Smart, C. W., Le Friant, A., Moreton, S. G. and Lang, M. J. (2013), Timing, origin and emplacement dynamics of mass flows offshore of SE Montserrat in the last 110 ka: Implications for landslide and tsunami hazards, eruption history, and volcanic island evolution, *Geochemistry, Geophysics, Geosystems*, *14(2)*, 385–406. doi:10.1002/ggge.20052

Urgeles, R., Canals, M., Baraza, J. and Alonso, B. (1997), The most recent megalandslides of the Canary Islands: El Golfo debris avalanche and Canary debris flow, west El Hierro Island, *Journal of Geophysical Resarch*, 102, 20305-20323

Urgeles, R., Masson, D. G., Canals, M., Watts, A. B. and Le Bas, T. (1999), Recurrent large-scale landsliding of the west flank of La Palma, Canary Islands, *Journal of Geophysical Research*, 104 (B11), 25331-25348, doi: 1999JB900243 0148-0227/99/1999JB 900243$09.00

Vezzoli, L., (1988), Island of Ischia, *CNR Quaderni de La ricerca scientifica*, 114(10), 122

Vincent, P. M., Bourdier, J. L., Boudon, G. (1989), The primitive volcano of Mount Pelée: its construction and partial destruction by flank collapse, *Journal of volcanology and geothermal research*, 38(1), 1-15

Wadge, G. (1985), Morne Patates volcano, Southern Dominica, Lesser Antilles, *Geological Magazine*, *122 (3)*, 253–260

Wadge. G., Voight, B., Sparks, R. S. J., Cole, P. D., Loughlin, S. C. and Robertson, R. E. A. (2014), An overview of the eruption of Soufrière Hills Volcano, Montserrat from 2000 to 2010, *in The Eruption of the Soufrière Hills Volcano, Montserrat from 2000–2010, Memoirs of the Geological Society of London 3*, edited by G. Wadge, R. A. E.Robertson, and B. Voight, *Geological Society of London,*1–4

Wall-Palmer, D., *et al*., (2014), Late Pleistocene stratigraphy of IODP Site U1396 and compiled chronology offshore of south and south west Montserrat, Lesser Antilles, *Geochemistry, Geophysics, Geosystems*, *15*, 1–21, doi: 10.1002/2014GC005402/full

Wang, W. N., Wu, H. L., Nakamura, H., Wu, S. C., Ouyang, S. and Yu, M. F. (2003), Mass movements caused by recent tectonic activity: the 1999 Chi-chi earthquake in central Taiwan. *Island Arc*, *12*(4), 325-334

Ward, S. N. and Day, S. (2003), Ritter Island Volcano-lateral collapse and the tsunami of 1888, *Geophysical Journal International, 154*, 891-902

Watt, S. F. L., *et al*., (2012a), Combinations of volcanic-flank and seafloor-sediment failure offshore Montserrat, and their implications for tsunami

generation, *Earth and Planetary Science Letters*, *319(320)*, 228–240, doi:10.1016/j.epsl.2011.11.032

Watt, S. F. L., *et al*., (2012b), Widespread and progressive seafloor-sediment failure following volcanic debris avalanche emplacement: Landslide dynamics and timing offshore Montserrat, Lesser Antilles, *Marine Geology*, *323(325)*, 69–94, http://dx.doi.org/10.1016/j.margeo.2012.08.002

Watt, S. F. L., Talling, P. J. and Hunt, J. E. (2014), New insights into the emplacement dynamics of volcanic island landslides, *Oceanography,* 27, 46–57

Weaver, P. P. E., Rothwell, R. G., Ebbing, J., Gunn, D. and Hunter, P. M. (1992), Correlation, frequency of emplacement and source directions of megaturbidites on the Madeira Abyssal Plain, *Marine Geology*, 109(1-2), 1-20

Wynn, R. B., Weaver, P. P. E., Stow, D. A. V. and Masson, D. G. (2002), Turbidite depositional architecture across three inter- connected deep-water basins on the northwest African margin, *Sedimentology*, 49, 1441–1462, doi:10.1046/j.1365– 3091.2002.00471.x

Yadava, M. G. and Ramesh, R. (1999), Speleothems—useful proxies for past monsoon rainfall, *Journal of Scientific and Industrial Research*, *58*(5), 339-348

Yoshida, H., Sugai, T. and Ohmori, H. (2012), Size-distance relationships for hummocks on volcanic rockslide- debris avalanche deposits in Japan, *Geomorphology*, 136, 76-87, doi:10.1016/j.geomorph.2011.04.044

Chapter 4:

The long-term evolution of construction and destruction processes at an island arc volcano: a 1 Ma long integrated stratigraphy for Montserrat.

Abstract

In this chapter all available onshore and offshore stratigraphic data are used to develop an integrated stratigraphy for Montserrat. This includes three International Ocean Drilling Program (IODP) sites, previously studied shallow marine cores, and the subaerial stratigraphy, that cover a large (>50 km) spatial extent. Correlating individual units over such distances is difficult and hindered by factors such as deposit preservation and transport direction. However, using this more complete stratigraphy, the past 1 Ma of eruptive and collapse history of Montserrat can be better determined, thus building on observations made in Chapters 2 and 3. In addition to numerous tephra fall and mass-flow deposits, which have a recurrence frequency of the order of $10^{3\text{-}4}$ years, IODP Site U1394 drills through a large landslide deposit (Deposit 2). This deposit represents a major flank collapse of Montserrat (the largest in the past ~250 ka), and is volumetrically an order of magnitude larger than the events that dominate the rest of the stratigraphy. Core U1394 thus also provides an opportunity to study the composition and emplacement processes of the infrequent but volumetrically significant large landslides that occur around volcanic islands.

Overall, three periods of heightened volcanic activity are identified on Montserrat between 1.1-0.9 Ma, at ~0.3 Ma and 0.2-0.1 Ma, and these coincide with periods of heightened mass-wasting. This suggests that eruptive activity may facilitate mass-wasting processes by destabilising island flanks through loading or increased seismic activity. No large pauses in activity are observed in the period between the end of volcanism at Centre Hills and the onset of volcanism at Soufrière Hills, suggesting relatively continuous (and possible overlapping) volcanism on Montserrat, albeit with a slight reduction in event frequency between 0.7-0.4 Ma.

The central to distal parts of Deposit 2 (as sampled by core U1394) comprise horizontally bedded marine sediments, as opposed to subaerially-derived volcanic material (i.e. as might be expected in a primary flank collapse deposit). This confirms previous interpretations of seismic data, and demonstrates that primary volcanic-collapse volumes cannot easily be interpreted from final deposit volumes (and may be far smaller). Such landslides can undergo complex transitions during their emplacement, with implications for the nature and magnitude of tsunamis that may be generated by such events.

1. Introduction

Volcanic islands such as Montserrat, pose a range of geohazards, including various types of volcanic eruption, and landslides that can trigger tsunamis. This chapter combines the onshore and offshore volcano-sedimentary sequences at Montserrat to develop a detailed record of island building and destruction over the past 1 Ma. The onshore stratigraphic data (described in Chapter 2) and observations from the marine Hole U1395B (described in Chapter 3) are incorporated with two further marine records, Holes U1394B and U1396C, to form a detailed 1 Ma stratigraphic record. This stratigraphy is then used to investigate how the frequency, magnitude and style of volcanic and mass movement events have varied on Montserrat over the past 1 Ma, including an examination of the largest-volume event to have affected Montserrat in the past ~250 ka (and possibly the past ~1 Ma), a major landslide deposit derived from a flank-collapse of Soufrière Hills volcano at ~130 ka (Deposit 2).

Integrated Ocean Drilling Program (IODP) Expedition 340 in 2012 provided some of the few long cores from offshore volcanic islands (>1 Ma), and the first that penetrated through major submarine landslide deposits (Le Friant *et al.*, 2012, 2014). Three sites, U1394, U1395 and U1396 were successfully drilled offshore Montserrat (Figure 1). At each Site, multiple Holes were drilled within a few tens of meters apart (e.g. U1394A, U1394B etc). These cores captured a series of

tephra fall deposits, turbidites, and large-scale landslide deposits (Deposit 2) that are representative of island building and island (and volcano) collapse processes.

Analysing both the onshore and offshore deposits provides a more complete stratigraphy that can be used to better understand the development and evolution of island arc volcanoes. Onshore deposits better preserve primary depositional features and can be easier to interpret, whereas offshore interactions with the water column can complicate features (Schneider *et al*., 2004; Jutzeler *et al*., 2014b, 2015). However, the terrestrial record is incomplete, due to erosion and burial of deposits (Chapters 2 and 3). Analyses of the Large Magnitude of Explosive Volcanic Eruption (LaMEVE) database (Crosweller *et al.,* 2012) suggests that smaller events and older events are less likely to be preserved, resulting in a stratigraphic record biased towards younger, larger magnitude event deposits (Brown *et al.,* 2014). A more complete record of past processes may be found offshore, in marine sequences, where much of the material produced in volcanic eruptions (in island settings) is ultimately deposited (Le Trofimovs *et al*., 2008). The marine record will still be biased towards younger, large magnitude event deposits, but to a lesser extent than the subaerial stratigraphy. Marine sediments are also more easily dated than their terrestrial counterparts, due to intervening layers of hemipelagic mud (Trofimovs *et al*., 2012).

Montserrat is an outstanding natural laboratory for understanding the growth and decay of a volcanic island. Previous offshore work includes: one of the most complete sets of shallow (< 10m) sediment cores around a volcanic island (Figure 1) (Trofimovs *et al*., 2006, 2008, 2010, 2013; Le Friant *et al*., 2008; Cassidy *et al*., 2013, 2014a); the first repeat bathymetric surveys of offshore pyroclastic flow deposits emplaced during recent eruptions (Le Friant *et al*., 2004, 2009, 2010; Trofimovs *et al*., 2006, 2008); and detailed 2D and 3D seismic reflection surveys (Deplus *et al*., 2001; Lebas *et al*., 2011; Watt *et al*., 2012a, 2012b; Crutchley *et al*., 2013; Kastens *et al*., 2013; Le Friant *et al*., 2004, 2014). These studies identified a series of offshore landslide deposits, with much larger volumes (0.3-20 km^3) than any of the 1995-recent eruptions. These landslides are termed Deposits 1 to

Deposit 8 (Figure 1) (Deplus *et al.*, 2001; Le Friant *et al.*, 2004; Lebas *et al.*, 2011; Watt *et al.*, 2012a, 2012b).

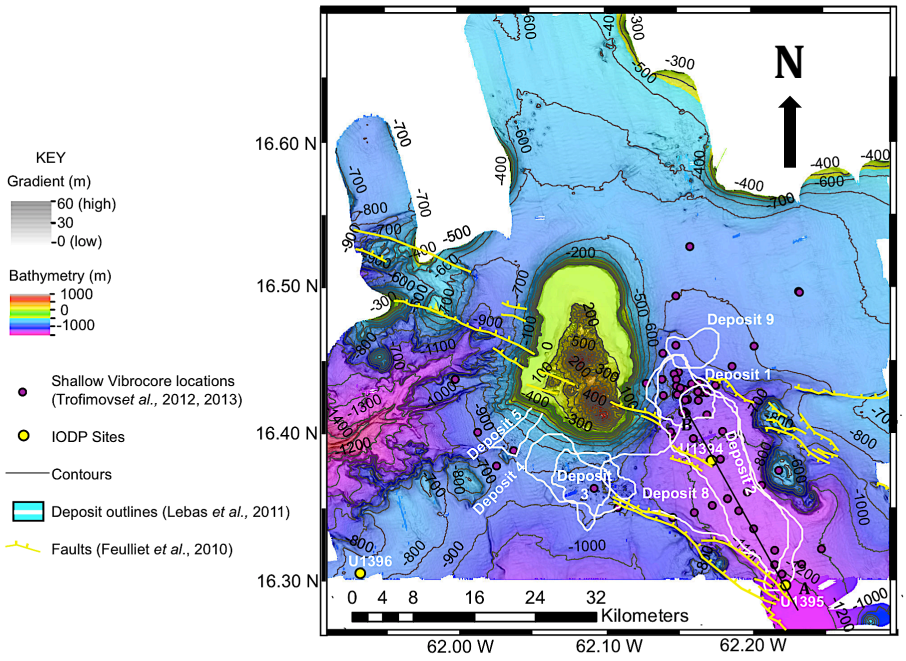

Figure 1: Topographic map of Montserrat showing the location of three IODP Sites (U1394, U1395, and U1396). Also shown are the outlines of major landslide deposits, numbered from 1 to 5 and 8-9 (Lebas *et al.*, 2011; Watt, *et al.*, 2012a, 2012b; Le Friant *et al.*, 2004; Boudon *et al.*, 2007). Grey dots are the locations of shallow (< 5m long) vibrocores from previous studies (Trofimovs *et al.*, 2013; Cassidy, *et al.*, 2012, 2013). Line A-B is the seismic section shown in figure 6. Also shown is the Montserrat-Havers Fault system in yellow.

1.1 Aims

This chapter aims to bring together all available offshore and onshore data around Montserrat to develop an integrated record of the island's volcanic history. This represents one of the longest and most detailed records of volcanic island history that can be used to better understand how volcanic islands evolve in terms of growth and collapse events. This record covers the extinction of the Centre Hills edifice, the activation of volcanism at the Soufrière Hills edifice, the South Soufrière Hills volcanism, and the largest flank collapse event at Soufrière

Hills (Deposit 2 - directly sampled by the marine cores). Using these offshore and onshore records we aim to investigate several key questions:

1) By building on Chapters 2 and 3 we extend our analysis to determine how eruptive styles and eruptive frequency has varied on Montserrat. We also investigate if there was a pause in volcanism during migration of activity from Centre Hills to Soufrière Hills.
2) Building on Chapter 3 we determine to see whether other marine sites show similar variations in mass-wasting composition and frequency, and if mass-wasting coincided with periods of more intense volcanism.
3) Using material from IODP Site U1394 we determine what comprised the large landslide, Deposit 2, and how the landslide was emplaced.

1.2 Past Offshore Work

1.2.1 Major landslide deposits

Offshore seismic surveys around Montserrat have identified seven debris avalanche deposits with volumes varying between 0.3 km^3 and 20 km^3 that were derived from Montserrat (Figure 1) (Deplus *et al*., 2001; Lebas *et al*. 2011; Watt *et al*., 2012a, 2012b; Crutchley *et al*., 2013; Kastens *et al*., 2013; Boudon *et al*., 2007) (Figure 1). The most recent large flank-collapse (Deposit 1; 1.8 km^3)) occurred at 12-14 ka towards the southeast of the island. IODP Site U1393 tried unsuccessfully to sample Deposit 1. A smaller landslide (Deposit 5; 0.3 km^3) originated from the shelf edge to the southwest of the island at a similar or slightly later time (8-12 ka; Cassidy *et al*., 2013; Wall-Palmer *et al*., 2014). A much larger landslide, Deposit 2 (~8.4 km^3) occurred at ~130 ka, and overlies an even larger landslide, Deposit 8 (20 km^3), as shown by seismic reflection data (Lebas *et al*., 2011; Watt *et al*., 2012a, 2012b; Le Friant *et al*., 2014), with an estimated age of >700 ka (Watt et al., 2012). Both Deposits 2 and 8 contain areas of well-bedded reflectors, as well as large blocks in their more proximal regions (Watt *et al*., 2012a, 2012b). Emplacement of material from the volcano onto the surrounding seafloor may have resulted in widespread failure of seafloor sediment (Watt *et al*., 2012a, 2012b, 2015; Le Friant *et al*., 2015).

1.2.2 Other volcaniclastic deposits

An extensive set of > 80 shallow (up to 6 m long) vibrocores and gravity cores have been collected from around Montserrat (Figure 1). These cores have been used to correlate and date a series of turbidites emplaced in the last 130 ka (Trofimovs *et al*., 2006, 2008, 2010, 2012, 2013; Cassidy *et al*., 2013, 2014a) (Figures 1 and 2). Forty accelerator mass spectrometry (AMS) radiocarbon dates have precisely constrained the ages of events in the last ~40 ka (Figure 2). These events include a stack of erosive turbidites at 11.5-14 ka, which may be linked to the emplacement of Deposit 1. Two smaller volume turbidites were emplaced at 2 ka and 6 ka, and were probably linked to later failures at English's Crater (Boudon *et al*., 2007; Trofimovs *et al*., 2013), and a complex sequence of volcaniclastic turbidites generated during the recent 1995-2010 eruption of the Soufrière Hills (Figure 2). An oxygen isotope stratigraphy from these vibrocores helps to establish the ages of older events, including basaltic scoria-rich turbidites at 110 ka. A detailed analysis of the CAR-MON2 core collected to the southwest of Montserrat (Figure 1) provides information on events during the last 250 ka (Le Friant *et al*., 2008). Cassidy *et al*. (2013, 2014) provide information on landslide and turbidite events during the last 110 ka on this southeast side of the island. More recently, Wall-Palmer *et al*. (2014) discuss events recorded in IODP Site U1396 (Figure 1) during the last ~250 ka. In general, this extensive set of shallower cores is useful for understanding the stratigraphy and age of layers in the upper parts (< 150-250ka) of the IODP Sites described here.

The onshore record is dominated by andesitic lithic breccias associated with dome eruptions (Roobol and Smith, 1998; Smith 2007; Chapter2). Deposits from Centre Hills are also regularly interlayered with thick pumice-rich sequences, but such deposits are rare within the Soufrière Hills deposits (Chapter 2).

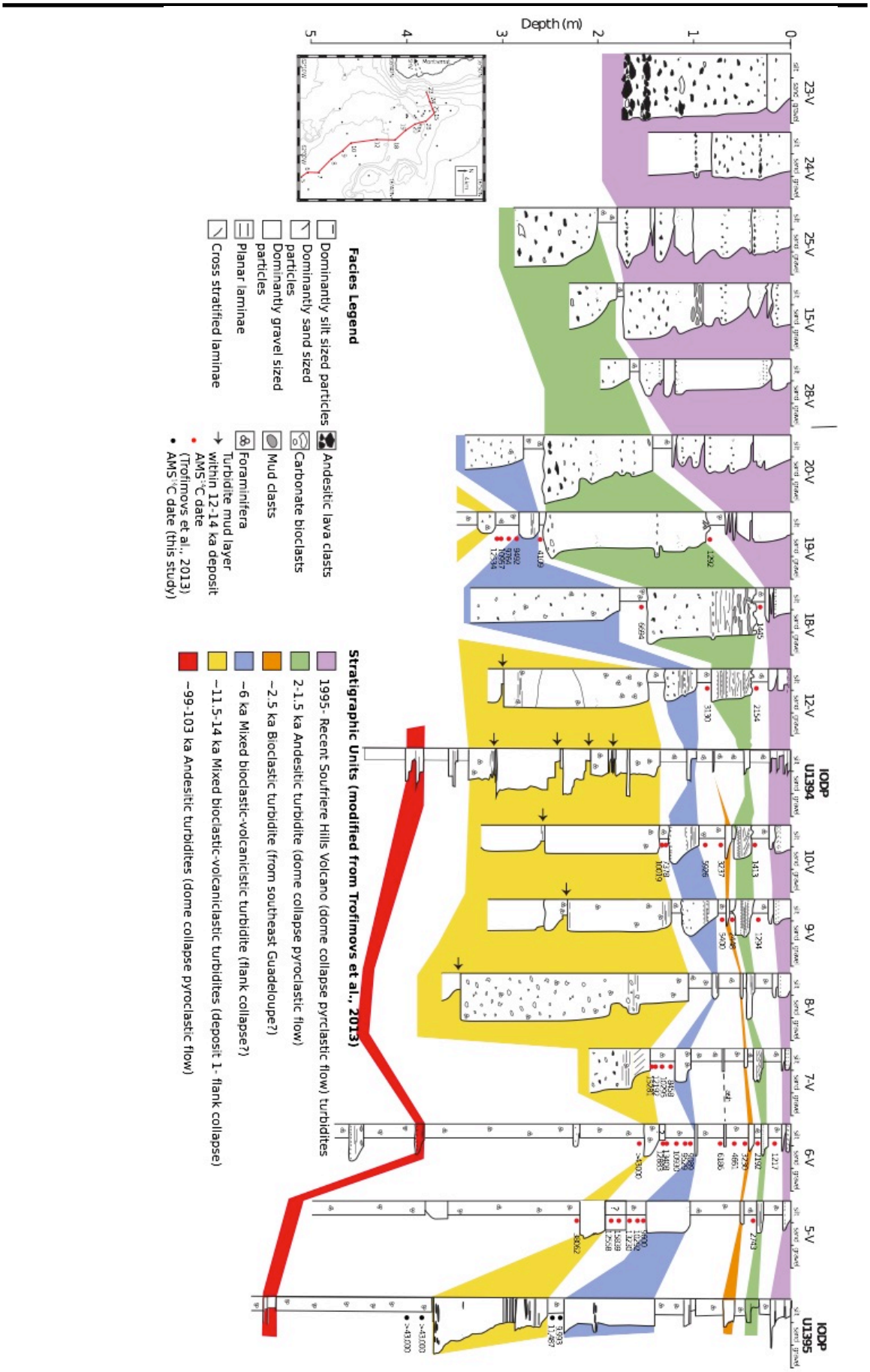
Depth (m)
0
1
2
3
4
5
23-V
24-V
25-V
15-V
28-V
20-V
19-V
18-V
12-V
10-V
9-V
8-V
7-V
6-V
5-V
IODP U1394
IODP U1395
Facies Legend
Dominantly silt sized particles
Dominantly sand sized particles
Dominantly gravel sized particles
Planar laminae
Cross stratified laminae
Andesitic lava clasts
Carbonate bioclasts
Mud clasts
Foraminifera
Turbidite mud layer within 12-14 ka deposit
AMS 14C date (Trofimovs et al., 2013)
AMS 14C date (this study)
Stratigraphic Units (modified from Trofimovs et al., 2013)
1995- Recent Soufriere Hills Volcano (dome collapse pyrclastic flow) turbidites
2-1.5 ka Andesitic turbidite (dome collapse pyroclastic flow)
~2.5 ka Bioclastic turbidite (from southeast Guadeloupe?)
~6 ka Mixed bioclastic-volcaniclstic turbidite (flank collapse?)
~11.5-14 ka Mixed bioclastic-volcaniclastic turbidites (deposit 1- flank collapse)
~99-103 ka Andesitic turbidites (dome collapse pyroclastic flow)

Figure 2: Correlation of units between Expedition 340 Sites U1394 and U1395, to the turbidites described and dated by Trofimovs *et al*., (2013). The red dots show previous AMS radiocarbon dates from Trofimovs *et al*., (2103) supplemented by new AMS dates from vibrocores. The four radiocarbon dates from Sites U1395 are shown as black dots.

2. Methods

2.1 Core descriptions

Sites U1394, U1395 and U1396 were drilled during March 2012. Sites U1394 and U1395 are situated in the Bouillante-Montserrat graben, which is a major channel for turbidites originating from the southeast of Montserrat.

2.1.1 Site U1394

Site U1394 B is the most proximal site (~10 km southwest of Montserrat), and thus samples deposits from smaller magnitude events derived from Montserrat that are unlikely to reach more distal core sites. Site U1394 also drilled directly through Deposit 2 (Figure 1). Two Holes were drilled, Hole U1394A recovered 24.17 m of core with at least 41% disturbed core and Hole U1394B recovered 137.42 m of core with an estimated core disturbance of ~29%. Hole U1394A had poor core recovery below 35 m due to the rotary drilling technique used below this depth. Hole U1394B has a gap between 15–60 m due to the rotary drilling technique; a subsequent change to advanced piston coring improved core recovery.

2.1.2 Site U1395

Site U1395 is located ~25 km southwest of Montserrat (Figure 1) and the stratigraphy at this site has been described in Chapter 3. Site U1395 captures a long and detailed record of volcanic eruptions and mass wasting events that extends over 1 Ma. At Site U1395 two sites were drilled. Hole U1395A recovered

124.29 m of core with 7-13% estimated core disturbance, Hole U1395B recovered 127.52 m of core with 12-16% core disturbance.

2.1.3 Site U1396

Site U1396 was drilled on a topographic high ~35 km southeast of Montserrat (Figure 1): turbidites are unlikely to reach Site U1396, due to its relatively elevated position, and it predominantly preserves tephra fall deposits. It can therefore be used to investigate the record of explosive volcanism at Montserrat. Three holes were drilled at Site U1396. Holes U1396A recovered 140.51 m of core with <1% estimated core disturbance, and U1396C recovered 145.92 m of core with 3% estimated core disturbance. The interval between 5 m to 15 m was deformed in U1396A during drilling; therefore, a short (10 m) third hole (U1396B) was drilled to recover this 5 m to 15 m depth interval.

Holes U1394B, U1395B, and U1396C were the most complete, and initial work was conducted primarily on these holes. Initial core logging was done during Expedition 340 on the RV Joides Resolution, including detailed graphical logs (at a detailed scale of 1 cm to 10 cm) and componentry (Appendix Figure 2) (Coussens *et al*., 2016). Coring artefacts, such as suck in, partial strokes, or coring-related deformation were identified using criteria outlined in Jutzeler *et al*. (2014a). In particular, advanced piston coring can suck in layers of massive sand, which may be mistaken for turbidites. These sand units can fill the core barrel, resulting in substantially increased apparent deposit thicknesses at the expense of real stratigraphy. A grey shaded box on the logs in Appendix figures 2 and 3 show sand layers that may have been sucked in, and which may therefore represent artefacts in the records (and missing strata).

2.2 Unit identification

Different event types produce deposits with distinct sedimentological characteristics, and distinguishing between deposit types is thus important in order to ascertain the nature of past activity. Within the IODP Holes five different lithofacies are present: 1) bioclastic turbidites, 2) mixed turbidites, 3) volcaniclastic turbidites, 4) tephra fall and 5) hemipelagic mud (Figures 3 and 4). Volcaniclastic deposits most likely associated with volcanic activity (explosive

eruptions, dome collapses) (Le Friant *et al*., 2008; Trofimovs *et al*., 2006, 2008, 2013; Cassidy *et al*., 2014a); mixed and bioclastic turbidites are associated with flank or carbonate shelf collapse events (Trofimovs *et al*., 2010; Cassidy *et al*., 2013); and hemipelagic intervals represent background sedimentation (Reid *et al*., 1996).

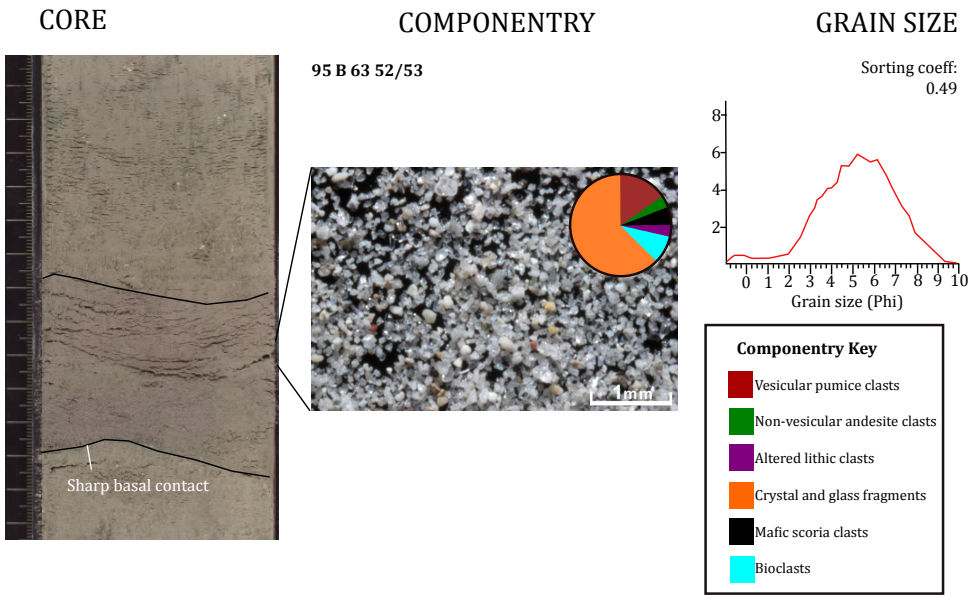

Figure 3: Fall deposit in Hole U1395B. To the left are core photos with millimetre and centimetre marks, in the middle is a photo of material >63 µm. Composition is given by the pie chart in the top right of the photo. Far right is the grain size distribution from analysing whole samples on the Malvern. Also shown are calculated Folk and Ward sorting coefficients.

Hemipelagic mud comprises high proportions of brown-yellow clays with interspersed foraminifera. Componentry analyses are used to distinguish between bioclastic turbidities, mixed turbidites, and volcaniclastic units (both volcaniclastic turbidites and tephra fall deposits) (Figures 3 and 4). Distinguishing between volcaniclastic turbidites and tephra fall can be difficult and we refer the reader to the paper by Cassidy *et al*. (2014b) for a fuller discussion. Tephra fall deposits are volcaniclastic rich, density sorted deposits that form volcanic rich horizons. However, bioturbation, bottom mixing, fluctuations in eruption intensity can increase the bioclastic content and decease deposit sorting. Furthermore, some volcaniclastic turbidite facies are also well

sorted. Here we use the Folk and Ward, (1957) sorting coefficient and unit thickness to distinguish between volcaniclastic turbidites and tephra fall deposits. Volcaniclastic turbidites are more likely to form the thickest (>1 m) layers observed at the IODP core sites (>10 km away from the edifice), whereas tephra fall deposits are more likely to form thinner layers (cm-scale) (see Chapter 3, Figure 6). Tephra fall deposits are better sorted than turbidites; although some turbidite lithofacies can be well-sorted.

Table 1 summarises the criteria used to identify each deposit type, but distinguishing between unit types can be difficult. Ocean bottom currents and bioturbation can winnow fine material (Wall-Palmer *et al*., 2014), or mix together thin tephra fall deposits with underlying hemipelagic mud (Carter *et al*., 1995). Turbidites can erode and entrain the substrate and as a result can change composition with distance (Trofimovs *et al*., 2008). Furthermore, turbidite and tephra fall deposition are complex processes. For example, turbidites may be reflected around a depositional basin, and can generate secondary turbidites from unstable seafloor sediments (Pickering *et al*., 1998; Watt *et al*., 2012b); tephra fall may form pumice rafts on the sea surface, prior to deposition on the sea floor (Jutzeler *et al*., 2014b), and tephra fall settling through the water can also form density currents (Manville and Wilson, 2004).

Detailed componentry analysis was conducted using >63 μm material from all volcaniclastic units, and some bioclastic units from Holes U1394B, U1395B, U1396A and U1396C. For each sample approximately 400 grains were point counted using a field counting method, where all grains within the microscopes field of view are counted. Grains were divided into one of six classifications: 1) vesicular pumice clasts; 2) non-vesicular lava; 3) altered lithic clasts; 4) crystal and glass fragments; 5) mafic scoria clasts; and 6) bioclasts (Figures 3 and 4). This follows the classification of Le Friant *et al*. (2008) and Cassidy *et al*. (2014a). Data is shown in Appendix figure 3 and Appendix table 10.

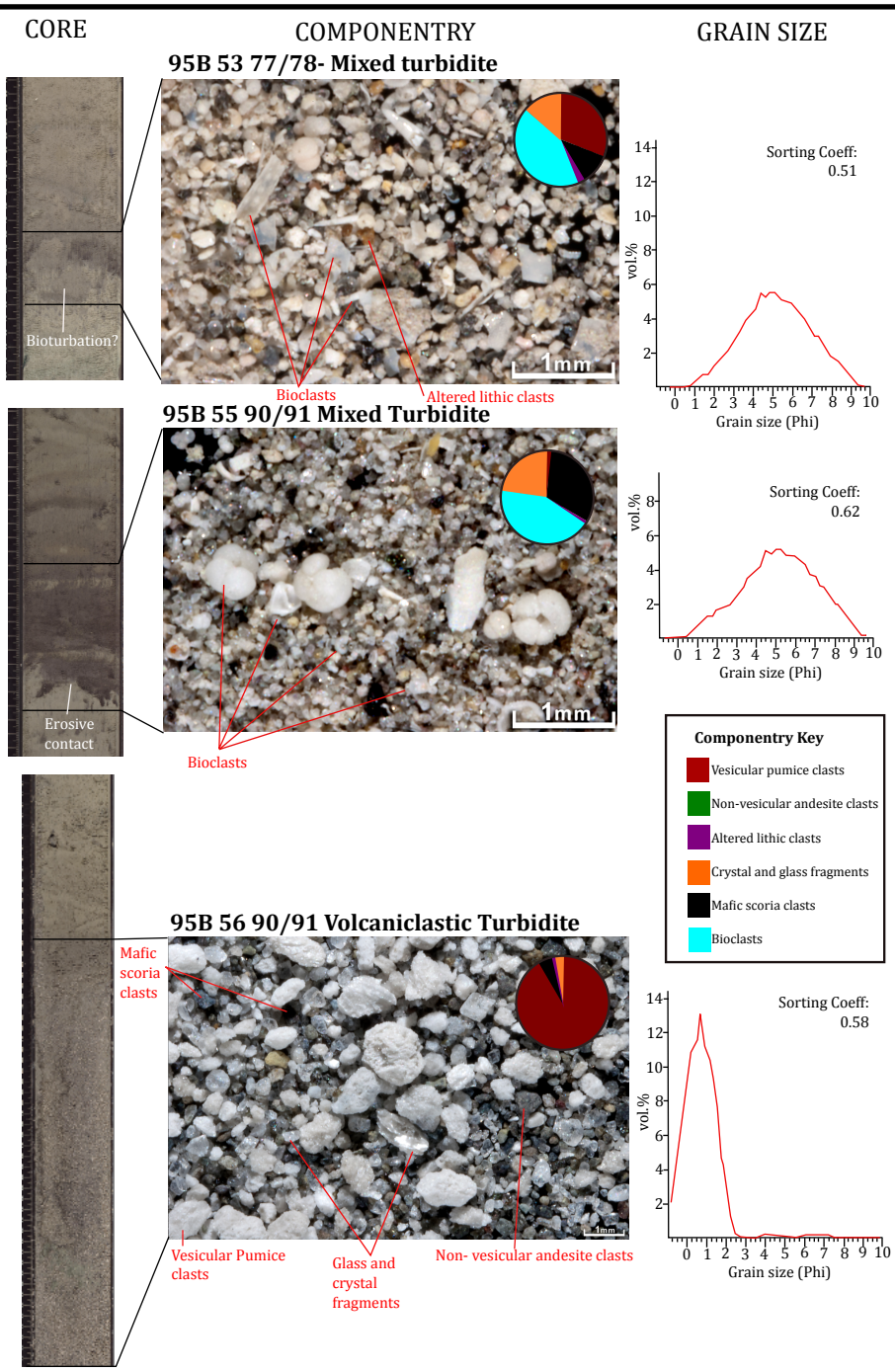

Figure 4: Turbidite deposits in Hole U1395B. To the left are core photos with millimetre and centimetre marks, in the middle are photos of material >63 µm. Composition is given by the pie charts in the top right of each photo and different clast types are labelled. Far right is the grain size distribution from analysing whole samples on the Malvern. Also shown are calculated Folk and Ward sorting coefficients.

To calculate Folk and Ward coefficients, grain sizes were analysed using a Malvern (Master-sizer 2000) laser diffraction particle size analyser. This instrument has a range from 0.2 –2000 μm and measures grain size using laser diffraction. 25 ml of reverse osmosis water with 0.05% sodium hexametaphosphate dispersant was added to 1 cm^3 of unsieved sample, and left overnight on a shaking table. Samples were analysed in triplicate, and accuracy was monitored using standard size particles (32 and 125 μm) (Appendix Tables 8 and 9).

Deposit Type	% Bioclasts	Folk and Ward sorting coefficient (phi)	Thickness (cm)
Bioclastic Turbidites	>70		
Mixed Turbidites	30-70		
Volcaniclastic Turbidites	<30	>0.5	
Tephra Fall	<30	<0.5	<20

Table 1: Summarises the criteria used in identifying each unit type

2.3 Providence of units

The IODP sites lie between Montserrat and Guadeloupe and tephra layers from Guadeloupe may be preserved within the IODP holes. Tephra from Guadeloupe can be distinguished using lead isotopes: magmas erupted on Guadeloupe are enriched in radiogenic lead relative to Montserrat (Cassidy, *et al*., 2012).

Tephra from Hole U1396C was analysed for lead isotopes: this is the site most dominated by tephra fall deposits. This was a combined effort between S. Hatter and myself. For each sample, 200 mg of pumice or scoria clasts were picked out and leached in 4 ml of 6 mol HCl at 140°C for 1-2 hours in sealed Teflon vials. Samples were then left on a hot plate at 130°C for 24 h to dissolve in HF-HNO_3. Samples were left to dry and then a further 0.5 ml of concentrated HCl and 0.5 ml of concentrated HNO_3 were added, evaporating till dry between each addition. To the remaining residue, 1.5 ml of HBr was added and heated for 1 h. A supernatent liquid for column chemistry was then produced by centrifuging samples for 5 min. Isolation of Pb from the matrix was achieved using AG1-X8 200-400 mesh anion

exchange resin. Blanks contained < 50 pg of Pb and the Pb standard NBS 981 was used. Isotope analyses were conducted on a VG Sector 54 thermal ionization mass spectrometer and multiple collector inductively coupled plasma mass spectroscopy (MC-ICP-MS) (Neptune and GV Iso Probe) at the National Oceanography Centre, Southampton. The double spike method was used to correct instrumental bias (Ishizuka *et al*., 2003). The sample preparation and analyses methods follows that of Cassidy *et al*. (2012).

2.4 Radiometric dating

Four different dating methods were used to develop an age model for each IODP Hole. These are: 1) oxygen and carbon isotope analysis; 2) biostratigraphic analysis; 3) paleomagnetic dating; and 4) AMS radiocarbon dating. Sedimentation rates of hemipelagic mud are estimated between each dated horizon. Using the estimated sedimentation rates, unit ages can be approximated.

Oxygen and carbon isotope analyses were conducted on the upper ~ 250 ka of stratigraphy in order to aid correlations with units found in nearby shallow vibrocores (Trofimovs *et al*., 2013). This was a combined effort between D. Wall-Palmer and myself. Marine isotope stages (MIS) can be identified in Sites U1394, U1395, and U1396 by comparing their respective oxygen isotope records with the global record (Lisiecki and Raymo, 2005). Holes U1394B, U1395B, and U1396C contain a near complete record of MIS, thus oxygen isotope stratigraphy was conducted primarily on these holes. However, the upper part of Hole U1394A was more complete than Hole U1394B, and therefore the upper 6 m of Hole U1394A was sampled. For Sites U1394 and U1395 ~20 *Globigerinoides ruber* specimens between 250-355 μm in size were picked every 7 cm, and for Site U1396 samples were picked every 4 cm. Specimens were reacted with 100% phosphoric acid at 90°C for two hours. The resulting CO_2 was analysed using an Isoprime Instruments continuous flow mass spectrometer with a Gilson Multiflow carbonate auto-sampler at Plymouth University. Oxygen and carbon isotope values ($\delta^{18}O$ and $\delta^{13}C$) are given as per mil (‰) deviations in the isotope ratios ($^{18}O/^{16}O$ and $^{13}C/^{12}C$) calibrated against VPDB using internal standards NBS-19, IAEA-CO-8 and IAEA-CO-9. Five NBS-19 standards were also evenly

distributed throughout the individual isotope runs to correct for daily drift. The mean standard deviation on replicate analyses was 0.17‰ for $\delta^{18}O$ and 0.19‰ for $\delta^{13}C$.

For biostratigraphic analysis microfossils and nannofossils were analysed and as a combined effort between D. Wall-Palmer and myself. For microfossils species counts were made on 300 specimens. Offshore planktik foraminifera do not follow the standard zonation of Wade *et al*. (2010) during the last 250 ka (Wall-Palmer *et al*. 2014) and were thus not used for biostratigraphy. However, the distribution of *Globorotalia menardii* was used, following the zonation previously published offshore of Montserrat by Le Friant *et al*. (2008). Calcareous nannofossils in the <63 μm fraction of hemipelagic samples were analysed using scanning electron microscopy (SEM). Dry pieces of sediment were adhered to metal stubs using a silver paint then sputter coated with gold. The zonation of Kameo & Bralower (2000) for the Caribbean Sea was used to determine the nannofossil stratigraphy for the three sites.

Paleomagnetic studies were conducted onboard the ship during Expedition 340. Cores were analysed every 2.5 cm using a 2G Enterprises model 760R superconducting rock magnetometer (SRM) with superconduction quantum interference devices (SQUIDs) and an in-line automated alternating field demagnetizer. For further details we refer the reader to Expedition 340 scientists, (2013), and Hatfield *et al*. (2015).

For AMS dates four samples in the upper 4 m of the Hole U1395B (aged < 43 ka) were dated. AMS samples selected were beneath two of the largest turbidites in the top 4 m of U1395B (Figure 2). Approximately 1,000 pristine (not reworked) tests > 150μm in size of *Globgerinoides ruber* were picked (~17mg) and sonically cleaned for each sample. Radiocarbon dates were measured at Scottish Universities Environmental Research Council (SUERC) laboratories using their in-house protocol (see Trofimovs *et al*., 2013). The AMS dates for the lower two analysis in Hole U1395B are close to the analytical limit of radiocarbon, so are reported as an uncalibrated age of >45 ka. This was a combined effort between D Wall-Palmer and myself.

2.5 Correlations

Correlations between sites use a combination of age dating and geochemical data. Stratigraphic horizons were dated using oxygen isotopes, biostratigraphic markers, paleomagnetic reversals and AMS dates. Geochemical correlations were based primarily on the glass chemistry of the coarsest-grained tephra fall layers within marine cores: these were considered to have the greatest potential for correlating with the subaerial pumice fall deposits (Chapter 2). We focussed on the coarse-grained deposits which are more likely to be the result of large magnitude eruptions and are more likely to form more extensive stratigraphic horizons. We also attempted to analyse a few coarse-grained volcaniclastic turbidites. However, turbidites are compositionally heterogenous, and correlations may be more ambiguous.

Glass chemistry was measured on a Cameca SX100 microprobe at the Department of Earth Sciences, University of Bristol. Multiple analyses were made for each unit, and totals <92 % were discarded. Totals were low because of high water contents in the samples due to the marine depositional environment. An analysis time of 3 minutes was used with a beam current of 4 nA with a beam diameter of 5 μm.

3. Results

3.1 Stratigraphy

3.1.1 Site U1394

The upper ~6 m of both U1394 Holes comprises stratigraphy seen previously in shallow cores (see Trofimovs *et al*. (2013) (Figure 2, *Section 3.5*). This comprises the 1995-recent eruption deposits that overlie a series of bioclastic and volcaniclastic turbidites. A thick pumice-rich turbidite occurs at ~6-14 m in Hole U1395B, which is overlain by a distinctive scoria-rich unit inferred to be a tephra fall deposit (Cassidy *et al*., 2015).

Between 16-60 m there is a gap in core recovery. A series of relatively thick (3-10 m) turbidites occur between 60-to-120 m in Hole 1394B (Figure 3). These sandy layers have variable compositions, with ~10-80 % of bioclastic and volcanic material. Some of the thick turbidites may have been sucked-in as an artefact of piston coring (see Jutzeler *et al.*, 2014a), and such intervals are shown by a shaded grey box in figure 5. However, a significant number of thick turbidite sand layers appear to be in-situ. Their presence is somewhat anomalous: this section of the core has a predominance of thick sandy beds with relatively little intervening hemipelagite, and contrasts in this respect to the sections of core above and below. This sand-rich sequence is interpreted as part of the marine stratigraphy that was mobilised during the emplacement of Deposit 2 (Figure 4).

The interval between 120 m to 175 m in Hole U1394B comprises a greater fraction of hemipelagic muds, and has thinner turbidite and tephra fall layers (Figure 3). A thick pumice-rich sand interval at 155-163 m may have been affected by flow-in during coring. Thinner bedded (<20 cm) turbidites and fallout deposits underlie the pumice-rich sand interval: a thick sand layer forms the base of Hole U1394B.

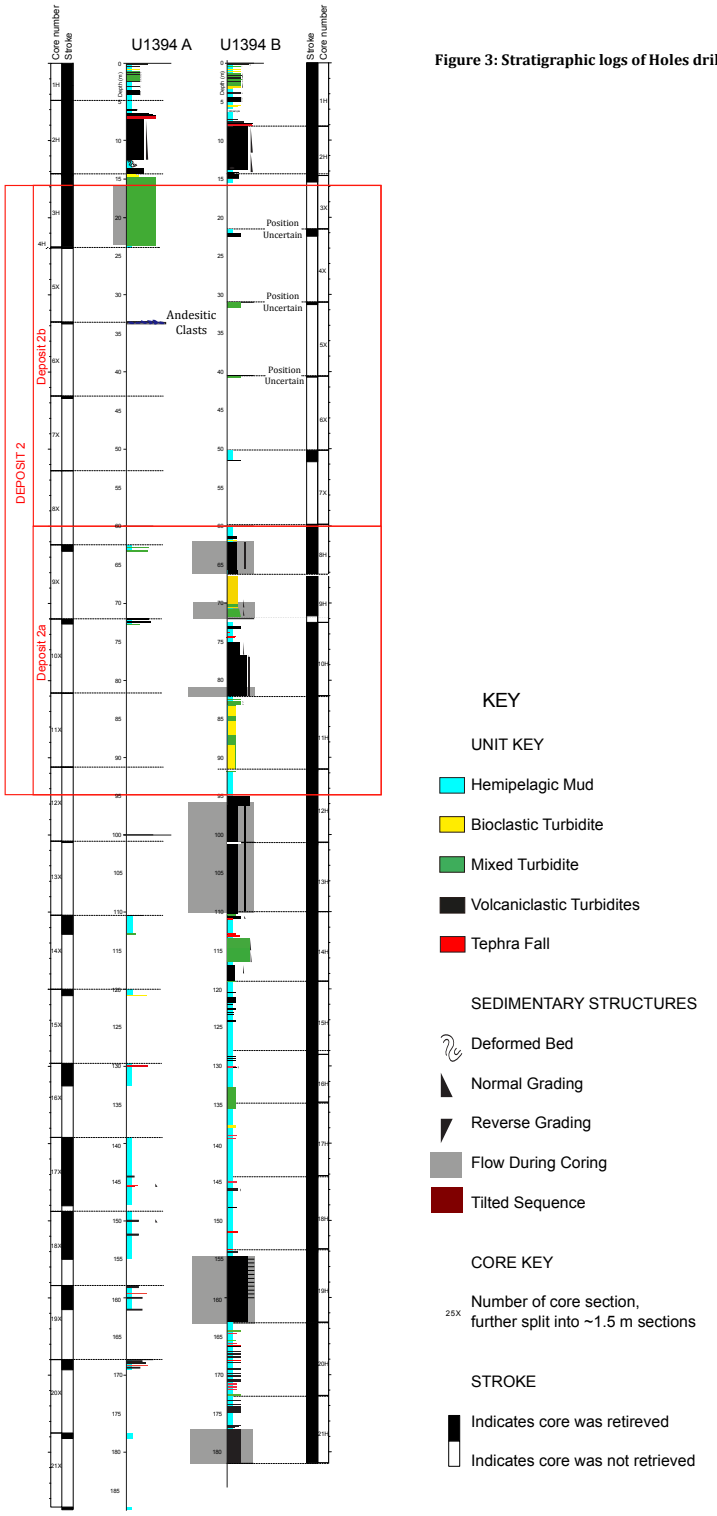

Figure 3: Stratigraphic logs of Holes drilled at IODP Site U1394

3.1.2 Site U1395

The upper 11.5 m of both holes comprises a series of turbidites separated by hemipelagic mud. These are are capped by a turbidite stack from the 1995-recent eruption on Montserrat. This turbidite stratigraphy can be correlated to Site U1394 and to the shallow cores described by Trofimovs *et al*., (2013) (Figure 2, *Section 3.5*).

A prominent thick turbidite sand layer occurs between ~11.5 m to 18 m at this site. This layer has been attributed to the turbidity current created during the emplacement of Deposit 2 (130 ka), and is most likely equivalent to the thick pumice-rich turbidite that occurs between 6-14 m at Site U1394 (i.e. immediately on top of Deposit 2; Figures 5 and 7). This turbidite is the thickest (excluding strata affected by flow-in) deposit in U1395B. This supports our correlation with Deposit 2, which is the largest landslide to have affected Montserrat during the period of Soufrière Hills volcanism.

Between 18-62 m Holes U1395A and B have relatively thick units of hemipelagic mud separated by thinner (<20 cm) turbidites and tephra fall layers (Figure 7). There are a small number of thicker (> 1 m) turbidites, some of which may have anomalous thicknesses associated with flow-in during piston coring (Jutzeler *et al*., 2014a). A grey shaded box in figure 7 shows intervals that may have been sucked in. The lower part of Holes U1395A and U1395B (62- 120 m) (700- 1000 ka) comprise numerous thin tephra layers (<10 cm) and thin volcaniclastic turbidites (<20 cm), with thin intervals (<50 cm) of hemipelagic mud (Figure 7), suggesting a sharp increase in the frequency of volcanic activity (or a sharp drop in sedimentation rate, which is not supported by palaeomagnetic data (*Section 3.3*)) around this time.

Unfortunately, a change from advanced piston coring to rotary drilling results in poor recovery below 120 m. However, at the base of the core is a thick volcaniclastic turbidite sequence. These may be associated with/ overlie the large landslide, Deposit 8 (Watt *et al*., 2012a) (Figures 1 and 6).

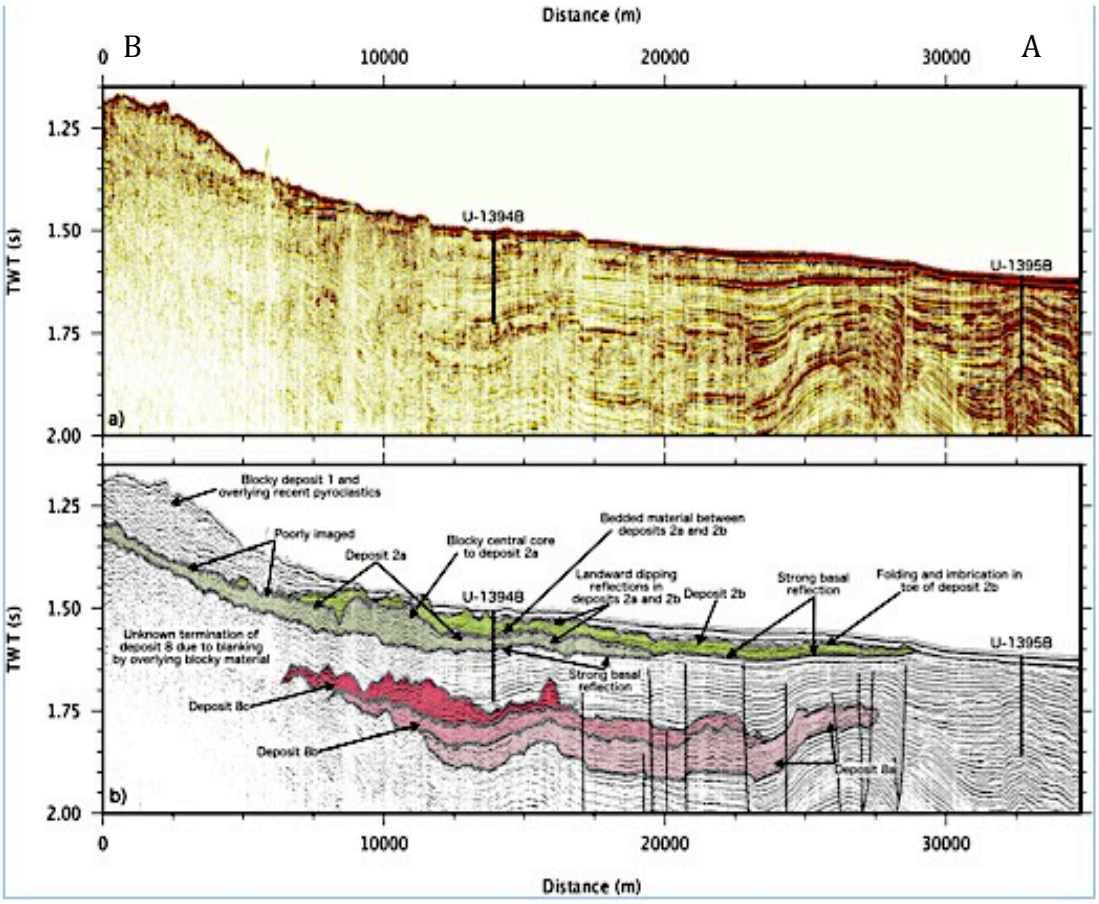

Figure 6: Top- 2D seismic profile trending NE-SW through IODP Site U1394 and U1395. Bottom- Interpretation of seismic profile outlining Deposits 2 and 8. Also shown are Holes. For seismic line see Figure 1.

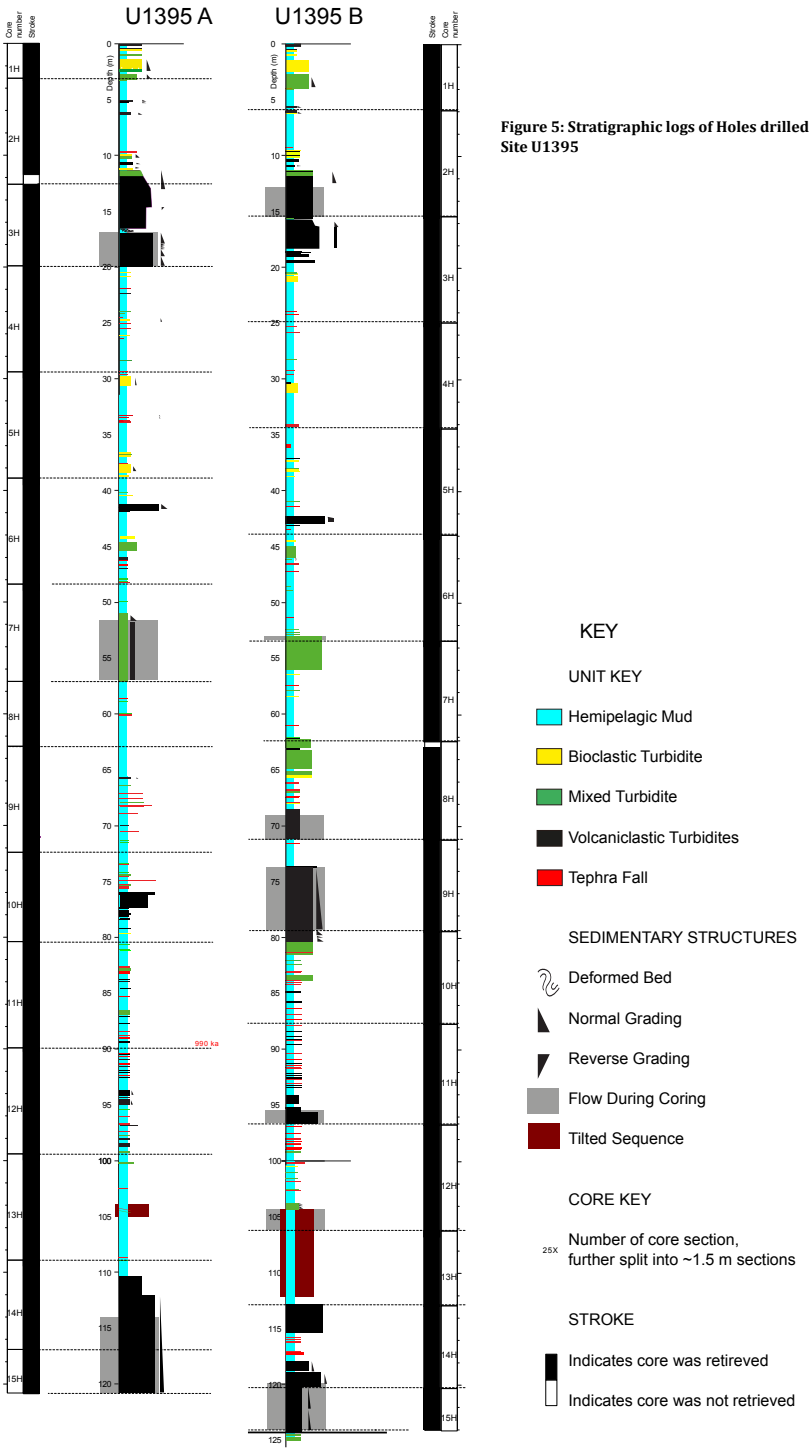

Figure 5: Stratigraphic logs of Holes drilled at IODP Site U1395

3.1.3 Site U1396

U1396C generally contains much finer-grained, thinly-bedded deposits than Sites U1394 and U1395. Tephra fall deposits and thin (<40 cm) turbidites dominate Site U1396 (Figure 8).

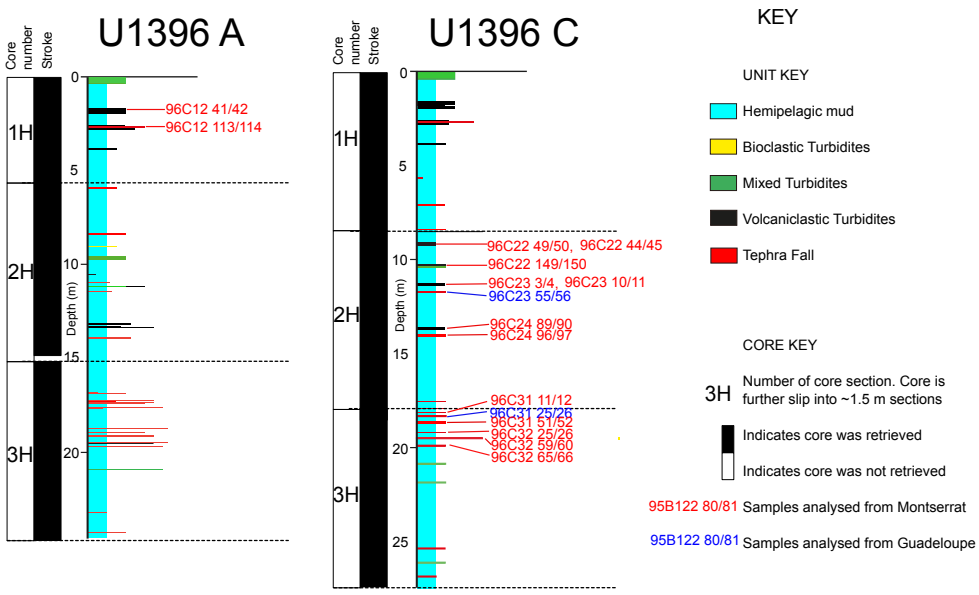

Figure 8: Stratigraphy of Holes drilled at IODP Site U1396. Also shown are samples analysed for Pb. Blue sample numbers indicate tephra layers that likely originate from Guadeloupe.

3.1.4 Deposit 2

Hole U1394B directly intersects Deposit 2, as defined by a region of disrupted marine sediment in seismic reflection profiles (Watt *et al.*, 2012a). At this location, Deposit 2 appears as a low amplitude sequence in seismic profiles with disrupted parallel-bedded reflectors (Figure 6). It is difficult to correlate core depth with the two-way time values in seismic reflection data, but depth conversion estimates suggest that Deposit 2 corresponds to the 16-95 m interval in Hole U1394B (Mark Vardy, personal communication). This fits well with our stratigraphic interpretation at the top surface (i.e. immediately beneath the scoriaceous fall unit and underlying turbidite), and would place the bottom surface of Deposit 2 within the sequence dominated by thick sandy turbidites (Figures 5 and 7). Notably, there is no horizon within the core that shows any visible signs of disturbance or systematic change, and which may be interpreted as the basal plane of Deposit 2.

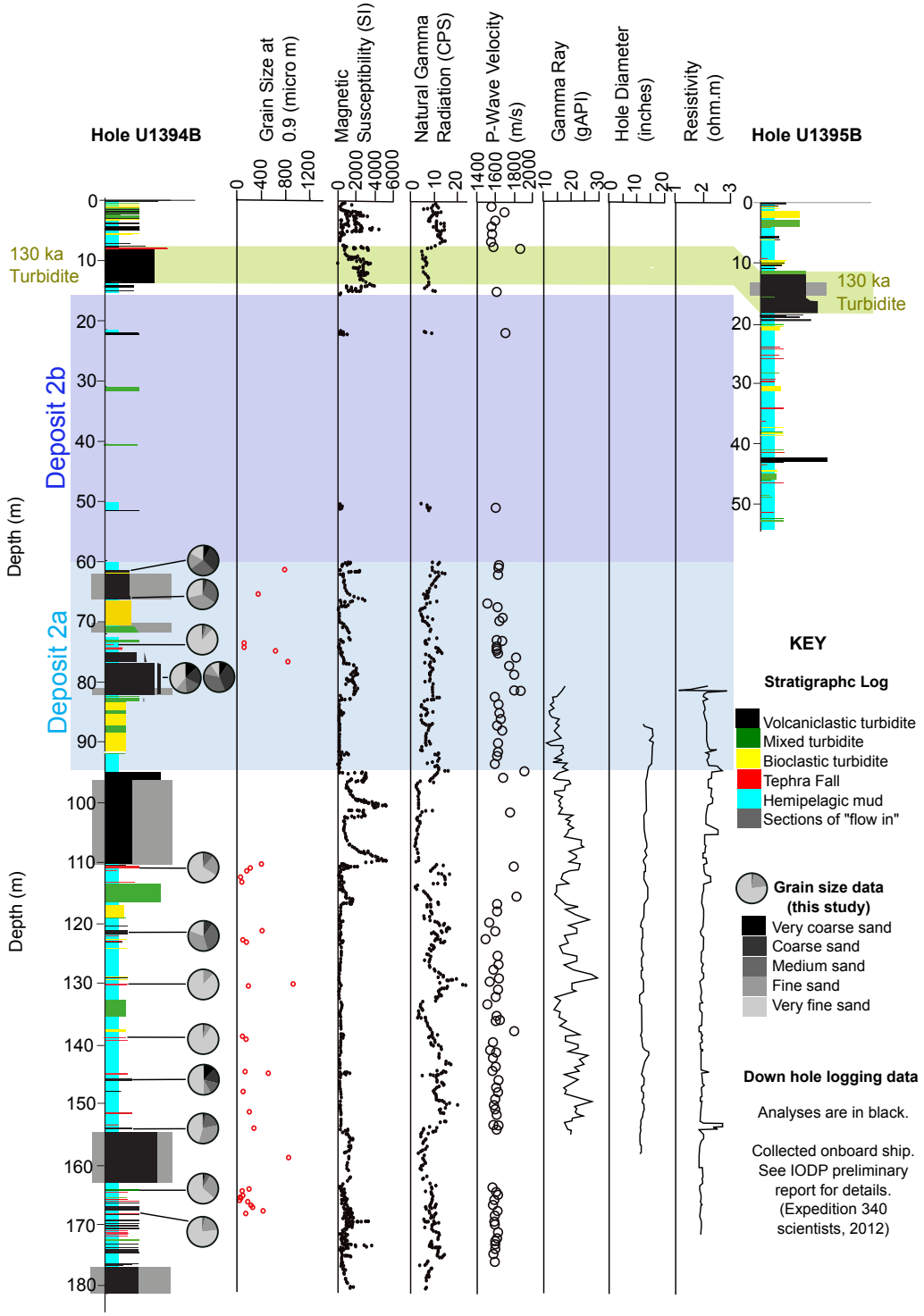
Hole U1394B
Grain Size at 0.9 (micro m)
Magnetic Susceptibility (SI)
Natural Gamma Radiation (CPS)
P-Wave Velocity (m/s)
Gamma Ray (gAPI)
Hole Diameter (inches)
Resistivity (ohm.m)
Hole U1395B
130 ka Turbidite
Deposit 2b
Deposit 2a
Depth (m)
KEY
Stratigraphc Log
Volcaniclastic turbidite
Mixed turbidite
Bioclastic turbidite
Tephra Fall
Hemipelagic mud
Sections of "flow in"
Grain size data (this study)
Very coarse sand
Coarse sand
Medium sand
Fine sand
Very fine sand
Down hole logging data
Analyses are in black.
Collected onboard ship. See IODP preliminary report for details. (Expedition 340 scientists, 2012)

Figure 9: Stratigraphic logs of Hole U1394B and the upper 50 m of Hole U1395B. Also shown is grain size data collected in this study and downhole log data from Hole U1394B collected on board the ship during Expedition 340 (Expedtion 340 scientists., 2013). The figure highlights Deposit 2 in blue and the 130 ka turbidite in green. Also shown are a selection of grain size pie charts. Many of the deposits within Deposit 2a are coarser than other deposits sampled in Hole U1394B.

Deposit 2 is separated in seismic reflection data into two vertically stacked halves, by a continuous set of parallel reflectors that extend 15 km downslope (Figure 6) (Watt *et al*., 2012b), defining Deposit 2a and 2b. Depth conversions suggest 2a extends between 60-95 m – and so is recovered within the core - and 2b extends between 16-60 m, and is therefore entirely absent in the core, since it corresponds to the gap in core recovery. Unfortunately, the core does not provide further insight into Deposits 2a and 2b are different, or on the nature of the internal reflectors that separate the two halves of the deposit.

Deposit 2a primarily comprises a sequence of thick (>1 m) turbidites that contain medium sand sized material (Figure 9) and little interlayered hemipelagic material. The absence of hemipelagic material is reflected in the down hole logging data (Expedition 340, 2013) where there is a reduction in gamma Ray and natural gamma radiation (Figure 9). Higher magnetic susceptibilities and faster P-wave velocities are observed in Deposit 2a, which suggests that there is an increase of volcaniclastic material and perhaps an increase in density (Figure 9).

3.2 Unit identification

The various volcaniclastic units in each IODP core were divided into specific categories using granulometric and thickness criteria (Chapter 3). Hole U1394B includes 16 bioclastic turbidites, 17 mixed turbidites, 44 volcaniclastic turbidites, and 30 tephra fall layers. Hole U1395B contains 18 bioclastic turbidities, 27 mixed turbidites, 41 volcaniclastic turbidites and 52 tephra fall layers. The top 7 m of Hole U1396C (we only consider this section, since the rest of the core is far

older than material in cores U1394 and 1395) contains 1 bioclastic turbidite, 1 mixed turbidite, 8 volcaniclastic turbidies and 13 tephra fall layers. Grain size data can be found in appendix table 8. Grain size data analyses using GRADISTAT are in appendix table 9. Componentry data can be found in appendix table 10.

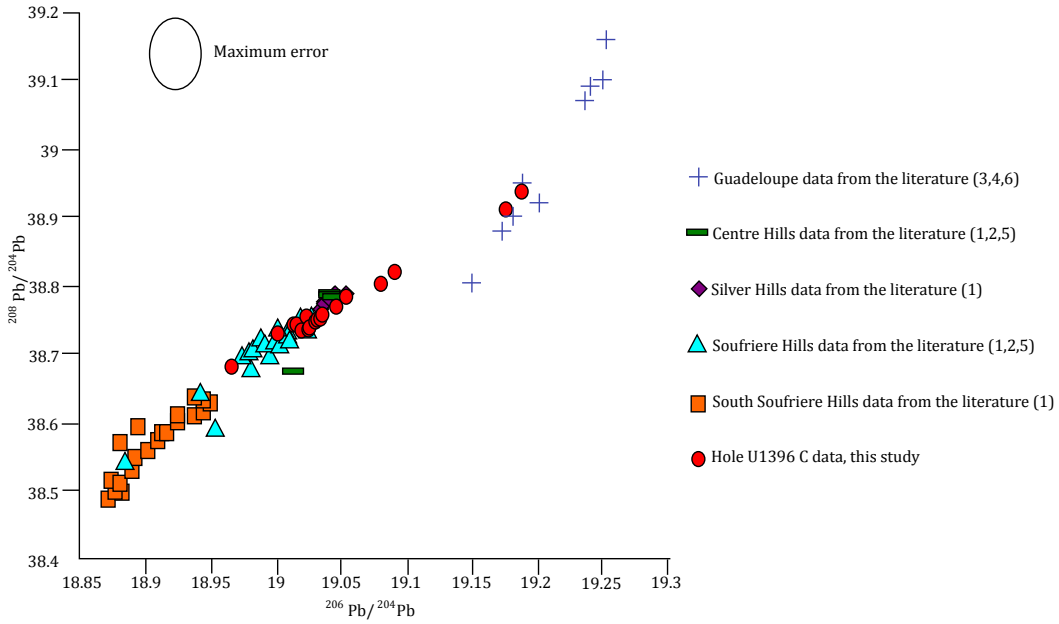

Figure 10: Comparison of Pb isotope data from U1396 C with Pb data from Montserrat and Guadeloupe obtained from the GEOROC database. (1= Cassidy *et al.*, 2012b; 2= Davidson, 1987; 3= Dufrane *et al.*, 2009; 4= Feuillard *et al.*, 1983; 5= Thirlwall, 2000; 6= White and Patchett, 1986). The ellipse in the top left indicates the maximum error of Pb isotope measurements, from this study.

Some of the tephra fall deposits in the IODP cores may be derived from Guadeloupe or neighbouring islands. Lead isotopes were used to distinguish between these sources, although analysis could only be conducted on a small number of deposits selected from Core U1396 (see Figure 8). We used this core because it is more dominated by tephra fall deposits than the other cores (and such deposits may be derived from widely spaced sources). By examining tephra fall deposits in this core, we can assess the proportion of events derived from Montserrat relative to other islands. The results indicate that out of 14 deposits analysed, 2 tephra units in core U1396C were derived from Guadeloupe ($^{208}Pb/^{204}Pb > 38.85$, $^{206}Pb/^{204}Pb > 19.1$) (Figures 8 and 10, Table 2): the rest

were sourced from Montserrat. We thus infer that the majority (>80%) of tephra fall deposits in holes U1394B, U1395B, and U1396C originated from Montserrat, although a larger number of Pb isotope analyses would be required to constrain this more precisely.

Sample name	$^{206}Pb/^{204}Pb$	Error +/-	$^{207}Pb/^{204}Pb$	Error +/-	$^{208}Pb/^{204}Pb$	Error +/-	$\Delta^{207}Pb/^{204}Pb$	$\Delta^{208}Pb/^{204}Pb$	Source
96c 2 2 44/45	19.04	0.0017	15.66	0.0016	38.76	0.0050	10.72	11.07	Montserrat
96c 2 2 49/50	19.08	0.0354	15.67	0.0325	38.81	0.1023	10.15	11.61	Montserrat
96c 2 2 149/150	19.02	0.0053	15.65	0.0049	38.74	0.0155	10.28	11.87	Montserrat
96c 2 3W 3/4	19.03	0.0016	15.66	0.0015	38.75	0.0047	10.97	11.60	Montserrat
96c 2 3 10/11	19.09	0.0015	15.67	0.0014	38.82	0.0044	10.55	12.49	Montserrat
96c 2 3 55/56	19.19	0.0090	15.69	0.0082	38.94	0.0260	12.10	11.21	Guadeloupe
96c 2 4 89/90	19.02	0.0025	15.66	0.0023	38.74	0.0071	10.30	11.56	Montserrat
96c 2 4 96/97	19.03	0.0022	15.66	0.0020	38.75	0.0064	10.63	12.13	Montserrat
96c 3 1 11/12	19.05	0.0020	15.66	0.0019	38.78	0.0059	11.76	10.23	Montserrat
96c 3 1 25/26	19.17	0.0016	15.69	0.0015	38.91	0.0046	10.51	11.88	Guadeloupe
96c 3 1 51/52	19.05	0.0017	15.66	0.0016	38.77	0.0049	9.67	11.10	Montserrat
96c 3 2 25/26	19.03	0.0022	15.65	0.0020	38.74	0.0063	10.29	12.20	Montserrat
96c 3 2 59/60	19.03	0.0017	15.66	0.0016	38.75	0.0050	10.34	12.77	Montserrat
96c 3 2 65/66	19.02	0.0017	15.66	0.0016	38.74	0.0050	10.05	12.69	Montserrat
96a 1 2 41/42	18.96	0.0031	15.65	0.0029	38.68	0.0091	10.05	12.69	Montserrat
96a 1 2 113/114	19.00	0.0034	15.65	0.0032	38.73	0.0099	10.17	13.27	Montserrat

Table 2: Lead isotope data from Site U1396. See figure 8 for locations. All samples were taken from the working half of the core.

Sites U1394 and U1395 are situated in the Bouillante-Montserrat graben, which is a major route for turbidites from Montserrat. Turbidites derived from Guadeloupe over the past 1 Ma are unlikely to be sampled in the Bouillante-Montserrat graben, since most of the volcanism on Guadeloupe has been focussed further south, where they would be funnelled westwards by an extensive canyon system (Samper *et al*., 2007). Only deposits discharged from the north of Guadeloupe could reach the IODP core Sites, but no subaerial volcanic deposits have been dated <1 Ma in the north of the island. Site U1396 is drilled on a topographic high (Figure 1), and it is unlikely that turbidites from Guadeloupe could reach Site U1396.

3.3 Radiometric dating of deposits

3.3.1 Site U1394

Marine Isotope Stages (MIS) 1 to 5 are identifiable in the upper 15 m of U1394B, but identifying the MIS boundaries below 15 m is difficult due to incomplete core recovery. The first occurrence of the nannofossil species *Emiliania huxleyi* (250 ka) is found at Sites U1395 and U1396 and in the CAR-MON2 core (Le Friant *et al*., 2008) near the MIS 7/8 boundary (Figure 11). In Hole U1394B the first occurrence of *E. huxleyi* is located at 133 m, and coincides with an increase in δO^{18} at ~133 m. Thus the increase in δO^{18} in Hole U1394B at ~133 m has been correlated with the MIS 7/8 boundary (Figure 11). At the base of the core MIS 8/9 is identified at ~ 150 m.

Shipboard NRM identifies no paleomagnetic reversals in Hole U1394B suggesting that all of the core material was deposited in the last 781 ka, this is in agreement with the oxygen isotope stratigraphy.

3.3.2 Site U1395

In the upper 45 m of Hole U1395B 9 MIS's have been identified. The oxygen isotope record from Hole U1395B correlates well to that in vibrocore JR 123-12-V, and to other shallow vibrocores described by Trofimovs *et al*. (2013) (Figure 2), to the more complete oxygen isotope record of CAR-MON2 (Figure 12), (shallow core from the southwest of Montserrat), and with the standard global oxygen isotope curve (Imbrie *et al*. 1984; Prell *et al*. 1986; Martinson *et al*. 1987).

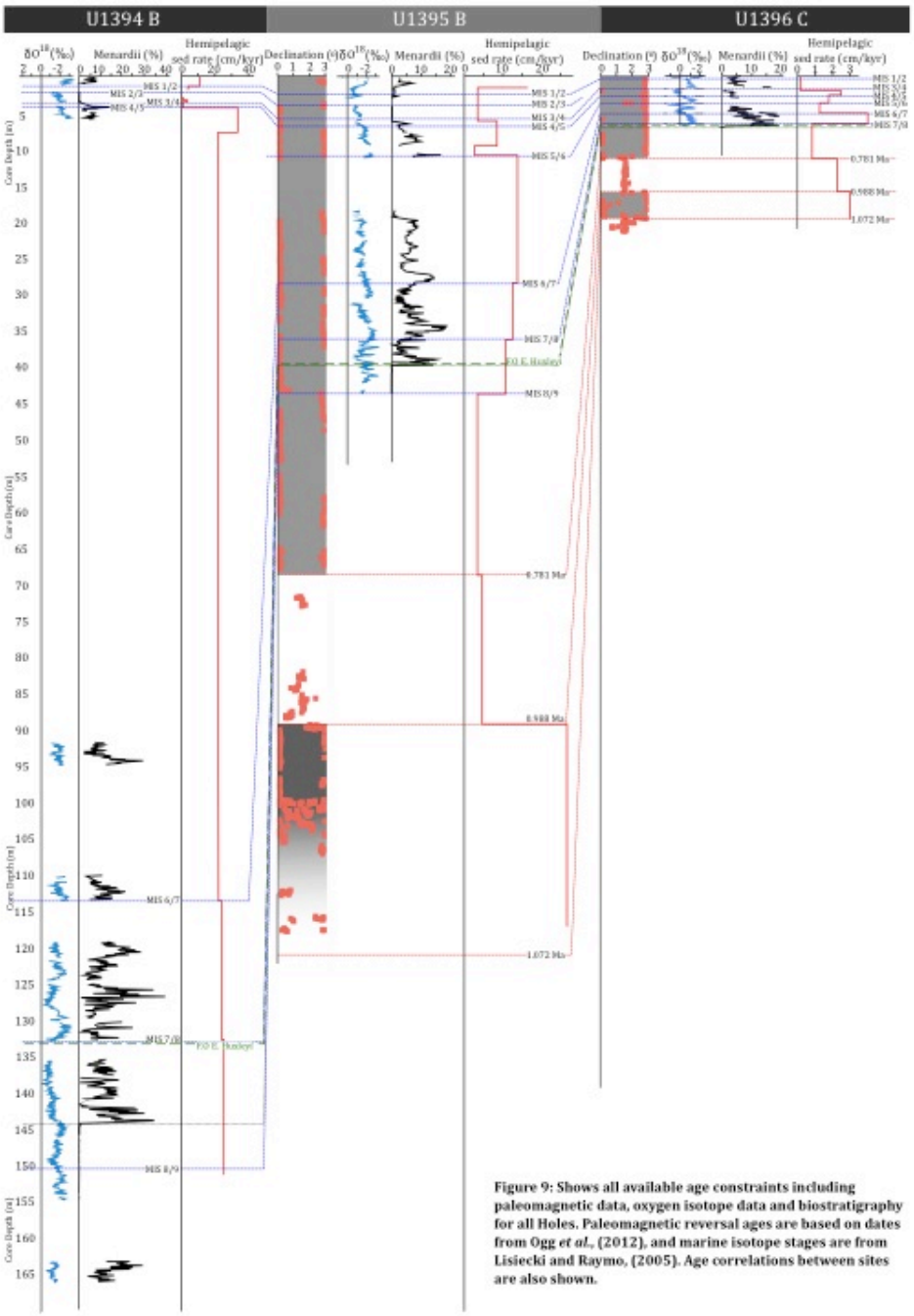

Figure 9: Shows all available age constraints including paleomagnetic data, oxygen isotope data and biostratigraphy for all Holes. Paleomagnetic reversal ages are based on dates from Ogg *et al.*, (2012), and marine isotope stages are from Lisiecki and Raymo, (2005). Age correlations between sites are also shown.

Using the oxygen isotope stratigraphy, several turbidites in the upper 15 m of Site U1395 can be correlated with deposits previously described from nearby vibrocore sites (e.g. core JR123-12V, Trofimovs *et al*., 2013; Cassidy *et al*., 2013, 2014a (Figure 2)), including deposits at 2-1.5 ka, 6 ka, 14 ka, 74-59 ka, and 110-103 ka (Figures 2 and 12; Section 3.5).

AMS dating in Hole U1395B yields ages of 9.93 ka and 11.49 ka beneath the 6 ka turbidite and >43 ka beneath the 14 ka turbidite (Figure 2, Table 3). This suggests that the 14 ka turbidity current event may have removed ~30 ka of underlying hemipelagic material (Trofimovs *et al*., 2013).

Publication code	Core number	Stratigraphic position (cm)	Conventional Radiocarbon Age (years BP)	$\delta^{13}C_{VPDB}$‰ ± 0.1	Calibrated age (years)
SUERC-46961	U1395 B	258-260	9993	1.1	10475+/-58
SUERC-46962	U1395 B	265-267	11489	1.1	12617+/-41
SUERC-46965	U1395 B	409-411	45806	1.2	>45000
SUERC-46966	U1395 B	416-418	44294	1	>45000

Table 3: Radiocarbon data from Hole U1395 B.

Two paleomagnetic reversals occur in Hole U1395B at 781 ka, and 988 ka. They are found at depths of 68.5–71 m and 89.08 m respectively (Figure 11). The exact location of the 781 ka reversal is obscured by a thick volcaniclastic turbidite. We date this turbidite at 781 ka as it is likely to have been emplaced at a similar time to the reversal.

At the base of U1395, declination begins to change indicating that a 1072 ka reversal may appear at the base of U1395B (Figure 11). In Chapter 3 the 1072 ka reversal was not included in any of the age models due to uncertainty of the placement. In Hole U1396C the 1072 ka reversal is well developed, and coincides with a visual increase in the number of tephra fall and turbidite deposits. At the base of U1395B a similar increase in the occurrence of tephra fall and turbidite deposits is observed. By correlating this sequence with U1396C, we have greater confidence that the 1072 ka reversal is present near the base of U1395B. We place the 1072 ka reversal at 115.45 m (at the base of a volcaniclastic turbidite). At the bottom of Hole U1395B is a thick volcaniclastic sequence that may be

associated with Deposit 8 (the largest landslide deposit observed offshore Montserrat). Dating of Hole U1395B may therefore suggest that Deposit 8 is > 1 Ma.

3.3.3 Site U1396

Oxygen isotope stratigraphy of core U1396C is the most complete, as there has been less erosion by turbidity currents. Site U1396 is located near the site of CAR-MON2 (Le Friant *et al*., 2008) and the oxygen isotope stratigraphies correlate well (Figure 12). Only the uppermost unit shows any evidence of significant erosion at its base, where MIS 2 is absent (Wall-Palmer *et al*., 2014) (Figures 11 and 12).

At Site U1396 there is a long and detailed paleomagnetic stratigraphy identifying 16 individual reversals. This shows that the entire core dates back to ~4.5 Ma. (Appendix Figure 3).

Differences between the data presented here and previously published data can be explained by the use of different methodologies (Figure 12). For example, oxygen isotope analysis of CAR-MON2 was carried out on homogenised <63 μm material, which contains both planktic and benthic organisms, whereas analysis of Hole U1396C was carried out on a single species of planktic foraminifera.

3.4 Sedimentation rates

Sedimentation rates for hemipelagic mud were calculated using all available dated horizons for each core. Event beds (e.g. turbidites and tephra fall deposits) were not included in the thicknesses used to calculate sedimentation rates (Figure 11). However, it should be noted that erosion beneath all beds (except a few units in the radiocarbon age window) is unquantifiable, and could potentially have removed tens of thousands of years-worth of hemipelagic mud in places (cf. Trofimovs *et al*., 2013). Such erosion may have systematically affected the calculated sedimentation rates throughout the cores especially in sequences (such as U1394) dominated by turbidites.

Estimated sedimentation rates are highest at Hole U1394B, as expected, because this site is most proximal to the island, and thus to a terrigenous sediment source. Calculated rates are 24-33 cm/ka between 300-101 ka (Figure 11), and decrease markedly in the 101-6 ka interval, to 0.6-3.8 cm/ka. Rates then increase to ~12 cm/ka from 6 ka (Figure 11). Sedimentation rates between 130-191 ka are uncertain due to a gap in coring between 15-60 m and the uncertainty of the 191 ka MIS 6/7 transition (Figure 11). The high variability (over an order of magnitude) in sedimentation rates potentially calls into question our assigned ages, or may indicate that parts of the core have been more subject to major erosive events. The presence of the Deposit 2 landslide unit (which mobilised marine sediment stratigraphy in this area) may also complicate the stratigraphy, but our interpretation of this is hindered by the stratigraphic gap from 15-60 m.

Sedimentation rates since 300 ka at Hole U1395B vary between 2-17 cm/ka (Figure 11). In the top 15 m of Hole U1395 B, there is a high resolution of dated horizons, thus sedimentation rates appear more variable. Higher dating resolutions pick up smaller-scale variability, including the measurable effects of erosion below turbidites. Sedimentation rates between 300-988 ka are ~3-5 cm/ka (Figure 11). Between 988-1072 ka sedimentation rates increase to >26 cm/ka (Figure 11).

In Hole U1396C sedimentation rates are the lowest estimated from this study, as expected due to the distal location of Site U1396. Sedimentation rates fluctuate between 0.2-4 cm/ka over the past 1 Ma (Figure 11). This corresponds very closely to the rate derived from 101-6 ka for site U1394, the most proximal core, and reinforces the puzzling nature of the apparently low sedimentation rates in the shallow part of U1394, which we would have expected to be far higher. This may be due to erosion, which would be greater at more proximal locations.

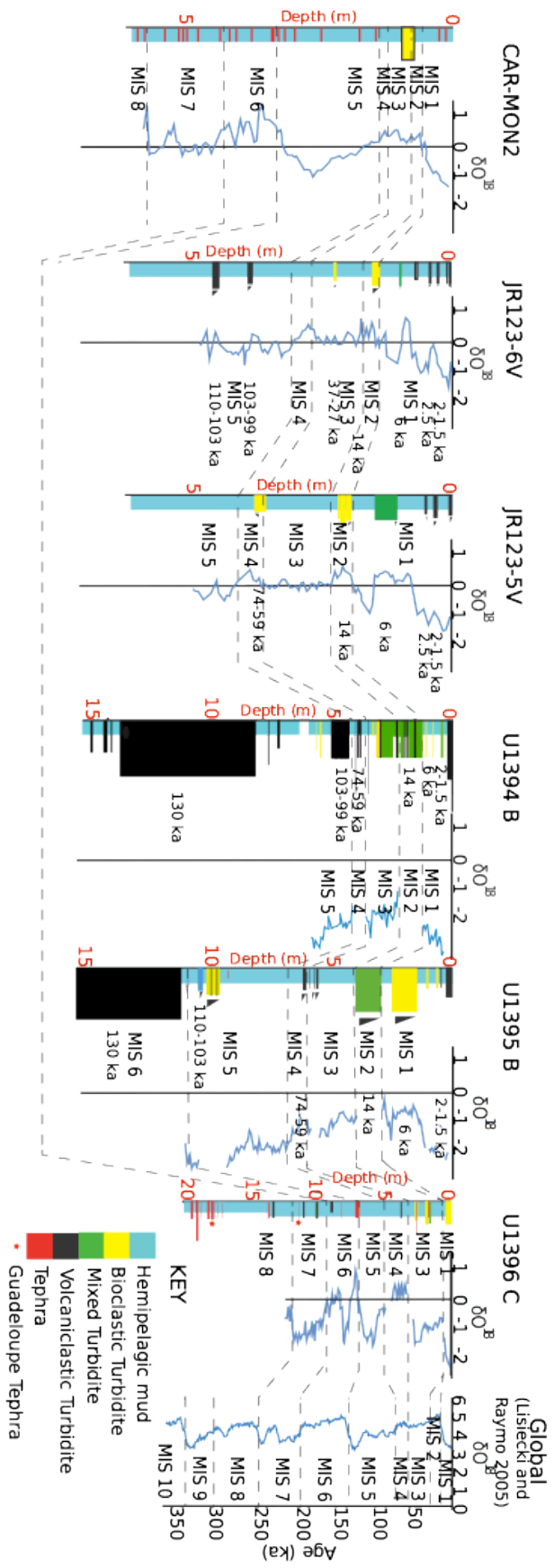

Figure 12: Comparison of oxygen isotope analyses of this study with CAR-MON-2, JR123-6V, JR123-5V (Le Friant *et al.*, 2008; Trofimovs *et al.*, 2013), and the global oxygen isotope curve (Lisiecki and Raymo, 2005). Oxygen isotope stages (MIS) are shown. Also shown are unit correlations based on dates and componentry.

Most sedimentation rates estimated in this study are broadly similar to previous estimates by Reid *et al*. (1996) of 5-10 cm/ka, from a relatively distal core (closest core location to Montserrat is ~30 km east (EN 16)).

3.5 Correlations

3.5.1 Correlations to units dated previously

Turbidites in the upper 3 to 5 m of Sites U1394 and U1395 can be correlated to turbidites in adjacent vibrocores, whose ages are well constrained by numerous radiocarbon dates (Figure 2, Trofimovs *et al*., 2013). These correlations are based on componentry analyses and oxygen isotope stratigraphies. Correlations are shown in figures 2 and 12, and allow turbidites in the upper parts of U1394B and U1395B to be dated more precisely. Below recent turbidites from the 1995 eruption, there are turbidites at ~2 ka, ~3 ka and 6 ka (Trofimovs *et al*., 2013). The 6 ka turbidite is relatively thick at Site U1395 (Figure 12). The 2 ka and 6 ka events are thought to originate from collapses of English's Crater on land, whilst the 3 ka turbidite may be the result of a more local carbonate platform failure (Trofimovs *et al*., 2013). The 6 ka turbidite is underlain by thick bioclastic-rich turbidites that were emplaced at 11.5-14 ka, and are most likely associated with landslide Deposit 1 (Figures 2 and 12; Trofimovs *et al*., 2013). Radiocarbon dating shows that the 11.5-14 ka turbidity current was particularly erosive. Basaltic scoria-rich turbidites dated to ~103-110 ka by Trofimovs *et al*. (2013) are found at Sites U1394 and U1395 (Figure 12).

Correlating Hole U1396C to the previously studied sites is difficult as there are few nearby cored locations (CAR-MON2 and JC18-19, Figure 13). The 30.5 ka (associated with Deposit 5), and 75±10 ka events found in shallow cores to the southwest of Montserrat (cores JR123-1 to 3) may be found at Site U1396 (Cassidy *et al*., 2012, 2014a, 2014b; Trofimovs *et al*., 2013; Wall Palmer *et al*., 2014) (Figure 13). In the CAR-MON2 core there is a sequence of reworked volcaniclastic material dated at 124-147 ka, and this may correlate to a volcaniclastic-rich unit in Hole U1396C (Figure 13).

3.5.2 Subaerial correlations

Glass compositions record the final pre-eruptive conditions in a magma reservoir; each tephra fall deposit is likely to have a unique glass composition even from stable magmatic systems (Lowe *et al*., 2011). Here, we analysed the coarsest-grained tephra layers and some prominent volcaniclastic turbidites, as these are likely to be from larger magnitude events that produce more extensive stratigraphic horizons. Given the relatively small number (< 30) of major (1 m thick proximal tephra fall) explosive eruptions apparent in the subaerial stratigraphy (Chapter 2), our expectation was that correlation with offshore units, focussing on the coarser and thicker fall deposits, would enable multiple correlations. However, this is not borne out by the data (Figures 14 and 15). While several tephra fall deposits have discrete glass compositions, relatively few show clear overlap with units from other sites. Thus, we can define only a few tie points between the various records; only one subaerial unit has been correlated with the marine record. TiO_2 and K_2O compositions are used to assess correlation, as these parameters provide the best separation between units. The small number of correlations based on geochemical data, and the uncertainty in the strength of these correlations, means that they have not been used to further refine the age models used here. Thus, the ages of the correlated units, quoted below, may be slightly different, but have been deemed close enough to suggest that the correlation is plausible.

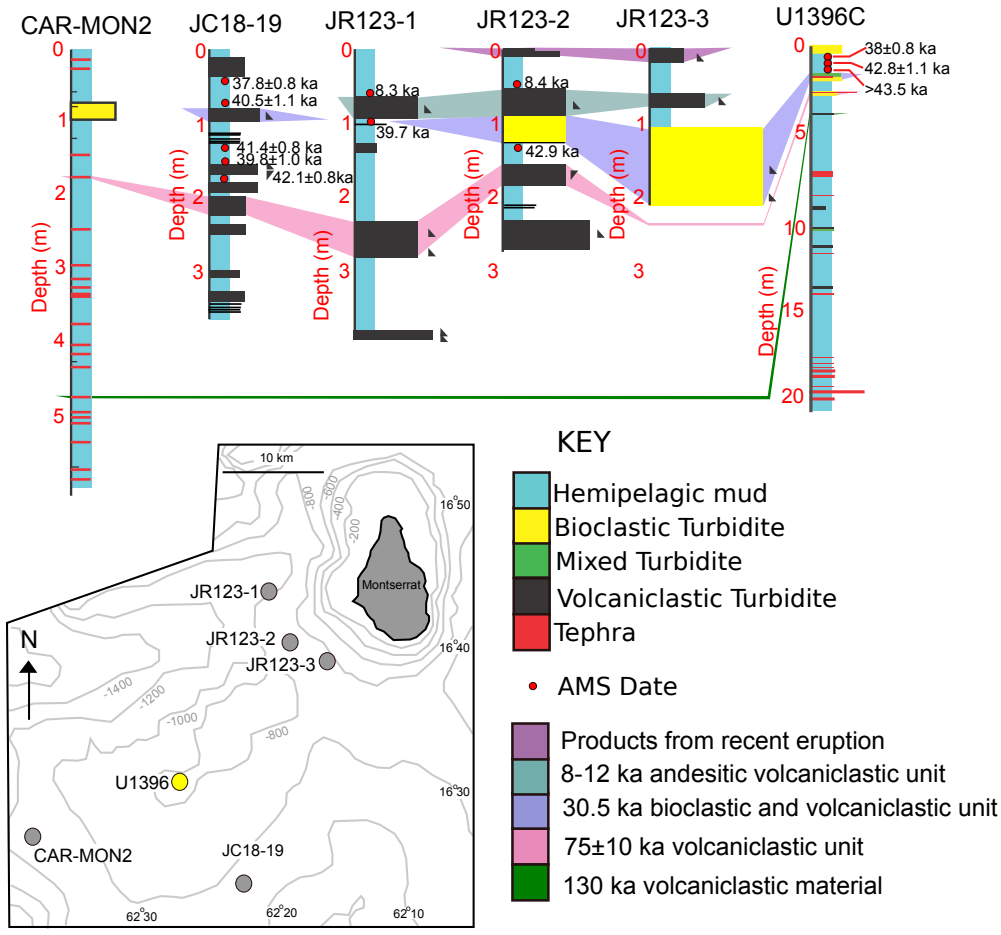

Figure 13: Correlations to the southwest of Montserrat (Le Friant *et al.*, 2008; Cassidy *et al*, 2012, 2014a, 2014b; Trofimovs *et al.*, 2013; Wall-Palmer *et al.*, 2014).

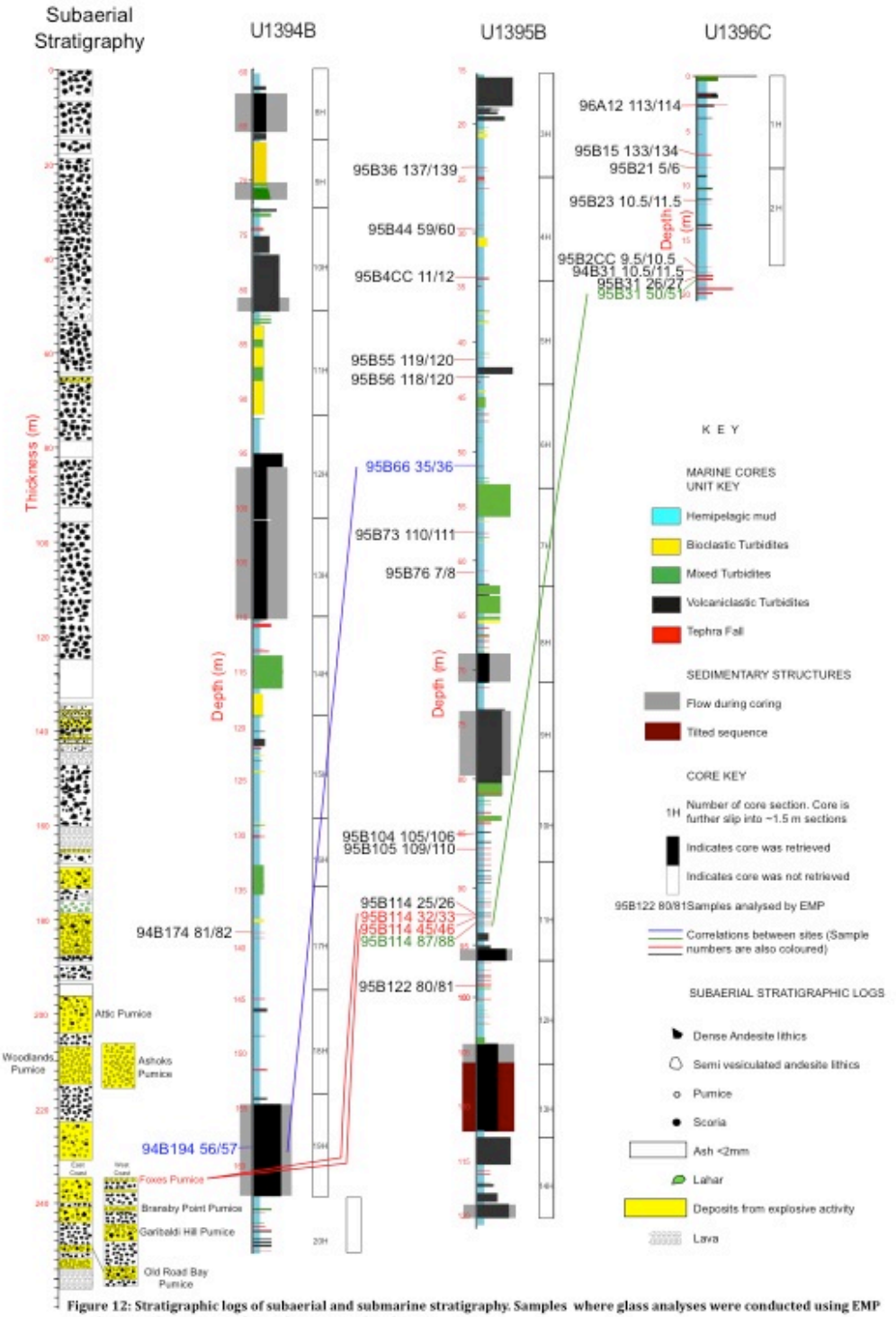

Figure 12: Stratigraphic logs of subaerial and submarine stratigraphy. Samples where glass analyses were conducted using EMP are shown and any potential correlations are also shown.

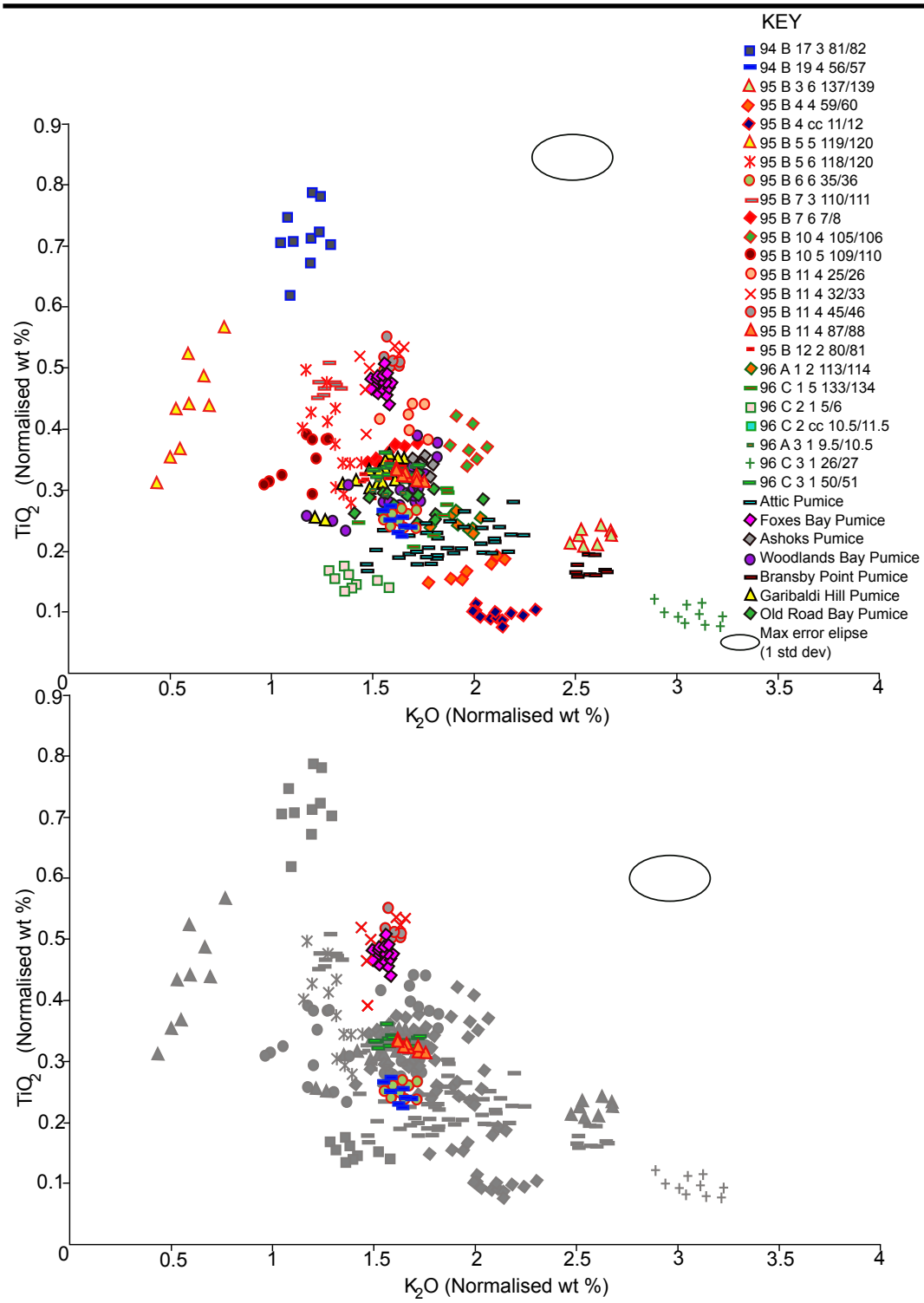

Figure 15: Major element compositions of glass from selected volcaniclastic layers. Blue outlined symbols are deposits from Site U1394, red outlined symbols are deposits from Site U1395, green outlined symbols are from Site U1396, and black outlined symbols are on-land deposits (data from Chapter 3). The lower figure shows only the correlated samples.

Two closely spaced volcaniclastic layers in Hole U1395B (95B 11 4 45/46 and 95B 11 4 32/33) have similar chemistries to the subaerial Foxes Bay pumice (Chapter 2) (Figures 14 and 15). The glass compositions in these deposits are distinct with high TiO_2 contents (0.4-0.5 wt %; Figure 15), suggesting that Foxes Bay pumice is likely to correlate with one of these two high-TiO_2 deposits. Ages estimated from subaerial and submarine data are broadly similar at 0.6-0.9 Ma and ~0.95 Ma respectively (Figure 16), and the correlation is considered reasonable.

3.5.3 Correlations between IODP sites

Correlations between IODP sites are made using date horizons, biostratigraphic horizons, and volcanic glass chemistry. Oxygen MIS are identified at all IODP sites back to MIS 9, and are useful stratigraphic horizons in the past 300 ka of Montserrat's offshore stratigraphy. Paleomagnetic reversals are useful for correlating stratigraphy between Holes U1395B and U1396C. However, no reversals were found in Hole U1394B. The 781 ka and 988 ka reversals are well developed in Holes U1395B and U1396C, but the 1072 ka reversal is only well developed in Hole U1396C (Figure 11).

The disappearance of *G. menardii* and the first occurrence *E. huxleyi* are useful stratigraphic horizons at all three of the IODP sites (Figure 11). The disappearance of *G. menardii* coincides closely with the first occurrence of *E. Huxleyi* and occurs near the MIS 7/8 boundary (Figure 11). The disappearance of *G. menardii* is likely to be related to a local environmental change, as at the base of Hole U1394B *G. menardii* reappears (Figure 11).

Two potential correlations between the IODP sites have been identified using glass compositions of volcaniclastic deposits. The first correlation is between a thick (>5 m) volcaniclastic turbidite in Hole U1394B (that may have been artificially thickened by flow-in during coring (Jutzeler *et al*., 2014a)) with a 5 cm thick tephra fall layer in Hole U1395B (Figure 14). Sample 94B 19 4 56/57 from Site U1394 has similar major element glass chemistry to 95B 6 6 35/36 in Site U1395 and both units have relatively low TiO_2 contents (0.2-03 wt %) (Figures 14 and 15).

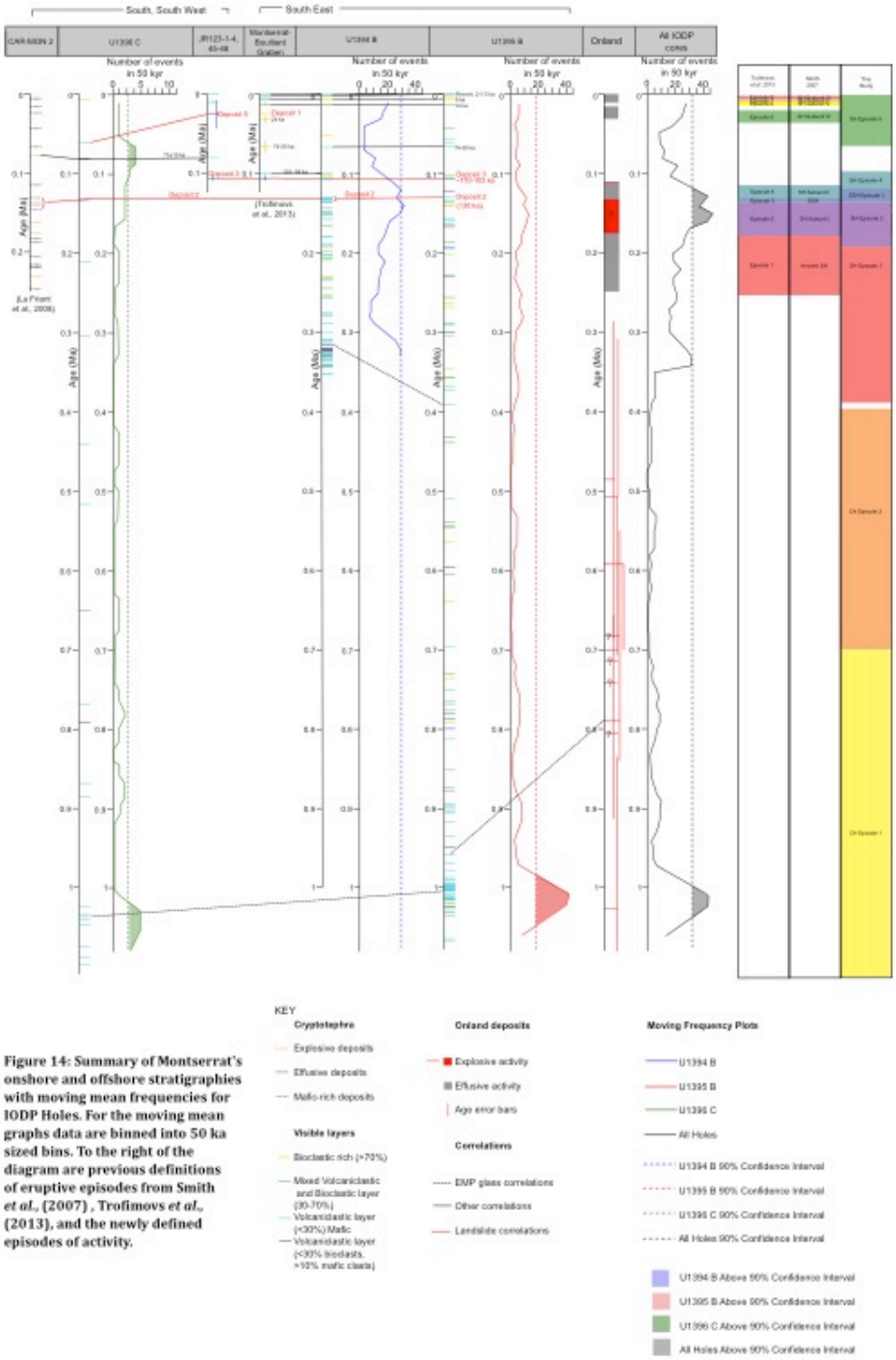

Figure 14: Summary of Montserrat's onshore and offshore stratigraphies with moving mean frequencies for IODP Holes. For the moving mean graphs data are binned into 50 ka sized bins. To the right of the diagram are previous definitions of eruptive episodes from Smith *et al.*, (2007) , Trofimovs *et al.*, (2013), and the newly defined episodes of activity.

The second correlation is between sample 96C 3 1 50/51 from Site U1396C and sample 95B 11 4 87/88 in Site U1395B (Figures 14 and 15). Both of these tephra layers have similar compositions to several of the analysed samples, but these two samples occupy a narrow compositional range (Figure 15) relative to the broader ranges of other units, and are in stratigraphically similar positions. The estimated ages of the units at sites U1395 and U1396 are ~1.1 and ~1.3 Ma respectively and both of the tephra layers are 2 cm thick.

4. Statistics

4.1 Frequency of tephra fall and turbidites

One age model is presented for each hole, which incorporates all available age data (Figure 11). Age data used for each hole are summarised in table 4. Moving frequency graphs are constructed, where data is binned into 50 ka wide bins and the bin window is incrementally moved by 10 ka (Figure 17). To determine the effects of binning data on observations, moving mean graphs are constructed using 10 ka and 100 ka wide bins (Figures 18 and 19). We define periods of heightened activity as time periods where event frequency is above the 90% confidence interval. We define periods of low activity as periods of <1 event per 50 ka. Four main periods are identified.

Hole U1394B		**Hole U1395B**		**Hole U1396C**	
Type	*Age (ka)*	*Type*	*Age (ka)*	*Type*	*Age (ka)*
Correlation	1.75	Correlation	1.75	Unit date (Wall-Palmer *et al.*, 2014)	19
Correlation	6	Correlation	6	Unit date (Wall-Palmer *et al.*, 2014)	60.25
Correlation	14	Oxygen Isotope	14	Unit date (Wall-Palmer *et al.*, 2014)	81
Oxygen Isotope	29	Correlation	66.5	Unit date (Wall-Palmer *et al.*, 2014)	131.5
Oxygen Isotope	57	Correlation	107	Oxygen Isotope	191
Correlation	66.5	Correlation	130	Oxygen Isotope	243
Oxygen Isotope	71	Oxygen Isotope	191	Paleomagnetic reversal	781
Correlation	101	Oxygen Isotope	243	Paleomagnetic reversal	988
Correlation	107	Oxygen Isotope	300	Paleomagnetic reversal	1072
Correlation	130	Paleomagnetic reversal	781		
Oxygen Isotope	191	Paleomagnetic reversal	988		
Oxygen Isotope	243	Paleomagnetic reversal	1072		
Oxygen Isotope	300				

Table 4: Date horizons used in constructing age models. Correlations are ages given by correlating units within the IODP cores to units in the shallow vibrocores. Unit dates are ages of units in Hole U1396C that are given by Wall-Palmer *et al.* (2014).

1.1-0.9 Ma

Between 1.1 Ma to 0.9 Ma high frequencies of volcaniclastic units (tephra fall deposits and volcaniclastic turbidites) (Figures. 17-19) are observed in Hole U1395B and U1396C. High frequencies of mixed turbidites are also found in Hole U1395B.

This peak is poorly developed in Hole U1395B (Chapter 3). This is because the age models in Chapter 3 do not include the 1072 ka paleomagnetic reversal (it is poorly developed). However, here the base of Hole U1395B is correlated with Hole U1396C where the 1072 ka reversal is well developed.

0.7-0.4 Ma

Between 0.7-0.4 Ma there are reduced frequencies of volcaniclastic events (both tephra fall and volcaniclastic turbidities) (Figures. 17-19) in Holes U1395B and U1396 B. However, at ~0.6-0.5 Ma there is a high frequency of mixed turbidites in Hole U1395B.

~0.3 Ma

At ~0.3 Ma high frequencies of volcaniclastic turbidites, tephra fall and bioclastic turbidites are observed (Figures 17-19) in Holes U1394B and U1395B.

0.2-0.1 Ma

In Hole U1349B, high frequencies of tephra fall deposits are observed at 0.22 Ma. Bioclastic, mixed and volcaniclastic turbidite frequency is high in Holes U1394B and U1395B.

4.1.1 The effects of erosion on frequency observations

The ages of turbidites and tephra fall deposits have been determined by estimating the sedimentation rates of interlayered hemipelagic mud. Accurately

determining hemipelagic sedimentation rates in marine cores is difficult due to the difficulties in constraining amounts of hemipelagite erosion, and the ambiguities in identifying oxygen MIS's within the cores.

The effects of dating errors on frequency observations made from marine cores around Montserrat were extensively discussed in Chapter 3 where different age models were tested. Age Model 1 used all available date horizons (oxygen isotope stratigraphy, biostratigraphy, and paleomagnetic stratigraphy), whereas age models 2 and 3 used the most reliable age data for Hole U1395B (paleomagnetic stratigraphy, and radiometric dates). Chapter 3 showed that broad frequency observations at Site U1395 were largely similar in all three age models, despite some unit ages varying up to the order 10^5 ka. Therefore, it is reasonable to assume that if dating errors did not affect the overall conclusions at Site U1395B, then it is valid to use a single age-model approach to also assess Sites U1394 and U1396, with the caveat that some (poorly constrained) uncertainties exist in terms of absolute event ages.

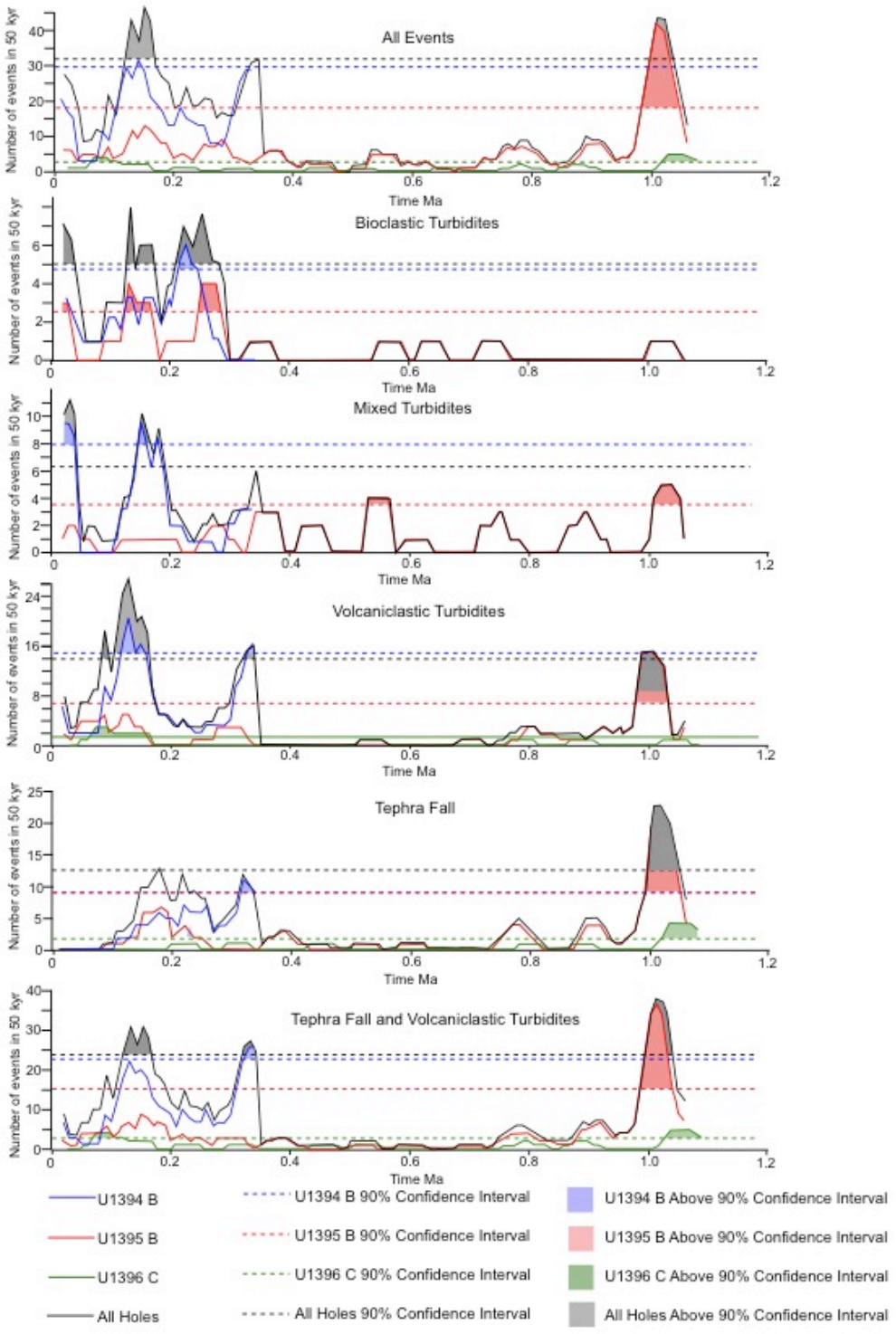

Figure 17: Moving frequencies of events. Data is binned into 50 ka windows. Windows are then moved at 10 ka increments to produce moving frequency graphs. Frequencies from individual cores are shown for Holes U1394B (blue), U1395B (green), and U1396C (red). Also shown is the sum of events in all Holes (black). Dashed lines show the 90% confidence interval, and shaded periods are above the 90% confidence interval.

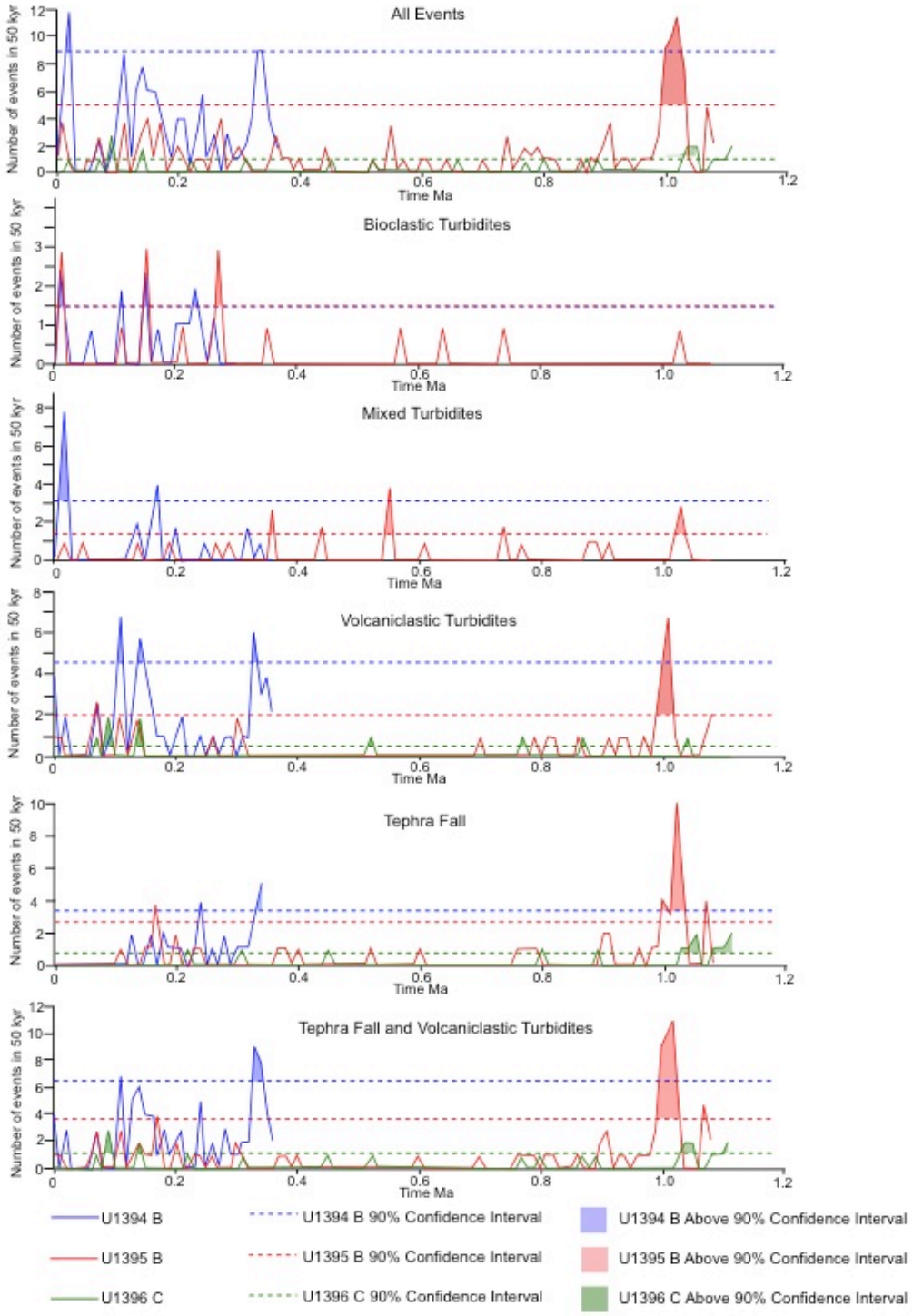

Figure 18: Moving frequencies of events. Data is binned into 10 ka windows. Windows are then moved at 10 ka increments to produce moving frequency graphs. Frequencies from individual cores are shown for Holes U1394B (blue), U1395B (green), and U1396C (red). Dashed lines show the 90% confidence interval, and shaded periods are above the 90% confidence interval.

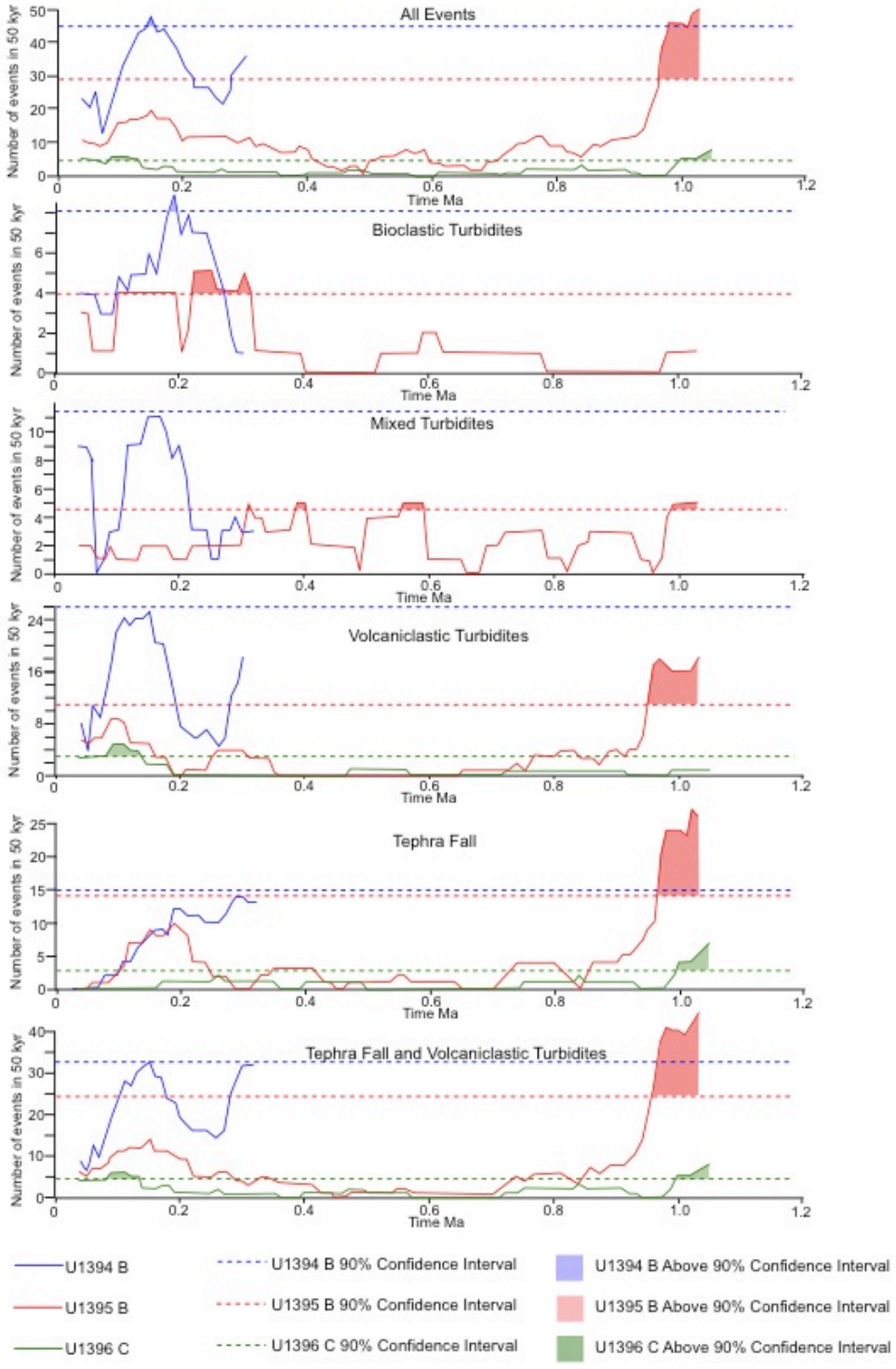

Figure 19: Moving frequencies of events. Data is binned into 100 ka windows. Windows are then moved at 10 ka increments to produce moving frequency graphs. Frequencies from individual cores are shown for Holes U1394B (blue), U1395B (green), and U1396C (red). Dashed lines show the 90% confidence interval, and shaded periods are above the 90% confidence interval.

4.2 Turbidite thickness

Holes U1394B and U1395B capture a detailed turbidite record that shows that turbidite thicknesses vary through time. Figure 20 is a moving mean where the average thickness of 5 turbidites is plotted, and is incrementally moved every 1 unit. Periods of thick turbidite occurrence are defined as periods where average turbidite thickness is above the 90% confidence interval. Turbidites that may have been artificially thickened by coring processes such as suck in (Jutzeler *et al.*, 2014a) are not included within the analyses.

In Hole U1394B thick volcaniclastic and mixed turbidites are observed at ~0.2 Ma, and in Hole U1395B thick mixed turbidites occur at ~0.6 Ma and thick volcaniclastic turbidites occur at ~0.8 Ma (Figure 18). Periods of thick turbidites coincide with periods of high event frequency (*Section 4.1*).

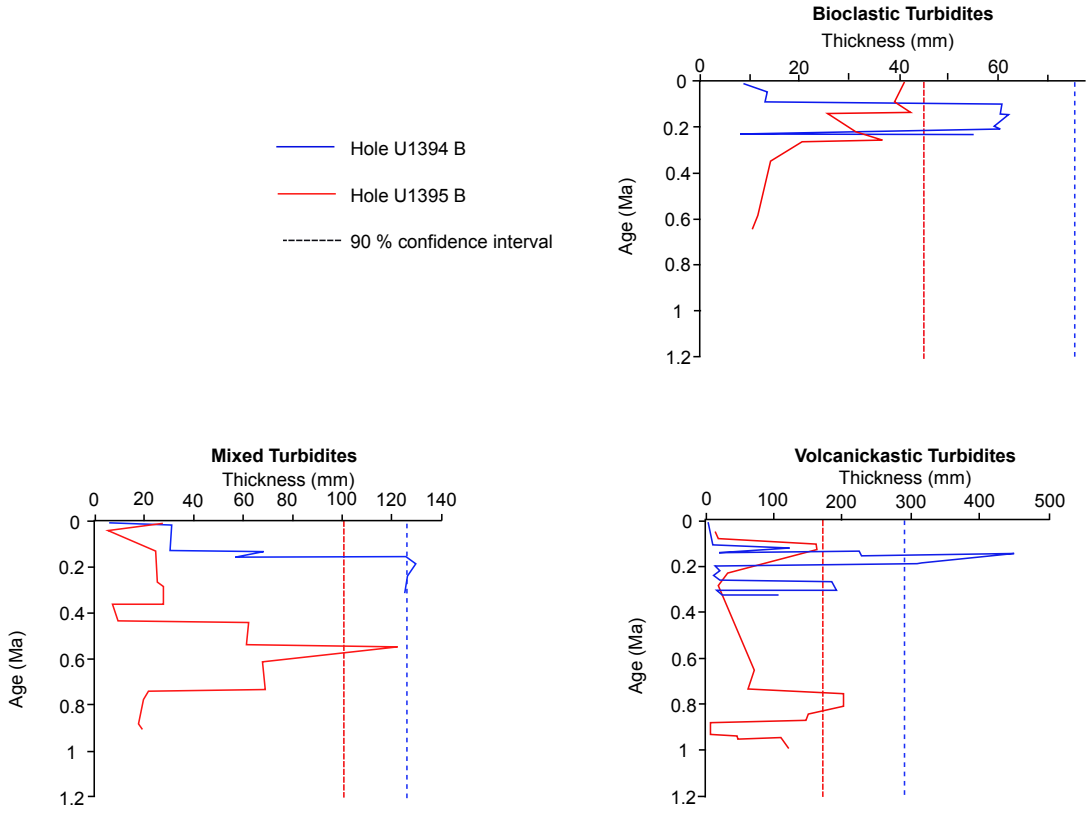

Figure 20: Thickness of turbidites from Holes U1394B (blue) and U1395B (red). Dashed lines show 90% percentile thickness. Turbidites that may have been artificially thickened by flow in have been removed.

5. Discussion

Using this stratigraphy we can better understand how eruptive and sedimentary processes (e.g. mass-wasting) vary over long time scales (1 Ma). Volcanic eruptions and mass wasting events pose significant hazards. Eruptions, particularly large-magnitude explosive eruptions can have significant environmental and economic impacts (e.g., Robock, 2000; Watt *et al*., 2009; Sammonds *et al*., 2010; Carlsen *et al*., 2012; Sigl *et al*., 2015). Mass-wasting events are hazardous to the local environment and populations through their erosive behaviour and via their inundation (Kokelaar *et al*., 2002; Ward and Day *et al*., 2003; Wadge *et al*., 2014). Thus understanding when and how frequently such events have occurred are important for future hazard mitigation.

5.1 Montserrat's stratigraphic framework

Centre Hills Episode 1 (>1- 0.7 Ma)

This oldest period of recorded activity is represented onshore by multiple thick pumice-rich sequences (representative of large-magnitude explosive eruptions) dated at ~0.8±0.2 Ma (Chapter 2) that are interbedded with dome-eruption style deposits. These subaerial deposits broadly correlate with a high event frequency observed in IODP sites U1395 and U1396 (above the 90% confidence interval; Figures. 17-19). Most events recorded within the core sites resulted in tephra fall deposits or volcaniclastic turbidites (Figures 17-19), suggesting that there may have been high levels of volcanism on Montserrat. Despite the large number of thick subaerial sequences, only the Foxes tephra correlates with a submarine tephra layer (Figures 14-16), and one tephra fall has been correlated between sites U1395 and U1396 (Figures 14-16).

The difficulty in correlating horizons is somewhat surprising. There are multiple thick pumice-bearing fall deposits identified in the subaerial stratigraphy, and multiple fall deposits in the marine record, spanning the same time interval, and it is reasonable to expect that the largest-volume events are best preserved in both datasets. However, very few events show clear correlation, based on the available glass data. This may mean that the subaerial events are simply not

represented in the marine record (and/or vice versa), counter to expectations, and that our assumptions about which events are preserved in the subaerial record (i.e. the largest magnitude), are not valid (Brown *et al.,* 2014). In addition to this, spatial effects arising from variable transport directions may mean that the subaerial exposures (east and west of the Centre Hills vent) and submarine core samples (southeast and southwest of Montserrat) are variably sampling events from Montserrat, such that there is only limited overlap in the events preserved in the subaerial exposures and those in the cores. If this is correct, it has significant implications for the completeness of any stratigraphy that is inferred only from a limited number of sites, without a wide spatial coverage.

Centre Hills Episode 2 (0.7-0.4 Ma)

Onshore, several pumiceous deposits occur during this period, including 3 units that can be correlated across Montserrat (Attic tephra, Woodlands tephra, and Bunkum Bay tephra). Some of these units have onshore pumice fall deposits >5 m thick (e.g. Woodlands tephra, Chapter 2) and have been dated to ~0.5±0.2 Ma. Andesitic lithic breccias associated with dome eruptions are found interleaved with these pumiceous successions (Chapter 2). Surprisingly, few events are recorded in the IODP sites between 0.7-0.4 Ma.

Subaerial outcrop patterns from this second pulse of behaviour suggest eruptive activity moved northwards, and may be associated with the Katy Hills vent site (Chapter 2). Many of the deposits generated from this activity may have been deposited towards the east and west of Montserrat, as the older, southerly Centre Hills vent site may have obstructed many southward-travelling pyroclastic desnity currents.

Soufrière Hills (SH) Episode 1 (0.38-0.2 Ma)

Onshore there is little evidence of early volcanic activity at Soufrière Hills, with only a few lava dome-forming eruptive products preserved on-land (Smith 2007). However, there is an increase in the occurrence of volcaniclastic deposits in the offshore record (Figures 17-19). This has been interpreted as the initiation of activity at Soufrière Hills. Such early deposits are unlikely to be preserved onshore or are likely to be deeply buried.

The offshore record is predominantly represented by volcaniclastic turbidites. High frequencies of tephra fall deposits are only observed in the most proximal core, at IODP Site U1394 (Figures 17-19) and this suggests that activity was dominated by lava dome-forming eruptions and small-scale explosive eruptions that dispersed ash over limited areas. In the recent eruption, pumice fall has largely been restricted to subaerial observations, but thicknesses of 1 cm, up to 7 km away have been identified from Vulcanian eruptions such as the 26th September 1997 event (Bonadonna *et al*., 2002). However, the lack of tephra fall at more distal IODP sites may also be a function of wind direction and unit preservation.

One unit has been correlated during this time period. A thick (>5 m) volcaniclastic turbidite in Hole U1394B is correlated with a thin tephra fall unit in Hole U1395B. Both units are considered part of the same eruption (Figures 14-16).

Soufrière Hills Episode 2 (0.2- 0.13 Ma)

This stratigraphic period is represented by an apparent change in the style of eruptive activity on Montserrat. This is best observed onshore where multiple pyroclastic density current deposits and ~1 m thick pumice fall deposits are found (Smith, 2007). Such deposits are rarely associated with Soufrière Hills volcano and are the only described deposits representative of large-magnitude explosive activity at Soufrière Hills. Offshore, an increase in tephra fall deposit occurrence is observed at Sites U1394 and U1395, and is consistent with large-magnitude explosive activity onshore (Figures 17-19).

South Soufrière Hills Episode 3 (0.13-0.12 Ma)

This period of activity is marked by a change in the composition of erupted magmas to more mafic compositions and a migration of volcanic activity further south to the South Soufrière Hills volcano. At 130 ka there is a large landslide deposit (Deposit 2) that is represented by a thick volcaniclastic turbidite sequence at Sites U1394 and U1395 (Figures 5 and 9), and a sequence of low amplitude reflections at Site U1394B (Figure 6). Some volcaniclastic rich units in

CAR-MON2 and U1396C may also correlate with this event (Figure 13). These landslide deposits are succeeded by the migration of activity to a short lived-basaltic centre, the South Soufrière Hills. In both the onshore and offshore stratigraphies basaltic units are identifiable (Figure 16).

Soufrière Hills Episode 4 (0.12- 0.1 Ma)

Activity migrates back to Soufrière Hills and is represented offshore by high frequencies of volcaniclastic deposits and bioclastic turbidites (Figures 17-19). The deposits of lava dome-forming eruptions dominate the subaerial stratigraphy, and erupted magmas return to andesitic compositions (Figure 16; Appendix Figure 3) (Smith *et al*., 2007). Offshore a large basaltic scoria rich turbidite, Deposit 3, is dated approximately to 103-110 ka (Cassidy *et al*., 2014a) (Figure 16). Deposit 3 has been correlated across Holes U1394B, U1395B and the shallow vibrocores described by Trofimovs *et al*. (2013) and Cassidy *et al*. (2014a). The 103-99 ka turbidite described by Trofimovs *et al*. (2013) has also been correlated with a turbidite in Hole U1394B (Figures 2, 12 and 16), and a sequence of volcaniclastic deposits dated at 124 ka.

Soufrière Hills Episode 5 (<0.07 Ma)

Onshore, the deposits of lava dome-forming eruptions dominate the stratigraphy (Smith 2007). Offshore, high frequencies of turbidites are observed suggesting a heightened frequency of mass-wasting or PDC events (Figures 17-19). This is in agreement with two large landslide deposits, Deposit 1 (14-11 ka) and Deposit 5 (12-8 ka) that occur to the southeast and southwest of the island respectively (Figures 1 and 16). Many of these more recent deposits are sampled in shallow vibrocores and the units have been correlated across the Bouillante-Montserrat graben, including in the IODP cores. These units include the 74-59 ka, 14 ka, 6 ka, and 2-1.5 ka turbidites (Figures 2 and 12). To the southwest of Montserrat the 12-14 ka, 30.5 ka, and 75±10 ka events can be correlated (Figure 13).

5.2 Difficulties in developing a stratigraphic framework.

Developing a stratigraphic framework is difficult. Stratigraphic differences are observed over decimetre scales (such as stratigraphic differences between Holes

drilled at a single IODP site (Figures 5, 7 and 8)), thus correlating units across large distances is complex. Issues that hinder correlation include: variation in deposit character/composition; differences in event transport direction; preservation and magnitude related bias; and poor age resolution. Below we discuss each factor.

Deposit composition varies laterally due to erosive incorporation of material and also because of deposition of denser material in more proximal regions. Consequently identifying a particular event at multiple sites is difficult as turbidites often become more enriched in low density bioclasts with distance from Montserrat (Trofimovs *et al*., 2010). Furthermore secondary turbidites may be generated from the remobilisation of unstable seafloor sediments, which may be compositionally distinct from the initial turbidite.

Deposit distribution is spatially variable around Montserrat. Turbidites are often unidirectional (Trofimovs *et al*., 2006, 2010, 2013) and tephra fall distributions are controlled by wind direction and speed (Carey and Sparks *et al*., 1986). As a result stratigraphic records are variable. In this study the IODP records show very few events between 0.7-0.4 Ma (Figures 17-19), but the subaerial record is represented by multiple eruptive deposits dated at ~0.5±0.2 Ma (Figure 6, Chapter 2). Correlating such variable stratigraphies can be difficult as few units are likely to appear across all sites.

Deposit preservation varies depending on the magnitude of the event, but also on the location of the deposit. Larger magnitude events are more likely to be preserved within the stratigraphic record as these produce laterally extensive, thicker deposits. Consequently the stratigraphic record is biased towards large magnitude events. This is a common problem observed in the geological record, and has been highlighted in work by Brown *et al*, (2014) who have studied deposit preservation using the LaMEVE database. Deposits on topographic highs, areas of extensive bioturbation, and in major turbidite pathways are also less likely to be preserved.

Constructing age models for each studied site is useful. Paleomagnetic reversals, Ar-Ar dating and AMS dating are the most robust age markers on Montserrat: biostratigraphic markers and oxygen isotope MIS are more ambiguous. Biostratigraphic markers, such as *G. menardii,* are sensitive to local environmental conditions and disappearances and reappearances may differ between sites (Wall-Palmer *et al*., 2014). Identifying MISs are also difficult. Erosion may completely remove a MIS (such as the removal of MIS 2 in Hole U1396C (Figure 11)) resulting in misidentification of MIS.

5.3 The evolution of eruptive activity and mass wasting processes on Montserrat over the past 1 Ma.

5.3.1 How does eruptive activity vary through time?

Periods of more frequent volcanism and more explosive volcanism have been identified using the onshore and offshore stratigraphies. Heightened volcanism has been identified in the offshore record during 1.1-0.9 Ma, 0.3 Ma, and 0.2-0.1 Ma (Chapter 3, Figures 17-15). Increased volcanism may have occurred at ~0.5 ± 0.2 Ma and is identified using subaerial deposits, but this is not well-represented in the marine cores (Chapter 2, Figure 16). Volcaniclastic deposits (likely to be representative of eruptive activity) are found throughout the marine cores and suggest that there were not long periods (>100 ka) of volcanic quiescence (Figures 17-19).

This compiled stratigraphy of Montserrat described here is one of the most complete stratigraphic records of volcanism. Pulses in volcanic activity are commonly observed (Houghton *et al*. 1995; Bacon and Lanphere 2006; Singer *et al*. 2008; Germa *et al*. 2010;), however periods of apparent quiescence may be generated by incomplete record preservation. By using a combination of subaerial observations, and observations from the more complete marine record, there is a greater certainty that that the observed pulsed behaviour is unlikely to be an artifact of record preservation. Instead, this pulsed behaviour in volcanism may be more likely attributed to long-term variations in magma production rates, or magma transportation processes through the crust.

Activity at Centre Hills and Soufrière Hills over the past 1 Ma has been largely dominated by lava dome-forming eruptions. However, at Centre Hills there appears to have been common large-magnitude explosive eruptions. Evidence of such large-magnitude eruptions is rare within the Soufrière Hills stratigraphy (Chapter 2, Figures 14 and 16).

5.3.2 How does mass-wasting vary through time?

Mass-wasting events have occurred throughout the past 1 Ma at Montserrat and are represented by turbidites of varying size and composition within the submarine record. High frequencies of volcaniclastic turbidites occur during 1.1-0.9 Ma, ~0.3 Ma, and 0.2-0.1 Ma (Figure 7). Mixed turbidite occurrence is more regular with 4 to 5 events every 50 ka. High frequencies of bioclastic turbidites are only observed after the onset of activity at Soufrière Hills (~0.3 Ma) (Figure 7), suggesting that the onset of activity may have destabilised the carbonate shelf, or that more bioclastic turbidites were directed southwards towards the IODP core sites.

Four periods of increased mass wasting are observed at 1.1-0.9 Ma, 0.6-0.5 Ma, ~0.3 Ma, and 0.2-0.1 Ma (Figures 17-19) with the thickest turbidites occuring between 0.8-0.5 Ma and between 0.3-0.1 Ma. These periods of increased mass-wasting (in terms of frequency and thickness (which may be used as a proxy for magnitude)), coincide with periods of increased volcanism.

During heightened periods of volcanism more material (lava and tephra) is added to the island flanks resulting in greater flank instability. There are also increases in volcano-tectonic earthquakes, increases in explosive volcanic behaviour and changes to local stress regimes. Such changes in flank stability, seismicity, and local tectonics may facilitate mass-wasting processes (Tommasi *et al*., 2005; Harris *et al*., 2011; Chadwick *et al*., 2012).

6. Deposit 2

Large landslides and their associated turbidites can transport and emplace large volumes of material (for example the Icod Landslide, Tenerife, Canary Islands, has a volume of 320 km^3 (Ancochea *et al*., 1990)) over long distances (McMurty *et al*., 2004a, 2004b; Hunt *et al*., 2013, 2014). Understanding the transport of such large volumes of material is important as such voluminous mass movements are important processes in sedimentary cycles, and are potentially hazardous due to the threat by inundation and generation of tsunamis. It is often inferred that the bulk of the material comprising landslide features is comprised of material that was either derived from the headwall, or has been incorporated from the underlying sea floor through erosive processes (Deplus *et al*., 2001, Le Friant *et al*., 2004; Lebas *et al*., 2011). Detailed seismic studies show that landslides may also comprise extensive sequences of failed sea-floor sediments (Sawyer *et al*., 2009; Watt *et al*., 2012a, 2012b).

6.1 What comprises large landslides and how are they emplaced?

In this study Hole U1394B drilled through Deposit 2 and directly samples the lower part of the landslide, Deposit 2a. Deposit 2a comprises thick sandy turbidites with very little interbedded hemipelagic material (Figure 9). At the base of Deposit 2a is a hemipelagic unit with no visible evidence of displacement or deformation (Section 3.1.4), thus suggesting that Deposit 2a comprises in-situ marine sediments. The sequence is unusually sand-rich with little hemipelagic material (Figure 9). Overlying Deposit 2 is the thick 130 ka volcaniclastic turbidite (Figure 9). It is proposed here that Deposit 2 was formed by sea-floor sediment failure during the emplacement of the 130 ka landslide (which also formed the overlying turbidite). This confirms earlier interpretations (Watt *et al*., 2012a, 2012b) based on seismic reflection profiles. It should be noted that, in this interpretation, the descriptor of "Deposit" for these disrupted packages of stratigraphy is something of misnomer, but is continued from its original identification of a low-amplitude and apparently chaotic region in seismic reflection profiles, interpreted as volcanic landslide deposits.

Watt *et al.* (2012b) propose four possible ways to deform underlying strata during landslide and associated turbidite emplacement. 1) Loading by landslide and turbidite emplacement can cause dewatering and compaction of underlying sediments resulting in increased density, reduced porosity and reduced permeability of underlying strata. 2) Loading by a landslide can cause sediment failure at the frontal toe of a landslide deposit, resulting in the development of a sequence of imbricate shear planes and plastic deformation. 3) Underlying sediments can undergo shear coupling resulting in a series of tight asymmetrical folding of some units. 4) Loading can propagate shear ruptures through a particular sedimentary horizon; this may result in shearing and ductile deformation of overlying strata, although it is unclear how extensive this deformation may be.

Deposit 2a appears undeformed in Hole U1394, and at site U1394 seismic reflections are horizontal and low amplitude. This lack of any apparent deformation, in addition to the absence of a clear basal plane in the cores, is surprising. It suggests that sea-floor sediment failure mechanisms 2-4 can be ruled out, unless the core happens to have intersected a horizontally bedded part of the deformed region (i.e. the crest of a fold), or unless the deformation (e.g. in Mechanism 2) is concentrated in particular bands, with undeformed blocks of seafloor existing between these. Alternatively, and as suggested in Mechanism 1, deformation may be relatively minor and widely distributed, such that dewatering and compaction is sufficient to alter the seismic reflection properties of sedimentary sequences (resulting in the observed decrease in the amplitude of seismic reflections). Some original stratigraphic features such as horizontal bedding may be maintained, but with a loss of coherent reflectors (perhaps in bands of slightly greater deformation) in parts of the package of sediment. Deposit 2a comprises an unusually coarse sequence that is poor in hemipelagic material. The coarse nature of the deposits may have increased the susceptibility of the deposits to compaction and dewatering due to the large pore spaces in coarser deposits. Similar examples have been observed in the Ursa Basin, northern Gulf of Mexico (Sawyer *et al.*, 2009).

6.2 Hazard Implications

During the recent eruption on Monserrat, the largest lava-dome collapse involved 0.2 km^3 of material, and generated a tsunami up to 1 m high along the coast of Guadeloupe (Kokelaar *et al*., 2002). The much larger landslide deposits identified in the offshore seismic reflection profiles are likely to have generated far larger tsunamis (Pannizo *et al*., 2005; Watts *et al*., 2005). However, since we have confirmed that a major proportion of the 8.4 km^3 Deposit 2 comprises marine sediments, this tsunami risk may be smaller than might be initially inferred from the deposit volume. Only a small proportion of the deposit is likely to have originated from above sea level. If other landslide deposits around Montserrat and other volcanic island arcs contain a significant proportion of marine sediments, the threat of these island arc systems producing "mega" tsunamis is significantly reduced.

7. Summary and Conclusions

In this study we begin to develop a stratigraphic framework that spans the last 1 Ma of Montserrat's volcanic history. The stratigraphy from three IODP sites is integrated with subaerial observations and observations from a large shallow vibrocore data set. Using this dataset the evolution of eruptive activity and mass-wasting processes at Montserrat can be studied. Fully integrating all datasets has not been possible due to complications when correlating stratigraphy over large distances, but this framework will be useful for future studies on Montserrat.

This stratigraphy presents the opportunity to better study the long-term evolution of volcanism and mass wasting at Montserrat. Three periods of increased volcanism have been observed based on submarine and subaerial observations. Heightened volcanic activity occurred between 1.1-0.9 Ma, at ~0.3 Ma and between 0.2-0.1 Ma. No extended periods (>100 ka) of volcanic repose have been identified within the stratigraphic record. Between 0.7-0.4 Ma there is a decrease in the number of volcaniclastic events in the IODP Holes, but numerous eruptive events dated at ~0.5 ±0.2 Ma are observed onshore. This

suggests that there was no long pause in activity while activity migrated from Centre Hills to Soufrière Hills (~0.5-0.4 Ma), but there may have been a reduction in volcanism.

High turbidite frequency and increased turbidite thickness coincide with periods of more intense volcanism. This suggests that most mass-wasting occurs during volcanic activity, as opposed to after more volcanically active periods. The edifice maybe less stable during periods of more intense volcanism due to growth and an increase in the number of earthquakes and explosive behaviour, thus facilitating mass wasting processes.

Drilling through Deposit 2 shows that much of this large landslide deposit comprises in-situ marine sediments. The reduced seismic amplitudes observed in the Deposit 2 stratigraphy may be due to compaction and dewatering of the stratigraphy during the emplacement of the overlying 130 ka turbidite. As Deposit 2 mostly comprises in-situ material, estimating volumes of large landslides and understanding their hazards is difficult due to the complex emplacement processes of these deposits.

8. References

Bacon, C. R. and Lanphere, M. (2006), Eruptive history and geochronology of Mount Mazama and the Crater Lake region, Oregon, *Geological Society of America Bulletin*, 118(11-12), 1331–1359

Bonadonna, C., Mayberry, G. C., Calder, E. S., Sparks, R. S. J., Choux, C. et al., (2002), Tephra fallout in the eruption of Soufrière Hills Volcano, Montserrat, *Geological Society, London, Memoirs*, *21*(1), 483-516

Boudon, G., Le Friant, A., Komorowski, JC., Deplus, C. and Semet, P. (2007), Volcano flank instability in the Lesser Antilles Arc: Diversity of scale, processes, and temporal recurrence, *Journal of Geophysical Research*, 112(B8), B08205

Bouysse, P. and Westercamp, D. (1990), Subduction of Atlantic aseismic ridges and Late Cenozoic evolution of the Lesser Antilles island arc, *Tectonophysics,* 175, 349-380

Branney, M. J. and Kokelaar, B. P. (2002), Pyroclastic density currents and the sedimentation of ignimbrites, *Geological Society of London*

Brown, K and Davidson, C., (2008), $^{40}Ar/^{39}Ar$ geochronology of the Silver Hills andesite, Montserrat, West Indies, B. A. Senior integrative excersize, Carelton College, Northfield, Minnesota

Brown, S. K., Crosweller, H. S., Sparks, R. S. J., Cottrell, E., Deligne, N. I., Guerrero, N. O. et al (2014), Characterisation of the Quaternary eruption record: analysis of the Large Magnitude Explosive Volcanic Eruptions (LaMEVE) database, *Journal of Applied Volcanology*, *3*(1), 1-22

Carey, S.N. and Sparks, R. S. J. (1986), Quantitative models of the fallout and dispersal of tephra from volcanic eruption columns, *Bulletin of Volcanology*, 48, 109–125

Carlsen, H. K., Gislason, T., Benediktsdottir, B., Kolbeinsson, T. B., Hauksdottir, A., Thorsteinsson, T. and Briem, H. (2012), A survey of early health effects of the Eyjafjallajökull 2010 eruption in Iceland: a population-based study, *Public health, BMJ Open*, 2, e000343, doi:10.1136/bmjopen-2011-000343

Carter, L., Nelson, C. S., Neil, H. L. and Froggatt, P. C. (1995), Correlation, dispersal, and preservation of the Kawakawa Tephra and other late Quaternary tephra layers in the Southwest Pacific Ocean, *New Zealand Journal of Geology and Geophysics*, *38*(1), 29-46

Cassidy, M., Taylor, R. N., Palmer, M. R., Cooper, R. J., Stenlake, C. and Trofimovs, J. (2012), Tracking the magmatic evolution of island arc volcanism: Insights from a high-precision Pb isotope record of Montserrat, Lesser Antilles,

Geology, Geochemistry, Geophysics., 13(5), 1525-2027, doi:10.1029/2012GC004064

Cassidy, M., Trofimovs, J., Palmer, M.R., Talling, P.J., Watt, S.F.L., Moreton, S. and Taylor, R.N. (2013), Timing and emplacement dynamics of newly recognised mass flow deposits at ~8-12 ka offshore Soufrière Hills volcano, Montserrat: how submarine stratigraphy can complement subaerial eruption histories, *Journal of Volcanology and Geothermal Research,* 253, 1-14

Cassidy, M., Trofimovs, J., Watt, S.F.L., Palmer, M.R., Taylor, R.N., Gernon, T.M., Talling, P.J. and Le Friant, A. (2014a), Multi-stage collapse events in the South Soufrière Hills, Montserrat, as recorded in marine sediment cores, *In The eruption of Soufriére Hills Volcano, Montserrat from 2000-2010,* Edited by Wadge, G., *et al*., 2014, *The Geological Society Special Publications*, 39, 383-397

Cassidy, M., Watt, S.F.L., Palmer, M.R., Trofimovs, J., Symons, W., Maclachlan, S.E. and Stinton, A.J., (2014b), Construction of volcanic records from marine sediment cores: A review and case study (Montserrat, West Indies), *Earth-Science Reviews*, 138, 137–155

Cassidy. M., *et al*., (2015), Rapid onset of mafic magmatism facilitated by volcanic edifice collapse, *Geophysical Research Letters, 42(12),* 4778-4785

Chadwick, W. W., Dziak, R. P., Haxel, J. H., Embley, R. W. and Matsumoto, H. (2012), Submarine landslide triggered by volcanic eruption recorded by in-situ hydrophone, *Geology*, 40(1), 51-54

Coussens, M. F., Wall-Palmer, D., Talling, P. J., Watt, S. F. L., Hatter, S. J., Cassidy, M., *et al*., (2016), Synthesis: stratigraphy and age control for IODP Sites U1394, U1395, and U1396 offshore Montserrat in the Lesser Antilles, *Proceedings of the IODP*, *340*, 19

Crosweller, H. S., Arora, B., Brown, S. K., Cottrell, E., Deligne, N. I., Guerrero, N. O. et al., (2012), Global database on large magnitude explosive volcanic eruptions (LaMEVE), *Journal of Applied Volcanology*, *1*(1), 1-13

Crutchley, G. J., Karstens, J., Berndt, C., Talling, P. J., Watt, S. F. L., Vardy, M. E., Huhnerbach, V., Urlaub, M., Sarkar, S., Klaeschen, D., Paulatto, M., Le Friant, A., Lebas, E. and Maeno, F. (2013), Insights into the emplacement dynamics of volcanic landslides from high-resolution 3D seismic data acquired offshore Montserrat, Lesser Antillies, *Marine Geology,* 335, 1-15

Davidson, J.P. (1987), Crustal contamination versus subduction zone enrichment: exampless from the Lesser Antillies and implication for mantle source compositions of island arc volcanic rocks, *Geochemica Cosmochemica Acta,* 51, 2185-2198

Deplus, C., Le Friant, A., Boudon, G., Komorowski, JC., Villement, B., Harford, C., Segoufin, J. and Chiminee, JL. (2001), Submarine evidence for large-scale debris avalanches in the Lesser Antillies Arc, *Earth and Planetary Science Letters,* 192, 145-157

Druitt, T.H., and Kokelaar, B.P. (2002), The eruption of Soufrière Hills Volcano, Montserrat, from 1995 to 1999, *Memoirs of the Geological Society of London*, 21, 45–69

Dufrane, S.A., Turner, S.P., Dosseto, A. and Van Soest, M.C. (2009) Reappraisal of fluid and sediment contributions to Lesser Antillies magmas, *Chemical Geology,* 265, 272-278

Expedition 340 Scientists (2012), Lesser Antilles volcanism and landslides: implications for hazard assessment and long-term magmatic evolution of the arc, *IODP Preliminary Report, 340* doi:10.2204/ iodp.pr.340.2012

Expedition 340 Scientists (2013), Paleomagnetism in methods, *In Proceedings*

IODP 340: Tokyo (Integrated Ocean Drilling Program Management International, Inc.), Le Friant, A., Ishizuka, O., Stroncik, N.A., and the Expedition 340 Scientists, doi:10.2204/iodp.proc.340.102.2013

Feuillard, M., Allegre, C.J., Brandeis, G. and Gaulon, R. (1983), The 1975-1977 crisis of La Soufrière Guadeloupe (F.W.I): a still-born magmatic eruption, *Volcanological Geothermal Research,* 16, 317-334

Folk, R. L. and Ward, W.C. (1957), Brazos River bar: a study in the significance of grain size parameters, *Journal of Sedimentary Petrology*, 27, 3-26

Friedman G. M. and Sanders J. E. (1978), *Principles of Sedimentology,* Wiley: New York

Germa, A., Quidelleur, X., Labanieh, S., Lahitte, P. and Chauvel C. (2010), The eruptive history of Morne Jacob volcano (Martinique Island, French West Indies): Geochronology, geomorphology and geochemistry of the earliest volcanism in the recent Lesser Antilles arc, *Journal of Volcanology and Geothermal Research*, 198(3-4), 297–310, doi:10.1016/j.jvolgeores.2010.09.013

Harford, C. L. Pringle, M. S., Sparks, R. S. J. and Young, S. R. (2002), The volcanic evolution of Montserrat using 40Ar/39Ar geochronology, *Geological Society, London, Memoirs*, 21:93–113, doi: 10.1144/GSL.MEM.2002.021.01.05

Harris, P. D., Branney, M. J. and Storey, M. (2011), Large eruption-triggered ocean-island landslide at Tenerife: Onshore record and long-term effects on hazardous pyroclastic dispersal, *Geology*, 39(10), 951-954

Hatfield. R.G. (2015), Data report: stratigraphic correlation of Site U1396 and creation of a composite depth scale and splice, *In Proceedings of the Integrated Ocean Drilling Program, 340: Tokyo (Integrated Ocean Drilling Program Management International, Inc.),* Le Friant, A., Ishizuka, O.,

Stroncik, N.A., and the Expedition 340 Scientists, doi: 10.2204/ iodp.proc.340.202.2015

Houghton, B. F., Wilson, C. J. N., McWilliams, M. O., Lanphere, M. A., Weaver, S. D., Briggs, R. M. and Pringle, M. S. (1995), Volcanic Zone , New Zealand Chronology and dynamics of a large silicic magmatic system : Central Taupo Volcanic Zone, New Zealand, *Geology*, 23, 13–16, doi: 10.1130/00917613(1995)023<0013:CADOAL>2.3.CO;2

Holz, C., Stuut, J. B. W. and Henrich, R. (2004), Terrigenous sedimentation processes along the continental margin off NW Africa: implications from grain-size analysis of seabed sediments, *Sedimentology*, 51(5), 1145-1154

Hunt, J. E., Wynn, R. B., Talling, P. J. and Masson, D. G. (2013), Turbidite record of frequency and source of large volume (>100 km^3) Canary Island landslides in the last 1.5 Ma: Implications for landslide triggers and geohazards, *Geochemistry, Geophysics, Geosystems*, 14(7), 2100–2123, doi: 10.1002/ggge.20139

Hunt, J.E., Talling, P.J., Clare, M., Jarvis, I. and Wynn, R.B. (2014), Long-term (17 Ma) turbidite record of the timing and frequency of large flank collapses of the Canary Islands, *Geochemistry, Geophysics, Geosystems,* 15, 3322–3345, doi: 10.1002/2014GC005232

Imbrie, J., Hays, J. D., Martinson, D. G., McIntyre, A., Mix, A. C., Morley, J. J. and Shackleton, N. J. (1984), The orbital theory of Pleistocene climate: Support from a revised chronology of the marine delta18 O record, *In Milankovitch and climate: Understanding the response to astronomical forcing*, Edited by Berger. A. *Springer Science & Business Media*, 126, 269

Ishizuka, O., *et al*. (2003), Fluid-mantle interaction in an intra- oceanic arc: Constraints from high-precision Pb isotopes, *Earth Planetary Science Letters,* 211(3–4), 221–236, doi:10.1016/ S0012-821X(03)00201-2

Jutzeler, M., White, J. D. L, Talling, P. J., McCanta, M., Morgan, S., Le Friant, A. and Ishizuka, O. (2014a), Coring disturbances in IODP piston cores with implications for offshore record of volcanic events and the Missoula megafloods, *Geochemistry Geophysics Geosystems*, 15, 3572–3590, doi:10.1002/ 2014GC005447

Jutzeler, M., Marsh, R., Carey, R. J., White, J. D., Talling, P. J. and Karlstrom, L. (2014b), On the fate of pumice rafts formed during the 2012 Havre submarine eruption, *Nature communications*, *5*

Jutzeler, M., McPhie, J., Allen, S. R. and Proussevitch, A. A. (2015), Grain-size distribution of volcaniclastic rocks 2: Characterizing grain size and hydraulic sorting, *Journal of Volcanology and Geothermal Research*, 301, 191-203

Kameo, K. and Bralower, T. J. (1998), Neogene calcareous nannofossil biostratigraphy of sites 998, 999, and 1000, Caribbean Sea, *Proceedings of the Ocean Drilling Program, Scientifc Results*, 165, 3–17

Karstens, J., Crutchley, G. J., Berndt, C., Talling, P. J., Watt, S. F. L., Huhnerbach, V., Le Friant, A., Lebas, E. and Trfomovs, J. (2013), Emplacement of pyroclastic deposits offshore Montserrat: Insights from 3D seismic data, *Journal of Volcanology and Geothermal Research,* 257,1-11, doi: 0.1016/j.jvolgeores.2013.03.004

Kokelaar, B.P. (2002), Setting, chronology and consequences of the eruption of Soufrière Hills Volcano, Montserrat (1995-1999), *In the eruption of* Soufrière *Hills volcano, Montserrat, from 1995 to 1991*, edited by Druitt, T., and Kokelaar, P. *Geological Society Special Publications,* 21:1–43, doi:10.1144/GSL.MEM.2002.021.01.02

Lebas, E., Watt, S. F. L, Talling, P. J., Feuillet, N., Deplus, C., Berndt, C. and Vardy, M. (2011), Multiple widespread landslides during the long-term evolution of a volcanic island: Insights from high-resolution seismic data, Montserrat,

Lesser Antilles, *Geochemistry Geophysics Geosystems*, 12(5), Q05006, doi:10.1029/2010GC003451

Le Friant, A., Harford, C. L. and Deplus, C. (2004), Geomorphological evolution of Montserrat (West Indies): importance of flank collapse and erosional processes *Journal of the Geological Society*, 161(1), 147–160, doi:10.1144/0016-764903-017

Le Friant, A., Lock, E. J., Hart, M. B., Boudon, G., Sparks, R. S. J., Leng, M. J., Smart, C. W., Komorowski, J. C., Deplus, C. and Fisher, J. K. (2008), Late Pleistocene tephrochronology of marine sediments adjacent to Montserrat, Lesser Antilles volcanic arc, *Journal of the Geological Society*, 165(1), 279–289, doi:10.1144/0016-76492007-019

Le Friant, A., Deplus, C. and Boudon, G. (2009), Submarine deposition of volcanicastic material from the 1995-2005 eruptions of Soufrière Hills volcano, Montserrat, *Journal of the Geological Society,* 166,171-182, doi: 10.1144/0016-76492008-047

Le Friant, A., Deplus, C., Boudon, G., Feuliiet, N., Trofimovs, J., Komorowski, J. C., Sparks, R. S. J., Talling, P. J., Loughlin, S., Palmer, M. R. and Ryan, G. (2010), Eruption of Soufrière Hills (1995- 2009) from an offshore perspective: Insights from repeated swath bathymetry surveys, *Geophysical research letters*, 37, L11307, doi:10.1029/2010GL043580

Le Friant, A., Ishizuka, O., Stroncik, N. A., Slagle, A. L., Morgan, S., Adachi, T., Aljahdali, M. and Boudon, G. (2012), Lesser Antillies Volcanism and Landslides. Implications for hazard assessment and long-term magmatic evolution of the arc, *Integrated Ocean Drilling Program, Expedition 340 preliminary report.* doi:10.2204/iodp.pr.340.2012

Le Friant., A., Ishizuka, O., Boudon, G., Palmer, M.R., Talling, P.J., Villement., *et al*. (2014), Submarine record of volcanic island construction and collapse in the Lesser Antilles arc: First scientific drilling of submarine volcanic island

landslides by IODP Expedition 340, *Geochemistry, Geophysics, Geosystems,* 16, 420-442, doi:10.1002/ 2014GC005652

Le Friant, A., Ishizuka, O., Boudon, G., Palmer, M. R., Talling, P. J., Villemant, B., *et al.,* (2015), Submarine record of volcanic island construction and collapse in the Lesser Antilles arc: First scientific drilling of submarine volcanic island landslides by IODP Expedition 340, *Geochemistry, Geophysics, Geosystems*, *16*(2), 420-442

Lipman, P. W., Normar, W. R., Moore, J. G., Wilson, J. B. and Gutmacher, E. (1988), The Giant Submarine Alika Debris Slide, Mauna Loa, Hawaii, *Journal of Geophysical Research*, 93(7), 4279-4299

Lisiecki, L. E. and Raymo, M. E. (2005), A Pliocene-Pleistocene stack of 57 globally distributed benthic $\delta^{18}O$ records, *Paleoceanography*, 20:1–17, doi:10.1029/2004PA001071

Lowe, D. J. (2011), Tephrochronology and its application: a review, *Quaternary Geochronology*, *6*(2), 107-153

Manville, V. andWilson, C. J. N. (2004), Vertical density currents: a review of their potential role in the deposition and interpretation of deep-sea ash layers, *Journal of the Geological Society*, *161*(6), 947-958.

Martinson, D. G., Pisias, N. G., Hays, J. D., Imbrie, J., Moore, T. C. Jr. and Shackleton, N. J. (1987), Age dating and the orbital theory of the ice ages: Development of a high-resolution 0 to 300,000-year chronostratigraphy, *Quaternary Research,* 27, 1–29, doi:10.1016/0033-5894(87)90046-9

Masson, D.G. (1996), Catastrophic collapse of the volcanic island of Hierro 15 ka ago and the history of landslides in the Canary Islands, *Geology*, 24(3), 231–234

McGuire, W. *et al*. (1997), Correlation between rate of sea-level change and

frequency of explosive volcanism in the Mediterranean, *Letters to Nature*, 389, 473–476

McGuire, W. J. (1992), Changing sea levels and erupting volcanoes: cause and effect, *Geology Today*, 8(4), 141–144

McMurtry, G. M., Watts, P., Fryer, G. J., Smith, J. R. and Imamura, F. (2004a), Giant landslides, mega-tsunamis, and paleo-sea level in the Hawaiian Islands, *Marine Geology*, 203:219–233, doi:10.1016/S0025-3227(03)00306-2

McMurtry, G. M., Fryer, G. J., Tappin, D. R., Wilkinson, I. P., Williams, M., Fietzke, J., Garbe-Schoenberg, D. and Watts, P. (2004b), Megatsunami deposits on Kohala volcano, Hawaii, from flank collapse of Mauna Loa, *Geology*, 32(9), 741–744, doi: 10.1130/G20642.1

Moore, J. G., Clague, D. A., Holcomb, R. T., Lipman, P. W., Normark, W. R. and Teorresan, M. E. (1989), Prodigious submarine landslides on the Hawaiian Ridge, *Journal of Geophysical Research*, 94(89):17465-17484

Moore, J. G. and Holcomb, R. T. (1994), Giant Hawaiian lantslides, *Earth and Planetary Science Letters*, 22:119–144

Oehler, J. F., Lénat, J. F. and Labazuy, P. (2008), Growth and collapse of the Reunion Island volcanoes, *Bulletin of Volcanology*, 70:717–742, DOI 10.1007/s00445-007-0163-0

Ogg, J.G. (2012), Geomagnetic Polarity Time Scale, *In: The Geologic Time Scale 2012,* Edited by Gradstein, F. M., Ogg, J. G., Schmitz, M. D., and Ogg, G. M., *Elsevier Publications,* 85-114

Palmer, M. R., Hatter, S. J., Gernon, T. M., Taylor, R. N., Cassidy, M., Johnson, P., Le

Friant. A. and Ishizuka, O. (2016), Discovery of a large 2.4 Ma Plinian eruption of Basse-Terre, Guadeloupe, from the marine sediment record, *Geology*, *44*(2), 123-126

Panizzo, A., De Girolamo, P., & Petaccia, A. (2005). Forecasting impulse waves generated by subaerial landslides, *Journal of Geophysical Research: Oceans*, *110*(C12)

Pickering, K. T., & Hiscott, R. N. (1985). Contained (reflected) turbidity currents from the Middle Ordovician Cloridorme Formation, Quebec, Canada: an alternative to the antidune hypothesis, *Sedimentology*, *32*(3), 373-394

Pindell, J. and Barrett, S. (1990), Geological evolution of the Carribean region. A plate- tectonic perspective, *In The Geology of North America,* vol H*, The Caribbean Region*, Edited by Dengo. G. and Case. J. E., *The Geological Society of America,* 405-432

Prell, W. L., Imbrie, J., Martinson, D. G., Morley, J. J., Pisias, N. G., Shackleton, N. J. and Streeter, H. F. (1986), Graphic correlation of oxygen iso-tope stratigraphy application to the late Quaternary, *Paleoceanography,* 1, 137–162, doi:10.1029/PA001i002p00137

Quidelleur, X., Hildenbrand, A. and Samper, A. (2008), Causal link between Quaternary paleoclimatic changes and volcanic islands evolution, *Geophysical Research Letters*, 35, 1–5. doi:10.1029/2007GL031849

Reid, R. P., Carey, S. N. and Ross, D. R. (1996), Geological Society of America Bulletin Late Quaternary sedimentation in the Lesser Antilles island arc Late Quaternary sedimentation in the Lesser Antilles island arc, *Geological society of America Bulletin,* 108, 78-100, doi: 10.1130/0016-7606(1996)108<0078:LQSITL>2.3.CO;2

Robock, A. (2000), Volcanic eruptions and climate, *Reviews of Geophysics*, *38*(2), 191-219.

Roobol, M. J. and Smith, A.L. (1998), Pyroclastic stratigraphy of the Soufrière Hills volcano , Montserrat - Implications for the present eruption, *The Journal of Geophysical Research Letters* 25(18), 3393–3396, Paper number 98GL00643. 0094-8534/98/98GL-006435$5.00

Rosi. M., Vezzoli, L., Castelenzano, A. and Grico, G. (1999), Plinian pumice fall deposit of the Campainian Ignimbrite eruption (Phlegraean Fields, Italy), *Journal of Volcanology and Geothermal Research,* 91, 179-198

Sammonds, P., McGuire, W. and Edwards, S. (2010), Volcanic Hazard from Iceland: Analysis and Implications of the Eyjafjallajökull Eruption, UCL *Institute for Risk and Disaster Reduction, London.* Available at: www.ucl.ac.uk/rdr/publications/irdr-special-reports/iceland

Samper, A., Quidelleur, X., Lahitte, P. and Mollex, D. (2007), Timing of effusive volcanism and collapse events within an oceanic arc island: Basse-Terre, Guadeloupe archipelago (Lesser Antilles Arc), *Earth and Planetary Science Letters*, *258*(1), 175-191

Sawyer, D. E., Flemings, P. B., Dugan, B. and Germaine, J. T. (2009), Retrogressive failures recorded in mass transport deposits in the Ursa Basin, Northern Gulf of Mexico, *Journal of Geophysical Research: Solid Earth*, *114*(B10)

Schneider, J. L., Torrado, F. J. P., Torrente, D. G., Wassmer, P., Santana, M. D. C. C. and Carracedo, J. C. (2004), Sedimentary signatures of the entrance of coarse-grained volcaniclastic flows into the sea: the example of the breccia units of the Las Palmas Detritic Formation (Mio–Pliocene, Gran Canaria, Eastern Atlantic, Spain), *Journal of Volcanology and Geothermal Research*, *138*(3), 295-323

Sigl, M., Winstrup, M., McConnell, J. R., Welten, K. C., Plunkett, G., Ludlow, F., Büntgen, U., Caffee, M., Chellman, .N, Dahl-Jensen, D. and Fischer, H. (2015), Timing and climate forcing of volcanic eruptions for the past 2,500 years, *Nature,* 523, 543-549

Singer, B. S., Jicha, B. R., Harper, M. A., Naranjo, J. A., Lara, L. E. and Moreno-Roa, H, (2008). Eruptive history, geochronology, and magmatic evolution of the Puyehue-Cordón Caulle volcanic complex, Chile, *Geological Society of America Bulletin*, 120(5-6), 599-618.

Smith, A. L., Roobol, M. J., Schellekens, J. H. and Mattioli, G. S. (2007), Prehistoric Stratigraphy of the Soufrière Hills – South Soufrière Hills Volcanic Complex , Montserrat , West Indies. , *The Journal of Geology,* 115(1),115–127, doi: 0022-1376/2007/11501-0007

Thirlwall, M. F. (2000), Inter-laboratort and other errors in Pb isotope analyses investigated using ^{207}Pb-^{204}Pb double spike, *Chemical Geology*, 163:299-322

Tommasi, P., Baldi, P., Chiocci, F. L., Coltelli, M., Marsella, M., Pompilio, M. and Romagnoli, C. (2005). The landslide sequence induced by the 2002 eruption at Stromboli volcano. *In Landslides,* Edited by Sassa. K., Fukuoka. H., Wang. F. and Wang. G., *Springer*, 251-258

Trofimovs, J. *et al*. (2006), Submarine pyroclastic deposits formed at the Soufrière Hills volcano, Montserrat (1995–2003): What happens when pyroclastic flows enter the ocean? *Geology*, 34(7), 549-552, doi: 10.1130/G22424.1

Trofimovs, J., Sparks, R. S. J. and Talling, P. J. (2008), Anatomy of a submarine pyroclastic flow and associated turbidity current: July 2003 dome collapse, Soufrière Hills volcano, Montserrat, West Indies, *Sedimentology*, 55,617-634, doi: 10.1111/j.1365-3091.2007.00914

Trofimovs, J., Fisher, J. K., MacDonald, H. A. Talling, P. J., Sparks, R. S. J., Hart, M. B., Smart, C. W., Boudon, G., Deplus, C., Komorowski, J. C., Le Friant, A., Moreton, S. G. and Leg, M. J. (2010), Evidence for carbonate platform failure during rapid sea-level rise; ca 14 000 year old bioclastic flow deposits in the Lesser Antilles, *Sedimentology*, 57:735-759, doi: 10.1111/j.1365-3091.2009.01117

Trofimovs, J., Foster, C., Sparks, R. S. J., Loughlin, S., Le Friant, A., Deplus, C., Porritt, L., Christopher, T., Luckett, R., Talling, P. J., Palmer, M. R. and Le Bas, T. (2012), Submarine pyroclastic deposits formed during the 20th May 2006 dome collapse of Soufrière Hills volcano, Montserrat, *Bulletin of Volcanology,* 74, 391-405, doi: 10.1007/s00445-011-0533-5

Trofimovs, J., Talling, P. J., Fisher, J. K., Hart, M. B., Sparks, R. S. J., Watt, S. F. L., Cassidy, M., Smart, C. W., Le Friant, A., Moreton, S. G. and Lang, M. J. (2013), Timing, origin and emplacement dynamics of mass flows offshore of SE Montserrat in the last 110 ka: Implications for landslide and tsunami hazards, eruption history, and volcanic island evolution, *Geochemistry, Geophysics, Geosystems*, 14(2), 385–406, doi:10.1002/ggge.20052

Wade, B. S., Pearson, P. N., Berggren, W. A., Palike, H. (2010), Review and revision of Cenozoic tropical planktonic foraminifera biostratigraphy and calibration to the geomagnetic polarity and astronomical timescale, 2010, *Earth Science Reviews,* 104, 111-142, doi:10.1016/j.earscirev.2010.09.003

Wadge, G., Robertson, R. E. A. and Voight, B. (2014), An overview of the eruption of Soufrière Hills Volcano, Montserrat from 2000 to 2010. *In The Eruption of Soufrière Hills Volcano, Montserrat from 2000 to 2010,* edited by G. Wadge, R. E. A. and Robertson, B. Voight, *Geological Societ of London Special Publications. 1-39,* ISBN: 978-1-86239-630-2

Wall-Palmer, D. *et al*. (2014), Late Pleistocene stratigraphy of IODP Site U1396 and compiled chronology offshore of south and south west Montserrat, Lesser Antilles, *Geochemistry, Geophysics, Geosystems*, 15,1–21, doi: 10.1002/2014GC005402/full

Ward, S. N. and Day, S. (2003), Ritter Island Volcano-lateral collapse and the tsunami of 1888, *Geophysical Journal International, 154*, 891-902

Watts, P., Grilli, S. T., Tappin, D. R., & Fryer, G. J. (2005). Tsunami generation by submarine mass failure. II: Predictive equations and case studies. *Journal of waterway, port, coastal, and ocean engineering*, *131*(6), 298-310

Watt, S. F., Pyle, D. M., Mather, T. A., Martin, R. S. and Matthews, N. E. (2009), Fallout and distribution of volcanic ash over Argentina following the May 2008 explosive eruption of Chaitén, Chile, *Journal of Geophysical Research: Solid Earth (1978–2012)*, *114*(B4)

Watt, S. F. L., Talling, P. J., Vardy, M. E., Heller, V., *et al*. (2012a), Combinations of volcanic-flank and seafloor-sediment failure offshore Montserrat, and their implications for tsunami generation, *Earth and Planetary Science Letters*, 319(320), 228–240, doi:10.1016/j.epsl.2011.11.032

Watt, S. F. L., Talling, P. J., Vardy, M. E., Masson, D. G., *et al*. (2012b), Widespread and progressive seafloor-sediment failure following volcanic debris avalanche emplacement: Landslide dynamics and timing offshore Montserrat, Lesser Antilles, *Marine Geology*, 323(325), 69–94, http://dx.doi.org/10.1016/j.margeo.2012.08.002

Watt, S. F. L., Jutzeler, M., Talling, P. J., Carey, S. N., Sparks, R. S. J., Tucker, M., *et al.,* (2015), New insights into landslide processes around volcanic islands from Remotely Operated Vehicle (ROV) observations offshore Montserrat, *Geochemistry, Geophysics, Geosystems*, *16*(7), 2240-2261

White, W. M., and Patchett, P. J. (1984), Hf-Nd-Sr isotopes and incompatible element abundances in island arcs: implications for magma genesis and crust-mantle evolution, *Earth Planetary Science Letters,* 67, 167-185

Wynn, R.B., Piper, D. J. W. and Gee, M. J. R. (2002), Generation and migration of coarse-grained sediment waves in turbidity current channels and channel-lobe transition zones.,*Marine Geology*, 192, 59–78

Chapter 5:

Conclusions

This thesis studies over 1 Ma of Montserrat's onshore and offshore stratigraphy to form one of the most detailed and extensive studies of an island arc volcano. This extensive record substantially improves our understanding of how volcanic and mass-wasting processes evolve at Montserrat over long time scales. Chapter 2 discusses how eruption styles vary through time using the terrestrial record. Chapter 3 describes the marine record at Site U1395, and analyses the effects of sea-level change and intensity of volcanism on the frequency of mass-wasting events. Finally, Chapter 4 constructs a stratigraphic framework for the past 1 Ma of volcanism at Montserrat, combining both the onshore and offshore stratigraphies. This integrated record is then used to build on Chapters 2 and 3 to better understand the past eruptive and mass-wasting activity at Montserrat.

Observations made using this dataset have wider implications for other island arc and ocean island volcanoes, particularly with regards to hazard mitigation. This thesis shows that more intense volcanic activity and rapid sea-level changes facilitate mass-wasting processes at Montserrat, and comparisons with a global dataset suggest that rapid sea-level change may promote mass-wasting at other island arc volcanoes (Chapter 3). This thesis also presents data from some of the few deep drill sites through large volcanic island landslides. Deposit 2 was drilled and sampled at IODP Site U1394 and largely comprises in-situ marine sediments that were deformed during the emplacement of the 130 ka turbidite. This suggests that landslide emplacement processes are complex and can cause large-scale deformation of underlying sea floor sediments. This study highlights the difficulties in determining accurate primary volcanic landslide volumes and thus understanding the tsunami hazards posed by large island flank collapses.

The main questions and conclusions from each chapter are summarised below.

1. Chapter 2- A 1 Ma evolution of explosive volcanic activity: chronostratigraphy of the Centre Hills Volcano, Montserrat.

This chapter conducts a detailed study of the Centre Hills subaerial stratigraphy, and compares it with the previously studied subaerial stratigraphy of Soufrière Hills (Roobol and Smith 1998, Smith 2007). Using this stratigraphic record we answer the following questions:

Qu 2.1: How does the eruptive style of Montserrat change over the past 1 Ma, and is activity at the Soufrière Hills and Centre Hills significantly different?

The onshore stratigraphy suggests that activity at Montserrat over the past 1 Ma has been dominated by dome-style eruptions. However, at Centre Hills regular large-magnitude explosive eruptions occurred. This contrasts to activity at Soufrière Hills where large-magnitude explosive eruptions are rare.

The stratigraphy of Centre Hills (dated between 0.48 ± 0.2 Ma to 0.8 ± 0.2 Ma) is composed of at least 24 thick (>1 m) pumiceous units that are interleaved with andesitic lithic breccias. These lithic breccias suggest that dome-style eruptions occurred throughout the activity of Centre Hills. The regular distribution of interlayered pumiceous sequences suggests that large-magnitude explosive eruptions were a frequent occurrence during the activity of Centre Hills (Figure 1). This contrasts with Soufrière Hills where thick pumiceous sequences only occur during Soufrière Hills Episode 2 (Figure 1). Volume estimates of the pumiceous sequences suggest that eruption magnitudes may have been up to 5.

The cause of more regular large-magnitude explosive eruptions at Centre Hills compared to Soufrière Hills is uncertain. The two volcanic centres are indistinguishable in terms of whole rock chemistry, glass chemistry, and mineral

1 Ma → TIME → RECENT

Volcano	CENTRE HILLS		SOUFRIERE HILLS		SOUTH SOUFRIERE HILLS	SOUFRIERE HILLS				
Vent Site	Vent destroyed	Katy Hill	Vent destroyed	Castle Peak and Gages Dome	Raspberry Hills	Chances and Castle Peak, Galways Dome	Perches Dome	Vent destroyed	Castle Peak	Castle Peak
Trofimovs et al. 2013			Episode 1	Episode 2	Episode 3	Episode 4	Episode 5	Episode 6	Episode 7	Episode 8
Smith 2007			Ancient Soufriere Hills	Subunit I	South Soufriere Hills	Subunit II	Subunit III	Subunit IV	Subunit V	Subunit VI
This study	CH Episode 1	CH Episode 2	SH Episode 1	SH Episode 2	SSH Episode 1	SH Episode 3				
Ages	0.92-0.56 Ma	0.71-0.38 Ma	>0.175 Ma	0.175-0.13 Ma	0.13-0.12 Ma	>0.112 Ma to recent				

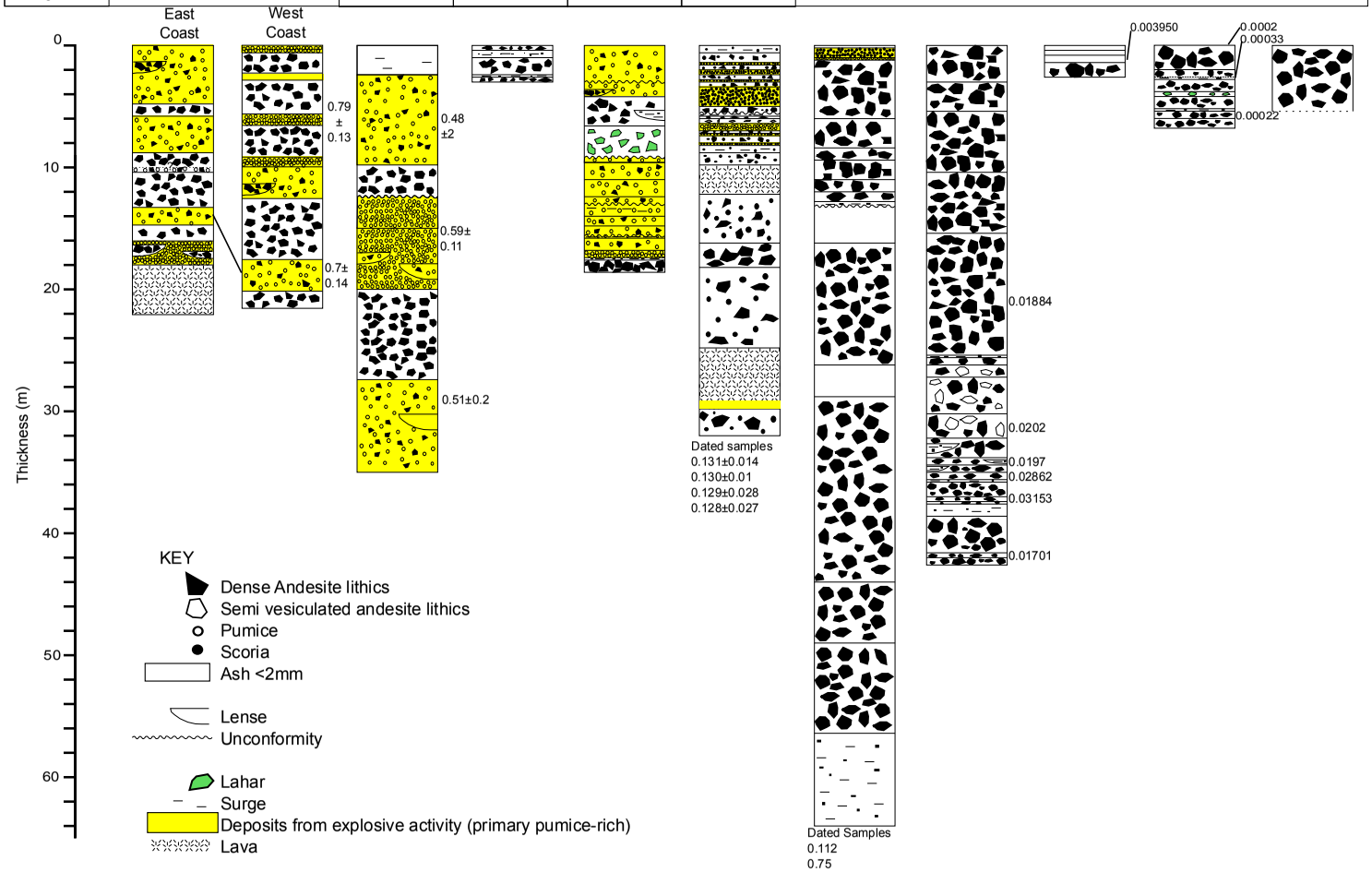

Figure 1: Summary of onshore stratigraphy of Centre Hills, Soufrière Hills, and South Soufrière Hills. Episodes of activity defined in this study are shown, with stratigraphic logs of representative on-land deposits. Scales are approximate and logs are primarily representative of deposits found at the distal margins of the subaerial edifice. Also shown are episodes of activity defined previously by Smith (2007) and Trofimovs *et al.* (2013). Data from Smith, (2007) are used in conjunction with data from this study.

chemistry, and thus differences in explosivity may be attributed to edifice and conduit morphology, or pre-eruptive volatile contents.

2. Chapter 3- The relationship between eruptive activity, flank collapse and sea-level at volcanic islands: a long-term (>1 Ma) record offshore Montserrat, Lesser Antilles.

In this chapter the stratigraphic record at IODP Site U1395B is studied. IODP Site U1395B captures >1 Ma of mass-wasting and eruptive events and forms one of the most complete stratigraphic sequences studied (IODP Site U1394 only extends to ~300 ka, IODP Site U1396 primarily samples tephra fall), and thus is used to answer the following:

Qu 3.1: How does the submarine stratigraphy at Site U1395 record volcanic activity at Montserrat?

Volcaniclastic turbidites and tephra fall are produced during eruptions, as observed in the recent 1995-present dome eruption of Soufrière Hills (Trofimovs *et al.,* 2006). Periods of high volcaniclastic turbidite frequency and tephra fall are likely to be representative of increased volcanism, however it is noteworthy that some volcaniclastic turbidites may also be associated with later re-sedimentation of deposits during periods of relative volcanic quiescence. Using the occurrence of volcaniclastic turbidites and tephra fall layers, periods of increased volcanism have been identified at ~930 ka to ~900 ka, ~810 ka to ~760 ka, and ~190 ka to ~120 ka (Figure 2).

Figure 5

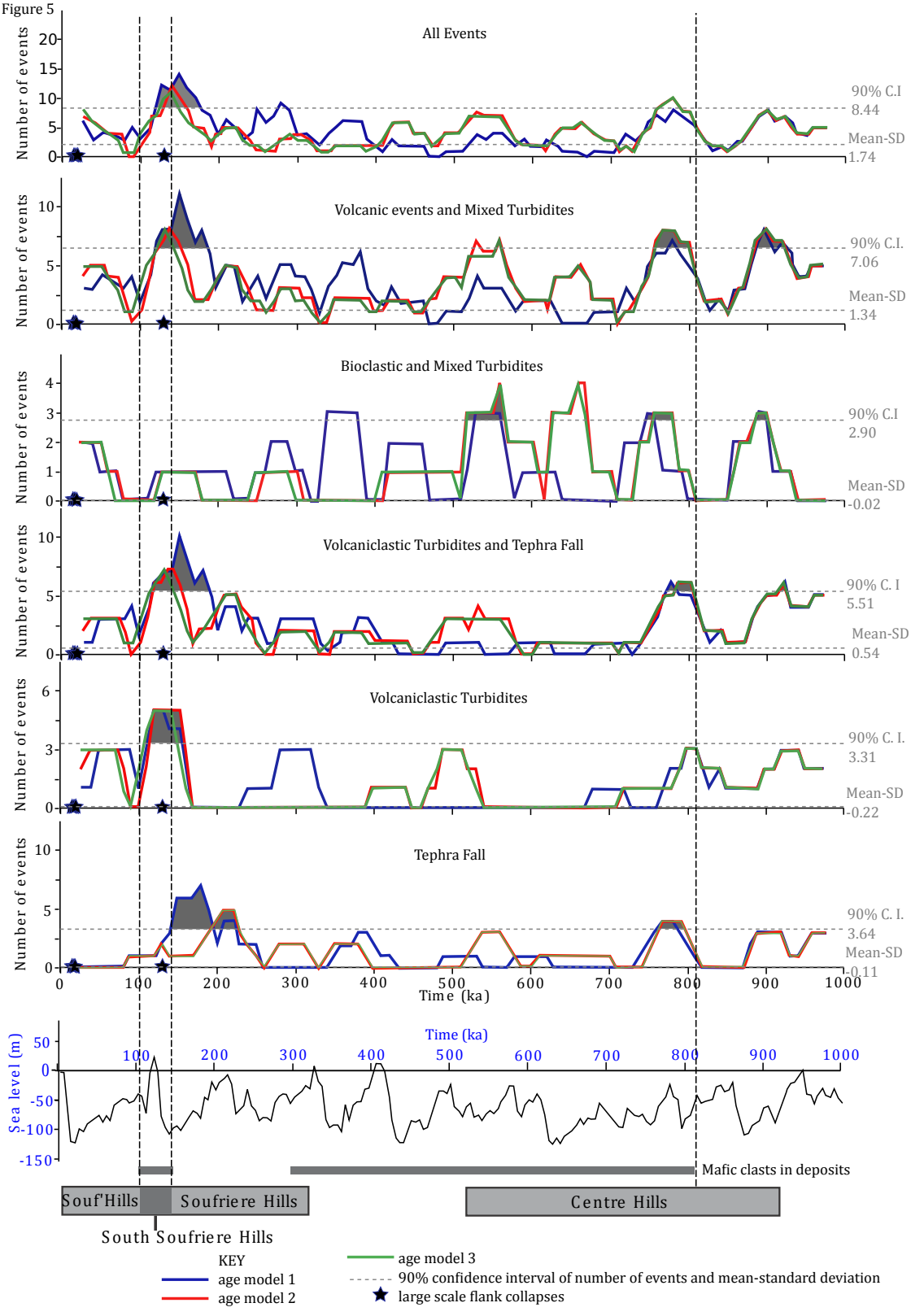
All Events
Number of events
90% C.I
8.44
Mean-SD
1.74
Volcanic events and Mixed Turbidites
90% C.I.
7.06
Mean-SD
1.34
Bioclastic and Mixed Turbidites
90% C.I
2.90
Mean-SD
-0.02
Volcaniclastic Turbidites and Tephra Fall
90% C. I
5.51
Mean-SD
0.54
Volcaniclastic Turbidites
90% C. I.
3.31
Mean-SD
-0.22
Tephra Fall
90% C. I.
3.64
Mean-SD
-0.11
Time (ka)
Sea level (m)
Mafic clasts in deposits
Souf'Hills
Soufriere Hills
Centre Hills
South Soufriere Hills
KEY
age model 1
age model 2
age model 3
90% confidence interval of number of events and mean-standard deviation
large scale flank collapses

Figure 2: Number of events within 50 ka (centred on window, at 10 ka increments). Peaks correspond to clusters in Figure 4. Age model 1 (green) uses oxygen isotope data, biostratigraphic data, AMS dates, and paleomagnetic dates. Age model 2 (red) uses Deposit 2 as a boundary at 130 ka (Figure 2), and the paleomagnetic intervals. Age model 3 (blue) uses only the paleomagnetic data. Peaks in event frequency occur at ~930 ka to ~900 ka, ~810 ka to ~760 ka, and ~190 ka to ~120 ka. Periods when event frequency is above the 90% confidence interval in all age models are shaded in grey. The black line is the Miller *et al.*, (2005) sea-level curve in meters from present day sea-level. Thin grey lines show occurrence of mafic scoria within Hole U1395B, the thick grey line shows known extents of activity at volcanic centres on Montserrat based on limited subaerial dating (Harford *et al.*, 2002). There is a peak in event frequency that coincides with the appearance of mafic scoria in Hole U1395B and all large flank collapses occur during periods of rapid sea-level rise.

Qu 3.2: Are mass-wasting events distributed evenly through time, or do events cluster?

The distribution of turbidites within Hole U1395B suggests that mass-wasting is not constant through time. Turbidite layers within Hole U1395B represent mass-wasting events (however, some volcaniclastic turbidites may have been generated from pyroclastic density currents entering the ocean as opposed to turbidites associated). The three well dated large landslides (Deposits 1, 2 and 5) occurred at 14-8 ka and at 130 ka (Figure 2) and high frequencies of turbidites are observed at 150-100 ka, 560-500 ka, 790-740 ka and ~0.9 ka, suggesting that these were periods of increased mass wasting.

Qu 3.3: What triggers mass wasting events, do volcanism and sea-level changes facilitate mass wasting events?

Periods of heightened mass-wasting (represented by bioclastic, mixed and some volcaniclastic turbidites) at Montserrat often coincide with periods of volcanism (represented by tephra fall and some volcaniclastic turbidites) (Figure 2), suggesting that volcanism may facilitate collapse events. Furthermore, all of the well-dated, large-scale (>0.3 km^3) landslides (Deposits 1,2 and 5) occurred during periods of volcanic activity on Montserrat. An increase in mass-wasting during volcanic activity may be caused by the priming of volcanic flanks that are loaded with eruptive products or are perhaps triggered by seismic or explosive events.

Comparing the occurrence of turbidites with the rate of sea-level change showed little correlation between increased mass-wasting and rapid sea-level change. However, all of the well-dated large landslide deposits at Montserrat (Deposits 1, 2 and 5) coincide with periods of rapid sea-level rise, suggesting that rapid sea-level change may facilitate the largest landslides at Montserrat (Figure 2) (perhaps due to pore pressure changes or increased erosion).

Comparing the emplacement of large landslides at other volcanic islands with the rate of sea-level change showed that at island arc volcanoes large landslides tend to coincide with rapid sea-level rise, but large landslides at ocean islands occur at all rates of sea-level change (Figure 3). The reason for this difference remains unclear, but may be attributed to the topographic, tectonic and lithological differences between island arc volcanoes and ocean islands. However, this is based on a limited dataset and further work is required.

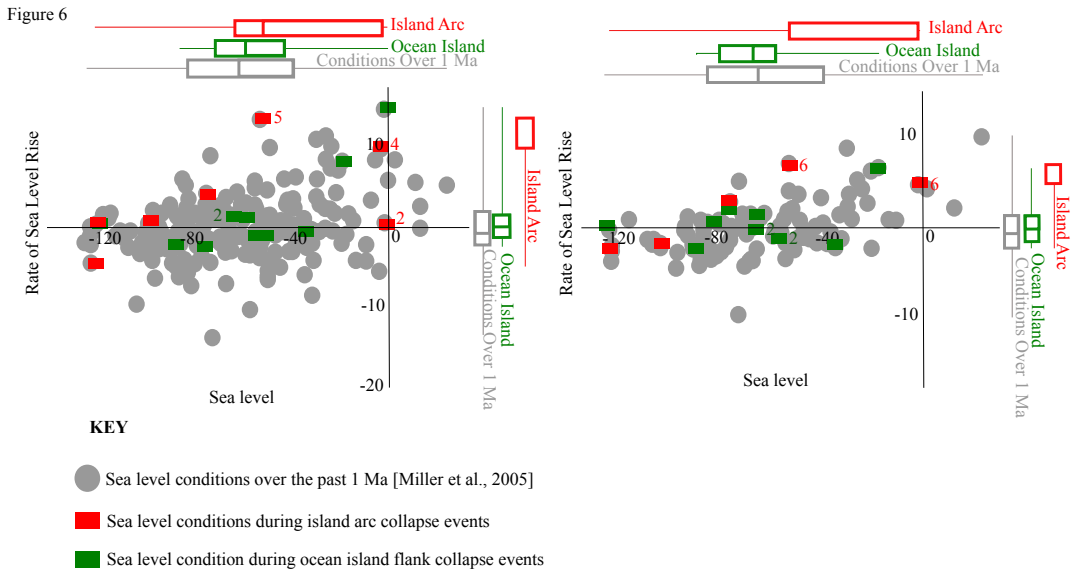

Figure 3: Comparison of sea level conditions with those at the time of documented landslides using data in 5 ka bins (A, left) and in 10 ka bins (B, right). Grey solid circles indicate the full range of conditions over the past 1 Ma at which no landslides were recorded. Annotated box and whisker plots indicate the spread of each data set, with boxes showing 25%, 50% and 75% of the data, whiskers showing the minimum and maximum. Numbers next to data points show the number of overlapping datum. A general skew of landslides occurring at rapid sea-level rises can be seen in the box and whisker plots.

3. Chapter 4- The long-term evolution of construction and destruction processes at an island arc volcano: a 1 Ma long integrated stratigraphy for Montserrat.

In this chapter we outline a stratigraphic framework for the past 1 Ma of stratigraphy for Montserrat, correlating both the onshore and offshore stratigraphies (Figure 4). Correlating units over large distances is difficult, thus further work is required. However, using this integrated stratigraphy we can better understand island growth and destruction processes, building on observations in Chapters 2 and 3.

Qu 4.1: Has eruptive styles and eruptive frequency varied on Montserrat and is there a pause in volcanism during migration of activity from Centre Hills to Soufrière Hills?

Eruptive frequencies and style varies through time. Three main periods of increased eruptive activity have been identified in the offshore record during 1.1-0.9 Ma, 0.3 Ma, and 0.2-0.1 Ma (Figures 4 and 5, Chapter 3). Another period of increased volcanism may have occurred at ~0.5 ± 0.2 Ma and is identified using subaerial deposits, but this is not well represented in the marine cores.

Activity ceased at Centre Hills and migrated to Soufrière Hills between ~0.4-0.5 Ma (Harford *et al*., 2002, Chapters 2 and 3). No large periods of repose (>100 ka) have been identified in the marine cores (denoted by an absence of volcaniclastic-rich units), but a reduction in the activity between 0.7-0.4 Ma is observed (represented by a decrease in the frequency of volcaniclastic deposits in the IODP Holes) (Figure 5).

Eruption styles have evolved over the past 1 Ma, where large-magnitude explosive events were more regular earlier in Montserrat's history. This evolution of behaviour can be seen in both the offshore and onshore records. Onshore at least 24 large-magnitude explosive eruptions have been identified throughout Centre Hills stratigraphy. Such large-magnitude explosive sequences are rare in the Soufrière Hills subaerial stratigraphy. Within the offshore record high frequencies of wide-spread tephra fall only occur during Centre Hills activity (Figure 5). Increases in tephra fall are only observed in the most proximal core site (IODP Site U1394) during Soufrière Hills activity (Figure 5).

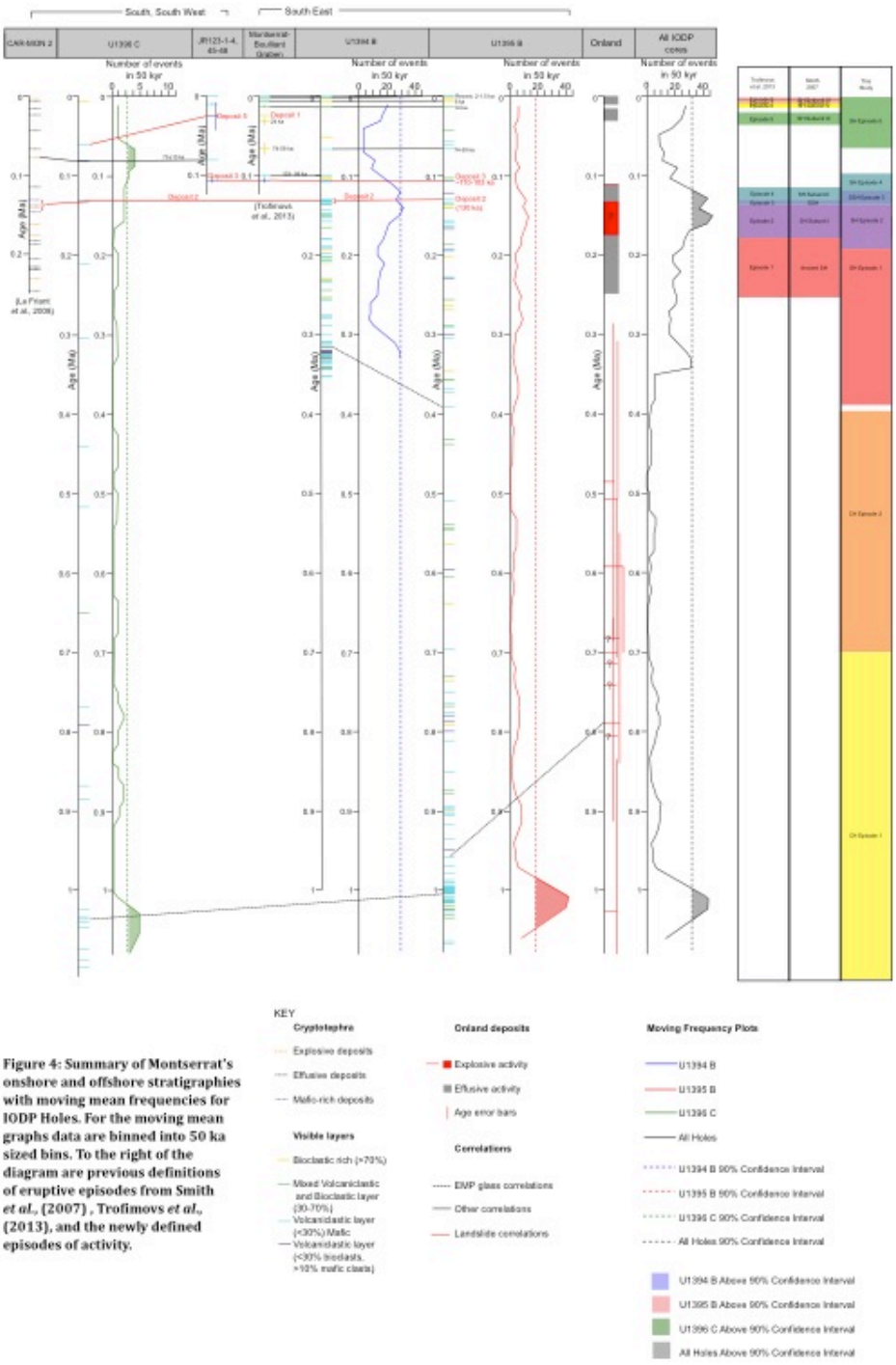

Figure 4: Summary of Montserrat's onshore and offshore stratigraphies with moving mean frequencies for IODP Holes. For the moving mean graphs data are binned into 50 ka sized bins. To the right of the diagram are previous definitions of eruptive episodes from Smith *et al.*, (2007) , Trofimovs *et al.*, (2013), and the newly defined episodes of activity.

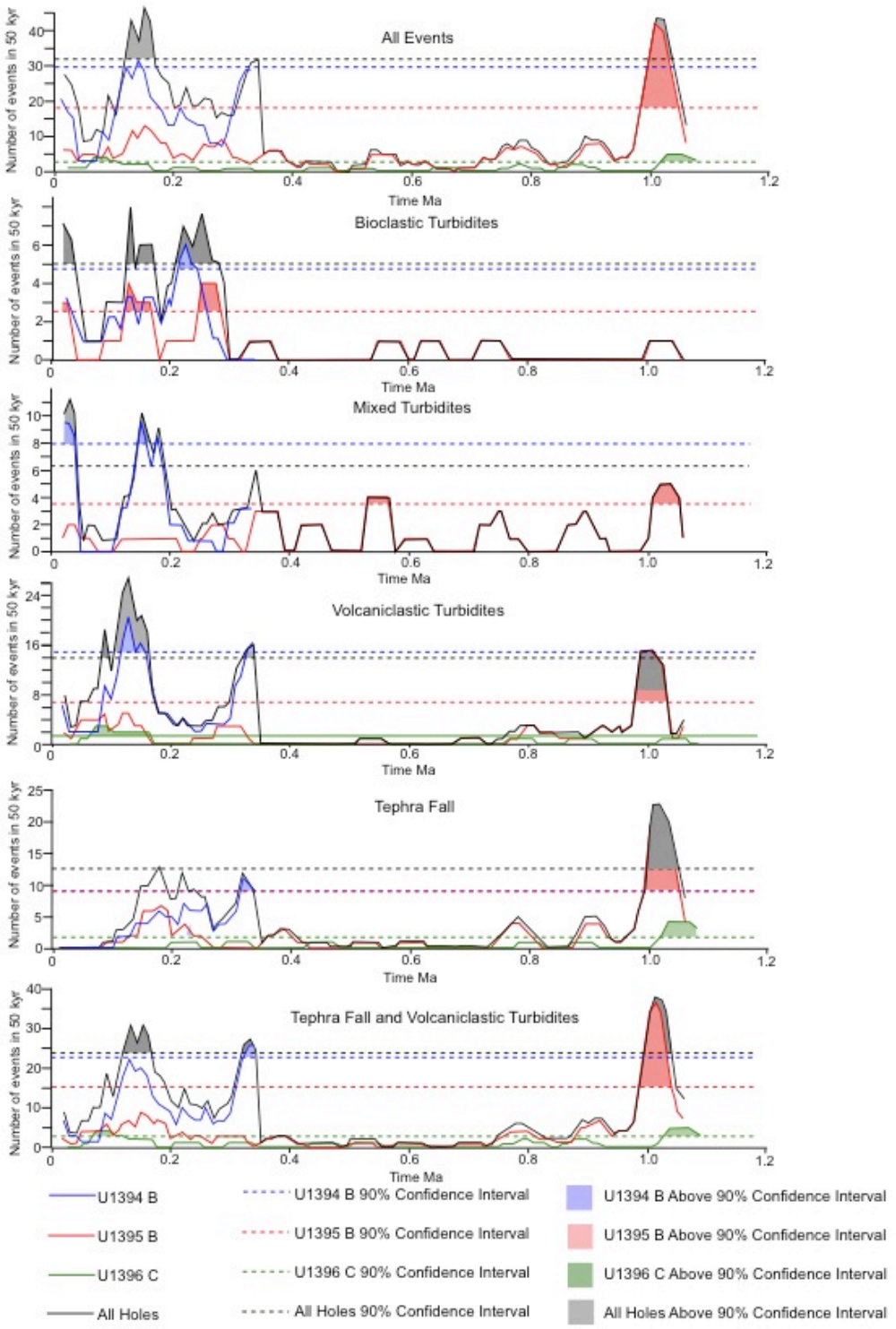

Figure 5: Moving frequencies of events. Data is binned into 50 ka windows. Windows are then moved at 10 ka increments to produce moving frequency graphs. Frequencies from individual cores are shown for Holes U1394B (blue), U1395B (green), and U1396C (red). Also shown is the sum of events in all Holes (black). Dashed lines show the 90% confidence interval, and shaded periods are above the 90% confidence interval.

Qu 4.2 Do other marine sites (IODP Sites U1394 and U1396) show similar variations in mass-wasting composition and frequency as U1395 (Chapter 3), and do mass-wasting events coincide with periods of more intense volcanism?

Mass-wasting histories between Sites U1394 and U1395 show similar trends through time (Figure 5). IODP Site U1396 captures few turbidite events as it is located on a topographic high, and is thus not useful for comparison. The IODP record suggests that the amount of mass wasting varies through time. High frequencies of volcaniclastic turbidites occur during 1.1-0.9 Ma, ~0.3 Ma, and 0.2-0.1 Ma (Figure 5). Mixed turbidite occurrence is more regular with 4 to 5 events after the onset of activity at Soufrière Hills (~0.3 Ma) (Figure 5), suggesting that the onset of activity may have destabilised the carbonate shelf, or that more bioclastic turbidites were directed southwards towards the IODP core sites. The

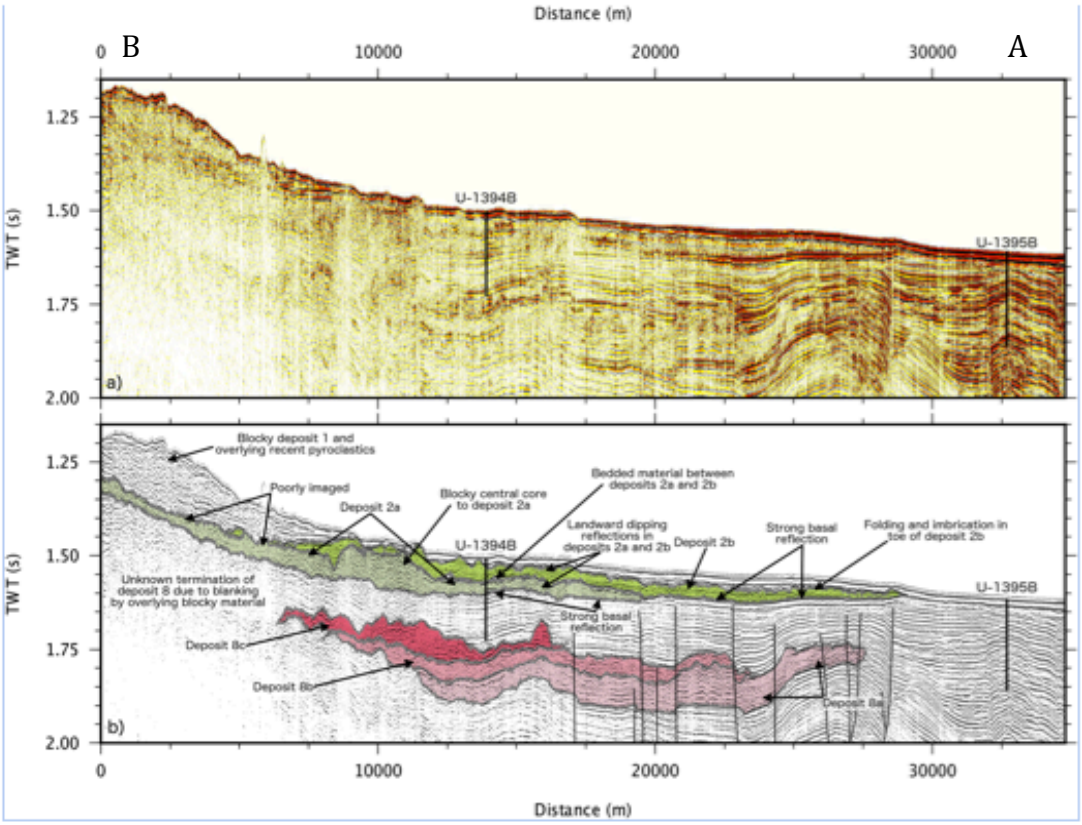

Figure 6: Top- 2D seismic profile trending NE-SW through IODP Site U1394 and U1395. Bottom- Interpretation of seismic profile outlining Deposits 2 and 8. Also shown are Holes. (For seismic line see Figure 1, Chapter 4).

thickest turbidites occur between 0.8-0.5 Ma and between 0.3-0.1 Ma, coinciding with observations of high turbidite frequency (Figure 5).

Observations of the highest turbidite frequencies and the thickest turbidites coincide with periods of increased volcanism (Figure 5), suggesting that volcanic activity may promote mass-wasting. During volcanic activity there is increased seismic activity and increased sedimentation (from eruptive volcanic products) on the island flanks. This may result in decreased flank stability, resulting in increased mass wasting.

4.3: What comprises the large landslide, Deposit 2, and what are the emplacement mechanisms?

IODP site drilled through the Deposit 2 landslide, which appears as a sequence of low amplitude reflections on seismic profiles (Figure 6). Deposit 2 comprises two parts, an upper unit (Deposit 2b) and a lower unit (Deposit 2a) (Figures 6 and 7). Seismic depth conversions estimate that Deposit 2b is at 15-60 m, and Deposit 2a is at 60-95 m. Due to incomplete coring between 15-60m, only Deposit 2a is sampled, thus the composition of Deposit 2b remains undetermined.

Deposit 2a comprises a sequence of turbidites that is unusually coarse with little interleaving hemipelagic material (Figure 7). The units are horizontally bedded and at the base of the deposit no evidence of shearing is found, therefore the deposits are interpreted to be in-situ. Emplacement of the thick (>5 m) overlying 130 ka turbidite may have resulted in dewatering and compaction of the underlying stratigraphy. The sequence that comprises Deposit 2a is coarse, and may have been more susceptible to compaction and dewatering (due to the large intervening pore spaces in coarser deposits), resulting in the observation of reduced seismic amplitudes (Figure 6).

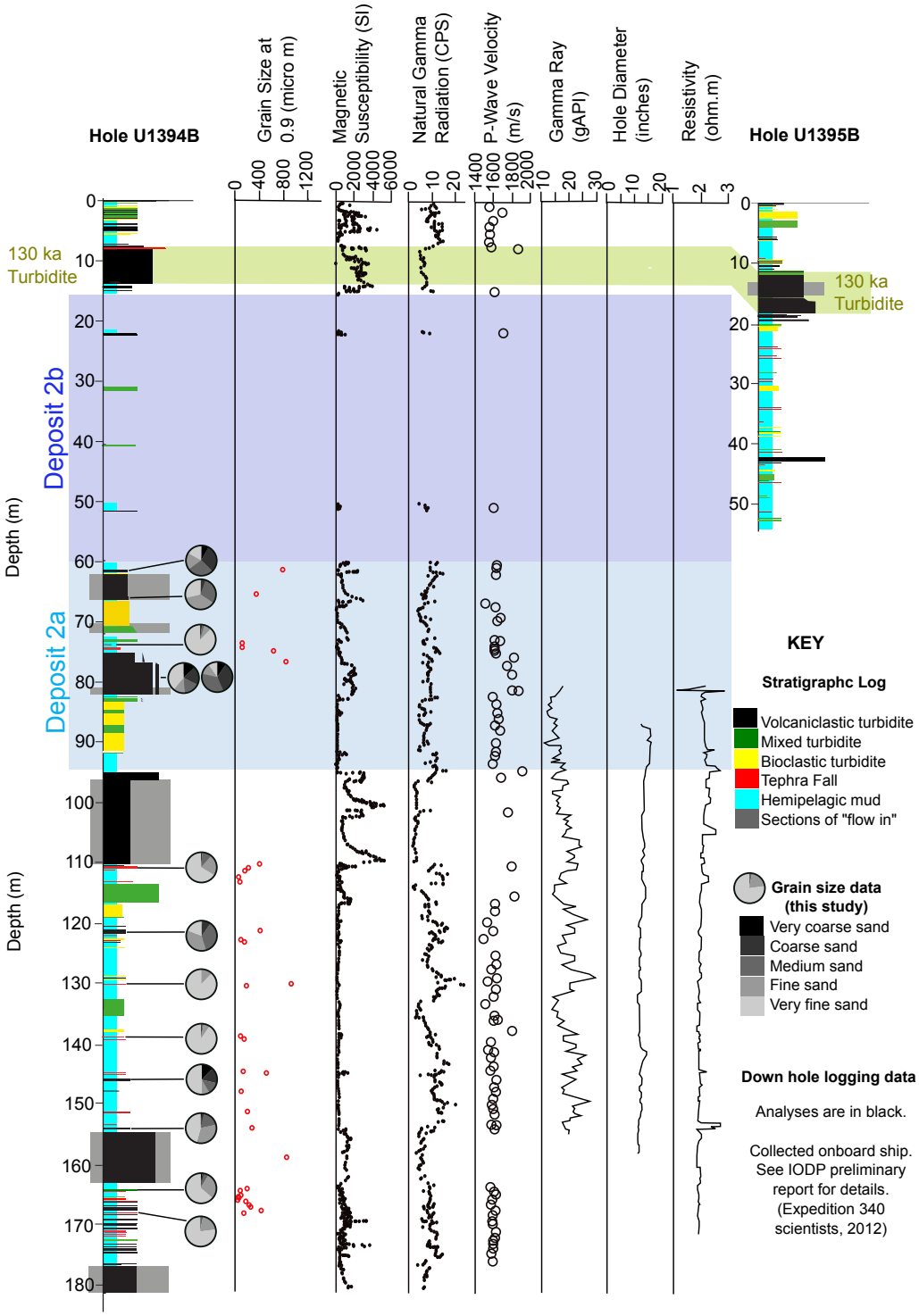
Hole U1394B
Hole U1395B
Grain Size at 0.9 (micro m)
Magnetic Susceptibility (SI)
Natural Gamma Radiation (CPS)
P-Wave Velocity (m/s)
Gamma Ray (gAPI)
Hole Diameter (inches)
Resistivity (ohm.m)
130 ka Turbidite
130 ka Turbidite
Deposit 2b
Deposit 2a
Depth (m)
Depth (m)
KEY
Stratigraphc Log
Volcaniclastic turbidite
Mixed turbidite
Bioclastic turbidite
Tephra Fall
Hemipelagic mud
Sections of "flow in"
Grain size data (this study)
Very coarse sand
Coarse sand
Medium sand
Fine sand
Very fine sand
Down hole logging data
Analyses are in black.
Collected onboard ship. See IODP preliminary report for details. (Expedition 340 scientists, 2012)

Figure 7: Stratigraphic logs of Hole U1394B and the upper 50 m of Hole U1395B. Also shown is grain size data collected in this study and downhole log data from Hole U1394B collected on board the ship during Expedition 340 (Expedtion 340 scientists., 2013). The figure highlights Deposit 2 in blue and the 130 ka turbidite in green. Also shown are a selection of grain size pie charts. Many of the deposits within Deposit 2a are coarser than other deposits sampled in Hole U1394B.

The observation that Deposit 2 largely comprises in-situ marine sediments has important implications for determining landslide hazards. This study suggests that large landslides may have much smaller volumes than initially estimated, which has implications for estimating tsunami size and the threat of inundation. The study also suggests that landslide emplacement is a complex process that can result in large-scale deformation of underlying marine sediments.

4. Future Outlook

This thesis is a substantial contribution to better understanding Montserrat's past eruptive history. However, the study also raises a number of new questions.

Chapter 2 studies the subaerial stratigraphy of Montserrat and demonstrates that the activity at Centre Hills is much more explosive than at Soufrière Hills, despite the two edifices having similar chemical budgets. The work raises the following questions:

How does Centre Hills and Soufrière Hill produce both effusive and explosive eruptions at the same time and why is Centre Hills a more explosive edifice than Soufrière Hills?

Large-magnitude explosive eruptions pose significant hazards to the environment, human health and the economy (Robock, 2000; Watt *et al*., 2009; Sammonds *et al*., 2010; Carlsen *et al*., 2012; Sigl *et al*., 2015). Understanding what

triggers such eruptions is important to help better predict future large-magnitude explosive events.

At Centre Hills and Soufrière Hills, transitions between dome-style eruptions and explosive eruptions are suggested by the changes in stratigraphy (Chapter 2; Kokelaar *et al*., 2002; Wadge *et al*., 2014). What causes these changes in behaviour is unclear. In the recent eruption less crystalline-more chlorine rich material is ejected during explosive phases when compared with effusive phases (Harford *et al*., 2003). This suggests that explosive phases source un-degassed magmas that have ascended relatively rapidly (Harford *et al*., 2003). More generally, at Centre Hills, a relatively large number of large-magnitude explosive eruptions are observed, but these are rare in the past activity at Soufrière Hills. Magmas from the two eruptive centres are compositionally similar, and a compositional different thus does not explain why the Centre Hills volcano is more prone to large-magnitude explosive eruptions than Soufrière Hills. However, differences in pre-eruptive volatile contents, geometries of the edifices and conduits or permeability of the edifices may either promote or reduce the development of large-magnitude explosive events. In order to determine if a more general pattern exists over longer timescales, whereby the more explosive episodes of Centre Hills volcanism are associated with more gas-rich magmas, perhaps with shorter periods of shallow storage, more detailed petrological studies are required (Barclay *et al*., 1998; Rutherford *et al*., 2003; Humphreys *et al*., 2009a, 2009b; Edmonds *et al*., 2014).

Chapter 3 focuses on when mass wasting events occur and what facilitates mass-wasting events. Chapter 3 showed that large mass-wasting events coincided with rapid sea-level rise at Montserrat and other island arcs, but not at ocean islands. The study raises the following questions.

How does rapid sea-level rise trigger/facilitate flank collapses at Montserrat and other island arc volcanoes and why do landslide processes at ocean islands appear unaffected by the rate of sea-level change?

Flank collapses are hazardous due to erosion and by the inundation of large volumes of material, thus better predicting of future events will help mitigate future hazards. How the rate of sea-level changes may affect island arc flank stability (thus triggering flank collapses) is not well understood, but may be attributed to increased pore-pressures, increased flank erosion, or increased volcanism.

Computer modelling and laboratory experiments may give insight into what factors affect pore pressure build up (porosity permeability, composition of flanks), and how large an overpressure is required to result in flank collapse (e.g. Flemmings *et al*., 2008). Laboratory experiments and fieldwork (such as Ramalho *et al*., (2013), Anderson *et al*., (2015)) may also give insights into whether increased erosion occurs during rapid sea-level rise, and if increased erosion can facilitate the development of large-scale landslides.

Rapid sea-level change may also potentially trigger increased volcanism (McGuire *et al*., 1997), in turn promoting mass-wasting events, but the evidence behind such processes remains somewhat speculative. Sea-level changes may trigger volcanism due to pressure changes acting on magmatic reservoirs, or due to interaction of the magmatic system with ground water. Computer modelling (such as those used to study the affects of de-glaciation on magmatic processes (Sigmundsson *et al*., 2010)) may give insight into the affects of sea-level change on magmatic systems, but detailed stratigraphic and petrological studies are required to fully test such ideas. This is not a trivial exercise. Even at a site such as Montserrat, where past work has been extremely extensive and where a uniquely detailed set of marine cores exists – as used in this study – there remain many challenges in generating a stratigraphy that is sufficiently detailed to analyse patterns in activity over $10^{3\text{-}5}$ year timescales.

Chapter 4 aims to construct a stratigraphic framework that includes the past 1 Ma of Montserrat's deposits. Due to the difficulties in correlating individual deposits across large distances, the framework is incomplete. Further work is required to further integrate the subaerial and submarine records. Such work

may include additional chemical analyses of deposits (glass analyses on finer deposits and also bulk rock chemical analyses), and further dating of deposits (extending the oxygen isotope stratigraphies and further Ar-Ar dating of subaerial deposits).

Chapter 4 also discusses emplacement mechanisms of large landslide deposits and includes results from drilling the Deposit 2 landslide. The work raises the following questions:

How are large landslides emplaced and do other large landslides dominantly comprise in-situ marine sediments?

Large landslides are hazardous due to their erosive nature, inundation and their potential to generate large tsunamis. It is important to understand what comprises these deposits and how they are emplaced. This thesis shows that Deposit 2 largely comprises in-situ marine sediments, thus reducing the potential hazards generated during this event. It is therefore necessary to understand if Deposit 2 is unique (in that it comprises mainly locally deformed/ in-situ sediments), as this has significant impacts on determining potential hazards from future landslide events at other volcanic islands.

To better understand landslide emplacement processes, further coring, seismic and bathymetric surveys are required on Deposit 2 and other landslides. Coring provides direct samples of these landslides and will help determine landslide compositions. Multiple cores of the same landslide will also reveal if landslide compositions are spatially variable. Seismic and bathymetric surveys will give detailed insight into the structure of large landslides and aid better understanding of their emplacement.

5. References

Anderson, T. R., Fletcher, C. H., Barbee, M. M., Frazer, L. N. and Romine, B. M. (2015), Doubling of coastal erosion under rising sea level by mid-century in Hawaii, *Natural Hazards*, *78*(1), 75-103

Barclay, J., Rutherford, M. J. and Caroll, M. R. (1998), Experimental phase equilibria constraints on pre-eruptive storage conditions of the Soufrière Hills magma, *Geophysical Research Letters,* 25, 3437-3440

Carlsen, H. K., Gislason, T., Benediktsdottir, B., Kolbeinsson, T. B., Hauksdottir, A., Thorsteinsson, T. and Briem, H. (2012), A survey of early health effects of the Eyjafjallajökull 2010 eruption in Iceland: a population-based study, *Public health, BMJ Open*, 2, e000343, doi:10.1136/bmjopen-2011-000343

Cassidy, M., Trofimovs, J., Palmer, M.R., Talling, P.J., Watt, S.F.L., Moreton, S. and Taylor, R.N. (2013), Timing and emplacement dynamics of newly recognised mass flow deposits at ~8-12 ka offshore Soufrière Hills volcano, Montserrat: how submarine stratigraphy can complement subaerial eruption histories, *Journal of Volcanology and Geothermal Research,* 253, 1-14

Edmonds, M., Humphreys, M. C. S. *et al*. (2014), Pre-eruptive vapour and its role in controlling eruption style and longevity at Soufrière Hills Volcano, *In The Eruption of Soufrière Hills Volcano, Montserrat from 2000 to 2010,* edited by Wadge, G., Robertson, R. and Voight, B., *Geological Society, London, Memoirs*, 39, 291 – 315, doi. org/10.1144/M39.16

Expedition 340 Scientists (2012), Lesser Antilles volcanism and landslides: implications for hazard assessment and long-term magmatic evolution of the arc, *IODP Preliminary Report, 340* doi:10.2204/ iodp.pr.340.2012

Expedition 340 Scientists (2013), Paleomagnetism in methods, *In Proceedings IODP 340: Tokyo (Integrated Ocean Drilling Program Management International, Inc.),* Le Friant, A., Ishizuka, O., Stroncik, N.A., and the Expedition 340 Scientists, doi:10.2204/iodp.proc.340.102.2013

Flemings, P. B., Long, H., Dugan, B., Germaine, J., John, C. M., Behrmann, J. H. and Expedition, I. O. D. P. (2008). Pore pressure penetrometers document high overpressure near the seafloor where multiple submarine landslides have occurred on the continental slope, offshore Louisiana, Gulf of Mexico, *Earth and Planetary Science Letters*, *269*(3), 309-325

Harford, C. L. Pringle, M. S., Sparks, R. S. J. and Young, S. R. (2002), The volcanic evolution of Montserrat using 40Ar/39Ar geochronology, *Geological Society, London, Memoirs*, 21:93–113, doi: 10.1144/GSL.MEM.2002.021.01.05

Harford, C. L., Sparks, R. S. J. and Fallick, A. E. (2003), Degassing at the Soufrière Hills Volcano, Montserrat, recorded in matrix glass compositions, *Journal of Petrology*, *44*(8), 1503-1523

Humphreys, M. C. S., Christopher, T. and Hards, V. (2009a), Microlite transfer by disaggregation of mafic inclusions following magma mixing at Soufrière Hills volcano, Montserrat, *Contributions to Mineralogy and Petrology,* 157, 609–624

Humphreys, M. C. S., Edmonds, M., Christopher, T. and Hards, V. (2009b), Chlorine variations in the magma of Soufrière Hills Volcano, Montserrat: insights from Cl in hornblende and melt inclusions, *Geochimica et Cosmochimica Acta* 73, 5693–5708

Kokelaar, B.P. (2002), Setting, chronology and consequences of the eruption of Soufrière Hills Volcano, Montserrat (1995-1999), I*n the eruption of* Soufrière *Hills volcano, Montserrat, from 1995 to 1991*, edited by Druitt, T.,

and Kokelaar, P. *Geological Society Special Publications,* 21:1–43, doi:10.1144/GSL.MEM.2002.021.01.02

Leatherman, S. P., Zhang, K. and Douglas, B. C. (2000). Sea level rise shown to drive coastal erosion. *Eos, Transactions American Geophysical Union*, *81*(6), 55- 57.

McGuire, W. *et al*. (1997), Correlation between rate of sea-level change and frequency of explosive volcanism in the Mediterranean, *Letters to Nature*, 389, 473–476

Miller, K. G., Kominz, M. A., Browning, J. V., Wright, J. D., Mountain, G. S., Katz, M. E., Sugarman, P. J., Cramer, B. S., Christie-Blick, N. and Pekar, S. F. (2005), The Phanerozoic Record of Global Sea-Level Change, *Science, 310*, 1293-1298, doi: 10.1126/science.1116412

Ramalho, R. S., Quartau, R., Trenhaile, A. S., Mitchell, N. C., Woodroffe, C. D. and Ávila, S. P. (2013), Coastal evolution on volcanic oceanic islands: A complex interplay between volcanism, erosion, sedimentation, sea-level change and biogenic production, *Earth-Science Reviews*, *127*, 140-170

Robock, A. (2000), Volcanic eruptions and climate, *Reviews of Geophysics*, *38*(2), 191-219

Roobol, M. J. and Smith, A. L. (1976), Mount Pelée, Martinique: a pattern of alternating eruptive styles. *Geology*, *4*(9), 521-524

Rutherford. M. J. and Devine, J. D. (2003), Magmatic conditions and magma ascents indicated by hornblende phase equilibria and reactions in the 1995-2002 Soufrière Hills Magma, *Journal of Petrology,* 44 (8), 1433-1454

Sammonds, P., McGuire, W. and Edwards, S. (2010), Volcanic Hazard from Iceland: Analysis and Implications of the Eyjafjallajökull Eruption, UCL *Institute for Risk and Disaster Reduction, London.* Available at: www.ucl.ac.uk/rdr/publications/irdr-special-reports/iceland

Sigl, M., Winstrup, M., McConnell, J. R., Welten, K. C., Plunkett, G., Ludlow, F., Büntgen, U., Caffee, M., Chellman, .N, Dahl-Jensen, D. and Fischer, H. (2015), Timing and climate forcing of volcanic eruptions for the past 2,500 years, *Nature,* 523, 543-549

Sigmundsson, F., Pinel, V., Lund, B., Albino, F., Pagli, C., Geirsson, H., & Sturkell, E. (2010). Climate effects on volcanism: influence on magmatic systems of loading and unloading from ice mass variations, with examples from Iceland, *Philosophical Transactions of the Royal Society of London A: Mathematical, Physical and Engineering Sciences*, *368*(1919), 2519-2534.

Smith, A. L., Roobol, M. J., Schellekens, J. H. and Mattioli, G. S. (2007), Prehistoric Stratigraphy of the Soufrière Hills – South Soufrière Hills Volcanic Complex, Montserrat, West Indies, *The Journal of Geology,* 115(1),115–127, doi: 0022-1376/2007/11501-0007

Trofimovs, J. *et al*. (2006), Submarine pyroclastic deposits formed at the Soufrière Hills volcano, Montserrat (1995–2003): What happens when pyroclastic flows enter the ocean? *Geology*, 34(7), 549-552, doi: 10.1130/G22424.1

Trofimovs, J., Talling, P. J., Fisher, J. K., Hart, M. B., Sparks, R. S. J., Watt, S. F. L., Cassidy, M., Smart, C. W., Le Friant, A., Moreton, S. G. and Lang, M. J. (2013), Timing, origin and emplacement dynamics of mass flows offshore of SE Montserrat in the last 110 ka: Implications for landslide and tsunami hazards, eruption history, and volcanic island evolution, *Geochemistry, Geophysics, Geosystems*, 14(2), 385–406, doi:10.1002/ggge.20052

Wadge, G., Robertson, R. E. A. and Voight, B. (2014), An overview of the eruption of Soufrière Hills Volcano, Montserrat from 2000 to 2010, *In The Eruption of Soufrière Hills Volcano, Montserrat from 2000 to 2010,* edited by G. Wadge, R. E. A. and Robertson, B. Voight. *Geological Societ of London Special Publications. 1-39,* ISBN: 978-1-86239-630-2

Watt, S. F., Pyle, D. M., Mather, T. A., Martin, R. S. and Matthews, N. E. (2009), Fallout and distribution of volcanic ash over Argentina following the May 2008 explosive eruption of Chaitén, Chile, *Journal of Geophysical Research: Solid Earth (1978–2012)*, *114*(B4)

Appendix

Note on sample names for IODP samples:

During IODP coring multiple sites are drilled (U1394, U1395, and U1396), and at each site multiple holes are drilled (A, B, C). During drilling, core is brought back up to the ship in ~10 m long barrels, these are labelled 1H, 2H and so on where 1H is the first barrel retrieved. These cores are split into ~1.5 m lengths and are numbered 1, 2 and so on. At the base of each core is a core catcher. This prevents loss of material, and are denoted by 'CC'. Cores are then split and all samples are from the working halves. Each sample location is identified by top and bottom depths in core sections.

Using the sample names in this study, the location of each sample can be found.

For example in sample number 95B73 7/8

95 refers to the IODP Site (U1395 in this case)
B refers to the Hole
7 refers to the core barrel (ie 7H)
3 refers to the section of core
7/8 refers to a sample top depth of 7cm, and a sample bottom depth of 8 cm in the core section.

Figures 2 and 3 are in the pocket due to their large size.

Figure 1- Stratigraphy of Centre Hills

This figure shows a more detailed stratigraphy of the E and W coasts of Montserrat. Also inset is a map identifying sample locations. Varying clast symols shows composition of each unit. Colours identify potential correlations.

Figure 2- Stratigraphic Logs of All IODP Holes in Pocket

This figure shows the stratigraphic logs of all Holes drilled offshore of

Montserrat during IODP Expedition 340. Also shown are potential correlations from biostratigraphic, oxygen isotope, and Paleomagnetic constraints.

Figure 3- Summary of All Data Collected on IODP Holes in Pocket

This figure summarises the stratigraphy of Holes U1394B, U1395B, and U1396C, and also all of the componentry, grain size, biostratigraphy, isotope stratigraphy and paleomagnetic analyses.

All tables are contained within the affixed CD. The tables are large, and are thus unsuitable for printing.

Table 1- Whole Rock ICP-MS RSD of Subaerial Material on CD

This table contains the RSD values of all ICP-MS analyses on subaerial samples described in Chapter 2. We refer the reader to Chapter 2 for the sample locations and for the whole rock trace element compositions (Table 5, Chapter 2).

Table 2- Plagioclase Compositions (SEM) of Subaerial Material on CD

This table contains SEM data of Plagioclase phenocrysts from select subaerial samples. We refer the reader to Chapter 2 for sample details.

Table 3- Clinopyroxene Compositions (SEM) of Subaerial Material. on CD

This table contains SEM data of Clinopyroxene phenocrysts from select subaerial samples. We refer the reader to Chapter 2 for sample details.

Table 4- Orthopyroxene Compositions (SEM) of Subaerial Material on CD

This table contains SEM data of Orthopyroxene phenocrysts from select subaerial samples. We refer the reader to Chapter 2 for sample details.

Table 5- Amphibole Compositions (SEM) of Subaerial Material on CD

This table contains SEM data of Amphibole phenocrysts from select subaerial samples. We refer the reader to Chapter 2 for sample details.

Table 6- Glass Compositions EMP on CD

This table contains all glass compositions from both subaerial and core

material. We refer the reader to Chapter 2 for subaerial sample details and Figure 7 in Chapter 2, and to Chapter 4 for core sample details and Figures 12 and 13 in Chapter 4.

Table 7- RSD of Glass Compositions on CD

This table contains RSD of all glass compositions from both subaerial and core material. We refer the reader to Chapter 2 for subaerial sample details and Figure 7 in Chapter 2, and to Chapter 4 for core sample details and Figures 12 and 13 in Chapter 4.

Table 8- Grain Size Data from laser analyses of Core Material on CD

This table summarises all of the grain size data collected using the Malvern laser grain size analyser. The 90% quartile is shown in Appendix Figure 3. For details see Chapters 3 and 4.

Table 9- GRADISTAT Results of Grain Size Data of Core Material on CD

Table 10- Componentry Data of Core Material on CD

This table shows all Componentry results of selected units in the IODP Holes. Results are summarised in Appendix Figure 3. See chapters 3 and 4 for further details on methods.

Table 11- Oxygen and Carbon Isotope analyses of Hemipelagic Mud on CD

This table shows all oxygen and carbon isotope data collected. See Chapters 3 and 4 for methods. Figure 2 in Chapter 3 summarises isotope data on Hole U1395B, Figure 9 in Chapter 4 and Appendix Figure 3 summarise isotope data on all analysed IODP Holes.

Table 12- Ages of Units in Hole U1395B on CD

Ages of units in IODP Hole U1395B that are estimated from hemipelagic sedimentation rates. In this table unit ages from all three age models (see Chapter 3 for details) are presented.

Table 13- Thicknesses and ages of Units in IODP Holes on CD

Ages of units in IODP Holes U1394B, U1395B, and U1396C that are estimated from hemipelagic sedimentation rates. For details on the age models used see Chapter 4.

Table 14- Descriptions of Units in IODP Holes and classification on CD

This table summarises all of the compositions (componentry), thickness, and sorting of units that were analysed from the IODP Holes. Also contained within this table are unit descriptions and the classification (e.g bioclastic turbidite tephra fall etc) of each analysed unit.